Hydrogen Powered VTOL Aircraft

Final Report

Design Synthesis Exercise

Group 05: H2-VTOO

Delft University of Technology

TU Delft

Hydrogen Powered VTOL Aircraft

Final Report

by

Group 05: H2-VTOO

Name	
Boersma, Mats	4861566
Comuth, Bas	4784626
Coutinho, Kirsten	4778707
Dahmani, Fabien	4824555
Deckers, Sam	4799135
Gouwy, Simon	4796918
Peeters, Michiel	4824504
Piera, Hielke	4667158
Pierreux, Brecht	4848292
Prencipe, Ynias	4777158

to obtain the degree of Bachelor of Science
at the Delft University of Technology,

Project duration: April 19, 2021 – July 2, 2021

Project tutors:
Dr. ir. J.M.J.F. van Campen, TU Delft, supervisor
Dr. ir. D.A.M. de Tavernier, TU Delft, coach
Ir. S.H.J. Westerbeek, TU Delft, coach
P. Meseguer, TU Delft, PM&SE TA

TU Delft

Contents

Preface

This report was written by ten third-year students from the Faculty of Aerospace Engineering at the TU Delft. In the last quarter of the third year we have been assigned a design of a ten-seater, hydrogen powered, VTOL aircraft, capable of conventional take-off and landing, to test our skills and knowledge acquired in the last three years. In this final report, a detailed conceptual design of the aircraft will be presented which will be followed by an analysis of the relevance of the aircraft in modern society and future steps.

In this report, the reader is assumed to have basic system engineering and technical knowledge in the field of aeronautical engineering. In the first six chapters a more elaborate overview is given of what the aircraft can do, what the relevance of the project will be and what the aircraft will look like. This will be followed by a detailed design of several subsystems from Chapter 7 till Chapter 13. After this the aircraft will be analysed for its performance on risk, RAMS, production, sustainability and cost alongside the future steps to be taken.

We would like to express our gratitude to Dr. ir. J.M.J.F. van Campen, Dr. ir. D.A.M. de Tavernier and Ir. S.H.J. Westerbeek for helping us out when we faced difficulties. Furthermore, a special thanks to P. Meseguer for helping out on the project management and systems engineering aspects of the project. Lastly, we would like to thank Ir. J.A. Melkert for his valuable feedback during times of doubt, lectures explaining the weekly deliverables, and smooth operation of on-campus activity during these difficult times.

This project provided all ten of us with large amounts of improvement in both our social skills when working in teams, but also in our technical and managerial skills. Not only due to this valuable experience, but also due the fact that we, as a team, designed a hydrogen powered VTOL aircraft, we deem this project successfully completed and feel prepared to embark on our next chapter in our academical or professional career.

Mats Boersma, Bas Comuth, Kirsten Coutinho, Fabien Dahmani, Sam Deckers, Simon Gouwy, Michiel Peeters, Hielke Piera, Brecht Pierreux and Ynias Prencipe. Delft, June 2021

Executive Overview

The world is progressing towards a more sustainable future. In all industries, emissions and production processes are carefully monitored to validate their level of sustainability. One industry that is traditionally held accountable for the hindrance of this progression, is the aviation industry [1]. Heavy taxation results in a desire for highly efficient sustainable fuels that produce low emissions and minimise their contribution to global warming. Along with this, sustainable aviation itself is seeing a rise in demand. Therefore, aircraft that can be recycled are experiencing a desire from this industry.

This demand has led to an initiative by the Delft University of Technology resulting in an assignment for the Design Synthesis Exercise; "Conceptually design a low capacity, 2500 km range, VTOL capable aircraft using H2 as energy carrier that reduces the door-to-door travel time in and between urban environments by 2040." The challenge to achieve such a conceptual design has been taken upon by ten aerospace engineering bachelor students at the university. The project will be carried out over a period of ten weeks. While the primary objective of this assignment will be to present the design of this aircraft, a secondary objective would be to also explore the capabilities of hydrogen as a fuel for aviation. This results in the generation of the following project objective statement: "In ten weeks time, ten students will design a ten-seater hydrogenpowered aircraft capable of VTOL and explore the possibilities of hydrogen powered flight." With this, the ten aforementioned students have formed the group 'H2-VTOO', which stands for '**H**ydrogen powered **V**ertical **T**ake-**O**ff and landing aircraft for urban envir**O**nment'.

When starting such a project where the goal is to contribute to a more sustainable future a sustainable development strategy needs to be generated. For sustainable development, there are three main pillars upon which one can develop a strategy. These are: economical, social and environmental sustainability. H2-VTOO tries to rest its design on each of these three pillars. Firstly, it is economically sustainable due to e.g. the use of lean manufacturing and circular economy. Secondly, it will provide entry level jobs for economically less favoured individuals which are motivated to work. Lastly, H2-VTOO will provide environmental sustainability not only by the use of the hydrogen, but also by making sure there are no toxic or scarce materials exposed to the environment during production. Furthermore, noise is kept to a minimum (which can be seen as social sustainability as well) and the design has a recyclability of 80%.
Next to this, it is important to assess the market situation. This is done in order to ensure that the product, in this case the aircraft, will perform successfully. From this market analysis, it could be concluded that the aviation industry is a market that contributes heavily to a region's economy (in this case the EU). The repercussions it has faced due to emissions have led to the development and shift of focus to more sustainable aircraft. H2-VTOO will be an aircraft that meets both the sustainable and convenience needs of (corporate) travellers.
After the market analysis, it is important to be able to provide an overview of which subsystems play an important role, and to assess in what way they provide this role, a functional analysis is made. From this it was clear that special attention is to be payed to the flight controls, structures, VTOL capabilities and sustainable development of the aircraft. Other parts that showed their importance were the electrical systems, production plan, control systems and communication diagram. These functions formed the basis of the subsequent design steps, and gave the team a clear overview of what functions the aircraft must at least be able to perform.

One of the strategies that was developed, are the operations and logistics of the aircraft. From this plan, it could be concluded that H2-VTOO will opt for a large tank, which is filled from either external or on-site hydrogen production sites. Hydrogen produced externally can be piped to the location of use, or brought there by trucks.

Next to these more general topics, the actual aircraft has to be designed. In aircraft design, one is always confronted with the very iterative nature in which this happens. Therefore, an iteration tool was developed in Python, which took into account various subsystem design parameters, and matched them together to converge to a viable aircraft design.

For any aircraft, it is vital to know it's performance in various flight conditions. Therefore, a performance analysis was conducted. For cruise performance, it was found that a cruise height of 1650 m would be optimum. At ideal conditions, the aircraft was found to have a maximum range of around 3200 km. During VTOL, the aircraft would climb at 9 m/s. It was also deduced that during conventional take-off, the aircraft would have a nacelle angle of 50 deg with the horizontal axis. A take-off speed of 56.5 m/s was calculated. From the climb performance analysis, an ideal climb speed for maximum ROC was deduced to be around 50 m/s.

Next to an aircraft's performance, the aerodynamics are of great importance. Upon analysis, the NACA 63(2)-215 was chosen for the main airfoil, and the NACA 0015 for both the vertical and horizontal tail airfoils. Apart from this, the

[1] https://www.bbc.com/future/article/20200218-climate-change-how-to-cut-your-carbon-emissions-when-flying

planform for the main wing and empennage were designed, together with a class I and II drag estimation, needed for sizing. Note that all of these methods, and the following to come, have been implemented in the iteration design tool.

No aircraft is able to fly without rigid structures, especially one that needs a large storage tank for hydrogen. A hydrogen tank at the back of the fuselage was designed based on its mechanical and thermodynamic properties. This resulted in a tank which weighs around 1000kg with a diameter of 2.5 m. It is able to store 807 kg of liquid hydrogen. Next to the hydrogen tank, the wing box and fuselage structures were designed, together with the analysis of structural dynamics. Lastly, the landing gears were sized.

An important topic of any aircraft is the stability and control. For this, the team started with the regulatory requirements for stability. Both the static and dynamic stability were analyzed based on a scissor plot and the eigenmodes during various dynamic motions, such as dutch roll, short period and spiral. It was than found that the aircraft is indeed stable. Next to stability, the controllability has to be assured. This is also done by means of the scissor plot. However, control surfaces such as ailerons, rudder and an elevator were designed in order to provide controllability around all three axes of the aircraft. Lastly, a preliminary overview of the aircraft control system was designed, which can be expanded to an autopilot system in the future.

Next to the stability and control, the power and propulsion have been analyzed. These resulted in the design of the propellers, fuel cell configuration of 6 stacks, the cooling system that accompanies this and the battery design needed for extra redundancy and to power the electrical system. Apart from this, an engine has been chosen and sized. In total, the aircraft will provide a total voltage 1330 V and 2570 kW of power. These systems are accompanied by a hardware, software and electrical block diagram, concluded with a data handling and communication system. These describe how the electrical systems will be built, programmed and are interlinked.

One of the most important topics of the project is the requirement to be sustainable. This was discussed in the sustainability analysis, in which a preliminary life cycle assessment was performed, together with an in-depth noise analysis. Resulting in the aircraft producing around 82dB of noise.

Finally, a RAMS analysis was performed together with an in-depth manufacturing plan. This will describe the processes, materials and assembly plan. This was concluded with a cost analysis which shows that the aircraft will have a total inflation-adjusted price of 17.5 million EUR. Lastly, a compliance matrix checking the requirements and a post-project planning have been set up.

The culmination of all the previously mentioned efforts resulted in the final conceptual aircraft design shown in Figure 1. It has a span of 18m, length of 18.5m MTOM of 11200kg and cruise speed of 470km/h.

Figure 1: Final design render of the H2-VTOO aircraft.

Nomenclature

Constants

π	Pi [-]

Symbols

α_h	Angle of attack of the horizontal tail [deg]
β	Sideslip angle [deg]
ΔT	Temperature difference [K]
Δ	Sweep angle [deg]
δ	Deflection angle [deg]
$\dot{m}$	Mass flow [kg/s]
$\dot{Q}$	Heat energy per second [J/s]
η	Efficiency [-]
η_p	Propulsive efficiency [-]
Λ	Sweep [deg]
λ	Taper ratio [-]
λ	Thermal conductivity [W/(m · K)]
μ	Advance ratio [-]
μ_c	Normalized velocity component [-]
μ_d	Dynamic viscosity [kg/ms]
ϕ	Roll angle [deg]
ψ	Turn over angle [deg]
ρ	Density [kg/m^3]
σ	Crab angle [deg]
τ	Chord to control surface chord ratio [-]
τ	Shear stress [Pa]
θ	Tip back angle [deg]
θ_{ground}	Angle between ground, propeller at MLG [deg]
θ_{nac}	Angle between the horizontal and the nacelle [deg]
θ_{tilt}	Tilt angle [deg]
A	Aspect ratio [-]
A	Rotor area [m^2]
A_b	Blade area [m^2]
B	Boom area [m^2]
b	Span [m]
C	Damping coefficient [Ns/m]
c	Chord [m]
C_L	Lift coefficient [-]
C_m	Moment coefficient [-]
C_p	Specific heat [J/kg K]
c_{d_0}	Zero lift drag coefficient airfoil [-]
C_{D_y}	Drag coefficient in lateral direction [-]
$C_{D_{misc}}$	Miscellaneous drag [-]
c_{dis}	Discharge coefficient [-]
C_{fe}	Equivalent skin friction coefficient [-]
c_{HT}	Horizontal tail volume coefficient [-]
c_{l_α}	Change in lift due to angle of attack of airfoil [-]
C_{L_h}	Lift coefficient horizontal tail [-]
C_{l_p}	Roll damping coefficient [-]
$C_{L_{\alpha_h}}$	Lift slope of horizontal tail [-]
$C_{l_{\delta_a}}$	Aileron roll control derivative [-]
$C_{L_{\delta_e}}$	Change in lift coefficient due to elevator deflection [-]
$C_{l_{\delta_r}}$	Rudder roll control derivative [-]
$C_{L_{A-h}}$	Tailless lift coefficient [-]
$C_{L_{h_0}}$	Lift at zero angle of attack horizontal tail [-]
C_l	Change in rolling moment[-]
C_{m_0}	Zero lift moment coefficient [-]
C_m	Change in pitching moment [-]
$C_{n_{\delta_a}}$	Aileron yaw control derivative [-]
$C_{n_{\delta_r}}$	Rudder yaw control derivative [-]
C_n	Change in yawing moment [-]
C_{rr}	Rolling resistance coefficient [-]
c_{vt}	Vertical tail volume coefficient [-]
C_{X_0}	X force coefficient in straight and level flight [-]
C_X	Change in X force [-]
C_{Y_β}	Change in lateral force due to sideslip [-]
C_{Y_p}	Change in lateral force [-]
$C_{Y_{\delta_a}}$	Aileron lateral force derivative [-]
$C_{Y_{\delta_r}}$	Rudder lateral force control derivative [-]
C_{Z_0}	Z force coefficient in straight and level flight[-]
C_Z	Change in Z force [-]
D_b	Differential operator in asymmetric flight [-]
D_c	Differential operator in symmetric flight [-]
d_f	Fuselage diameter [m]
D_p	Propeller diameter [m]
$d_{n,p}$	Distance between propeller blades and the motor nacelle [m]
E	Young's modulus [Pa]
e	Oswald efficiency factor [-]
f	Component diameter divided by diameter [-]
f	Natural frequency [Hz]
F_w	Lateral force exerted by crosswind [N]
G	Shear modulus [Pa]
h_{clear}	Clearance height of the propeller tip and the ground [m]
H_{evap}	Evaporation heat [J/kg]
h_{MLG}	Height of the MLG [m]
I	Moment of inertia [m^4]

J	Polar moment of inertia [mm^4]
K	Stiffness [Pa]
k	Skin roughness factor [-]
k_c	Buckling coefficient [-]
K_X^2	Normalized moment of inertia constant in X direction [-]
$K_Y^2 2$	Normalized moment of inertia constant in Y direction [-]
K_{XZ}^2	Normalized moment of inertia constant in XZ direction [-]
L	Column length [m]
$L1$	Nose cone length [m]
$L2$	Cabin length [m]
$L3$	Tail cone length [m]
l_f	Fuselage length [m]
l_{fc}	Tail cone length [m]
l_{nac}	Length of the motor nacelle [m]
M_{cruise}	Cruise mach number [-]
N_e	Number of engines [-]
N_p	Number of propellers[-]
N_{bl}	Number of blades [-]
P	Roll rate [deg $/s$]
p	Pressure [Pa]
P_{fc}	Fuel cell power output [W]
P_{TO}	Take-off power [W]
Q	Heat energy [J]
Q	Heat flux [W]
q	Dynamic pressure [N/m^2]
q_i	Shear flow [N/m]
R	Thermal resistance [W/K]
r	Distance from rotor center [m]
r_{prop}	Radius of a propeller blade [m]
Re	Reynolds number [-]
S	Surface area [m^2]
S_h	Horizontal tail surface area [m^2]
S_S	Projected side surface area [m^2]
S_v	Vertical tail surface area [m^2]
S_x	Shear force in x-direction [N]
S_y	Shear force in y-direction [N]
s_{land}	Landing distance [m]
S_{ref}	Reference area [m^2]
s_{to}	Take-off distance [m]
S_{wet}	Wetted area [m^2]
T	Temperature [K]
t	Thickness [m]
t/c	Thickness-over-chord ratio [-]
T_L	Thrust at engine failure [N]
U	Speed [m/s]
u	Upsweep angle [rad]
v	Poisson ratio [-]
V_c	Minimum control speed [m/s]
V_h	Horizontal tail volume [m^3]
V_R	Rotate speed [m/s]
V_T	Tangential wind speed crabbed landing [m/s]
V_W	Crosswind speed [m/s]
V_y	Vertical climb speed [m/s]
V_{cruise}	Cruise speed [m/s]
V_s	Stall speed [m/s]
V_{yc}	Vertical climb speed at ceiling [m/s]
W_p	Payload weight [N]
$w_{f_{landing}}$	Landing friction [-]
W_f	Fuel weight [N]
x_{cg}	Centre of gravity location [m]
x_{np}	Neutral point location [m]
y_T	Thrust arm [m]
y_{MLG}	Lateral position of the MLG seen from center fuselage [m]
z_T	Vertical thrust arm [m]
m	Mach number [-]

Abbreviations

CH_2	Compressed hydrogen [-]
LH_2	Liquid hydrogen [-]
AR	Aspect ratio [-]
CFRP	Carbon Fibre Reinforced Polymer [-]
CTOL	Conventional Take-Off and Landing [-]
EOW	Empty Operating Weight [N]
FF	Form Factor [-]
FoM	Figure of Merit [m^2]
GDP	Gross Domestic Product [-]
GFRP	Glass Fibre Reinforced Polymer [-]
HLD	High lift device [-]
HOT	Higher order term [-]
IF	Interference Factor [-]
LC	Load case [-]
LCA	Life cycle assessment [-]
MAC	Mean Aerodynamic Chord [m]
MLG	Main Landing Gear [-]
MOI	Moment of inertia [m^4]
MTOW	Maximum Take-off Weight [N]
RDTE	Research, development, test and evaluation [-]
RoC	Rate of Climb [m/s]
ROI	Return of investment [%]
SPL	Sound Pressure Level [dB]
TCL	Thrust Control Lever [-]
VTOL	Vertical Take-Off and Landing [-]
WBS	Work Breakdown Structure [-]
WFD	Work Flow Diagram [-]

1. Introduction

The aviation industry contributes to roughly 5% of global warming[1]. This is a big problem and results in an all-round backlash towards the industry. However, the latter should not be taken as a threat but rather be interpreted as motivation to develop a more sustainable aircraft and to de-carbonise aviation. As it will not only benefit the industry, but more importantly, the planet as whole.

The objective of this final report is to provide a detailed conceptual design of the final aircraft configuration, which has received preliminary sizing in previous reports. This together with the backbone structures necessary for successful aircraft design, such as cost analyses and risk assessments. To achieve this, several major subsystems have been worked out to a certain level of detail. These encompass the structures, control surfaces, power and propulsion. All of these systems have been sized in an iterative process, which resulted in a converged design layout. Next to this, several analyses have been performed which aim to not only design the aircraft, but the systems around it. These analyses will for example determine how the aircraft will be produced, how the design will be sustainable and whether the aircraft is fully controllable and stable.

This report starts off with a sustainable development strategy in Chapter 2. This is followed by a market analysis in Chapter 3 and a presentation of the final top level design in Chapter 4. Next, a functional analysis of the aircraft will be presented in Chapter 5. After this, the operations and logistics of the aircraft will be discussed and planned for in Chapter 6. Following, several analyses were performed, these encompass the system characteristics, performance, aerodynamics, structures, stability and control, propulsion and power, electrical subsystems of the aircraft. These can be found in Chapter 7 to Chapter 13. After these analyses, a technical risk analysis, RAMS analysis and manufacturing plan are presented in Chapter 14 to Chapter 16. This will be followed by and important chapter namely the sustainability analysis in Chapter 17. After this, the cost analysis is presented in Chapter 18. Finally, it is assessed whether or not the requirements have been met by means of a compliance matrix in Chapter 19. The report is than concluded by discussing the post-DSE planning in Chapter 20 and the conclusion and recommendations in Chapter 21.

[1] https://www.bbc.com/future/article/20200218-climate-change-how-to-cut-your-carbon-emissions-when-flying

2. Sustainable Development Strategy

Yearly, the aviation industry grows by around 5.4% in terms of kilometers flown. However, the amount of fuel required and thus also CO2 emissions, per kilometer flown only decreases by 1.5% per year. This net yearly increase of 3.9% in CO2 emissions will result in an untenable situation. Rather than spending effort on incrementally improving certain aspects of the aircraft, an overhaul in design and approach is required in order to ensure a sustainable future. In this chapter, the sustainability of the H2-VTOO aircraft will be discussed. First, the definition of sustainability, according to multiple sources, will be clarified. Furthermore the sustainability that follows from the requirements will briefly be discussed. However, the main part of this chapter will be about other sustainability aspects, in design, production, use and end-of-life of the product.

2.1. Sustainability Introduction

Before being able to start a sustainable design, it is important to exactly define what is meant with sustainability and on what should be focus on. After going more in depth into the sustainability definition, a look will be taken at the ideas of both the United Nations and the TU Delft, in particular the Aerospace Engineering faculty, on what they believe are the main goals to be achieved in order to reach sustainability.

2.1.1. Sustainability Definition

Currently, sustainability is an essential part in the process of designing products and services. The United Nations defines sustainability as: "Development that meets the needs of the present without compromising the ability of future generations to meet their own needs [147][1]". Broadly, sustainability can be divided into three pillars: environmental, economic and social sustainability.

Firstly, environmental sustainability is all about conserving the Earth's natural resources and the responsible management of those resources. For this pillar, H2-VTOO will contribute by using sustainable fuels such as hydrogen and recyclable materials.

Secondly, economic sustainability refers to activities that support (long-term) economic growth and enables future generations to consume (similar) products and services in the future as are consumed now. The successful completion of this project will encourage the green aviation sector, provide new jobs and contribute to the more efficient use of time and money of companies, due to the VTOL capability.

Thirdly, social sustainability is about handling human and social capital in a responsible manner and creating services and products that support the society and the well-being of humankind. As an example, the hydrogen VTOL can help in reducing the noise produced by aviation while reducing the need for an airport.

These three pillars are interrelated and often an increase in one comes at the cost of another. For example, increasing environmental sustainability might not be the best option economically as it can be more expensive, while the most cost efficient option might not be the best environmentally or socially. Due to this, a good balance between the three pillars has to be reached, by finding the minimum combination of the three, in order to guarantee adequate sustainability on all aspects.

2.1.2. Sustainability Goals by the United Nations

In 2015, the United Nations outlined 17 sustainable development goals in order to improve the quality of life around the globe [34]. Due to the nature of this project, a contribution to these goals can be made by the product. Note that not all of these 17 goals are directly applicable to the project. However, wherever possible attention will be spent in order to contribute to these goals. An overview of these 17 goals can be found in Figure 2.1.

2.1.3. Sustainability Goals within Aviation according to TU Delft Standards

In order to advance climate neutral aviation, the Delft University of Technology, and in particular the dean of the Aerospace Engineering faculty, defined 4 goals [2]. First of all, they want to reduce the energy consumption as the most sustainable fuel is the one you do not use. This is done through advanced concepts like the Flying V [3]. Secondly, a push towards sustainable fuels is present. Through usage of both (green) electricity and green fuels, for example hydrogen, a reduction or complete elimination of CO2 emissions during flight can be achieved. Thirdly, the aviation operations,

[1] https://en.unesco.org/themes/education-sustainable-development/what-is-esd/sd
[2] https://www.tudelft.nl/en/ae/sustainable-aviation
[3] https://www.tudelft.nl/lr/flying-v

Figure 2.1: The 17 Sustainable Development Goals of the United Nations [34].

including maintenance and service, should be sustainable. This also includes optimising the flight plans and mission profiles to maximise sustainability. Finally one may not forget that producing the aircraft also comes at a environmental cost, both in terms of scarcity and emissions. Therefore, the last goal is to minimise the environmental impact of the materials and structures. It can be noted that these goals all relate to the environmental definition of sustainability. This is in contrast with those from the United Nations, who defined their goals for all three fields within sustainability.

2.2. Sustainability from Requirements

There are several user requirements relating to sustainability. These requirements define the nature of the project. However, since they are requirements, they are considered as basic aspects of, and thus inherently present within, the design. They will be quickly introduced, but not analysed in depth.

First of all, HVA-GP-01 dictates that the final product should be climate neutral, which can be related to UN sustainable development goal number 13 about climate action [34]. The CO2 emissions throughout the development, production and use will be minimised, but in some phases, like for example transport, it might not be fully eliminated. Therefore, the emissions during these phases will have to be estimated, using a life cycle assessment, and be compensated for. This compensation will be done through usage of a currency called carbon credits. Carbon credits represent an investment in a CO2-negative project. These projects work either by directly capturing CO2 from the air, or by providing more environmental friendly solutions where there currently are none, thus reducing the amount of CO2 emissions. These projects are organised by companies like for example South Pole. One example of a current investment opportunity is a hydro-powerplant installation on the Musi River in Indonesia [4]. The cost of removing 1 kg of CO2 equals 9 EUR for this particular project. The project also shows which UN sustainability goals it supports, which are goals seven, eight, nine, twelve, thirteen and fifteen for this particular example. Most of these projects are organised in third world countries, who are not able to fund them by themselves. Therefore, apart from helping in environmental sustainability, these investments aid in social sustainability. Participating in a project like this is to be preferred over setting up an own method of compensation, especially due to the limited resources of the company.

The next requirement is HVA-GP-02: The aircraft shall use hydrogen as an energy carrier. This contributes to UN sustainability goal seven, concerning clean energy, and to the TU Delft goal of sustainable fuels [34]. This hydrogen is generated through electrolysis and should be produced in a sustainable fashion. If fossil fuels would be used to provide the required power for hydrogen production, using hydrogen would in no way be better than directly combusting these fossil fuels.

Another requirement that drives the design, is HVA-GP-03: The final product shall be able to re-purpose 80% of its materials as spare parts or scrap. This contributes to achieving UN sustainable development goal 12, concerning responsible consumption and production [34]. Furthermore this helps with realising the TU Delft goal of minimising the environmental impact of materials and structures. Due to this requirement, recyclability will be taken into account heavily throughout the design. For example, wherever possible, metals are chosen over composites, as those are more recyclable. Whenever this is applicable, it will be discussed in the relevant chapter.

The third relevant user requirement, namely HVA-GP-04, states that the aircraft shall have Aviation Induced Cloudiness (AIC) not higher than conventional aircraft. These condensation trails left in the wake of the aircraft can be adverse to the climate, due to their greenhouse effect. The presence of these so called contrails are dependent on altitude and ambient conditions. Generally, they can be neglected below 7000m at normal ambient conditions [24].

[4] https://market.southpole.com/home/offset-emissions/project-details/73

Finally, user requirement HVA-GP-05 states that the noise levels, 100 meters from the aircraft, should be no more than 70 dB. This requirement stems from social sustainability and relates to UN goal 11 about sustainable cities and communities [34]. Due to the complex nature of the requirement, it will be investigated further later on in Chapter 17.

2.3. Sustainability during the Design Process

After having discussed the sustainability aspects that stem from the nature of the product, it is time to contemplate additional sustainability measures that can be taken throughout the multiple phases throughout the cycle. In this section, sustainability during the design process will be considered. A list of the measures taken to increase sustainability while designing is shown in Table 2.1. These actions rely on a team effort and will be actively monitored by the sustainability manager and discussed during the mid-week meetings. In case action is required, or the team starts to become less aware of these points, an additional meeting will be scheduled to reiterate these points. Sustainability aspects related to the design itself will be discussed in the chapter where the design of that part is explained.

Table 2.1: Sustainability measures that are taken during the design process.

Sustainable improvement
Recycling/reusing coffee cups and water bottles.
Travel to fellowship by bike, foot, public transport or carpool.
Do not print unnecessary things to reduce paper use.
Split the generated waste in corresponding bins waste (plastic, organic waste, glass).
Reduce the waste of food.
Cut down unnecessary spending on electronics, clothing and other items that do not add value to the project itself.
Wear an extra sweater, so that less heating of the building is required.
Use urinoirs so less water is dispersed (for all male group members).
Turn off the lights at the Fellowship and at home when they are not necessary.
Unplug power cords when not used.
Drink tap water instead of buying a new bottle every time.
Bring the plastic bag for the self test so it can be reused.
Bring lunch in a reusable lunchbox.
Spread sustainability awareness amongst fellow users of the fellowship.
Borrow resources instead of buying new ones (markers, books etc.).

Furthermore, during the design process, effort is spent on ensuring all aspects of the design are sustainable. This is done both for technical aspects and more aesthetic or functional parts. For example the interior of the aircraft can not be neglected in this process. Seats should be covered in recycled leather, which is recovered from previously used leather or waste during production. Finally, the amount of scarce or energy intensive materials used in the design should be minimised.

2.4. Sustainability during Production

Sustainability should also be taken into account during production. Within this production phase a difference will be made between the three pillars of sustainability, namely environmental, economic and social.

2.4.1. Environmental Sustainability during Production

Environmental sustainability plays a big role during production. It dictates what materials and processes can be and those that can not be used. Most of these follow from the requirements as discussed earlier, like the example of using metals over composites and will not be further elaborated upon.

A first method to improve upon environmental sustainability is lean manufacturing. Lean manufacturing is, in short, defined as 'manufacturing without waste' [133]. This is relevant to both environmental and economic sustainability. However, only the environmental benefits will be discussed here, while economic aspects will be considered in the next subsection. In this process, the goal is to eliminate all waste, which is defined as activities that do not directly add to the value of the product, while using resources. This definition is really broad and encompasses everything from minimising transport to reducing the actual waste in terms of materials as this also has an environmental impact. Lean manufacturing requires a well-informed and driven working force as they are often able to detect waste and can help resolve it. This can be done by manufacturing the parts and performing the assembly at a single location. Than, the transport required is minimised. This is beneficial as transport comes at the cost of CO2 emission, while not directly adding value.

One more aspect to be taken into account during production is the effect the factory has on its surroundings. It should be climate neutral and on top of this it should not contaminate, pollute or toxify its surroundings. This will be

assured through periodic testing, monitoring and adjusting where necessary in order to meet a range of sustainability goals. Furthermore at the start it will be required to fulfill certification.

VTOL systems can take off and land vertically. This feature ensures that large areas of land are not unnecessarily used, which mitigates the decrease of biodiversity caused by the destruction of ecosystems. This is part of sustainable development goal 15 of the UN [34], which aims at protecting, restoring and promoting the life on land. Furthermore, by avoiding the construction of airfields noise hot spots can be avoided.

The production process of hydrogen has to be investigated as well. There are three types of hydrogen. Green hydrogen, meaning it is produced using fully renewable energy, is the preferable method for the production of hydrogen. Currently, only a small part of the available hydrogen is green. However, by 2040, this part is expected to reach a majority of all hydrogen, with green hydrogen representing a total energy delivery of 12% of the total EU energy supply [5]. Due to its abundant presence by the time the first products will be sold, green hydrogen will be considered as the main energy carrier. Note that green hydrogen might have a slightly higher cost than the other types depending especially on the region. This will be taken into account during the cost analysis. Furthermore, it has to be noted that in order to produce green hydrogen, the green energy does not necessarily have to be produced in the same location. This means it is possible to have one location of renewable energy generation per region (e.g. BeNeLux), while being able to have a hydrogen generation and liquefying plant in every major city. It is only required to put as much green energy on the net as you require. It does not matter whether the electricity you use is actually the one you generated yourself or not. As long as the net effect is zero.

2.4.2. Economic Sustainability during Production

Economic sustainability relies mainly on three things: lean manufacturing, circular economy and local manufacturing. Lean manufacturing, which has already been discussed before, also provides economical benefits. Through reducing all kinds of waste, a lower cost can be achieved. A list of possible actions that can be taken to reduce waste is shown in Table 2.2. All of these aim to reduce wasted resources. For example if parts are only produced when they are needed (Just In Time), no expensive storage spaces are required. Lean manufacturing is a continuous process where the plans need to be updated constantly.

Table 2.2: A table presenting several actions to minimise waste.

Actions to Minimise Waste
Put manufacturing and assembly close together to minimise transport.
Use maximum possible amount of material out of a single quantity.
Produce just enough - no overproduction.
Reduce waiting times throughout production.
Reduce amount of defects which requires rework.
Produce parts only when needed (JIT).
Minimise movement within factory.

Another economical concept which can help improve sustainability is circular economy. In this concept, materials are reused and recycled at the end of life. In a perfect scenario, no new materials are required to produce a new product. This is beneficial not only in terms of the environment, but also saves quite some financial resources as no new materials have to be mined or generated. Furthermore, this concept helps to achieve UN sustainability goal number 12, which deals with sustainable consumption and production [34].

Finally, all of the production should be done within the European Union, with preferably the majority of manufacturing located within the BeNeLux. By producing locally, jobs are created within the region on top of reducing waste, which is beneficial for the economy [75].

2.4.3. Social Sustainability during Production

Social sustainability during the production will mostly be focused on certain initiatives. These will be based on the UN sustainable development goals [34]. A first initiative will be to hire some people within the production process based on motivation rather than on previous experiences. They would then require a course in order to get them up to speed, but this would allow some very eager people who might come from a bad (economic) environment or background to improve their situation. This is related to the United Nations first goal, ending poverty [34]. Another example would be to perform the hiring process 'blindly'. By not knowing a persons ethnicity, gender or orientation as recruiter, no bias can be present and a person would just be selected on how they fit within the company. This would help reduce

[5] https://energypost.eu/german-hydrogen-scenarios-271-twh-of-green-hydrogen-by-2040/

inequalities as discussed in UN goal number 10 [34]. As this paper only discusses the preliminary design, no further examples will be given here.

2.5. Sustainability during Product Life

After having produced the aircraft and ensured sustainability within that process, it is time to investigate how it fares throughout its lifetime, including operations and end-of-life. All of this will be discussed in this section.

2.5.1. Sustainability during Operations

During operations, the aircraft should be sustainable as well. First of all, the fuel consumption should be minimised as stated in the TU Delft goals, which is related to the power required, which in turn is related the velocity. For the considered speed regime, lower velocities result in a lower fuel weight. Contrails are unlikely to form below 9000 m, due to the condensation with the cold air temperature outside at this altitude. They can also form below this altitude, but only when the air is cold and moist. Therefore, the aircraft should be able to climb to the service ceiling of 7000 m with a low likelihood of forming contrails in normal weather conditions [24]. Since the cruise altitude will be significantly lower than the ceiling, the altitude can be decided based on solely minimizing the drag and power required, without taking contrails into account.

The design should contribute to the overall quality of life. One of the goals is to reduce the door-to-door travel time within Europe, enabling quick transport for humans, and aiding the further integration of (sub)cultures and economies. Additionally, by using hydrogen as a fuel, the air quality is improved, which will also improve the quality of life. This is part of UN sustainable development goal 11 which states that cities and communities should be made more inclusive, safe, resilient and sustainable [34]. Furthermore, a quiet aircraft will not negatively impact the overall living conditions around the take-off sites.

On top of this, the waste generated through operations should be minimal. This entails both actual waste, for example from food served on flight, as well as waste as was defined earlier, within the lean thinking.

2.5.2. Sustainability during End-Of-Life

Once the aircraft is retired, as much parts as possible should be reclaimed for down cycling or recycling as has been discussed before. Starting from the design phase, all material and other choices are made while keeping this in mind. Not all parts will be able to be reused for the aircraft, instead some will be down cycled into lower-value applications. The respectability of the used materials will be further discussed in the production plan.

2.6. Execution of Sustainability Strategy

To make sure that sustainability is addressed sufficiently in the design process, a flow block diagram is constructed. This block diagram is depicted in Figure 2.2. Following all steps in the diagram will lead to a feasible and sustainable design. Firstly, sustainability requirements need to be set. These requirements are divided in development and production requirements, operational requirements and after-life requirements. After this, the design of the (sub)system takes place. This will be done according to the stated sustainability requirements. Afterwards, the (sub)system will be tested to see if it complies with the three different kinds of sustainability requirements. If it does comply, it shall be assessed if the (sub)system is feasible to build. If this is the case the (sub)system will be further optimised and integrated into the final design. However, if the sustainability requirements are not met it can be indicated per kind of requirement what possible solutions may quickly fix this problem. If the problem can not be fixed and it is already the minimum requirement, it might be necessary to discuss with the client if certain requirements can be changed. By walking through this loop, a converged design will be reached. The actual implementation of this strategy will be discussed in Chapter 17.

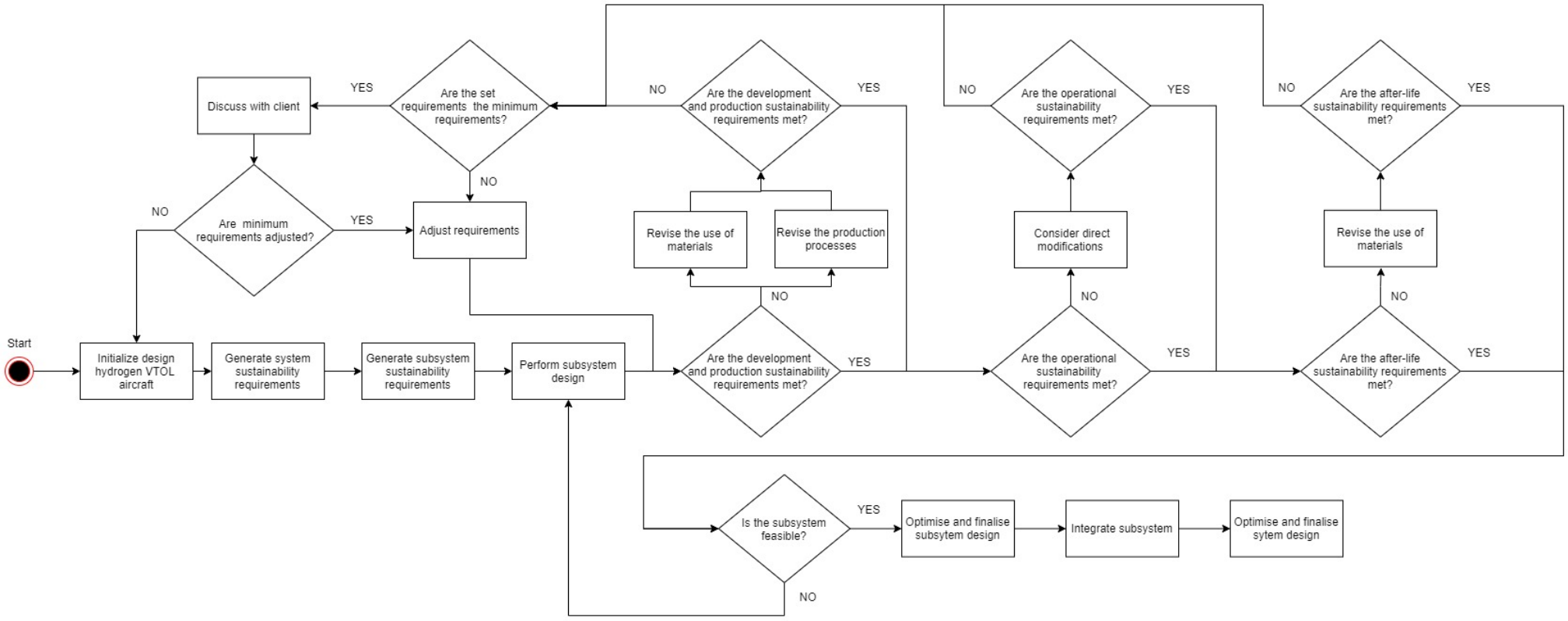

Figure 2.2: A block diagram presenting the execution of the sustainability strategy.

3. Market Analysis

The main aim of this chapter is to present the market analysis. A market analysis will help greatly in showcasing the strengths and weaknesses of the product to be designed. A more systematic approach to analysing the market is also crucial as it aids in the identification of customers and generation of a viable business strategy. This chapter first starts with a market segmentation which begins with an analysis on the aviation market as a whole, and then dives deeper into the market of choice within the industry - the sustainable aviation market, of which the size of the market is analysed. Stakeholders and competitors along with the differentiating factors can then be identified following this. Anticipation of the future of the chosen market is then elaborated on in Section 3.2. This is done by evaluating the growth rates and trends within the market. From this, the profitability of the product can be qualitatively evaluated. With the knowledge of the chosen market and the assurance of a profitable product, a business plan can then be constructed. This is done in a systematic way using a SWOT analysis found in Section 3.3.1 as well as a business model canvas in Section 3.3.2. The chapter ends with summarising the focal points of the market analysis as well as the final conclusion on it.

3.1. Market Segmentation

This section will conduct the market segmentation to arrive at the most beneficial markets to focus on for profitability of the H2-VTOO project. First, the chosen industry and reasons why the aircraft could be beneficial in it are discussed. This then leads to the rise in sustainable aircraft and the gap in the market which H2-VTOO seeks to fill. Following this, an estimation on the size of the market is presented. With these parameters, a better understanding of the customers to be satisfied is gained. From this, the stakeholders and their needs can be identified. Lastly, the key elements of the H2-VTOO design will be addressed displaying how different the aircraft is and what gives it the competitive edge.

3.1.1. Industry Analysis: Aviation

Before choosing a market within the aviation industry itself, the aviation industry as a whole will be analysed. This is important as the H2-VTOO aircraft will be an innovation for the industry. Therefore, the expected growth of the market must be analysed to determine a market gap as well as how lucrative the industry is to have a profitable entry into the market. If this sector itself is not concluded to be fruitful, then there would be no reason to pursue market segmentation. As the main region of operation for the H2-VTOO aircraft will be in the European Union (EU), the contributions of the aviation industry to this region specifically will be a primary focus.

The aviation industry itself is one that consistently displays growth in the number of adopters (in this case passengers), and consequentially, revenue due to the technological advancements and proficient capability for scaling and profitability within this sector. In the EU itself, the number of passengers travelling by air has increased by 39% between 2009 and 2017 [81]. As can be seen from Figure 3.1, the majority of travelling passengers of the EU are accounted for by intra-EU travel. As the H2-VTOO aircraft has a primary goal of operating within the EU while reducing the door-to-door travel time, investments into intra-EU travel would be beneficial for aviation [78].

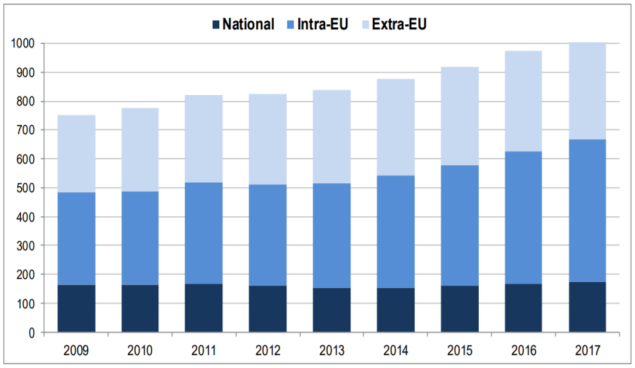

Figure 3.1: Graph showing the increase in travellers and the respective travel category from 2009-2017.

The industry contributes to 4.4% of all GDP in the EU, providing 13.5 million jobs and close to a trillion USD in economic activity[1]. However, while demand for flights has increased, the aviation industry has seen a steady-growing backlash from

[1] https://aviationbenefits.org/around-the-world/europe/

society due to its contribution to global warming (about 5% to global warming and 2.4% to global CO2 emissions) [2]. This emerging prejudice against the industry has grown so much that it has lead to an international movement - flight shaming: presenting scientific facts and raising awareness of climate change such that the public are 'shamed' into discarding any 'unnecessary' flights they may have otherwise taken [16]. This movement is especially present in Europe due to the its development in Sweden. With society's rising concerns on climate change and their new-found understanding of just how much aviation contributes to this, investors have made the reduction of emissions a primary focus. Airlines have realised that if they are incapable of presenting more climate neutral designs and making them available to the public, the public themselves will cancel any non-essential flights [1]. This has led aircraft manufacturers to re-evaluate the designs they offer, most even considering developing new fleets to satisfy demands for more sustainable aircraft. With an ever-increasing demand for flights threatened by an increasing concern about global warming, a gap in the market is created for sustainable aircraft. The sustainable aircraft market, especially with respect to hydrogen aircraft will be further discussed in Section 3.1.2.

3.1.2. Hydrogen Aircraft Market

Across the globe, and within the EU especially, climate change has started to drive the generation of sustainable aircraft. The EU, leading the movement of sustainable aircraft has already implemented a plan 'destination 2050' to improve public opinion on aviation and increase revenue. Jointly, hydrogen technology and sustainable aviation fuels make up more than half of the elements predicted to reduce emissions for aviation[45]. This is something that the H2-VTOO aircraft will offer and therefore it would excel in meeting these future demands.

Multiple concepts are being explored for sustainable aircraft, such as battery-powered flight, bio-fuels and hydrogen-powered flight. The latter is a very interesting option, mainly for short to medium range aircraft; a category in which H2-VTOO falls into. However, up until now, few fully hydrogen-powered aircraft have been developed and successfully flown. The largest being a six-seater plane designed by ZeroAvia, which took off on September 23, 2020 [140][3]. This illustrates the early stages of hydrogen powered aviation and the difficulty of designing such an aircraft. However, the economic opportunities that lie in successfully developing a sustainable hydrogen powered business aircraft are huge, since the market segment is yet to be capitalised on.

3.1.3. Market Size Analysis

At this point in time, the aviation industry is still very much centered around the use of fossil fuels. This can be seen in the recent developments in the sustainability of aircraft that are operated today. Most of these developments are improvements in fuel efficiency of kerosene powered aircraft. On the other hand, there is still no widely used type of passenger aircraft that uses a sustainable on-board energy carrier such as bio-fuel, batteries or hydrogen. As of today only 0.1% of the total fuel consumed by aircraft are sustainable aviation fuels, clearly indicating the premature state in which the sustainable aviation market finds itself [23][4]. Due this premature state in which this market finds itself, very little data is available about its size and volume, however, data was available on the market size of sustainable aviation fuel and which was estimated to be 66 million USD in 2020 [88][5]. Comparing this to the regular aviation fuel market size of which was 179.2 billion USD in 2018, one can see the almost insignificant part of sustainable fuels in the aviation industry as mentioned before [15][6]. This small market size does however show a big market gap which could be capitalised on by H2-VTOO. If further analysis on the market growth and future trends shows to be encouraging, the two main conditions are satisfied for the sustainable aviation market to be a highly profitable market for the H2-VTOO project.

3.1.4. Stakeholders

With the market segment now identified, the customers that the product will create value for may also be identified. These can be summarised in the following list:

- **Users:** The users, which will mainly be business people, are the ones who will actually use the system. They thus have major stakes in how the system works and what it is capable of. Furthermore they might have additional preferences in lay-out. In addition, users are also companies that want to transport cargo with H2-VTOO and therefore their needs will be analysed as well.

[2] https://www.bbc.com/future/article/20200218-climate-change-how-to-cut-your-carbon-emissions-when-flying
[3] https://newatlas.com/aircraft/zeroavia-first-commercial-scale-hydrogen-fuel-cell-electric-flight/
[4] https://www.euractiv.com/section/alternative-renewable-fuels/news/eu-planning-staggered-increase-in-use-of-green-jet-fuel/
[5] https://www.globenewswire.com/en/news-release/2021/04/21/2213864/28124/en/Global-29-75-Bn-Sustainable-Aviation-Fuel-Biofuel-Hydrogen-Fuel-Power-to-Liquid-Fuel-Market-to-2026-Analysis-by-Fuel-Type-Manufacturing-Technology-Biofuel-Blending-Capacity-Platfor.html
[6] https://www.alliedmarketresearch.com/aviation-fuel-market

- **General public:** One of the main stakeholders in the design is the general public. They are influenced by the aircraft in a number of ways, both directly by for example noise, or indirectly by for example the pollution. Through the sustainable design, an improve in quality of life shall be achieved which strongly benefits the general public.
- **Airlines/leasing companies**: Airlines and leasing companies are the ones who will actually purchase and own the aircraft. This means that they are important stakeholders, and are mainly interested in long term behaviour and financial affairs.
- **Aircraft Manufacturer:** The final aircraft is manufactured by the aircraft manufacturer and therefore they determine the feasibility of the aircraft. Therefore, their requirements should be carefully considered during the design process.
- **EASA:** As the main flight area is considered to be in Europe, the European flight regulation and certification, which is created by EASA, should be adhered to.
- **Government:** Next to flight regulations, the government also has certain regulations that should be adhered to. This makes the government an additional stakeholder. Next to these regulations the government is also interested in certain economical aspects.
- **Airports:** As the aircraft should also be able to take off and land as a regular fixed wing aircraft, airports should be considered to be a stakeholder as well.

It is important to identify stakeholders as the product can then be designed using the requirements from each group. By doing so, a more desirable and profitable product is made.

3.1.5. Competitors

The competitors chosen within aviation were the manufacturers that produced aircraft that most closely resembled H2-VTOO; these corresponded to leading companies within the business jet aircraft market. Currently, while there are multiple competitors within the market, only a few of these hold a significant market share as can be seen in Figure 3.2. For example, Gulfstream and Bombardier jointly make up more than two thirds of the market share. Other notable companies include Beechcraft, Cessna, Dassault and Embraer. All these companies are progressing towards more fuel efficient and sustainable advanced business jet models in order to increase their market share and competitive presence.

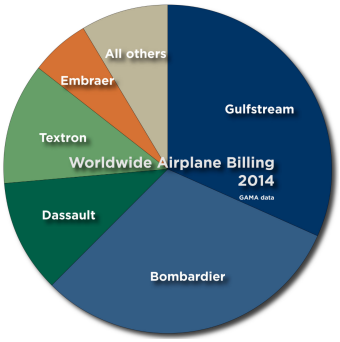

Figure 3.2: Pie chart of the competitors in global business jet market and their market share

Table 3.1 encompasses the parameters of competing super mid-sized jet aircraft to give a better overview of the current expected specifications in the market [68][7]. Upon analysis of Table 3.1, the H2-VTOO aircraft does perform lower than current service ceiling, range and design cruise speed standards. While these numbers do seem prominent at first glance, they deviate from the norm due to the functionality of the aircraft itself; while the H2-VTOO aircraft is indeed seen as a competitor of the super-mid sized business jet market, it caters more to companies and business people seeking to reduce their door-to-door travel time. In addition to this, with a competitive maximum target price of 12 million euros (14.5 million USD), the H2-VTOO aircraft is a new innovation in the market as it incorporates both sustainability and low emissions with VTOL capabilities. Characteristics like these will be in high demand in the future, making the aircraft a worthwhile product to develop. The demand for these characteristics and growth in the market will be further elaborated on in Section 3.2.

[7] https://www.mordorintelligence.com/industry-reports/business-jet-market

Table 3.1: A table displaying comparable business jet models and their specifications against those of the H2-VTOO project.[8]

Model	Price [M$]	Range [nmi]	Service ceiling [m]	Passengers [-]	Design cruise speed [kts]	Price per passenger [M$
Bombardier Challenger 300	7.5	3065	13716	8-16	459	0.94
Gulfstream G280	25	3420	13716	8-10	470	3.1
Cessna Citation Longitude	27	4000 max	13716	8	476 max	3.4
Dassault Falcon 50EX	4.5	3260	15000	9	459	0.5
H2-VTOO	14.5 max	1350	7000	10	351	1.4

3.1.6. Differentiating Factors

The H2-VTOO aircraft will set itself apart from other aircraft in the market due to its convenience and innovation. It will be beneficial to companies seeking to increase their business travel for more efficient meetings: the aircraft is capable of taking off and landing from virtually anywhere, provided the landing area is installed with the necessary equipment. The VTOL capabilities of the aircraft aid it in reducing door-to-door travel time for travellers-one of the focal points of the project itself. By 2018, the amount of money spent on business travel surpassed $ 1.4 trillion, this value accounts for nearly a quarter of the global travel and hospitality sector. Therefore, business travel is an important aspect of the market to consider for profitability which the H2-VTOO aircraft will significantly cater to. Corporate travel forms an essential part of the aviation and hospitality sector. This segment of the market contributes to nearly the majority of the profits acquired by airlines while only forming a fraction of the adopters. This is because business men and women have more urgency to travel and therefore expend more money on tickets. Along with this, hotels rely heavily on business people and thus, the aircraft could be seen as a worthwhile investment for not only aviation but also hospitality [9].

Another differentiating factor that H2-VTOO manages to incorporate is the sustainability aspect that is clearly a problem in the aviation industry. H2-VTOO will help decarbonise aviation and help meet the goals of many chief executives within the market and relieve their concerns of the future of the aviation industry. H2-VTOO will run on hydrogen and be fully electric. It will have zero carbon dioxide emissions and will be 80% recyclable. These are all important characteristics that many companies may be interested in, especially those looking into investments for the development of more sustainable aircraft fleets.

3.2. Market forecast

In this section, the predictions of the future of the market are discussed. This includes how current competitors in the ten-seater business jet aircraft market are handling the rising demand for sustainable aircraft. Along with this, some considerations on how the government has an impact on the market's future. Both the hurdles for H2-VTOO along with its competitive edge and future prospects are also analysed in this section.

3.2.1. Market Trends and Growth Rate

Roughly a third of currently operating business jets are over 10 years old. This opens the possibility of charter providers and jet operators to adopt new fleets, which could further accelerate the growth of this market[68]. Recently, despite the pandemic, Embraer SA (one of the competitors within the market) signed a contract for a sum of 1.4 billion USD with Flexjet for the production of mid-sized and super-midsized business jets [68]. Bombardier (another competitor) also signed an order worth 267 million USD for the provision of 10 business jets. Statistics and developments like these only provide additional evidence and motivation for the production of an innovative super mid-sized business aircraft [66].

Another positive market trend could be the rise in multiple governments adopting new regulations which both favour and incentivise the use of sustainable fuels for aircraft in the aviation sector. This is due to the increased awareness of climate change across the globe. Furthermore, the hydrogen aircraft market has also recently seen growth. With the demand for low emission aircraft and sustainable fuel ever increasing, this market is projected to reach a value of nearly 7.5 billion USD by the year 2030 alone [89]. Considerations like these could potentially be a driving factor for airlines and aircraft leasing companies to adopt new fleets of sustainable aircraft; the development of a hydrogen fuelled aircraft, such as the H2-VTOO project, may therefore become a competitive advantage for many of these businesses.

A prime example showing the implementation of new rules by the government to promote sustainability is the EU emissions trading system. With this new system, the emissions of a system produced by a country will be carefully monitored, with heavy fines being given out if they do not meet a certain limit[9]

3.2.2. Barriers to Entry

Considering fuel cost, kerosene is still the only fossil fuel which is not being taxed, this makes it so that aircraft powered by kerosene are economically very hard to compete with, however it is expected that by 2040 this will have changed in

[9] https://ec.europa.eu/clima/policies/ets_en

the favour of more renewable fuels [46].

Today, only 0.1% of the total hydrogen produced is considered "green hydrogen", i.e. hydrogen produced by electrolysis which is powered by renewable energy sources [6][10]. This number must increase dramatically by 2040, as using grey or blue hydrogen would only shift the emission of greenhouse gasses from operation to the production of the fuel; using grey and blue hydrogen as a means of fuel production would make the operation of H2-VTOO unsustainable. Airports and urban VTOL landing spots should also be equipped with hydrogen providing systems to refuel aircraft, this could impose serious additional costs to build large hydrogen storage tanks and pipelines. However, an investment is needed one way or another to achieve a sustainable future.

Another barrier may be the higher market share of already established competitors in the market. As stated before in Section 3.1.5, Gulfstream and Bombardier both hold a substantial percentage of the market share. Competing with much larger companies could be a huge barrier when trying to enter the market. Typically, startup businesses in today's economy are only developed for a few years before being acquired for an attractive price by another company [141]. This is an important phenomena to consider when assessing the business strategy of H2-VTOO in Section 3.3.

If it is decided that the business is capable of being scaled much larger, then pursuing to capitalise on the market share may be worthwhile. To facilitate this decision, as previously mentioned, competitors are seeking to design new sustainable aircraft and new fleets to meet the demands and future demands of sustainability. Investing in a design that is capable of disrupting the market and becoming a first adopter of such technology may therefore offer a significant advantage over current competitors. However, as previously explained, in the case of sustainable aircraft(the market chosen for H2-VTOO) there is still much development to be made. Many competitors are seeking to renew their fleets to shift focus on the sustainability aircraft market. This will take money, time and other resources, giving the H2-VTOO aircraft a first adopter advantage.

3.2.3. Product Prospects

Despite constant backlash, incorporating sustainability into products still remains a resentment from businesses. Offering sustainable products incurs development expenses and also extra procurement expenses due to the sustainable products not being as widespread and available as conventional products [116]. However, in the case of sustainable aircraft it appears that investments into research and technology to bring about a more green future will be profitable in the long term. Sustainability should not be seen as a trade-off where the cost is a restraint, but rather it should be reason to innovate further and capitalise on the market.

H2-VTOO will do just that, having zero carbon emissions, while still meeting the demands of people and providing a more time-efficient method of transportation, H2-VTOO has a great potential to capitalise on the sustainability and hydrogen aircraft market. Figure 3.3 Illustrates the predicted technologies that will help reduce CO2 emissions until the year 2050. From this we can see that 20% of the reduction in emissions is expected to be due to advancements in hydrogen technology. If one assumes that these different contributions would form the market share of the sustainable aircraft market, this means that H2-VTOO would be capable of capitalising on 20% of the market which is quite significant and shows potential for profitability.

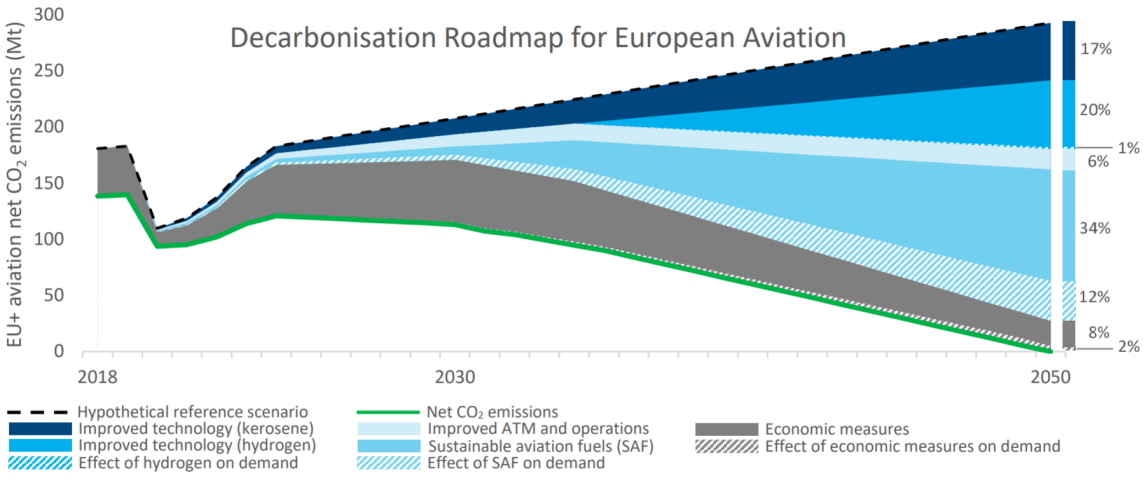

Figure 3.3: Decarbonisation roadmap of the EU showing the technologies that will help reduce CO2 emissions

[10] https://www.airbus.com/newsroom/stories/hydrogen-aviation-understanding-challenges-to-widespread-adoption.html

With well known companies such as the likes of Uber, investing into eVTOL aircraft and promoting the development of VTOL aircraft for on-demand mobility gives high prospects for investing into the design of the H2-VTOO aircraft. The demand for VTOL aircraft seems to be growing in recent years. Research has shown that the market for VTOL aircraft could grow to 14.7 billion USD by the year 2041 [118].

With regards to the benefit of sustainability to aircraft, it is becoming more and more apparent that companies pursuing investments and technology acquisition to help improve their sustainability ratings generally have a higher market value than less sustainable companies. This trend may lead to a rising amount of companies to shift their focus on sustainability to drive innovation. A phenomenon like this may be an incentive for aviation companies to invest in the development of H2-VTOO as well as companies that are customers to adopt the product and use them for business travel rather than conventional non-sustainable aircraft [20]. The early adoption of a sustainable innovation such as H2-VTOO could be seen as a competitive edge due to the gap and relatively new presence of sustainable aircraft in the market.

The exact numbers and estimations on the profitability like the Return on Investment(ROI) can be found in Chapter 18.

3.3. Business Strategy

This section lays the basis for a business plan in a systematic matter. This is done with the use of a SWOT analysis along with the corresponding SWOT analysis diagram in Figure 3.4. The business model itself of H2-VTOO is summarised using the business model canvas. Lastly, the channels with which the product can be distributed are elaborated upon, and their feasibility is discussed in Section 3.3.3.

3.3.1. SWOT Analysis

In order to properly formulate a business plan and strategy it is quintessential to determine four things. First of all one must identify which opportunities which will benefit the previously mentioned stakeholders. Secondly the strengths of the product should be identified, these strengths will be the main selling points with which potential buyers will be persuaded. Also the weaknesses of the product must be acknowledged such that the customer knows what the downsides of the product are. Finally the threats need to be identified in order to raise awareness of what prevent a successful launch and operation of the product. The identification of these four categories is called a SWOT analysis and can be illustrated via a SWOT diagram as depicted in Figure 3.4.

3.3.2. Business Model Canvas

The key elements of the H2-VTOO business model are illustrated by a business model canvas which consists out of nine segments as can be seen in Figure 3.5. Note that the canvas is centralised about the value proposition that the product offers. These are the main reasons on why a potential buyer would purchase the product and thus of extreme importance to the business plan.

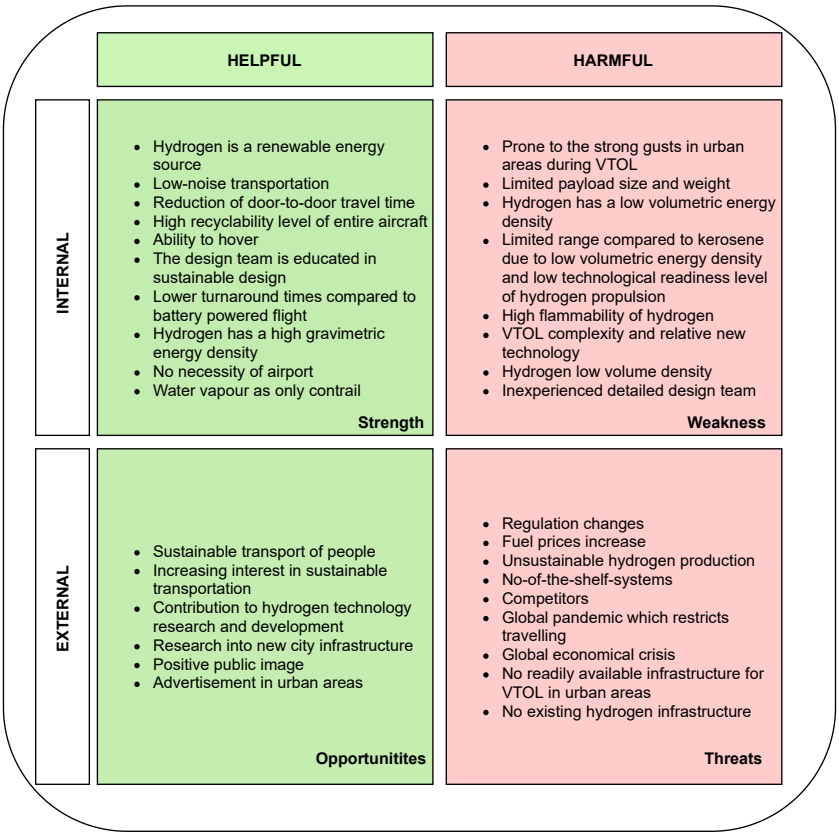

Figure 3.4: SWOT Diagram

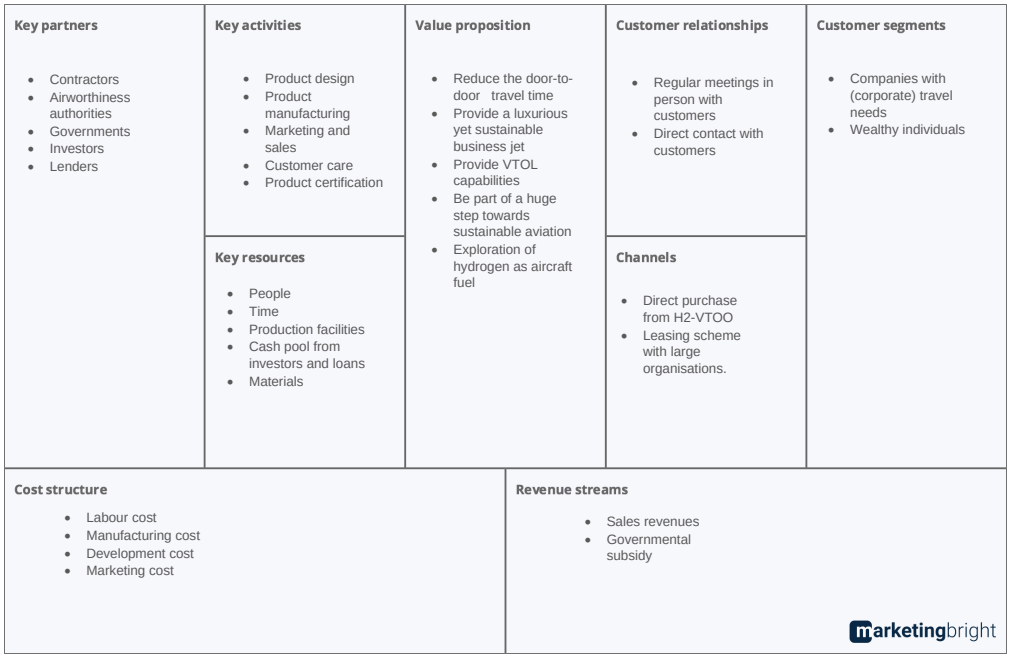

Figure 3.5: Business model canvas [21]

3.3.3. Distribution Channels

An important factor to consider in the market analysis of the aircraft would be to determine how exactly it will be provided to the respected customers. H2-VTOO's primary customers are business people and wealthy individuals both capable and willing to pay higher prices for more comfortable and luxurious travel [9]. Due to H2-VTOO being a new innovation from a new company within the market, the capacity to produce large amounts of aircraft per year may not be existent, and therefore it may not be possible to have economies of scale such that the price of production is lower. Hence, a leasing program may be a much more preferable option when distributing the aircraft; building an aircraft to sell to one specific company each time may be more resource-demanding compared to building an aircraft that can be leased to multiple companies, each at different periods of time. This may be especially beneficial for the first few years after completion until the number of adopters begins to rapidly increase such that multiple aircrafts are in demand at one period of time which will require more aircraft to be produced. The time at which this increase occurs can be modelled in further detail by the use of a Bass diffusion model[149].

H2-VTOO will be seen as more of a service than anything else; one that provides value in the form of convenience as continuously mentioned within this chapter. Secondly it also improves the image and social status of people or companies that use it due to its sustainable nature. Leasing aircraft to companies rather than selling them can be extremely beneficial as it has a higher chance of creating long-term relationships with companies. Providing one company with a high quality product and a pleasant experience can lead to forming more relationships with other companies within the market due to something as simple as a good review [70].

On the other hand, it may be advantageous to also consider selling the aircraft as a whole to customers. This may especially be easier to sell to wealthy individuals who would rather have their own private aircraft than sign a contract for a certain period of time. One main concern about this may be the significantly larger market share of other competitor companies offering similarly sized aircraft as discussed in Section 3.1.5. With such a large market share, these other companies will have a higher channel power structure and be capable of manipulating the distribution channels and prices indirectly. This means that it may be possible that the well established portfolio of other companies within the market may force a decrease in the retail price of H2-VTOO. The numbers associated with the profit margins of the aircraft will be later computed and analysed in Chapter 18.

3.4. Key Takeaways and Conclusion

From the market analysis, it is clear that the aviation industry first and foremost is still a growing industry despite backlash due to its non-sustainability. To combat this, the design and development of new sustainable aircraft has begun. The sustainable aircraft market is blooming and is expected to do so over the years to come. Currently, while not commercially available, there appear to be many sustainable aircraft, each using different configurations, designs and fuels in development. This has been further encouraged by government initiatives and pressure from society. The primary customers will be wealthy individuals and large organisations.

Some of the biggest challenges the project will face, will be the significantly larger market share of the competitors offering similarly sized aircraft, the currently more economical price of alternative conventional fuel and the switching costs that will come to provide they infrastructure required for hydrogen aircraft. However, it is believed that the benefits will outweigh these barriers when it comes to the convenience and sustainability of the H2-VTOO aircraft. The aircraft has potential to be an extremely profitable and attractive aircraft to many investors due to it being one of the few sustainable aircraft currently in development. It will meet the needs of many corporate travellers whom pay significantly more per ticket than majority of travellers. A leasing scheme to large organisations seems like the most beneficial business model to offer the aircraft as it forms long-term partnerships which in turn could lead to exponential growth due to networking. At such a time like this, where innovation may strike at any moment, it is crucial to invest in the right design capable of bringing about such a market-shifting innovation. H2-VTOO along with all its desirable characteristics may be the aircraft to do just that.

4. Final Top-Level Design

At the end of the conceptual phase of the design process, a final concept design should be achieved. This will be discussed in this chapter. First, a summary of the previous concept trade-off will be discussed. After this, some more design decisions will be elaborated upon. Finally, to conclude the chapter, an overview of the design will be given.

4.1. Trade-off Summary

Previously, a trade-off had been made to determine the optimal concept out of the possible alternatives. In this trade-off, the concepts were graded on weight, cost, energy consumption, sustainability, noise pollution and technology readiness level. These criteria were in turn subdivided into relevant subcriteria. The final trade-off table, showing how each of the concepts scored on the different main criteria, is shown in Table 4.1. CON-EIW is the engine integrated in wing concept, CON-LSE is a distributed propulsion concept, CON-TRP is a two large tilt rotor concept, CON-TWP is a tilt wing concept and CON-TBP is a twin boom concept. From Table 4.1 it is easy to identify in which areas certain concepts perform good or bad. Additionally, by looking into the trade-off tables for each of the different criteria, one could identify exactly what the strength and weaknesses are for the different concepts. Finally, it can be found which concept performs the best all round, by taking the weighted average.

Table 4.1: Trade-off matrix including the final concept where the column width represents the weight of the criterion and red, orange, yellow, green and blue mean very bad, bad, average, good and very good respectively.

Concept	**Weight**	**Cost**	**Energy consumption**	**Sustain-ability**	**Noise pollution**	**TRL**	**Weighted average**
Weight ->	0.15	0.15	0.25	0.2	0.15	0.1	
CON-EIW	2.1	1.6	2	2.9	3.1	3	2.4
CON-LSE	2.6	2.9	3.5	3.8	3.2	1	3.0
CON-TRP	3.9	3.4	3.25	3.0	3	4	3.3
CON-TWP	2.8	2.6	3	3.3	2.6	3	2.9
CON-TBP	3.2	3.3	2.3	2.9	3.2	4	3
CON-FIN	3.3	2.9	4.5	2.9	3.5	4	3.5

Out of the five concepts, the tilt-rotor aircraft was chosen as the most promising one. It performed good in terms of energy consumption, weight and cost. On the other hand it lacked in sustainability, due to emissions as it uses combustion, stability and noise. In order to overcome these weaknesses, a new design concept was proposed. This new concept will be identified as CON-FIN and can also be seen in Table 4.1. As CON-TRP performs the best, the final concept will be based on this, with some changes in specific aspects.

First of all, the final concept will use fuel cells, supported by batteries, rather than combusting the hydrogen directly. This is beneficial due to not having NOx emissions, an increase in efficiency and a decrease in noise. This comes at the cost of an increase in cost and weight. Next, the concept will use cryogenic stored hydrogen. This allows for a higher density and lower weight. However due to having to be liquefied, more energy is required in the storage process and the maximum allowed storage time is lower, meaning a more efficient hydrogen distribution is required. Finally, a rotor is added in the tail in order to improve upon stability at the cost of an increase in weight and cost. By adding this engine, a larger cg range can be supported during VTOL.

In Table 4.1 it can be seen that this new final concept does indeed perform better than the five previously proposed concepts. One remarkable thing is that the score for sustainability is actually lower for the final concept compared to CON-TRP, which might be counterintuitive. The reason for this is twofold. First, one of the main advantages of fuel cells is the efficiency, which is represented in energy consumption rather than in sustainability. Furthermore, the recyclability of the fuel cells and especially that of the batteries is expected to be very good, but can not be guaranteed yet. Therefore, a bad score is given for recyclability, as a conservative approach.

4.2. Design Decisions

After selecting the final concept, this concept can be investigated more in depth. This means that slightly lower level design decisions can be made, in combination with sizing for the previous options.

A further investigation was started on the tail rotor, in order to size it. For this, a few things are required. First, an estimation should be made of the cg range, depending on the wing position. This is based on the potato diagram method,

which estimates the shift in center of gravity throughout the loading of the aircraft. A more in depth explanation and examples will be given in Chapter 11, where the stability will be analysed further. Next an estimation has to be made for the forces active during VTOL. The thrust of the main engines can be easily found, while the thrust from the back rotor follows from moment equilibrium around the center of gravity.

Taking an estimate of wing position at 8 m, as that is the position with the smallest cg variation, the required force of the back rotor is estimated to be 100 N. This force is smaller than was estimated during the trade-off and is even negative for some cg positions. This is not desirable, as a negative thrust, even though it is small, means that more thrust is required by the main propellers. In addition, designing a propeller that can generate both upward and downward lift, results in a more complex and heavier system. It was considered to move the wing more forward so the cg range would shift backwards relative to the mean aerodynamic chord. However, this increased the (S_h/S) ratio to unfeasible values for the stability constraint, that would drastically increase the weight of the empennage and complete aircraft. Therefore, it has to be reconsidered whether this small thrust is worth the increase in weight, especially as it is adverse to the cg due to being placed at the tail.

As this result is slightly concerning, the main point in favour of having the back rotor is further investigated. This point was that achieving stability with just the main rotors was considered significantly harder. If one were to try this anyway, there are two methods. First of all the entire rotor can be slightly rotated. As the point of thrust application is not on the longitudinal axis, this changes the location of intersection on that particular axis. Thus by rotating the propeller, the line of action of the thrust can be made to follow the center of gravity, preferably through an automated control system during VTOL. Secondly, the pitch of the propeller blades can be varied through its rotation. This shifts the line of action forward or backward. As these two options both require a complex control system, a back rotor was considered beneficial. However, as the usefulness in additional vertical thrust was overestimated, it now has to be checked what the effect on thrust loss is for the other option.

To do this, a look is taken once again on the cg ranges. By once more taking the wing location at 8m, in order to minimise the variation, a range of 24 cm both forwards and backwards of the cg is found. If the propeller would then be attached, and thus also have its rotating point, straight above the center of gravity, the required angle of rotation can be computed.

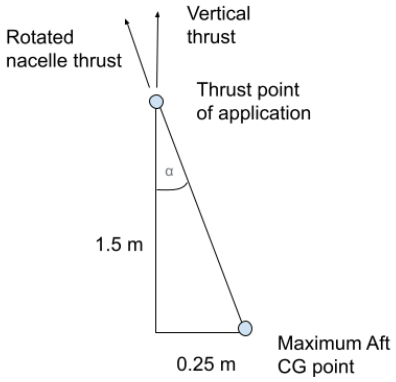

Figure 4.1: A depiction of the change in thrust direction through turning the propeller.

As can be seen in Figure 4.1, having a cg range of 24 cm to both sides and having the point of thrust application 1.5 m above the longitudinal axis, results in an angle of 9.09 deg. By taking the cosine of this angle, the percentage of useful (vertical) thrust to total thrust is found. This 1.5 m is quite a conservative distance, but even for a vertical distance of 1 m, the same analysis results in a angle of 13 deg, which still means 97.2% of thrust will be useful during VTOL. This proves that the controlling of the stability will not result in a significant loss of thrust. If the rotating of the blades would be used as well, the effect would be even smaller.

This means that the downside of a two rotor configuration was overestimated, while the upside of the three rotor configuration was overestimated as well. Thus, the decision was made to remove the back rotor from the concept. However, the fuel cells, batteries and cryogenic storage which were found from the trade-off still remain. Note that the in-depth analysis required to make this decision was not yet possible in earlier stages due to having too many unknowns and time constraints.

From this previous decision, another design decision arises. In earlier stages of the design, a rotor had to be implemented in the center of the tail. This meant that quite some standard tail designs became unfeasible, which ultimately resulted in the selection of an H-tail. However, having removed the tail rotor, other tails become feasible once again.

Ultimately, due to large rotors and high wing configuration, a T-tail will be selected, which will be elaborated upon in Section 9.1.

Another major design decision concerns the door-to-door travel time. Initially, the user requirement HVA-US-01 stated that the door-to-door travel time of 90% of the flights within Europe should have a door-to-door time of less than four hours. However, reaching this requirement means reaching a cruise velocity of 650 km/h. For propeller aircraft, whose power required scales with velocity to the third power, this is a very high speed, which results in an absurd power requirement. An investigation was launched into how much more time would be needed in order to realise more feasible numbers. From this analysis it was found that by adding just half an hour, the cruise velocity could be lowered to 472 km/h, taking into account block times. In terms of the requirement, this still means that 80% of the European flights reach their destination within the defined four hour timeframe, while an additional 10% of the flights reach their destination within the next 30 minutes. This change was discussed with the client, who considered this enough reason to loosen the requirement. Therefore, requirement HVA-US-01 will henceforth be known as HVA-US-01-n: The system shall have a door-to-door time of less than 4.5 hours within Europe for 90% of the business jet market for a maximum range of 2500 km.

4.3. Design Overview

Finally, after briefly discussing the trade-off, its results and changes that were made afterwards, it is time to take one final look at the configuration. The concept will have two rotors. These two rotors will be placed at the wing tip and will be able to rotate. Stability will be guaranteed to an automatic control system that varies the pitch of the rotor blades with a swashplate throughout the rotation and by varying the angle of the nacelles. Furthermore, the concept will use hydrogen as its primary energy supplier, which it will convert by means of fuel cells, supported by batteries. Apart from these batteries, capacitors will be used to regulate the electric flow, which is required as fuel cells are not are not suited to deal with quick variations in power during e.g. throttling. A better, more detailed visualisation of the chosen final concept can be found in Figure 4.2. This drawing gives a three-dimensional view of the aircraft with all design decisions mentioned in this chapter incorporated.

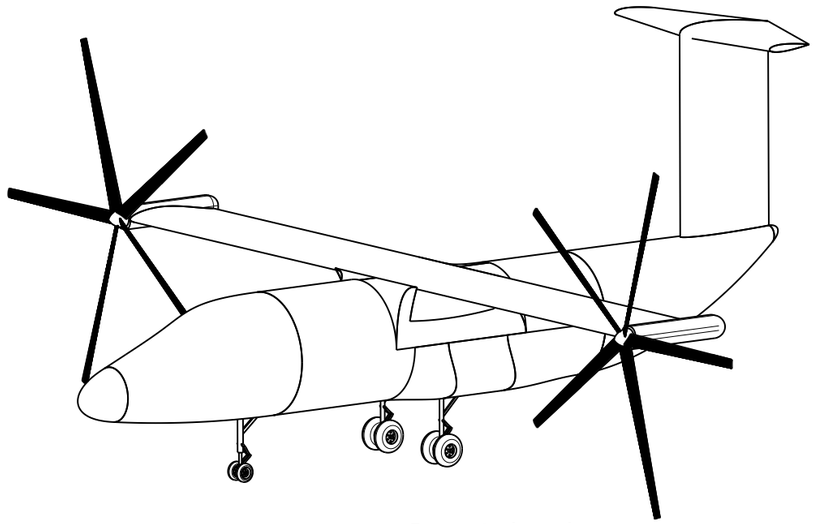

Isometric view
Scale: 1:100

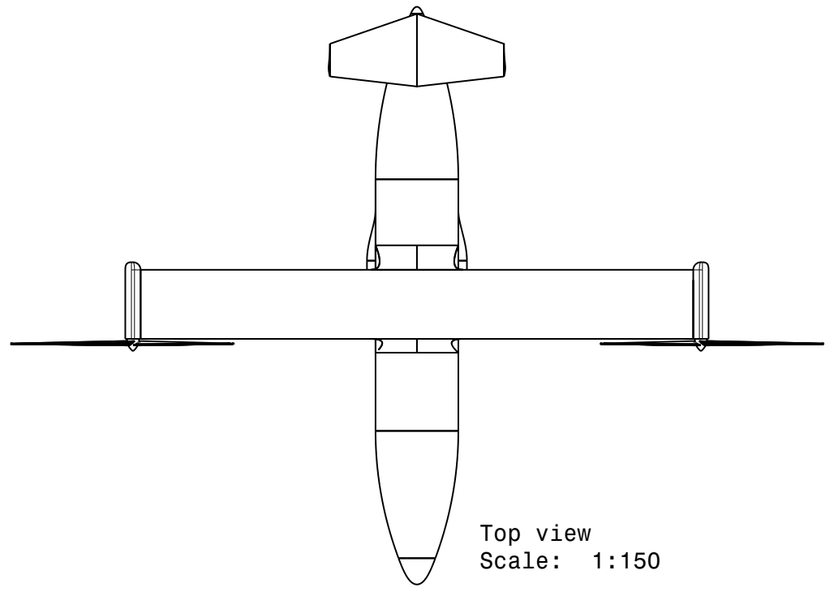

Top view
Scale: 1:150

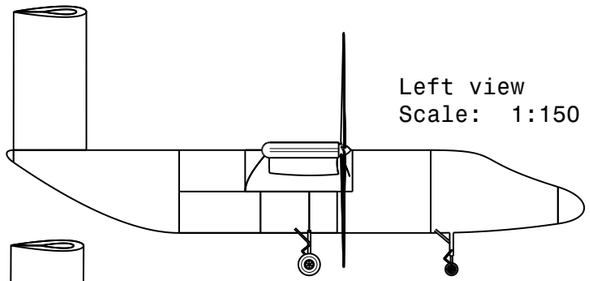

Left view
Scale: 1:150

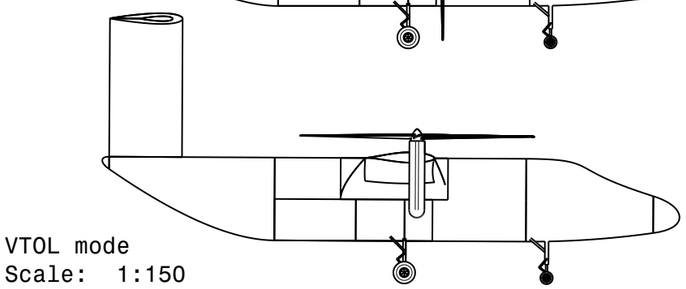

VTOL mode
Scale: 1:150

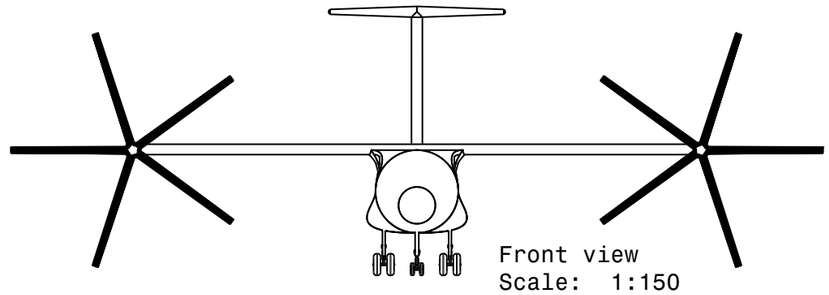

Front view
Scale: 1:150

This drawing is our property. It can't be reproduced or communicated without our written agreement.		DASSAULT SYSTEMES	
DRAWN BY: Bas Comuth	DATE: 22-6-2021	DRAWING TITLE: H2-VTOO aircraft	
CHECKED BY: Hielke Piera	DATE: 22-6-2021	SIZE: A3	DRAWING NUMBER: 1 / REV: 1
DESIGNED BY: H2-VTOO	DATE: 22-6-2021	SCALE: 1:1	WEIGHT(kg): 11217 / SHEET: 1/1

Figure 4.2: Three-dimensional drawing of the H2-VTOO aircraft, in conventional and VTOL mode.

5. Functional Analysis

In order to start the detailed design phase of the aircraft it first needs to be clear what the different functions of the aircraft are. In this chapter the different functions of the aircraft will be identified with a functional breakdown structure after which a functional flow diagram could be constructed that indicates the order in which the different functions should be executed. Finally, some specific functions will be elaborated upon on Section 5.3.

5.1. Functional Breakdown Structure

The functional breakdown structure (FBS) provides the opportunity to list all of the main functions that shall be provided by the aircraft, as shown in Figure 5.1. In this diagram the main functions together with the smaller subsystem functions of the aircraft are listed in no particular order. This diagram is split up into five main parts: designing, producing, customising and distributing, operating and retiring the aircraft system.

5.2. Functional Flow Diagram

To indicate the flow of each function described in the FBS, a functional flow diagram (FFD) is created. The functional flow diagram is divided over Figure 5.2 and Figure 5.3 and is split up into the same five parts as the FBS. They will be the main focus of this DSE and has been extensively discussed in the project plan under the name of Work Flow Diagram. Note that the numbering in the functional breakdown structure is not corresponding to that in the FBS. This stems from the fact that functions such as ”provide variable thrust” are now split up into ”increase throttle” and ”decrease throttle” for a more detailed diagram. Secondly, the production of the aircraft is listed. The focus in this case has been on assembly of the aircraft and the assembly site itself. In this step of the process, a lot of attention is payed to the sustainability of production and the general functioning of the factory. During the retirement of the aircraft, the end-of-life is put into the spotlight. It is determined that 80% of the aircraft should be recyclable. Therefore, the retirement of the aircraft is carefully structured so that the disassembly process categorises the recyclable and non-recyclable parts, and either reuses, recycles, resells, repairs or discards the part.

5.3. Elaboration on Specific Functions

To fully understand the functional diagrams, some functions or topics are explained more elaborately in the following list:

- **UN Sustainable Development Goals**: When comparing this functional flow with the UN Sustainable Development Goals, then one can clearly see that H2-VTOO tries to stay in line with responsible consumption and production, climate action (in terms of providing sustainable aviation) and sustainable cities and communities (due to the urban environment operating site for the aircraft) [34] [1]. The UN sustainable development goals are further elaborated upon in Chapter 2.
- **Recyclability**: In terms of recyclability, three distinctions of recycling a material are made: primary, secondary and tertiary. Primary being when a product is directly reused again, secondary when the same material and a similar form is used, and tertiary when chemical methods are needed to recycle the materials for a completely different use case [2].
- **In-flight emergency operations**: It should be noted that the in-flight emergency operations are not discussed in this functional flow diagram, as these would be too extensive to include here. Rather, they will be included in a more extensive failure mode and effects analysis (FMEA).

[1] https://sdgs.un.org/goals
[2] https://ecogreenequipment.com/secondary-recycling-what-it-is-and-why-we-need-more-of-it/

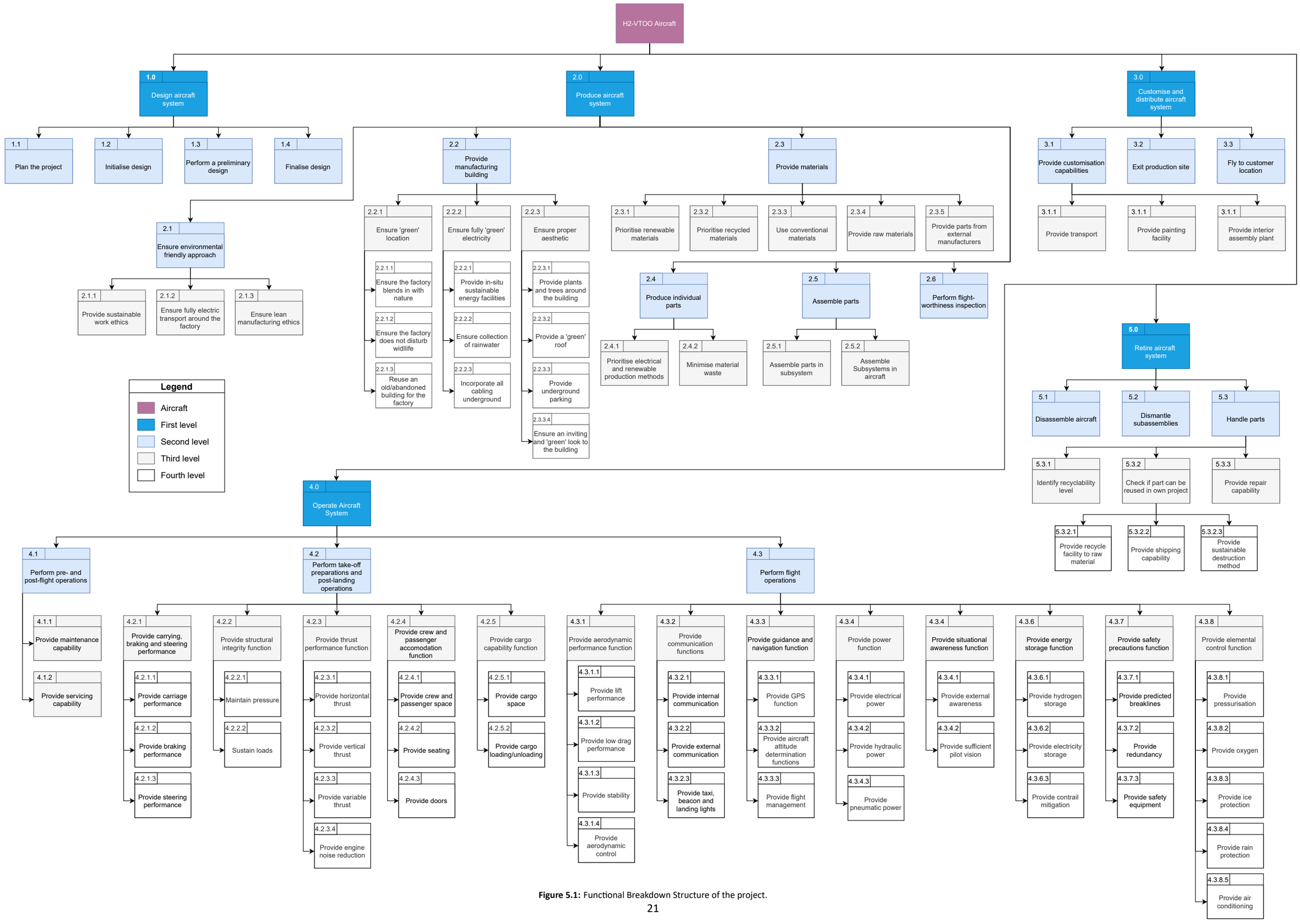

Figure 5.1: Functional Breakdown Structure of the project.

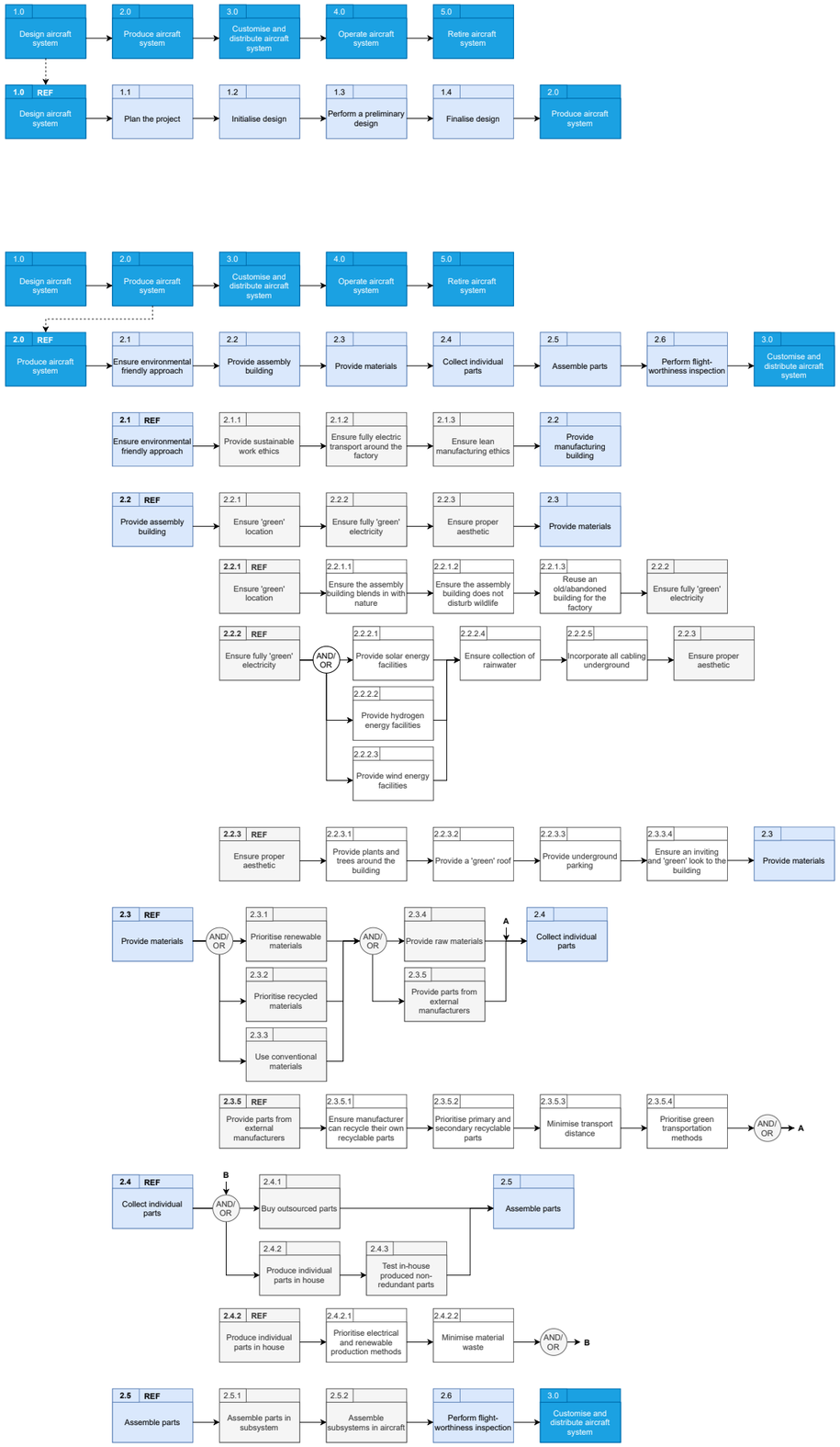

Figure 5.2: Functional Flow Diagram part 1 of the project.

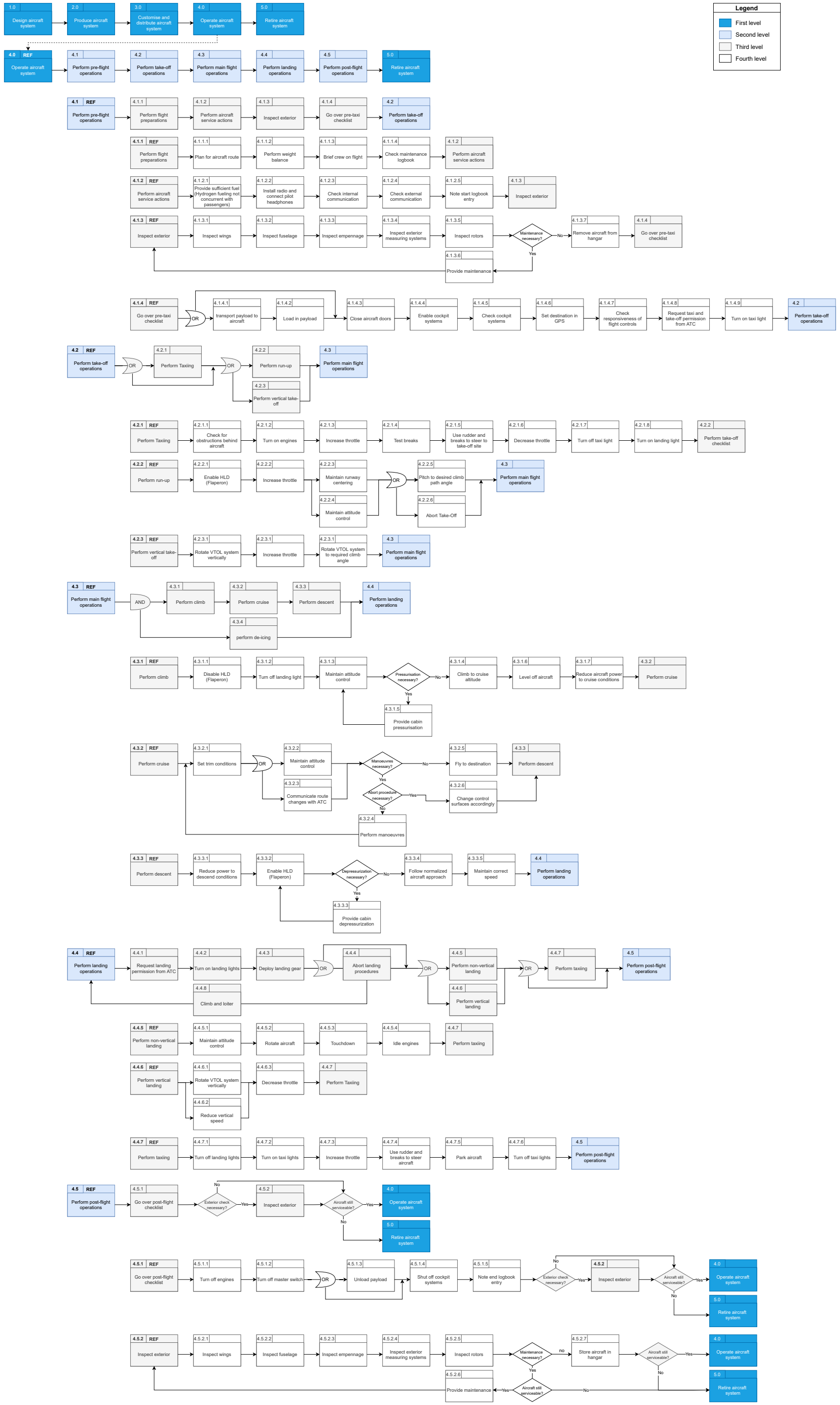

Figure 5.3: Functional Flow Diagram part 2 of the project.

6. Operations and Logistics

In this chapter, the main operational flows of the H2-VTOO aircraft and the logistics concerning the hydrogen fuel and VTOL/CTOL capabilities of the aircraft are described. Firstly, the operational flow shall be discussed in Section 6.1. This section will describe the flows concerning the training of the crew, operations and maintenance of the aircraft. After this, the hydrogen logistics are discussed in Section 6.2. This section describes the external production of hydrogen, followed by the internal production, also known as on-site production, and concluded by the modular hydrogen tank system provided by a central hub. Thirdly, the logistics concerning take-off and landing in both vertical and conventional take-off and landing are discussed in Section 6.3. Lastly, the final chosen logistical system, together with the logistical diagram and time budgeting are shown in Section 6.4.

6.1. Operational Flow

In this section, the operational flow of the H2-VTOO aircraft shall be described. Firstly, one can see the top-level operational flow diagram in Figure 6.1, further elaborations will be presented on the training phase, pre-flight operations, take-off and maintenance operations.

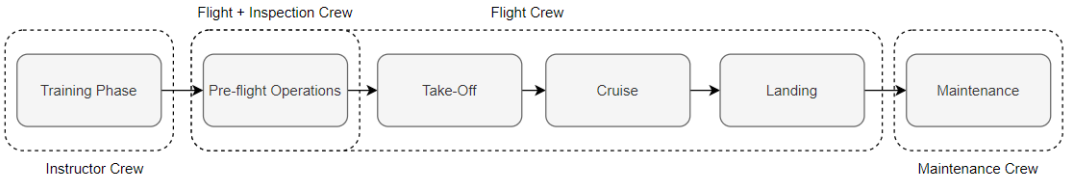

Figure 6.1: Top-level phases of the operational flow of the H2-VTOO aircraft.

As can be seen, the operational flow is depicted by means of a flowchart, accompanied by the indication of the different crews involved in each section of the operations. The phases mentioned previously will be explored deeper, with the exception of the cruise and landing phases. Note that the emergency flight operations have not yet been elaborated upon. This is due to the fact that these procedures are beyond the scope of the design at this stage.

First of all, the flight crew must undergo flight training to be able to operate the aircraft. This flow is depicted in Figure 6.2. These flow of operations do not only occur in the beginning of the pilot's service, but also when minor or major changes are introduced to the aircraft. These are addressed in the form of update briefings. In the beginning of the pilot's service, they will have to undergo supervised learning (potentially on a simulator), followed by a solo flight phase. It must be noted that due to the exotic nature of the aircraft, the ground crew should be specifically trained as well.

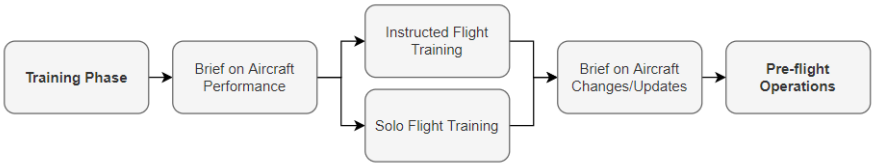

Figure 6.2: Operational flow of the training phase, performed by the instructor crew.

After this, the pre-flight operations take place, as depicted in Figure 6.3. These always consist of the planning of the flight, accompanied by the paperwork needed for landing and perimeter crossing permissions. In parallel, the inspection crew, or the flight crew in some occasions, thoroughly inspect the aircraft and provide the fuel needed. This is than followed by the startup, taxiing and ATC clearances. Note that ATC does not only play a vital role during take-off and landing, but throughout the entire flight. However, their guidance is especially important during these phases.

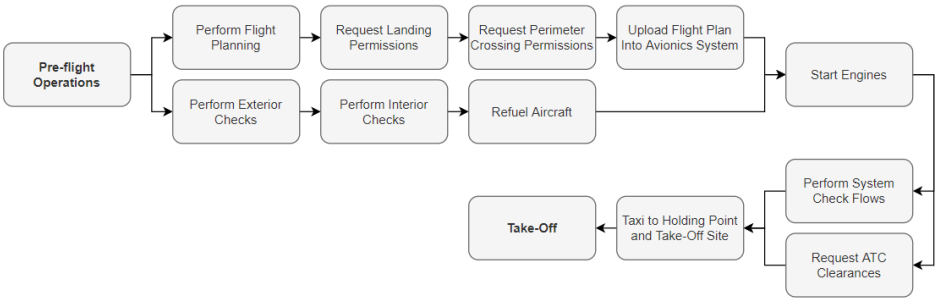

Figure 6.3: Operational flow of the pre-flight operations, performed by the inspection and/or flight crew.

When the aircraft has properly aligned on either the runway or VTOL site, it can perform its take-off, as shown in Figure 6.4. Due to the versatility of the H2-VTOO aircraft, this can be done in both conventional manners, or by means of a VTOL procedure. For the VTOL, the pilot or automatic control system must properly orient the engines. For more information on the take-off performance, the reader can refer to Section 8.3 for VTOL and Section 8.4 for CTOL. After the take-off, the cruise phase starts. In this phase, the aircraft is trimmed, altitude is maintained and the passengers receive the appropriate entertainment/accommodations. This is followed by either conventional or VTOL landing. In case of emergency, the aircraft will have to perform the emergency flows between cruise and landing.

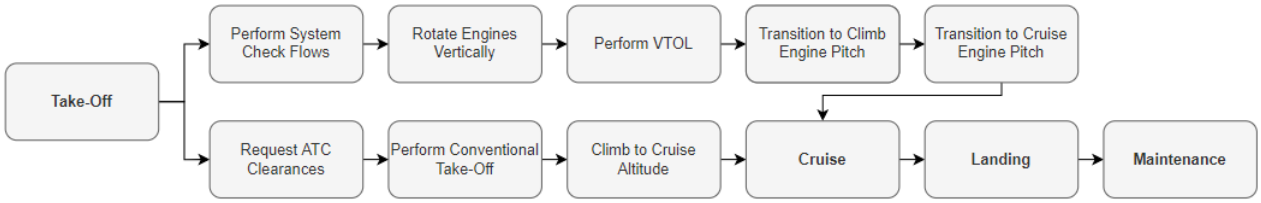

Figure 6.4: Operational flow of the take-off operations, performed by the flight crew.

Lastly, the aircraft has to be checked and maintained properly, to ensure proper functioning during flight, as visualized in the operational flow of Figure 6.5. This is split up into both the hardware and software side of the aircraft, which can be checked in parallel, by different members of the maintenance crew. More elaboration on the maintenance can be found in Section 15.3.

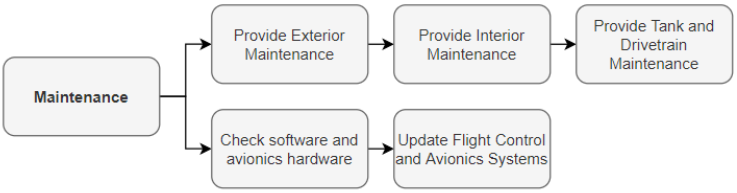

Figure 6.5: Operational flow of the maintenance of the aircraft, performed by the maintenance crew.

6.2. Hydrogen Logistics

In this section, the main logistical challenges concerning the production, transportation and storage of the hydrogen used for the airplane are discussed. A comparison between external, on-site and modular hydrogen production is made. These show the possibility of both using hydrogen being produced in a facility outside of the take-off and landing side, in a facility on-site or by using a swappable hydrogen tank system.

6.2.1. External Hydrogen Production

Currently, major projects concerning the production and transportation of large hydrogen facilities are being discussed in Europe. One of these discussions concern the plan to create a European Hydrogen Backbone by the year 2040 [87] (coinciding with the availability year of H2-VTOO). It can be seen in Figure 6.6 that major hydrogen pipelines will either be newly constructed, or upgraded from previously existing gas piping. Convenient start-up locations would be placed close to an existing pipeline, to reduce transport and infrastructure costs. When there would be an increase in hydrogen

usage further away from pipelines, there is an incentive to construct new pipelines there as well. On the same figure, one can also find the industrial production clusters of H2 sites. The closer the main aircraft sites are to one of these pipelines or these production sites, the cheaper it will be to transport hydrogen to the aircraft site.

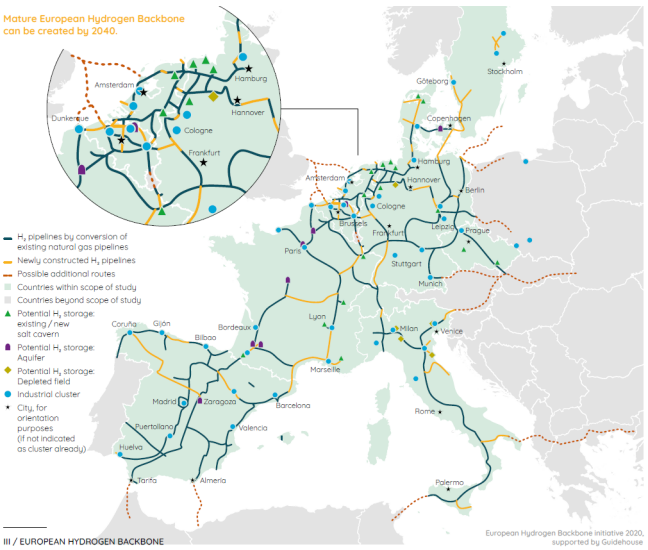

Figure 6.6: Projected Mature European Hydrogen Backbone for in the year 2040 [87].

An interesting proposal by Port of Rotterdam is being made to the European government to build Europe's largest Hydrogen production site, starting in 2022, in Rotterdam [87]. This project should supply Europe with additional hydrogen pipelines, and an additional 2 GW [87] of hydrogen power by the year 2030, which could be even more in 2040. This would not only be beneficial for the H2-VTOO project in terms of fuel availability, but for the entire hydrogen sector. Impacting energy production, automotive industries and aviation.

Transportation of hydrogen can be performed in several ways. The hydrogen can either be collected in a tank directly from existing pipelines, it can be refuelled by trucks, or transported by boats. One has to make sure that these trucks and/or boats do not interfere with the sustainability goals of H2-VTOO. Hence, these transportation methods are required to be environmentally neutral transport vehicles as well, either in the form of electric or even hydrogen powered vehicles.

After transportation, the hydrogen has to be stored in some way to be able to refuel the aircraft after landing. Logically, most of the airports H2-VTOO lands at shall have a hydrogen storage facility. These storage tanks will hold enough fuel to provide the desired frequency of aircraft landing at this site of sufficient fuel. As will be discussed in the following section, these tanks will be located on conventional airfields or on building rooftops. These buildings, offering a hydrogen helipad on their roof, shall be equipped with a safe and reliable pipeline system. This makes it possible to fill the roof-tank from the road using a hydrogen tank, or similarly, create a hydrogen tank on the ground, using pipelines to fuel the aircraft on the rooftop.

6.2.2. On-Site Hydrogen Production

Apart from external hydrogen production, one can also look at the on-site production of hydrogen. In 2018, Shell and ITM Power teamed up to build the first on-site hydrogen production facility destined for hydrogen powered cars [114]. This on-site production facility was powered by green electricity from the grid, but this could be further improved on by using on-site solar panels. This facility was able to produce 80 kg of hydrogen per day using a footprint area of under 55 m^2 [114].

When using this on-site production facility, one has to make sure that the system is able to provide enough hydrogen to fill all the incoming aircraft in a certain time interval. Another use of this on-site production system has been demonstrated by Japan, which was able to construct 135 hydrogen fuelling stations for the automotive industry in the year of 2021 [73]. The first advantage of on-site hydrogen production is the on-demand availability of hydrogen. The second advantage is the possibility to use self-produced solar energy as an electricity source, eliminating or reducing the electricity costs needed to produce the hydrogen. The last advantage is the elimination of transport costs. Some drawbacks are the large initial investment costs, need for available area, and limited hydrogen production rates.

If multiple buildings in one city would make use of the H2-VTOO systems, it could be more beneficial to create

a centralized hydrogen production hub. This should be accompanied by the corresponding pipeline grids in the roads and in the buildings. The main advantage of this system is the fact that higher quantities of hydrogen can be produced if the available area allows for it. A drawback is the need for road- and building-works to provide the needed piping in the city and buildings, together with the regulatory clearance from the city council.
It is an interesting question to ask how the hydrogen providing facilities will get into cities, together with the hydrogen powered aircraft. The hydrogen will probably not come before the aircraft are there and request it, but the aircraft will probably not come before the hydrogen facilities are accessible, a so called 'chicken and the egg' problem. Therefore it is worth to have discussions to find solutions which will help ease this transition. It might be an interesting idea to use the already existing, less sustainable hydrogen variants, such as grey and blue hydrogen, to start up the infrastructure. Facilities to provide these types of hydrogen for hydrogen-powered cars can be built, with the focus on the ability to transition to green hydrogen in the future. This will encourage the automobile industry in producing more hydrogen cars, and provide a framework to be expanded upon for the urban environment hydrogen business jet market. A problem that arises in certain countries like the Netherlands, is that the consumer can not choose the source of their energy. Therefore, it can be really valuable to try and encourage the automobile industry to use more hydrogen, and ride along the wave of increasing hydrogen facilities for the hydrogen business jet market. Further details however, are beyond the scope of this logistical analysis, however, a rough idea has been sketched.

6.2.3. Modular On-Demand Hydrogen Tanks

Another creative solution for fuelling the aircraft with hydrogen is by the use of a modular hydrogen tank system. This system assumes that interchangeable tanks with liquid hydrogen are available to be inserted and extracted from the aircraft. The main problem concerning these tanks holding liquid hydrogen is that the hydrogen can only be stored for 42 hours [56]. This however, can be solved by placing a liquid hydrogen production hub in a central location in the city. The tanks that are filled here can than be distributed among the users in the city. They are also are an inefficient use of volume, since there exist large gaps between the tank of unused space. Comparing this method to the cases discussed above, one can eliminate the needed of bulky and expensive hydrogen production/storage sites on or next to the customer buildings. Crew capacity would also decrease, which would decrease cost for the company but would mean an increase for the city's taxpayers. Finally, and perhaps most importantly, is the benefit of reducing the refuelling time. If timed properly, the fuel tanks could be delivered by the time the aircraft lands, and the empty tanks would simply have to be swapped with the full tanks, eliminating any refuelling time.

An important note that can be made is the modularity of the system outside of the H2-VTOO system. It would be possible to fuel hydrogen cars or other hydrogen-using vehicles as well using this system. The ability to make sure that these modular tanks would be able to get to the required destination, would require human intervention, to make sure these get distributed properly.

6.3. Take-off and Landing Logistics

In this last section concerning the logistics of the take-off and landing of the aircraft will be discussed. This will be split up into the vertical and conventional (VTOL and CTOL) logistics respectively.

6.3.1. VTOL Logistics

In Vertical Take-Off and Landing (VTOL) conditions, there are not many requirements for the landing site. The landing site should be physically accessible for the aircraft, while providing enough rigidity to support the aircraft with zero power applied. The main VTOL site of interest are business rooftop buildings and airports. The roofs on these buildings should have a flat roof with enough surface area and clearance available for the aircraft to land safely, while providing passengers and flight crew with enough clearance to exit the aircraft and withdraw their luggage. Other VTOL sites could be on (or near) hospital buildings, military sites or virtually anywhere with clearance.
Apart from the main VTOL sites, the aircraft should be able to undergo maintenance, therefore, special maintenance sites where the aircraft is able to VTOL, shall be available. These could be specialised H2-VTOO maintenance sites, or regular airport sites.

6.3.2. CTOL Logistics

Apart from being able to VTOL, H2-VTOO shall be able to conventionally land on relatively short runways, to be specified in future design steps, in emergency landings. Therefore, small to medium sized airports should be available. Since the European (member)states have an abundance of these airports within the specified range of 2500 km, no further logistical steps have to be taken to provide this function.

6.4. Logistical System

In this section, the final choice of the hydrogen proudction logistics is described, together with a logistical diagram. This diagram shows the flow of how to logistics are carried out by the main stakeholders. Finally, a time budget is set up which can be used in the thermal insulation design of the tank in Section 10.1.5

6.4.1. Hydrogen Production Logistics

Due to the technical disadvantages of a modular tank system, such as the inefficient use of volume, and larger fuselage required, H2-VTOO will opt for a non-modular tank design. Further elaboration on this choice can be found in Section 10.1.

This leaves the choice for either external or on-site hydrogen production. Since none of these influence the actual design of the aircraft, it is decided that depending on the location of the landing site, the choice for hydrogen production can be made. As explained earlier, it can become costly and difficult to construct a hydrogen production site on an office building. Therefore it might be more convenient to use a large tank on the building. This tank can be filled by either tapping into existing pipelines or pumping hydrogen into the tank from 'delivery'-trucks. On larger sites however, such as an airport, it can become an interesting choice to produce the hydrogen on-site. This is due to the fact that it might become more cost-beneficial, and that the required space might be available.

6.4.2. Logistical Diagram

From all of the previously discussed logistical aspects of the H2-VTOO aircraft, one can construct a diagram which shows the main logistical groups making sure the final product has a smooth operation. This is visualized in Figure 6.7.

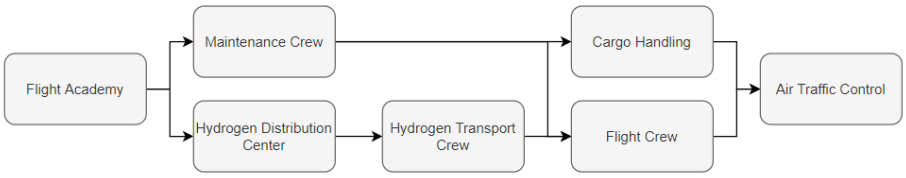

Figure 6.7: Logistics diagram covering the main logistical stakeholders of the aircraft.

Firstly, one starts off at the flight academy. In here, the mechanics and pilots will receive the required training to operate and maintain the aircraft. Than, the crews are defined. These are split up as shown in Figure 6.7. An important thing previously covered is the hydrogen distribution. For this, one can define the distribution center and transporting service of the hydrogen. The ATC section is especially important during CTOL.

6.4.3. Logistical Time Budget

To be able to design for thermal insulation in Section 10.1, and have an indication for how long the aircraft would need on the ground, it is useful to estimate a time budget consisting of the major parts of the ground activity. The main logistical activities that the aircraft undergoes when stationed are listed in Table 6.1, together with the estimated time per activity. This results in a maximum time on the ground of one hour, in the case that the tank has to be fully refilled, and some extra time delays take place.

It is assumed that the luggage is placed into the aircraft simultaneously with the fuelling of the hydrogen. For safety reasons, all passengers and pilots must wait with entering the aircraft until the refuelling has been completed. The entering of the passengers and pilot checklist are also assumed to be performed simultaneously. For redundancy of the system, 20 minutes of extra time are taken into account for any unforeseen circumstances. This than results in a total time budget of 60 minutes. Note that these values are based on experience.

Table 6.1: Time budget of the ground activity of H2-VTOO.

Phase	Time [min]
Entering of the passengers and pilots	5
Entering luggage	15
Checklist sequences by pilots	10
Filling the tanks with hydrogen	30
Unforeseen circumstances allowance	20

7. Aircraft System Characteristics

This chapter describes the iterative design and sensitivity analysis in Section 7.1 and Section 7.2, where-after the weight, flight and power charactersitcs are described in Section 7.3 to Section 7.5.

7.1. Iterative design

In aircraft design, the weight is decisive in determining the basic planform size. Changing the weight means changing the size of different subsystems, which changes the weight again. Due to this iterative behaviour, it is impossible to design an aircraft sequentially. That's why for the H2-VTOO aircraft, an iterative design method was established.

The method was set up, such that different subsystems could be tested and used individually as well as combined in a main file integrating the entire aircraft. The principle is explained by Figure 7.1.

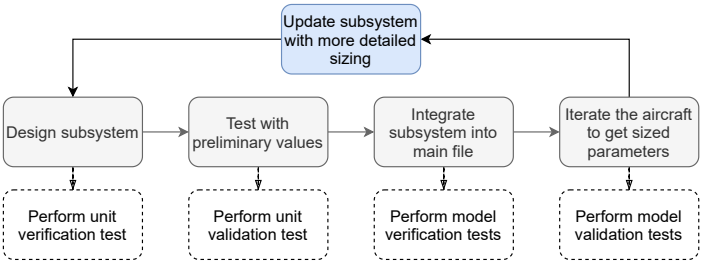

Figure 7.1: Simple overview of designing and updating the system including the verification and validation procedures

This method can easily be expanded upon to add and update subsystems/optimisers. At the start of the project, most methods were based on historical data. Over the course of the design process, these empirical methods were updated to sizing tools mostly based on physics. For the H2-VTOO project, the final iteration diagram can be seen in Figure 7.5. The boxes on the main diagonal all represent different submodels that can convert certain inputs into new outputs.

- Orange boxes represent models where the method for calculations changes after a full outer iteration loop (displayed by a grey dashed line).
- Red boxes represent models that only start working after one internal loop, shown by the blue dashed line.
- Green boxes represent models that are only used once at the very start.
- Blue boxes represent models that are only activated after one internal loop. They also change method (from empirical to physics-based) after one full loop.
- grey boxes represent the external inputs of the system, white boxes represent the in- and outputs of the models.

For every full iteration, the two internal loops, displayed by the blue dashed line and the green dashed line, iterate until they have converged, before continuing to the next box. The entire iteration stops when the MTOM of two subsequent iterations has converged to within 0.1 kg. Depending on the initial guess of the OEW/MTOW, the system either converges to a higher value than its initial value, or to a lower value. In the case of H2-VTOO, the mass steadily increases before converging. This is most likely due to the unconventional set-up of the aircraft, utilising fuel cells and hydrogen as a fuel. In Figure 7.2 it can be seen that the system converges after 17 full loops.

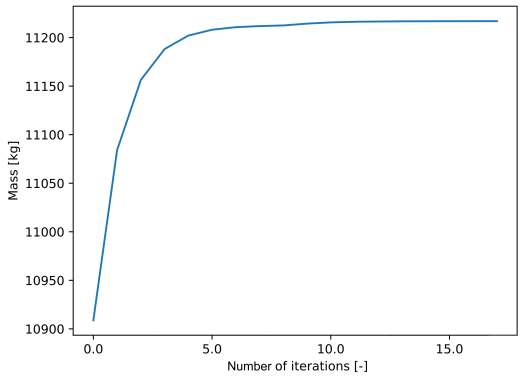

Figure 7.2: MTOM progression after iteration.

7.2. Sensitivity analysis

To check the robustness of the program, a sensitivity analysis was performed. The sensitivity analysis aims to show how the system reacts to a change in its input parameters. The results are analysed to check whether the system behaves as expected. If an anomaly is detected the system can be checked for errors. Hence, apart from a tool to show sensitivity to inputs, it can be used as a high level form of verification of the model. In the case of the H2-VTOO model, displayed in Figure 7.5, the input parameters are explained below, the results can be found in Figure 7.3 and Figure 7.4.

- *Disk Loading design point*. The design point determines how much power is necessary for a VTOL operation, and scales with the rotor area. This input was chosen since the VTOL capability is one of the main design goals.
- *Altitude*. During the design phase it was noticed that the efficiency of the aircraft was greatly influenced by the cruise altitude. This analysis was done to check whether small deviations in altitude had a big influence, as you cannot always fly at the desired cruise altitude.
- *Travel time within Europe*. The travel time within Europe largely determines the cruise speed. The cruise speed plays a major role in the required power, which largely determines the mass of the system. Normally the altitude changes with a change in velocity. In this case the altitude was kept constant in order to properly look at the effect of increasing the velocity.
- *Range*. The system is designed for 2500 km of range. This input was chosen to find out how scaleable the system can be for longer ranges, provided that the cruise speed and altitude stay the same.

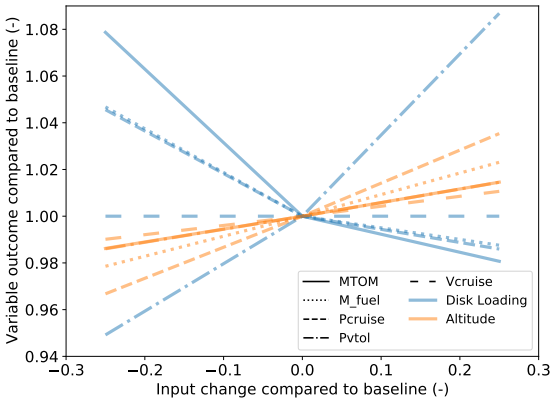

Figure 7.3: Sensitivity analysis with disk loading and Altitude as inputs

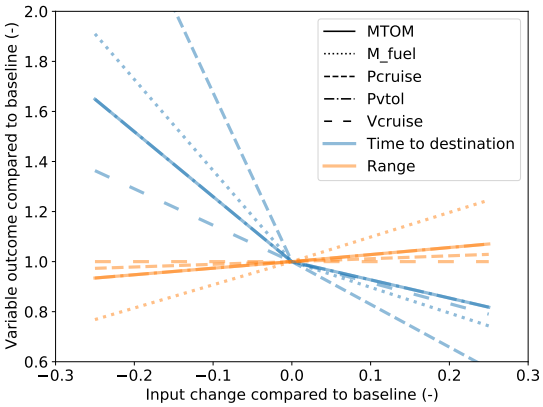

Figure 7.4: Sensitivity analysis with Time to destination and Ranges as inputs.

The figures above show the response of a variable, depicted by different linestyles as seen in the legend, to a change in input variable, depicted by the different colors, compared to the baseline (which is the current H2-VTOO design). It should be noted that the lines are generated using linear approximation between three data points at -0.25, 0 and 0.25. When looking at the solid line for the MTOM, it can be seen in Figure 7.3 that decreasing the altitude by 25 % decreases the MTOM by about 2 %. This is logical as in Section 8.1.2 it is explained that the H2-VTOO flies above its optimal cruise altitude. The opposite is true when the cruise altitude is increased. Luckily, however, the change in fuel mass is not drastic, so the aircraft can fly quite safely a bit lower and a bit higher, Which is necessary, since aircraft cannot always fly at their desired height. The disk loading shows an interesting result. Increasing the disk loading apparently slightly decreases the MTOM, as the propellers shrinkage induced by the higher disk loading causes drag and the weight in general to decrease. However the efficiency for VTOL operations decreases (as can be seen by the power needed for VTOL) and the rpm of the rotors need to increase, which could cause drag divergence on the tip of the propeller blade, and increase the noise. Further analysis on this subject is hence needed.

Figure 7.4 Shows the input values with the largest responses. It can be seen that reducing the time to reach a destination, increases the cruise velocity, which in turn increases the power during cruise dramatically, since the power scales cubic with cruise speed. Even though the system is very sensitive to this input change, the results are easily explained and logical. That is why the design time to reach a destination has been changed, as decreasing it improved the feasibility of the design substantially (the baseline in this plot already takes this design change into account). The range looks to be quite scaleable, as the increase in fuel weight does not seem to snowball to a massive MTOM increase, in comparison to the velocity.

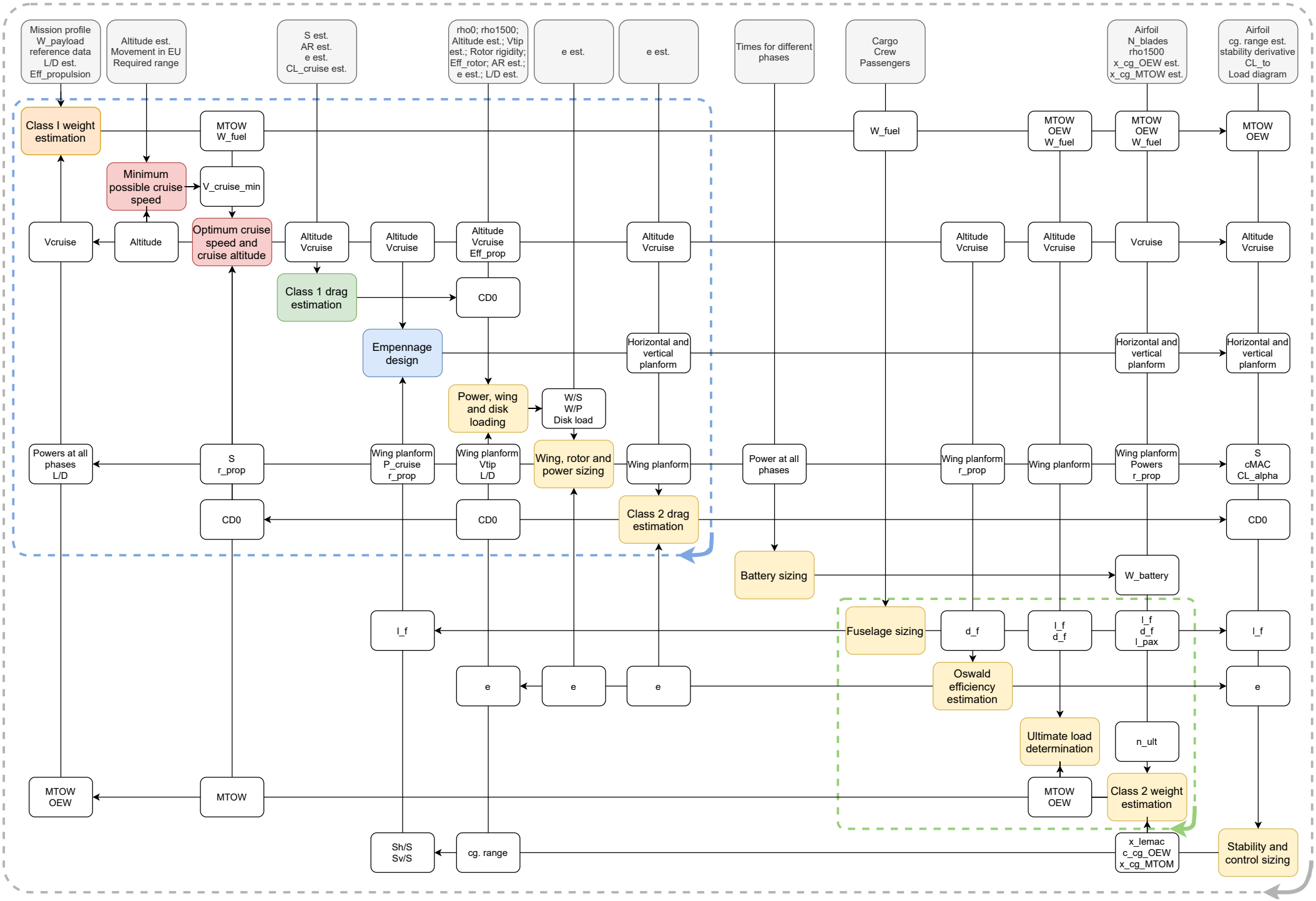

Figure 7.5: Main iteration layout. In one iteration (grey loop) both inner loops (blue and green) converge/iterate first before continuing.

7.3. Weight Estimation

This section will be dedicated to discussing how the weight was generated in the iteration file. For this, it is first required to develop the mission profile, after which the actual weight estimation methods will be discussed.

7.3.1. Mission profile

As per the requirements the aircraft should be able to fly 2500 km, whilst picking up and dropping off people at any stage. The aircraft should also be able to take off vertically and land vertically at all locations of the mission profile. Hence the following mission could be established, see Figure 7.6.

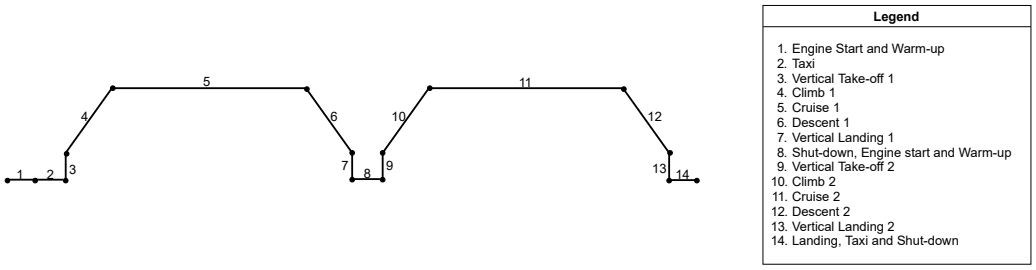

Figure 7.6: Mission profile of the H2-VTOO aircraft

7.3.2. Class I and Class II weight estimations

The class I weight estimation first uses statistical data from similar VTOL capable aircraft. Since hydrogen is yet to be used, the first OEW/MTOW estimation was performed using data from VTOL capable kerosene aircraft. It was known beforehand that the fuel mass for hydrogen would be significantly lower, and the OEW would be significantly higher. That's why correction factors were implemented, estimated using data on the fuel mass and the OEW found in earlier research [153].

Once the OEW and MTOW from the class II weight estimation and the power needed for different cruise phases were calculated, the class I weight estimation switches to using that data instead of the empirical data.

The class II weight estimation was first set-up using mostly empirical data. Along the design process the methods were updated from empirical data to actual mass data of the components. All exotic components were added to the weight estimation: the fuel cells, electric motors, battery, large rotors and the hydrogen tank were all sized accordingly.

7.3.3. Fuel fractions

For every stage of the mission profile a fuel fraction could be established, first using statistical data, later using the power needed for the different stages of the flight. The usage of hydrogen in combination fuel cells causes the the fuel fractions to be relatively large, since the gravimetric energy density and the efficiency of fuel cells are considerably higher than conventional combustion.

The final calculated fuel fractions, and the total fuel fraction can be seen in Table 7.1. Note that the fuel fractions for VTOL (3, 7, 9, 13) are determined compared to the MTOW (also using the power needed to VTOL the aircraft at its MTOW), since hydrogen mass change is low compared to the OEW. This adds some contingency to the design as well. Also note that due to the rounding, the fuel fractions seem more similar than they are in reality.

1	2	3	4	5	6	7	8	9	10	11	12	13	14	tot
0.99877	0.99939	0.99931	0.99817	0.97045	0.99817	0.99931	0.99878	0.99931	0.99817	0.96955	0.99817	0.99931	0.99939	0.92802

Table 7.1: Fuel fractions at different flight phases

These fuel fractions calculations were implemented in the class 1 weight method, which also calculates the final fuel mass.

7.4. Flight envelope

The flight envelope is a tool to find the maximum, and therefrom the ultimate, load factor the aircraft experiences during operation. It depends on the MTOW, the cruise speed, stall speed and more variables incorporated in Figure 7.1, since they change constantly. The final envelope from the converged values is seen in Figure 7.7. The gust loading diagram is constructed taking into account a reference gust velocity of 17.07 m/s according to CS25 regulations,

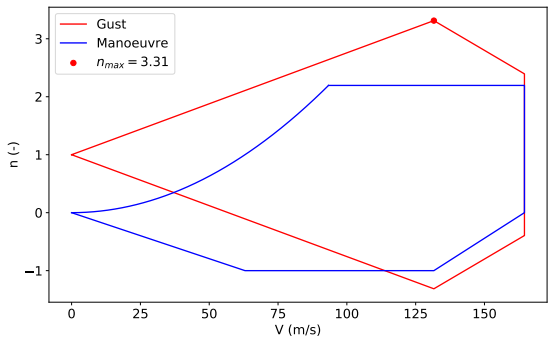

Figure 7.7: Flight envelope of the H2-VTOO

As seen in the diagram, the maximum load factor is determined to be 3.31. The ultimate load factor n_{ult} is defined as $1.5 \cdot n_{max}$ and found to be 4.97.

7.5. Power and wing Loading

During the iterative design it is key to determine the shaft power required for each flying phase, an estimate for the required propeller disc area and finally an estimate of the required wing surface area. These parameters are calculated via two power loading diagrams of which the first is used to size the power required (P) and the wing surface area (S) needed during conventional flight operations by plotting the power loading (W/P) versus the wing loading (W/S). The second diagram is used to size the power required during VTOL operations (P) and the required propeller disc area (A) which is done by plotting the power loading (W/P) versus the disc loading (W/A).
Considering conventional flight first, relations between W/P and W/S were plotted for take off, climbing flight, cruise flight and service ceiling. In addition stall limits and a landing limits are added, however, these are added for the sake of completeness and will not be constraining due to the rotating engines, which in practise can increase the lift by rotating upwards. The plotted lines provide a design space within which all feasible W/S - W/P combinations can be found.
For VTOL operations, relations between W/P and W/A were plotted for hovering at sea level, vertical climb, hovering at the hover ceiling and finally for transitioning flight. Again these lines provided a design space with plausible W/A-W/P combinations.

From these diagrams, the iteration program is able to select the most optimal wing loading and disc loading which turned out to be 2709.9 N/m^2 and 1100 N/m^2 respectively. Once the wing loading and disc loading values are obtained, the required power for each flying phase could be determined as illustrated in Figure 7.8. The most demanding phase of conventional flight is cruise, for which 2239.3 kW is required. For VTOL operations, hovering at the hover ceiling is the most demanding phase where a power of 3451.7 kW is required. These two mission phases are the most demanding in terms of required shaft power, therefore they will be the leading mission phases for which the power system will be designed for in Chapter 12. For a more in-depth explanation on the power, disc and wing loading, the reader is referred to the H2-VTOO midterm report [8].

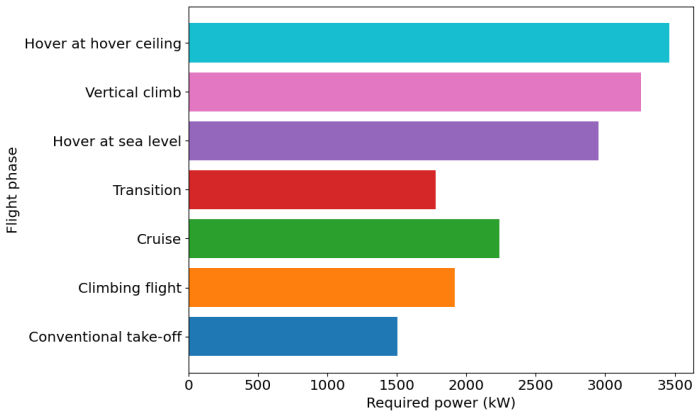

Figure 7.8: Required shaft power per flight phase

8. Performance Analysis

This chapter will focus on reviewing how and whether the performance requirements are achieved. First of all the cruise phase will be investigated. After this the payload-range diagram is presented. Next the take-off is considered, which is done for both vertical and conventional take-off. Finally, to conclude the chapter, the climb and rotor will be analysed.

8.1. Cruise Performance

There are several important parameters during cruise, including velocity and altitude. These will be discussed in this section.

8.1.1. Cruise speed

One of the top-level requirements of the aircraft design was to provide air travel which can provide passengers with a travel (or transfer) time less than 4.5 hours for 90% of all air travel in the EU. From this requirement, it could be found that 90% of all travel within the EU are below 2000 km [49]. Hence, the aircraft must be able to fly 2000 km in under 4.5 hours with the mission profile as described in Section 7.3.1. From this mission profile, it was estimated how long each phase would take based on taxi, climb, and descend speeds. After this, a block fraction was calculated using Equation 8.1. Here, T_{transf} is the transfer time in minutes, B the block fraction, and T_{total} the total time required for each flight phase except for cruise in minutes. From this fraction, one can calculate the cruise speed as shown in Equation 8.2. Here, $R_{90\%}$ is the 2000 km as described above, which results in a cruise velocity of 132 m/s.

$$B = \frac{T_{transf} * 60 - T_{total}}{T_{transf} * 60} \tag{8.1}$$

$$V_{cruise} = \frac{R_{90\%}}{T_{transf} * B} \tag{8.2}$$

8.1.2. Cruise altitude

Cruise is the most important phase in the mission profile, as the aircraft spends the majority of the mission in this phase, which is visualised in the mission profile in Figure 7.6. For this reason, aircraft are designed to be optimised for the cruise phase. It is therefore essential to select an optimal cruise altitude, as the changing density in the atmosphere will have a significant effect on the performance parameters of the aircraft. Determining the aircraft's cruise altitude is striking a balance between parasitic drag and lift-induced drag. The former increases with the square of the velocity, while the latter increases with the inverse of the square of the velocity, suggesting there is a minimum for some velocity. In this design, it is opted to select the altitude that optimises the power loading, as a higher power loading will lead to a lower weight, and a lower weight will lead to less fuel needed, which will help to achieve the sustainability goals. Naturally, this needs to be within the regulations, as well as the mission requirements. The power loading is calculated with the help of Equation 8.3.

$$W/P = 0.95\eta_p \left(\frac{\rho}{\rho_0}\right)^{3/4} \cdot \frac{1}{\frac{C_{D,0} \cdot 0.5\rho \cdot V_{\text{cruise}}^3}{W/S} + (W/S)\frac{1}{\pi \cdot AR \cdot e \cdot 0.5 \cdot \rho \cdot V_{\text{cruise}}}} \tag{8.3}$$

The density can be replaced with a function of altitude, as described in the International Standard Atmosphere using Equation 8.4.

$$\rho = \rho_0 \left(\frac{T_0 + ah}{T_0}\right)^{\frac{-g}{aR}-1} \tag{8.4}$$

The propeller efficiency η_p in Equation 8.3 is a function of the propeller advance ratio, a property that is dependent on airspeed, rotational speed of the propeller, and propeller diameter. The relationship is visible in Figure 8.1. The propeller rotational speed is limited by noise constraints, and the fact that the propeller tips may not exceed the speed of sound. For this reason a propeller advance ratio of 2.2 is chosen to optimise for noise and efficiency at the same time at the cruise speed determined in Section 8.1.1, as increasing the propeller rotational speed will increase the noise, but decreasing it will decrease the efficiency. After selecting the cruise altitude it must be checked that the propeller tips indeed do not exceed the speed of sound. The current cruise speed and propeller diameter resulted in a propeller rotational speed of 450 rpm, and therefore the propeller tip speed (229 m/s), is smaller than the speed of sound at the cruise altitude (334 m/s).

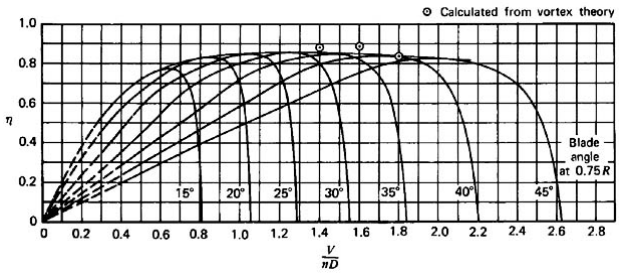

Figure 8.1: Propeller efficiency versus propeller advance ratio for multiple blade angles [93].

Combining Equation 8.3, Equation 8.4, and Figure 8.1 yields Figure 8.2: the power loading versus the altitude. From this figure the maximum power loading can be selected, and the corresponding altitude will be the cruise altitude, 420 m for the current design case.

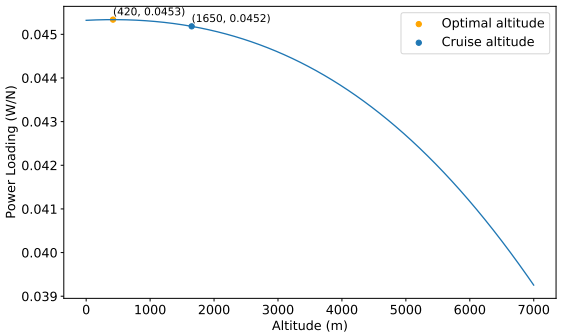

Figure 8.2: Power loading versus altitude, using the aircraft's parameters after the final iteration.

Now, the selected altitude is measured from sea level, and therefore a cruise altitude of 420 m will give some problems when flying over countries that have a high elevation. For example, Switzerland has an average elevation of 1350 m [3]. At low altitudes, the visual flight rules (VFR) are applicable. Aircraft do not fly in flight levels, but rather fly on sight. As VFR rules state that 'except when necessary for take-off or landing, or except by permission from the competent authority, a VFR flight shall not be flown over the congested areas of cities, towns or settlements or over an open-air assembly of persons at a height less than 300 m (1000 ft) above the highest obstacle within a radius of 600 m from the aircraft' [4]. Therefore, the cruise altitude that is selected is 1650 m, to be able to fly within the regulations over the majority of Europe in cruise. Moreover, the power loading is fairly constant up until altitudes of around 2000 m, after which it starts to drop rapidly, as is visible in Figure 8.2. A few things should be kept in mind with the above cruise altitude. Firstly, note that Andorra has the highest average elevation in Europe, but is not taken into account due to the country's size [3]. Then, it should be noted that the cruise altitude cannot be in the transition layer airspace. At altitudes lower than the transition altitude (the lower boundary of the transition layer), the altitude is measured with respect to the elevation, while at altitudes higher than the transition level (the lowest flight level above the transition layer), the altitude is measured with respect to a standard air pressure. To avoid collisions, it is not allowed to cruise in the transition layer. As the transition altitude can be as low as 914 m (3000 ft), the flight route needs to be planned out in such a way that these regulations are respected [44]. The transition altitude differs per country, and therefore it is not taken in consideration in determining the optimal cruise altitude. Lastly, it is decided that the cruise altitude is high enough to fly over the entirety of Europe, albeit with some climbing or rerouting over sea, for example when crossing the Alps or the Pyrenees.

These calculations, however, only hold for ISA-conditions. A sensitivity analysis should be done, in order to estimate the effect of having an offset from these conditions in terms of temperature. For this, the calculation will be repeated with ISA + 15 conditions, meaning a sea level temperature of 30 degrees Celsius instead of 15. The reason to elevate the considered temperature instead of lowering it, is because a lower density has an adverse effect on performance. Due to the decrease in density, the velocity has to be increased from 131.6 to 134.4 in order to generate enough lift. This increase in velocity in turn causes a decrease in power loading and hence an increase in power required of about 2%. Furthermore, it can occur that due to terrestrial constraints, the required altitude becomes higher. By flying higher, the density is lowered as well, which means the same effect as for higher temperatures occurs, namely

more power required and a lower power loading. In hotter regions or regions with a higher elevation, the operator can hence choose to either lower the range or the MTOW in order to continue the aircraft's operation.

8.2. Payload-Range Diagram

A payload-range diagram is used as it is a handy tool to illustrate the compromise made between the amount of payload, fuel and shows their effect on the range. Three types of weights are identified. These are: the fuel weight, the operative empty weight and the payload weight. The last one includes the passengers, crew and cargo. The payload-range diagram is constructed with the use of Equation 8.5 [152] to calculate the range.

$$R = \left(\frac{\eta_p}{g c_p}\right)_{cruise} \left(\frac{L}{D}\right)_{cruise} ln\left(\frac{W_4}{W_5}\right) \tag{8.5}$$

Here, the η_p is the estimated propeller efficiency (which can be iterated using Figure 8.1), c_p the specific fuel consumption, W_4 and W_5 the weight of the aircraft at the beginning and end of the cruise phase. W_5 is W_4 without the total fuel weight, except for 3.85 kg of hydrogen which are needed to land.

Two payload-range diagrams can be seen in Figure 8.3 and Figure 8.4. The first one corresponds to purely the weight of the payload, while in the second diagram the other weight components have been added as well. Now, the diagram is constructed on the basis of four points. The first one can be found on the most left vertical axis. This represents the situation where the aircraft has a maximum payload and no fuel on board. The maximum payload was determined on the basis of the weight of the conventional payload of ten passengers and a 1000 kg cargo, plus the equivalent weight of five extra passengers. It was chosen to add five passengers as this would implies the addition of a single seat on each row of the aircraft. However, the weight of these extra passengers could also be exchanged in the form of extra cargo.
Next, the second point is the situation where the aircraft carries its maximum payload for a range determined by Equation 8.5. Now, the total weight equals to the MTOW as the aircraft carries fuel. The amount of fuel that is carried in this situation is calculated from subtracting both the payload and OEW from the MTOW.
The third point is the one with the normal amount of payload and the maximum amount of fuel. The total weight once more is equal to the MTOW. This point is the combination of payload and range that is sized for. It can be noted however that the range largely overshoots the required distance of 2500 km at this point 3. This is due to two things, first of all a contingency but also due to the ideal mission profile consisting of 2 VTOLs on top of the range, while this graph only depicts the cruise phase, including a normalisation for vertical take off and landing at the start and finish.
The fourth point corresponds to the situation where there is no payload (only the crew is still in the aircraft, which is why the payload weight is not zero) and a full tank of fuel. Here the total weight does not equal the MTOW as the tank can only hold about $807kg$ and cannot compensate the reduced payload.
Now, Figure 8.4 encompasses more than the four sets of points that were discussed. The points that are located on the graph between the sets corresponds to intermediate configuration in which the H2-VTOO can be loaded.

Next, the structure of Figure 8.4 is explained. The grey box represents the EOW. The area between the green dotted line and the EOW represents the weight contribution of the payload. The area between the blue dot dashed and green dotted line is the fuel contribution.

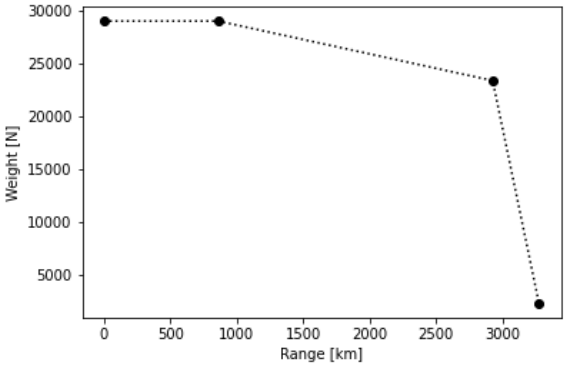

Figure 8.3: Payload-Range Diagram.

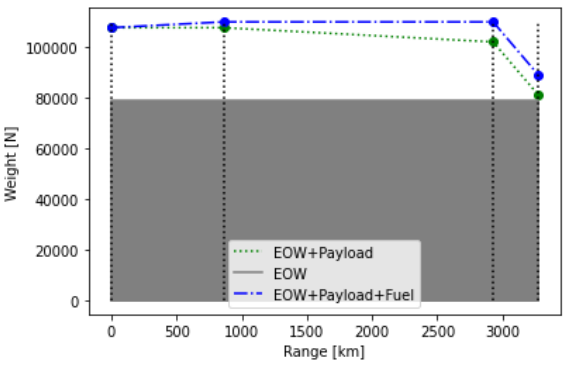

Figure 8.4: Payload-Range Diagram, including the other weights.

8.3. VTOL Performance

VTOL performance can best be discussed by going through the most critical procedure. First, the aircraft lifts off at 900 m altitude where it will be able to hover for a maximum of ten seconds. After those ten seconds it will climb for 600 m until the hover ceiling, at a velocity of 9 m/s, this procedure will take a total of 66.67 seconds. After it reaches the hover ceiling at 1500 m, the aircraft will be able to hover for an additional 10 seconds. Thereafter the aircraft needs to initiate transitioning flight which is allowed to take 93.33 seconds such that the entire VTOL procedure has lasted a maximum of three minutes. The power and energy required for these maneuvers can be found in Figure 7.8.

8.4. Conventional take-off performance

In this section conventional take-off will be investigated. First off the propeller blade radius is bigger than the height at which the propeller is attached. Taking off truly conventionally would hence not be possible. Aside from this, CS25 aircraft need to have a minimum angle between the wheels of the MLG and the most outboard propeller (in this case there is only one propeller) of 5°.

In the case of H2-VTOO, a lateral ground clearance angle θ_{ground} of 6° was chosen to keep some contingency compared to the minimum of 5°. Using the span b, the lateral position of the MLG y_{MLG} and the lateral ground clearance angle θ_{ground}, the minimum ground clearance height h_{clear} was calculated to be 0.73 m, using Equation 8.6. knowing this height, the minimum angle that the propeller nacelles can make, could be calculated to be $\theta_{nac} = 27.4°$. This was done using an estimate of the Nacelle length l_{nac}, the chord position about which the nacelle rotates (1/4), an estimate of the distance between the nacelle and the propeller $d_{n,p}$, the rotor radius r_{prop}, the MLG height h_{MLG}, and the fuselage diameter d_f, as shown in Equation 8.7.

$$h_{clear} = \tan\theta_{ground} \cdot \left(\frac{b}{2} - y_{MLG}\right) \tag{8.6}$$

$$h_{clear} = 2r_{prop} - (d_f + h_{MLG}) - r_{prop}\cos\theta_{nac} + \left(\frac{1}{4}l_{nac} + d_{n,p}\right)\sin\theta_{nac} \tag{8.7}$$

The height of the lowest point of the aircraft's rotor system can be visualised for every angle. This can be seen in Figure 8.5. Most notable from the plot is that the nacelle of the motor will become the lowest point of the aircraft starting at around 55 degrees. Before that the tip of the propeller is the lowest point.

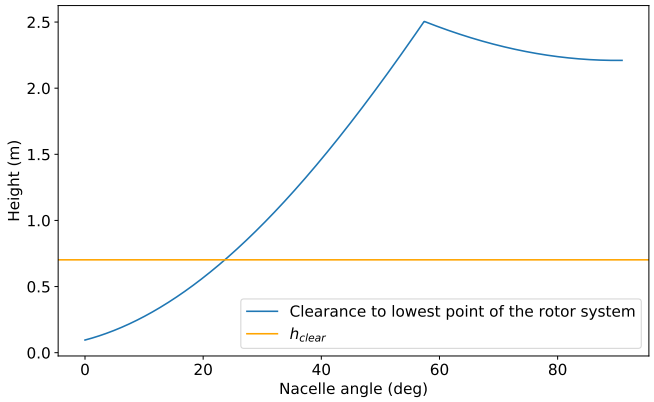

Figure 8.5: Height of the lowest point of the aircraft's rotor system compared to the nacelle angle. A zero degrees nacelle angle would mean that the engine is parallel to the body.

It is now known that 27.4° is the minimum angle needed for conventional take-off. The optimum value, however, is yet to be determined. In order to calculate the optimal θ_{nac} for take-off, simplified equations of motion were determined. To find them, multiple assumptions were made. The main assumptions are listed below.

1. The change in total drag coefficient due to the change in θ_{nac} is assumed to be negligible.
2. Thrust during take-off is assumed to be constant.
3. The normal force throughout take-off is assumed to be constant and equal to the MTOW.
4. The rolling resistance coefficient C_{rr} is constant at 0.015 [26].

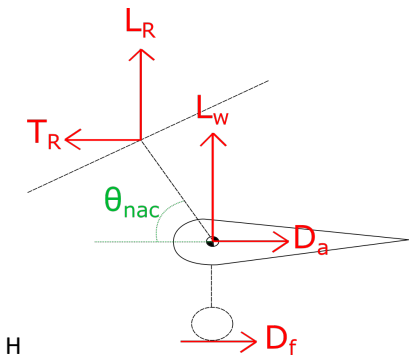

Figure 8.6: Simplified FBD to set up the EOM for conventional take-off (upwards and left positive coordinate system).

5. The weight is assumed to be constant and equal to the MTOW.
6. The drag polar is assumed to be parabolic.
7. Acceleration on the runway is constant.
8. The acceleration in the vertical direction is zero.
9. The runway length for take-off s_{to} should be 1500 m.
10. Ground effect is neglected.
11. Required power for a certain thrust can be deduced using actuator disk theory [157].
    (a) Airflow is modelled to be steady, homogenous, inviscid, incompressible and irrotational.
    (b) The number of blades is infinite (as per an actuator disk).
    (c) The ambient static pressure is undisturbed upstream and downstream.
    (d) Flow and thrust is modelled to be uniform across the actuator disk.

Using the above assumptions and the FBD, shown in Figure 8.6, the equations of motion could be set up, where the necessary thrust and velocities, were the unknowns. The thrust generated by the propeller was decomposed in a horizontal and vertical component, using the angle of the nacelle. The acceleration on the runway was rewritten to $a = \frac{2V^2}{s_{to}}$, using the assumptions stated above. The finalised equations of motion, in matrix notation, are shown in Equation 8.8.

$$\begin{bmatrix} \cos\theta_{nac} & -\frac{1}{2}\rho S C_D - \frac{2\text{MTOW}}{g \cdot s_{to}} \\ \sin\theta_{nac} & \frac{1}{2}\rho S C_L \end{bmatrix} \begin{bmatrix} T \\ V^2 \end{bmatrix} = \begin{bmatrix} C_{rr}\text{MTOW} \\ \text{MTOW} \end{bmatrix} \quad (8.8) \qquad P = \sqrt{\frac{T^3}{2\rho A}} \quad (8.9)$$

The power can be derived from the thrust using disk actuator theory. A first estimation of the power is given by Equation 8.9 [79]. Note that the propeller efficiency needs to be taken into account as well.
The lift coefficient greatly influences the amount of power needed for take-off. For a low lift coefficient, most upwards force needs to be produced by the propeller, whereas for a high lift coefficient, more lift will be produced by the wing. It was first considered to not install HLD on the aircraft, since the tiltable rotors could act as an alternative for both take-off and landing. This section checks whether this is possible. The chosen wing set-up, has a low lift coefficient at zero angle of attack of 0.132. For landing, the entire aircraft can pitch up a bit to increase the angle of attack, during take-off, pitching is possible once the elevator has enough pressure to pitch the aircraft. The angles in Figure 8.7 are shown w.r.t. the horizontal plane, not compared to the body axis.

At the current lift coefficient, without pitch, a rolling take-off is barely more efficient than a vertical take-off. This can be seen when looking at the necessary power for take-off compared to the lift coefficient. The black line in Figure 8.7 represents the lift coefficient during take-off without HLD, nor pitch. Purely from a power stand-point, the optimal nacelle angle would be 80°. In that case it would not be beneficial to use a rolling start instead of a vertical start.

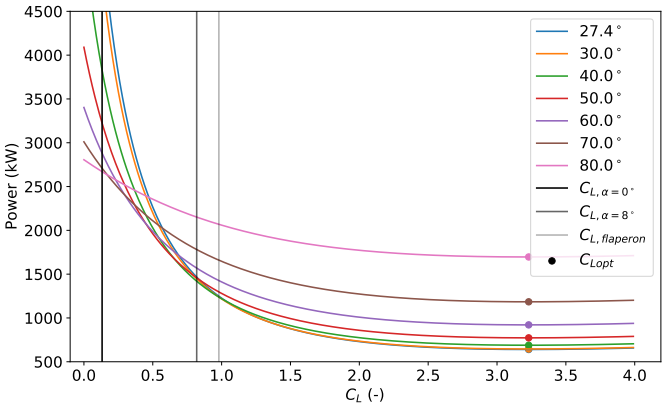

Figure 8.7: Engine power needed for take-off compared to the lift coefficient. With $s_{to} = 1500$ m and an altitude of zero.

In Figure 8.7 it can be seen that an increased lift coefficient causes a decrease in necessary power for a conventional take-off. Note that the optimal lift coefficients displayed in the figure do not take the increased weight and parasitic drag due to possible introduction of HLD into account. The figure does show at which lift coefficient, which nacelle angle is optimal. It also shows the point at which an increase in lift coefficient yields diminishing results. To see at what lift coefficient the H2-VTOO can operate without HLD, a pitch angle must found at which the lift coefficient is sufficient to make a rolling take-off efficient. In the subsequent paragraph it is assumed that the pitch angle and the AoA coincide.

An estimate of the lift coefficient vs AoA curve can be obtained using XFOIL. XFOIL is based on a panel method, which is based on potential flow theory for generating the airfoil lift coefficient at varying AoA, airspeeds and altitudes. The DATCOM method can be used to find the wing lift coefficient based on physical and semi-empirical parameters. This methods holds only for the linear part of the curve seen in Figure 8.8.

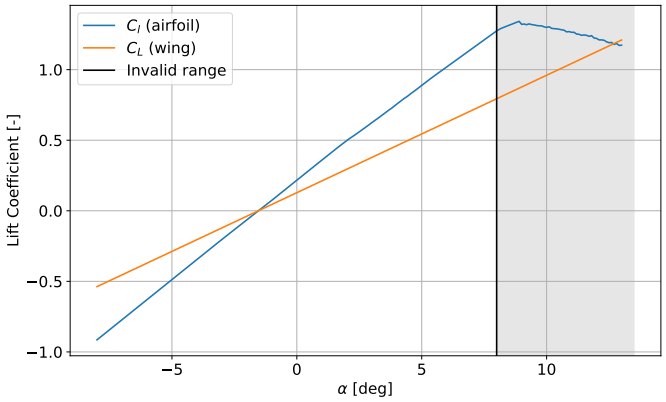

Figure 8.8: Lift coefficient and AoA for an airfoil and a wing.

It can be seen from Figure 8.8 that the lift coefficient curve stays linear up until an AoA of 8°. It can also be seen that the maximum lift coefficient is not drastically higher than the lift coefficient at 8°. At 8° the lift coefficient of the wing is estimated to be 0.819. From Figure 8.7 It can then be seen that the optimal nacelle angle is around 40° (39.3°, to be exact), with a required power of 1419 kW, drastically lower than the hover power. The corresponding speed at that instance is 56.5 m/s (around 203 km/h). Looking further into the graph it can be seen that improving the C_L further has ever diminishing return, up until the point where the induced drag coefficient causes the required power to rise again.

If the ailerons are used as flaperons, as described in Section 11.2.1, the maximum lift coefficient for the linear part of the curve can be estimated using Equation 11.15 to be 0.98. The power required then drops to 1238 kW.

8.5. Climb Performance

Now, the H2-VTOO's climb performance is analysed making use of the rate of climb. The steady rate of climb can be defined as the vertical speed of the aircraft without any accelerations. The unsteady rate of climb, often referred to as just the rate of climb, is defined as the vertical speed that allows for accelerations throughout the climb phase. The first one can be determined according to Equation 8.10 [95]. Where P_a, P_r and W are the power available, power required and weight of the aircraft. The weight was chosen to be the MTOW as this is the most critical weight and the fuel used for take-off is negligible relative to the total weight during cruise. Furthermore, The power required can be determined by multiplying the drag experienced by the airspeed as can be seen in Equation 8.11.

$$ROC_{steady} = \frac{P_a - P_r}{W} \tag{8.10}$$

$$P_r = D \cdot V \tag{8.11}$$

Now, the drag of the aircraft has to be estimated to calculate the required power. This is done with the use of Equation 8.12. The drag coefficient can be computed by Equation 8.13 [95]. Here, $C_{D,0}$, A and e are the zero-lift drag coefficient, the aspect ratio and the Oswald factor, which are already discussed in earlier chapters. The lift coefficient can be retrieved by equaling the weight of the aircraft to the lift.

$$D = \frac{1}{2} C_D \rho V^2 S \tag{8.12}$$

$$C_D = C_{D,0} + \frac{C_L^2}{Ae\pi} \tag{8.13}$$

The following step is to determine the the power available at the correct altitude. The power is scaled with the use of Equation 8.14 [124]. P_{a_0} and ρ_0 are the power required and density at sea-level conditions. It is assumed that the power available remains nearly constant with airspeed. However, it is important to mention that this assumption does not hold for very low and very high speeds, but these velocities are not relevant within the mission profile. [95]

$$P_a = P_{a_0} \left(\frac{\rho}{\rho_0}\right)^{0.75} \tag{8.14}$$

Now, it was already mentioned that the steady RoC and the RoC are not the same. The latter can be computed with Equation 8.15 [95] and Equation 8.16 [95].

$$RoC = \frac{1}{1 + \frac{V \frac{dV}{dH}}{g}} \tag{8.15}$$

$$\frac{dV}{dH} = V_{EAS} \frac{d\left(\sqrt{\frac{\rho_0}{\rho}}\right)}{dH} \tag{8.16}$$

Combining all the formulas result in the following graphs:

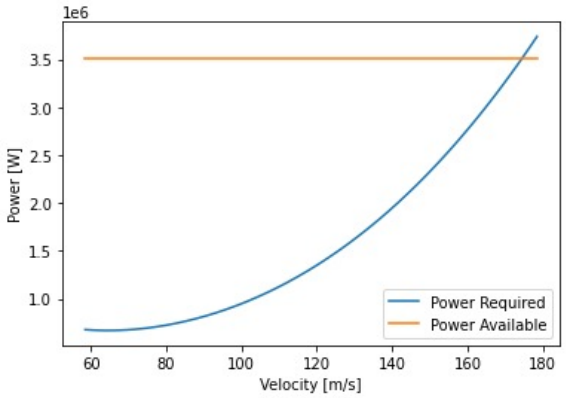

Figure 8.9: Power Required and Power Available.

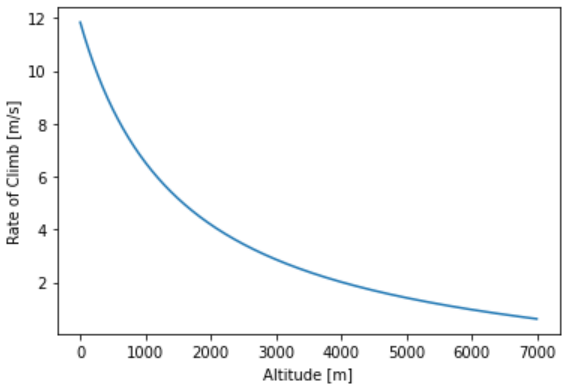

Figure 8.10: Rate of Climb.

Figure 8.9 illustrates the available and required power at an altitude of 1650m at a speed of 131m/s. It is only visualised for this altitude range as 131m/s is the cruise speed. When the power available is bigger, there is excess power that is not being used to overcome the drag and can be used to climb. Where the lines cross, the possible rate of climb will be zero. On the other hand, when the power required is the lowest, the rate of climb will be at its maximum. Important to note is that power required in Figure 8.9 for a speed of 131 m/s differs from other power required for cruise that are mentioned in this report. That is because those required powers also factor in the efficiencies and therefor come to a higher required power. Figure 8.10, visualises the rate of climb in function of the height for at a speed of 131m/s. It is clear that when the aircraft flies at a lower altitude, the possible rate of climb is bigger.

Finally, the maximum and required rate of climb are examined. This is done with the aid of Figure 8.11 and Figure 8.12 respectfully. Firstly, it is important to remember the requirement HVA-AM-10: The final product shall have a maximum climb rate of 9 m/s. Figure 8.11 shows all the combinations of speed and altitude where a rate of climb of

9m/s is attained by the blue line. Furthermore, the plot also shows the maximum rate of climb for the combinations of altitude and speed by the solid orange line. The green line indicates the stall speed for all the altitudes. It is clear that the requirement is met and that the H2-VTOO can reach a RoC of 9m/s. However, it is not clear what the RoC exactly is for each combination. That is why the Figure 8.12 is shown. It shows the maximum rate of climb in function of the altitude. Generally, one can say that the maximum rate of climb decreases with increasing altitude. However, in Figure 8.11 it can be seen that for the largest part of the altitude range, flying at the ideal climb trajectory is not possible. This is due to the constraint posed by the stall speed. However, up to altitudes of 3000 m it is possible to climb at a steady rate of 9 m/s, which is the required rate of climb and thus this does not pose a significant problem.

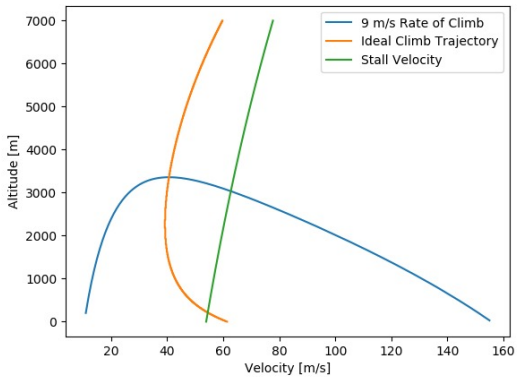

Figure 8.11: Combination of Velocity and Altitude for the RoC requirement and maximum.

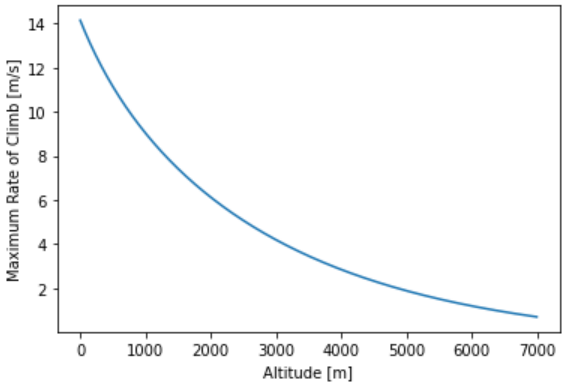

Figure 8.12: Maximum Rate of Climb.

8.6. Propeller/rotor performance:

The propulsion of the propellers were analysed for both their thrust and rpm in VTOL(as rotors) and in cruise(propellers).

8.6.1. Propeller performance in cruise

The rpm and thrust of the propellers in cruise were computed by using actuator disk theory. By applying several valid assumptions, the propeller is modelled as a disk with the propellers smeared of their circular area. It is important to note that doing this means that the performance of the propeller calculated within this chapter is for an infinite amount of blades and thus in the future when designing the actual propeller, the shape of it must be considered and more detailed calculations and modelling must be conducted. Actuator disk theory is better visualised in Figure 8.13.

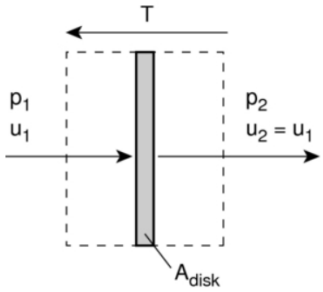

Figure 8.13: Propeller modelled as a disk

This model allows for a much simpler, time efficient method to determine the thrust and sequentially the rpm of the propellers in horizontal and vertical flight.

The thrust in cruise was calculated by simply using the computed L/D ratio of 9.05. The thrust in cruise can then be estimated as it equals to the drag. This gives a value of 12154.743 N. This value was then divided by 2 to find the thrust of each propeller.

Following this, the rpm of the propellers is then of importance. The rpm of the propellers in cruise was determined by simply using the advance ratio previously determined in Section 8.1. This value of 2.2 for the advance ratio was chosen due to noise constraints and the drag divergence that may occur at the propeller tips

The rpm was then calculated by solving Equation 8.17 for n (RPS of the propellers), resulting in an rpm of 449.82

$$J \equiv \frac{v_0}{nD} \tag{8.17}$$

8.6.2. Rotor performance in VTOL

For VTOL flight, hovering was taken as a critical condition. Therefore, the thrust to be produced by the propellers was then taken as the MTOW. In order to ensure that the aircraft does indeed take-off the ground a safety factor of 10% was also included in this thrust calculation. This led to a thrust in VTOL of 121000.517 N.

The rpm then followed from this. For this calculation, the actuator disk theory was not used. Instead, a relation between thrust, blade diameter and rpm was derived from the relation between these in Equation 8.18.

$$T = k_T \rho n^2 D^4 \tag{8.18}$$

where T is the thrust, n is the revolutions per second, D is the diameter of the rotor and k_T is the thrust coefficient. This formula was used as it indeed shows a relation between the speed of the propeller and the diameter of it. Equation 8.19 was then derived:

$$n^2 = \frac{k1.1MTOW}{D^4} \tag{8.19}$$

where k is a constant. Note, the density was not included in this equation because in vertical flight, the change in value with respect to the density at sea level is negligible. k was then determined by retrieving the required parameters from literature including those of helicopters and other VTOL aircraft[5][19][33]. A constant was then found, for which n could be solved, this resulted in an rpm of 596.9842.

A last comment on the calculated performance of the propeller, it should first be understood that actuator disk theory smears the propellers over a 'disk' area and therefore the values calculated are for an infinite number of blades. In reality, the number of blades along with their dimensions will influence these values. Therefore, it is advised to conduct more detailed analysis such that these dimensions can be calculated and a more accurate thrust and rpm can be calculated for the propellers. A suggested method to start on this is blade element momentum theory. This theory is much more accurate as it will take into account the mechanics and geometry of the propellers rather than a 'disk' area[85].

9. Aerodynamic Analysis

Analysing the aircraft's aerodynamic characteristics is an essential part in the design process as they determine the performance and the efficiency of the aircraft. In sizing all the aerodynamic surfaces, one has to make sure the aircraft is operable during all phases of the mission. In this chapter estimations of lift and drag are performed, as well as the design of the airfoils sections and planforms of all the aerodynamic surfaces.

9.1. Configuration

Before sizing the aerodynamic surfaces, one has to decide on the configuration of the main wing and the empennage as the design of the aerodynamic surfaces depends on that configuration. First of all, a high-wing configuration is selected, as the large rotors at the wing tips prevent any other configuration from obtaining enough ground clearance. Then, a T-tail empennage configuration is selected. Certain advantages made a T-tail the better option over a conventional tail. For example, the vertical tail will have an increased effective aspect ratio due to the horizontal tail on top of it. Moreover, the downwash effect on the horizontal tail will be much less (in the current design the conventional tail will experience 2.35 times as much downwash as the T-tail) and therefore the elevators are more effective. The smoother airflow over the horizontal tailplane (as it is not disturbed by the fuselage) will induce a slight decrease in drag. An additional advantage is that the T-tail will certainly keep the horizontal tailplane out of the wake of the engines, even if further design iterations significantly increase the rotor size. It must be noted that the T-tail comes with an increase in weight as the horizontal tail needs to be supported by the vertical tail. It was decided that all the advantages outweigh this disadvantage, that is also neutralised to some extent by the fact that a more effective horizontal tail can be lighter. Lastly, it is essential to notice that for a T-tail the risk of a deep stall is present if for large angles of attack the horizontal tail will enter the wake of the main wing. This risk can be mitigated by sizing the vertical tail such that the horizontal tail will stay out of the wake, something that needs to be checked afterwards.

9.2. Airfoil Selection

The geometry of an airfoil section of a wing determines all its two-dimensional aerodynamic characteristics, and therefore it is essential to pick the right airfoil according to the design case and mission profile. After completing the conceptual design, the Mach number was found to be lower, and the Reynolds number was found to be higher. As the compressibility effects of a higher Mach number and the viscous effects of a lower Reynolds number are detrimental to the aerodynamic characteristics, the analysis can be considered conservative.

9.2.1. Main Wing Airfoil

Before the selection of the airfoil can be discussed, it is important to explain the effect the Reynolds number has on it. This is done in the following section.

Reynolds number

The Reynolds number is a dimensionless parameter that needs to be determined to select an airfoil as it impacts the C_l, C_m and C_d. The Reynolds number can be determined with the following formula:

$$Re = \frac{\rho u L}{\mu} \tag{9.1}$$

Where ρ represents the density, u the velocity, L the mean aerodynamic chord and μ the dynamic viscosity of the fluid (in this case the air). The altitude at which the aircraft flies is important as it influences both ρ and μ (as the dynamic viscosity is influenced by temperature and therefore altitude). The H2-VTOO has a chord-based Reynolds number of 1754300.

Overview Airfoil Selection Strategy

This section discusses the selection of the airfoil of the wing. This is done according to the method presented in AE2111-II [108]. The procedure is laid out below. Important to note is that this is a general strategy. Some deviation is possible if some parameters become more important during the design phase. An example could be that a higher $C_{l_{max}}$ becomes more important due to a low transition speed.

1. Assume the thickness to chard ratio.

2. Establish the airfoil design lift coefficient with the following formula:

$$C_{l_{des}} = \frac{1.1}{2q_{eff}}\left[\left(\frac{W}{S}\right)_{scr} + \left(\frac{W}{S}\right)_{ecr}\right] \quad (9.2) \qquad q_{eff} = \frac{1}{2}\rho[V_\infty cos(\Lambda)]^2 \quad (9.3)$$

   Where $(W/S)_{scr}$ and $(W/S)_{ecr}$ are the weight to wing surface ratio (wing loading) at the start and end of the cruise phase respectively, V_∞ the freestream airspeed and Λ the wing sweep angle.
3. Select the airfoils with the lowest C_d for the $C_{l_{des}}$ and widest drag bucket. As the $C_{l_{des}}$ is fixed for the aircraft, selecting the lowest C_d results in the highest C_l/C_d-ratio.
4. Now, select the airfoil with the largest $C_{l_{max}}$. Important to note is that airfoils that suffer from a sharp drop in lift coefficient after they have stalled have to be avoided.
5. Finally, it is desired that the selected airfoil has an as low as possible C_m at $C_{l_{des}}$ as this is beneficial for stability.

Execution Airfoil Selection Strategy

Firstly, it is essential to understand that the stall speed and the lift-over-drag ratio are important factors in choosing an airfoil for a VTOL aircraft. The former is due to the transition from VTOL to the conventional configuration and vice-versa. A low stall speed is desired in this scenario. That is why the $C_{l_{max}}$ is an important parameter. This would assure that enough lift is produced by the wings so that the aircraft can fly at low speeds. The latter is to ensure an efficient operation of the aircraft. That is why there is a great interest for a high C_l/C_d by picking an airfoil with a low C_d for the $C_{l_{des}}$.

As a consequence, a NACA 6-series is chosen as it has a relatively high maximum lift coefficient. Important to note is that the angle at which the $C_{l_{max}}$ is reached, should be realistic. If that is the case this assures a low stall speed. Another characteristic of a NACA 6-series is a region of very low drag for a small interval of lift coefficients. This interval is called a drag bucket [22].

Now, a thickness to chord ratio slightly bigger than or equal to 14% is chosen as this implies that the airfoil will stall from the trailing edge as can be seen in Figure 9.1, retrieved from [108]. If one takes a look at the lift coefficient curve, it is clear that the stall will gradually propagate instead of having a sharp drop in lift coefficient, like the thin and moderately thick airfoils. Besides, the pitching moment does not vary as much as for the other airfoils. Airfoils thicker than 14% are more prone to lower critical mach numbers and have a higher suction peaks. The latter lead to higher drag while the former can lead to a unnecessarily lowering maximum speed of the aircraft.

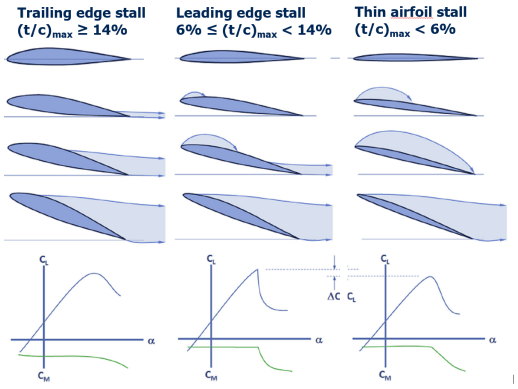

Figure 9.1: Effect of the thickness to chord ratio [108].

Thirdly, the airfoil design lift coefficient is estimated with use of the international standard atmosphere. To do this, it was assumed that the aircraft will cruise at an altitude of 1650 m at 131 m/s. Furthermore, the aircraft will use 7.7 kg and 800 kg of fuel during vertical take off and the total cruise. It has a MTOM of 11217 kg and 0 degrees of sweep.

Using Equation 9.2, a value of 0.305 is found for the $C_{l_{des}}$, which is rounded-off to 0.2 and 0.4 as there was no airfoil found with a $C_{l_{des}}$ equal to 0.3. This results in the selection shown in Table 9.1.

Table 9.1: Selection of Airfoils[144]

Airfoil	C_d at $C_{l_{des}}$ at (α)	$C_{l_{max}}$ at (α)	C_m at $C_{l_{des}}$
NACA 63(2)-215	0.00413 (0.70°)	1.3400 (8.90°)	-0.0485
NACA 63(2)-215 MOD B	0.00542 (0.80°)	1.7700 (10.9°)	-0.0332
NACA 64(2)-215	0.00390 (0.90°)	1.5200 (12.9°)	-0.0467
NACA 65(2)-215	0.00355 (0.90°)	1.2090 (13.4°)	-0.0478
NACA 66(2)-215	0.00452 (1.20°)	1.3681 (12.5°)	-0.0437
NACA 67(2)-215	0.00628 (2.60°)	1.1061 (10.6°)	-0.0046
NACA 63(2)-415	0.00430 (-0.75°)	1.7173 (14.0°)	-0.0877
NACA 64(2)-415	0.00526 (-2.85°)	1.7039 (13.8°)	-0.0884
NACA 65(2)-415	0.00521 (-2.90°)	1.6014 (13.2°)	-0.0860
NACA 65(2)-415a	0.00448 (-0.40°)	1.6017 (14.2°)	-0.0663
NACA 66(2)-415	0.00432 (-0.80°)	1.5012 (13.3°)	-0.0940

Now, the airfoils with the lowest C_d at $C_{l_{des}}$ and widest drag bucket around $C_{l_{des}}$ have to be picked from Table 9.1. This results in the elimination of the NACA 67(2)-215, 63(2)-215 MOD B and the 65(2)-415.

From the remaining airfoils, those with the largest $C_{l_{max}}$ and no pronounced drop in C_l after the stall have to be chosen. This results in the elimination of the NACA 63(2)-215 and NACA 65(2)-215.

Finally, the airfoil with the lowest C_m at $C_{l_{des}}$ is kept. So, this leads to the elimination of the NACA 64(2)-215, NACA 66(2)-215 and NACA 65(2)-415a. In conclusion, the airfoil chosen is the NACA 63(2)-415 due to its all round good performance.

Important to mention is that the selection of the NACA 63(2)-415 is the result of an iteration that should be kept in mind for the further design of the aircraft. However, in the calculations of other subsystems the airfoil of the previous iteration was used. This is the NACA 63(2)-215. It changed as the aircraft flew at a height of 6000m at a speed of $650 km/h$. This results in a different Reynolds number and mach number. Furthermore, the MTOM, amount of fuel used (during VTOL) and the sweep have changed. This resulted in an increase of the $C_{l_{des}}$. Furthermore, it is essential to note is that the wing will consist only out of one airfoil. This has a drawback that the entire wing will tend to stall all at once. However, a multi-airfoil wing will be harder to manufacture, design and model. This will tend to increase the cost rapidly. Besides, the airfoil was specifically optimized for the cruise phase. Other airfoils would be less optimal for this phase. In terms of the transition phase, the $C_{l_{max}}$ should be sufficient to guarantee a successful operation.

9.2.2. Empennage Airfoils

The selection of the airfoils of the empennage follows a different procedure from that of the main wing described in Section 9.2.1. The design criteria are different for the horizontal and vertical tail.

The horizontal tailplane should have an airfoil that has a high lift slope C_{l_α} and a large range of usable angles of attack, such that the tailplane has a large operable window, meaning that the airfoil should have a high stall angle. As the horizontal needs to be able to produce both positive and negative lift, a symmetrical airfoil needs to be selected. The thicker NACA 00xx airfoils are good options, as their large nose radius postpones the stalling of the tailplane [145]. Moreover, a good lift-to-drag ratio (C_l/C_d) would imply the minimum drag for a certain required lift force. As this lift-to-drag ratio changes with the angle of attack, the *slope* of the lift-to-drag curve has been selected as a design parameter, as that means the highest lift-to-drag ratio for all angle of attacks. The NACA 00xx airfoils considered in the selection are displayed in Table 9.2, along with the lift slope, lift-to-drag ratio slope, and stall angle, generated by XFOIL [32]. A viscous analysis has been performed with a Mach number of 0.5 and a Reynolds number of $13.6 \cdot 10^6$. These values do not correspond to the determined cruise speed, as this quantity is not known yet at the start of the aerodynamic analysis. As an increase in both Mach and Reynolds number is detrimental to the aerodynamic characteristics, the approach can be considered conservative. Note that all the slopes have an R^2-value of at least 0.996. Thicker airfoils than the NACA0018 exist, but have not been taken into consideration, as they have increasingly lower lift and lift-to-drag ratio slopes. It can be observed that the NACA0015 has the highest lift slope, and together with its good lift-to-drag ratio slope and high still angle, it is selected as the best airfoil.

Table 9.2: Analysis of different airfoil options for the empennage. M = 0.5, Re = $13.6 \cdot 10^6$, N_{crit} = 9

Airfoil	C_{l_α} [1/rad]	$(C_l/C_d)_\alpha$ [-]	α_{stall} [deg]
NACA0009	0.125	22.3	7.7
NACA0010	0.137	22.5	8.4
NACA0012	0.137	22.3	9.4
NACA0015	0.138	21.4	11.7
NACA0018	0.134	20.7	13.6

The vertical tail has less objectives than the horizontal tail. It again needs a large operable window, and a symmetrical airfoil, for the same reasons as the horizontal tail. As previously discussed, the empennage will have a T-tail configuration. A thicker airfoil for the vertical tail is beneficial in carrying the increased loads, as it allows for a wingbox with a larger moment of inertia. It has been decided that the NACA0015 has the lowest thickness that has the benefit of increased strength, and as it appeared to be the most efficient airfoil as described above, it has been selected as the best airfoil for the vertical tail as well.

9.3. Planform Design

Now that the two-dimensional characteristics of the main wing and empennage have been determined, the three-dimensional geometry can be designed such that an accurate estimate of the aircraft's lift and drag can be made.

9.3.1. Main Wing Planform

The sizing of the wing strongly depends on the wing loading, the maximum take-off weight and the placement of the engines. Now, the geometrical parameters needed to describe the wing planform can be calculated as demonstrated below.

Wing surface area

The wing surface area is an important parameter in quantifying how much lift a wing can generate. It is sized for the most critical point in the mission, which is when the aircraft is the heaviest: the MTOW. The design wing loading is determined at take-off. However, when the mission starts with a vertical take-off phase, the wing loading is determined at the point the aircraft will go to its cruise configuration. It is assumed that the fuel burnt during vertical take-off does not have a significant effect on the wing loading and therefore the wing surface area. The wing surface area is then calculated using Equation 9.4.

$$S = \frac{MTOW}{(W/S)_{TO}} \tag{9.4}$$

With the previously determined values, the wing surface area will be 40.6 m^2.

Aspect Ratio

The aspect ratio is a measure for the slenderness of the wing. It greatly influences a number of parameters that describe the behaviour of the wing, like the stall angle, drag, and lift. Moreover, a larger aspect ratio increases the wing weight [108].

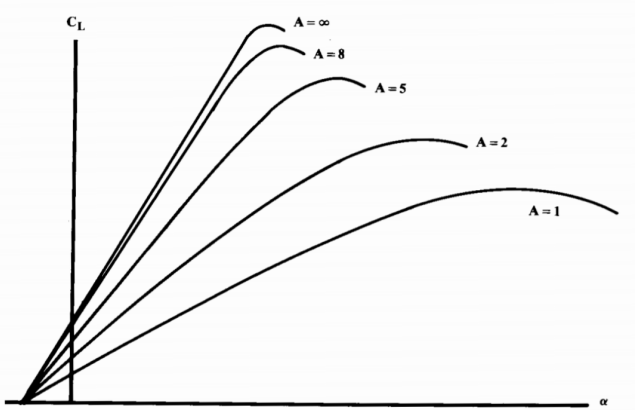

Figure 9.2: Effect of aspect ratio on lift. [117]

As can be seen in Figure 9.2, a smaller aspect ratio increases the stall angle and accelerates the stall behaviour. Stall is a critical scenario for the design case, as the aircraft will fly rather slowly in the conversion from VTOL-mode to the normal configuration. A low aspect ratio is therefore preferred. The same figure also shows that an increase in aspect ratio will increase the lift curve slope and the maximum lift coefficient. From a standpoint of lift, one needs an aspect ratio that is as large as possible. Then, the drag consists of two parts: parasitic and induced drag. As the induced drag scales with the inverse of the aspect ratio, a larger aspect ratio is again preferred. Although a larger aspect ratio would benefit the lift and drag of the wing, an aspect ratio of eight is opted for, as the wing weight was deemed to be the more important argument. A larger aspect ratio increases the wing span and therefore the bending stresses, resulting in a

heavier structure. This argument is especially important in the current design case, as the heavy engines at the wing tips would create exceptionally large bending moments for large wing spans. Another argument for the moderate aspect ratio of eight can be found when looking at Table 9.3, where the equivalent aspect ratios (including canard surface areas if present) of several types of propeller aircraft can be found. These indications found by Raymer [117] show that a ratio of eight would be a reasonable initial value. Note that this relatively low aspect ratio and the high thickness of the chosen airfoil in the following section suits the positioning of batteries in the wing.

Propeller aircraft	Equivalent aspect ratio
General aviation - single engine	7.6
General aviation - twin engine	7.8
Agricultural aircraft	7.5
Twin turboprop	9.2

Table 9.3: Typical equivalent aspect ratios for propeller aircraft categories. The equivalent aspect ratio includes potential canard surface area. [117]

Taper Ratio

Taper ratio is the ratio between the root chord and the tip chord of the aircraft's wing. Two factors are considered essential in selecting the optimal taper ratio for the conceptual design. First of all, the tip chord needs to be large enough to support the engines mounted on the wing tips, a taper ratio of 1 provides the most structural support. Moreover, a taper ratio of 1 ensures a constant cross-section, hence facilitating the manufacturing of the wing. Now, the tip of the (unswept) wing needs to be as close to 0.45 as possible, as this would result in a lift distribution that resembles an elliptic lift distribution the most [117]. In absence of a rotor, an elliptic lift distribution will result in an Oswald efficiency number (e) of 1 (in absence of the engines), minimising induced drag. However, the effect of tip vortices is considered to be negligible, as the rotors of the main engines per definition already create a large vortex, something that cannot be solved with taper. Even if the tip vortex on the wing tip would be of such size that it contributes to the vortex generated by the rotors, the effect on the drag will be mitigated by the fact that the engines work as winglets, increasing the effective aspect ratio and thereby decreasing the induced drag. Combining all of the arguments discussed above, a taper ratio of 1 is selected.

Sweep

The sweep angle of the wing can be determined by analysis of the mission profile. First, it must be noted that as the wing will be untapered, the sweep at any chord location will be the same, and therefore quarter-chord sweep and leading edge sweep are equivalent. Now, when the aircraft will change from VTOL-mode to its cruise configuration, the aircraft's speed will be rather low. As sweep is used decrease the local velocity over the wing, to increase its efficiency, the total lift generated will be lower. A sweep of 0 degrees is therefore selected, as maximum lift will be generated by utilising the entire incoming freestream velocity. This will ensure the aircraft can continue flying in this critical phase. For a cruise speed of 474 km/h and a cruise altitude of 1675 m, it can be calculated that the cruise Mach number is 0.39. Hence, it can be safely assumed that the critical Mach number will be higher than the cruise Mach number, so no sweep is needed with respect to this aspect.

Dihedral

Dihedral is the angle under which the wing is positioned when looking at it from the front. In Table 9.4, typical values of dihedral can be seen [117]. The conceptual design falls in the top-right category, with dihedral ranging from 0 to 2 degrees. In the this stage of the design a dihedral of 0 degrees is selected. As in this case the wing will be straight along its entire span, the structure can be lighter as there are no kinks that need to be reinforced. Moreover, dihedral is also used to improve roll stability. For high-wing configurations this is not necessary as the positioning itself already has a beneficial contribution.

Table 9.4: Dihedral guidelines (degrees). [117]

	Wing position		
	Low	Mid	High
Unswept (civil)	5 to 7	2 to 4	0 to 2
Subsonic swept wing	3 to 7	-2 to 2	-5 to -2
Supersonic swept wing	0 to 5	-5 to 0	-5 to 0

Twist

Typically, geometric twist of the wing is used to prevent tip stall and reshape the lift distribution to a more elliptic shape [117]. This optimisation of the lift distribution, however, is only valid for one lift coefficient, and is therefore not used

in this design case [117]. As the wing is unswept, tip stall will not be a problem as the stall will progress from root to tip [108]. A geometric twist of 0 degrees is therefore selected for the wing.

9.3.2. Empennage Planform

An initial sizing of the surface areas needed for the horizontal and vertical tail can be performed by analysing the OEI-case (one engine inoperative, a set of six engines that is) for the vertical tail, and analysing the moment generated by the lift vector during cruise for the horizontal tail, something that will be discussed later on in this section. These cases can be analysed for a multitude of combinations of geometrical parameters, as the surface area sizings depend on the planforms, and vice versa. This implies an iteration can be performed to come to an optimal solution. In this case the tail with the smallest amount of total surface area as a first indication for the tail weight. The design variables are both aspect ratios (A_h and A_v), and the quarter-chord sweeps ($\Lambda_{c/4,h}$ and $\Lambda_{c/4,v}$) of both tailplanes. Historical data on these variables will serve as an indication for the intervals over which they are iterated, being 1.3-2 for A_v, 3-5 for A_h, 0-20 degrees for $\Lambda_{c/4,v}$, and 0-25 degrees for $\Lambda_{c/4,h}$ [145, 117]. Note that [117] advises a ratio for A_v of 0.7-1.2 if a T-tail is used, to prevent any excessive structural weight. However, the configurations in this range were deemed unfeasible, as the surface areas increased significantly. The accompanying weight increase was of such size that the larger aspect ratios including the structural weight penalty would result in a more optimised configuration.

Now, the first parameter that can be determined from these design variables is the taper ratio of the horizontal tailplane. There are no limitations to this quantity but efficiency. In Equation 9.5 the taper ratio that resembles an elliptic lift distribution the most for a certain sweep angle (in degrees) is calculated [105].

$$\lambda_{\text{opt}} = 0.45 \cdot e^{-0.0375\Lambda_{c/4,h}} \tag{9.5}$$

Next, the surface areas are estimated using the loads in certain cases. The vertical tail load can be estimated by considering the OEI-case as described in Equation 9.6.

$$L_v = \frac{T_{max} \cdot (b/2)}{l_v} \tag{9.6}$$

In this equation T_{max} is the maximum thrust that occurs during cruise, as the vertical tail will be of little use in case of an engine failure in VTOL-mode. Then, l_v is the moment arm, from the center of gravity to the aerodynamic center of the vertical tail. The center of gravity is in its most aft position, as that will result in the largest tail surface and is therefore the critical scenario. The horizontal tail load can be calculated with Equation 9.7.

$$L_h = \left| \frac{L_{cruise} \cdot X_{LEMAC} + 0.25 \cdot c_{MAC} - X_{CG}}{l_h} \right| \tag{9.7}$$

Here, the aerodynamic center is taken to be at the quarter-chord position, and l_h is the moment arm, from the center of gravity to the aerodynamic center of the horizontal tail. As the position of the center of gravity can vary, the extreme cases need to be analysed, which can give a negative load, resulting in the need to the take the absolute value. A couple of assumptions have been made in the loads that the horizontal tail needs to counteract. In a full free body diagram, the moments generated by the fuselage $M_{fuselage}$, nacelles $M_{nacelle}$, and rotors M_{rotor} (due to the change in lift distribution due to the propeller wake), as well as the moment around the aerodynamic center M_{ac} should be taken into account. However, M_{ac} and M_{rotor} were assumed to be negligible compared to the moment generated by the lift force. Moreover, not taking into account $M_{fuselage}$ and $M_{nacelle}$ can be considered to be a conservative estimate [130].

With the loads calculated, the only things that are needed to estimate the surface areas are the lift slopes and the leading edge sweeps. Using the DATCOM method one can obtain the lift slopes as presented in Equation 9.8.

$$C_{L_{\alpha,h/v}} = \frac{2\pi A_{h/v}}{2 + \sqrt{4 + \left(\frac{A_{h/v}\beta}{\eta_{airfoil}}\right)^2 \cdot \left(1 + \frac{\tan^2 \Lambda_{c/2,h/v}}{\beta^2}\right)}} \quad \text{with} \quad \beta = \sqrt{1 - M_\infty^2} \tag{9.8}$$

Subsequently, the surface areas can be calculated with Equation 9.9

$$S_{h/v} = \frac{L_{h/v}}{\frac{1}{2}\rho V_{cruise}^2 C_{L_{\alpha,h/v}} \text{ angle}} \tag{9.9}$$

First of all, in order to calculate the leading edge and half-chord sweep, an initial estimation of the taper ratio of the vertical tail is needed. Next, the angle in Equation 9.9 is the cruise angle of attack in case of the horizontal tail. The

angle in case of the vertical tail is a sideslip angle of five degrees, as it then can be ensured that the vertical tailplane has not stalled yet, with an added twenty degrees of rudder deflection. As the increase in camber due to the rudder deflection simply shifts the lift curve upwards, this rudder deflection angle can be added to the sideslip angle to account for the extra lift generated. Note that the twenty degrees rudder deflection is less than the maximum, to ensure that the aircraft is still able to steer. Additionally, it is assumed that the thrust vector still acts in the direction of the freestream velocity regardless of the five degrees sideslip, as $\cos(5deg) \approx 1$.

From these surface areas, the spans of both tailplanes can be calculated. Now that the geometry of the horizontal tailplane is complete, the root and tip chord can be determined. As the empennage will have a T-tail configuration, the root chord of the horizontal tailplane can be set equal to the tip chord of the vertical tail. The geometry again being complete, the root chord of the vertical tail and its (updated) taper ratio can be determined. The entire empennage is now defined, and therefore the aerodynamic centers can be determined (being at 25 per cent of the mean aerodynamic chord), after which the moment arms can be updated and the next iteration loop can be initiated.

The only thing that is left to do now is to check for deep stall, as mentioned in Section 9.1. The location of the tail is visible in red in Figure 9.3 [117]. As the wing will not experience any pitch-up behaviour (no wing tip stall will occur as there is no sweep), which means that the location of the tail is feasible and safe.

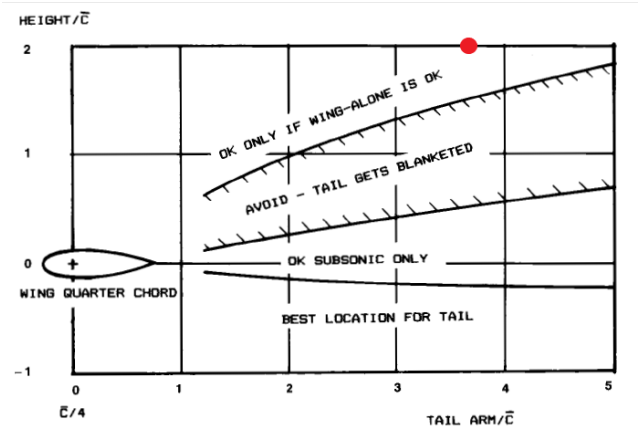

Figure 9.3: Safe tail locations with respect to deep stall, with in red the tail location of the design [117].

In Table 9.5, an overview of the entire empennage is visible.

Table 9.5: Overview of the planform layout of the tailplanes.

Quantity	Value	Quantity	Value	Quantity	Value	Quantity	Value
A_h	3.3	S_h	9.74	b_h	5.67	l_h	10.48
A_v	1.9	S_v	10.70	b_v	4.51	l_v	8.80
λ_h	0.45	$\Lambda_{c/4,h}$	0.0	$c_{root,h}$	2.37	$c_{tip,h}$	1.07
λ_v	1.00	$\Lambda_{c/4,v}$	0.0	$c_{root,v}$	2.38	$c_{tip,v}$	2.37

9.4. Drag Estimation

The drag of the aircraft is split up into two main contributors, induced drag and zero-lift drag, and will therefore be discussed in two different sections.

9.4.1. Class II Drag Estimation

The first part of the class II drag estimation is to determine the zero-lift drag. This is the static drag induced by for example the shape of the fuselage and wing. In order to determine the total zero-lift drag, the zero-lift drag for the different components needs to be determined. These different components are identified to be the wing, fuselage, horizontal tail, vertical tail and engine nacelles. The main method to determine the zero-lift drag of every component is the component build up method which can be seen in Equation 9.10. All the methods and equations used in this subsection are deduced from Raymer [117].

$$C_{D_0} = \frac{1}{S_{\text{ref}}} \sum_c C_{f_c} FF_c IF_c S_{\text{wet}\,c} + \sum C_{D_{\text{misc}}} \tag{9.10}$$

C_{fc} is the skin friction coefficient, FF is the form factor, IF is the interference factor, S_{wet} is the wetted area and $C_{D_{misc}}$ is miscellaneous drag.

Wing zero-lift drag
The skin friction coefficient of the wing is calculated in two parts. One part account for the laminar flow over the wing and the other accounts for the turbulent flow over the wing. In Equation 9.11 and Equation 9.12 the equation used for laminar and turbulent flow can be seen respectively.

$$\text{Laminar}: C_f = \frac{1.328}{\sqrt{Re}} \tag{9.11}$$

$$\text{Turbulent}: C_f = \frac{0.455}{(log(Re))^{2.58}(1 + 0.144M_{cruise}^2)^{0.65}} \tag{9.12}$$

In this equation M_{cruise} is the mach number during cruise and Re is the Reynolds number that can be determined for subsonic speeds with help of the following equation.

$$\text{Subsonic}: Re = \min\left(\frac{\rho V l}{\mu_d}, 38.21(l/k)^{1.053}\right) \tag{9.13}$$

ρ is the air density, V is the velocity, l is the component length (in case of the wing this is the MAC), μ_d is the dynamic viscosity and k is a factor that takes into account the roughness of the skin. The final skin friction coefficient can be determined by adding weighted values for the for the laminar skin friction and turbulent skin friction. These weights are obtained by estimating what part of the component is covered by laminar flow and what part is covered by turbulent flow.

Now that the skin friction coefficient can be determined the form factor can be estimated. This is done by using Equation 9.14.

$$FF = \left[1 + \frac{0.6}{(x/c)_m}\left(\frac{t}{c}\right) + 100\left(\frac{t}{c}\right)^4\right]\left[1.34M^{0.18}\left(\cos\Lambda_m\right)^{0.28}\right] \tag{9.14}$$

$(x/c)_m$ is the location of the maximum thickness over chord as percentage of the chord, t/c is the maximum thickness over chord and Λ_m is the sweep at the location of the maximum thickness over chord. The only unknowns that remain for the zero-lift drag estimation of the wing are the interference factor and the wetted area. The interference factor for the wing is assumed to be one since it is a high wing configuration aircraft. Next to this, the wing wetted area can be determined by Equation 9.15 where S_{ref} is the wing area. The final value for the wing zero-lift drag can be seen in Table 9.6

$$S_{wet_{wing}} = 2.14S_{ref} \tag{9.15}$$

Fuselage zero-lift drag
The skin friction coefficient of the fuselage is calculated with the same method as for the wing. However, for this case the length of the component l, is equal to the fuselage length. The form factor of the fuselage can be determined by Equation 9.16.

$$FF = \left(1 + \frac{60}{f^3} + \frac{f}{400}\right) \tag{9.16}$$

Where f is defined as the length over the diameter of the fuselage. Furthermore, the interference factor was again assumed to be one and the wetted are can be determined by Equation 9.17.

$$S_{wet_{fuselage}} = \frac{\pi D}{4}\left(\frac{1}{3L_1^2}\left[\left(4L_1^2 + \frac{D^2}{4}\right)^{1.5} - \frac{D^3}{8}\right] - D + 4L_2 + 2\sqrt{L_3^2 + \frac{D^2}{4}}\right) \tag{9.17}$$

D is the fuselage diameter and L_1, L_2 and L_3 are nose, cabin and tailcone length respectively. The final value for the zero-lift drag of the fuselage can be seen in Table 9.6.

Horizontal tail zero-lift drag
For the horizontal tail exactly the same method is used as for the estimation of the wing zero-lift drag. There are two main changes however. The first change is that the component length is equal to the horizontal tail MAC. Next to this, the wetted area of the horizontal tail can be determined by Equation 9.18 where S_h is the horizontal tail surface area. The interference factor of the horizontal tail is assumed to be 1.04 since this is the interference factor of a T-tail. The final value for the horizontal tail zero-lift drag can be seen in Table 9.6.

$$S_{wet_{tail}} = 2.1 S_h \tag{9.18}$$

Vertical tail zero-lift drag
The vertical tail is approximated almost the same as the horizontal tail. However, the component length is equal to the vertical tail MAC and the wetted area is also calculated by Equation 9.18 but this time the input will be the vertical tail area (S_v) instead of the horizontal tail area (S_h). Next to this, the interference factor is the same since it is still a T-tail configuration. At last, the final value for the vertical tail zero-lift drag can be seen in Table 9.6.

Nacelle zero-lift drag
Last but not least, the nacelle drag is taken into account. Again Equation 9.11 and Equation 9.12 are used to calculate the skin friction coefficient but this time the component length is the length of the nacelle. Next to this, the form factor of the nacelles can be determined by the following equation where f is the nacelle diameter divided by the nacelle length.

$$FF = 1 + \frac{0.35}{f} \tag{9.19}$$

The interference factor of the nacelle is determined to be one since it is place quite a distance away from fuselage and the wetted area is approximated by assuming that the nacelle is a straight cylinder. The final value for the nacelle zero-lift drag can be seen in Table 9.6.

Final zero-lift drag
Before the final zero lift drag can be determined one kind of miscellaneous drag still needs to be taken into account. This is the upsweep drag. This is a drag that is induced by the upsweep of the tailcone of the aircraft and can be determined by Equation 9.20.

$$C_{D_{upsweep}} = 3.83 u^{2.5} A_{max} \frac{1}{S_{ref}} \tag{9.20}$$

In this equation u is the upsweep angle, A_{max} is the maximum fuselage area and S_{ref} is the wing area. The final values for the zero-lift drag and its summation can be seen in Table 9.6.

Table 9.6: The final values for the zero-lift drag estimation.

Component	C_{D0}
Wing	0.00688
Fuselage	0.00736
Horizontal tail	0.00111
Vertical tail	0.00205
Nacelles	0.00030
Upsweep	0.00872
Total	0.02642

9.4.2. Induced Drag

The induced drag coefficient is calculated using Equation 9.21.

$$C_{D_i} = \frac{C_L^2}{\pi A e} \tag{9.21}$$

The aspect ratio of the main wing is already determined, and the lift coefficient depends on the mission phase. Hence, the only factor not yet known is the Oswald efficiency factor e, which is determined following the procedure in [105]. The theoretical Oswald factor can be determined using Equation 9.22.

$$e_{\text{theo}} = \frac{1}{1 + f(\lambda) \cdot A} \quad \text{with} \quad f(\lambda) = 0.0524\lambda^4 - 0.15\lambda^3 + 0.1659\lambda^2 - 0.0706\lambda + 0.0119 \tag{9.22}$$

Then, the actual Oswald factor is determined per Equation 9.23, taking into account a compressibility correction factor, an inviscid and a viscid term.

$$e = \frac{k_{e,M}}{Q + P\pi A} \quad \text{with} \quad Q = \frac{1}{e_{\text{theo}} \cdot k_{e,F}}, \quad P = KC_{D,0} \quad \text{and} \quad K = 0.38 \tag{9.23}$$

The fuselage and compressibility correction terms are then calculated with the help of Equation 9.24.

$$k_{e,F} = 1 - 2\left(\frac{d_F}{b}\right)^2, \quad k_{e,M} = \begin{cases} a_e\left(\frac{M}{0.3} - 1\right)^{b_e} + 1, M > 0.3 \\ 1, M \leq 0.3 \end{cases} \quad \text{with} a_e = -0.001521, \quad \text{and} \quad b_e = 10.82 \tag{9.24}$$

The wing is modelled as a theoretical wing, without engines present at the wing tips. In reality, as the rotors are turning inboard-up, the wing will experience an upwash. The total force vector on the wing will tilt forward, and therefore the lift will have a component in the positive axial direction, counteracting the drag (and therefore increasing e) [134]. As it is not known to what extent this effect is present, the theoretical wing is used as a conservative estimate. As a side note, the impingement of the rotor blade wakes and the tip vortices will cause a fluctuating wing loading, but the effect of this unsteady interaction on the time-averaged performance will be negligible [134].

All factors combined, the method in this section yields an Oswald efficiency factor of 0.66 for the current design.

9.5. Drag Polar

Combining the zero-lift drag coefficient $C_{D,0}$ and the Oswald efficiency factor e, as determined in Section 9.4.2 and Section 9.4.1, one can plot the drag polar, as visible in Figure 9.4, defined by Equation 9.25. It must be noted that the range of lift coefficients is that in which the main wing will not have stalled yet, as determined in Figure 8.8.

$$C_D = C_{D,0} + \frac{C_L^2}{\pi A e} \tag{9.25}$$

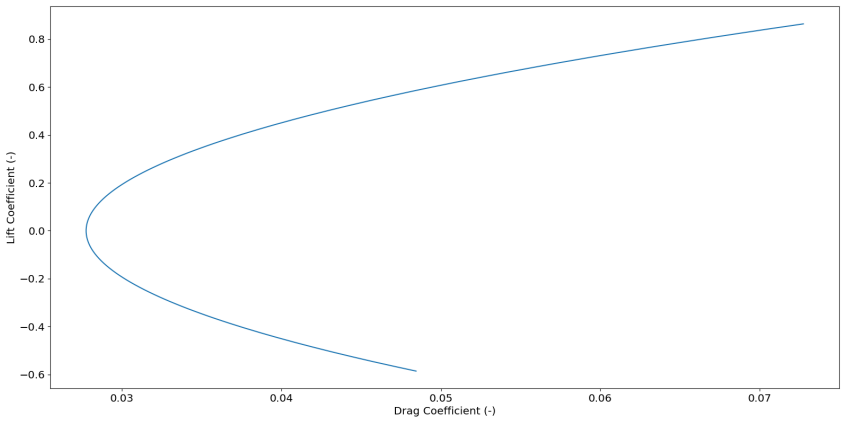

Figure 9.4: Drag polar of the aircraft in cruise.

9.6. Validation

It is essential to verify the results in order to come to a realistic design. In verifying the aerodynamic parameters, the parameter is considered validated if the difference is less than ten per cent.

9.6.1. XFLR5

Now, certain calculated parameters can be validated with the use of XFLR5, for example the lift slopes of the main wing and the tailplanes, and the zero-lift angle of attack of the main wing. Moreover, the $C_{D,0}$ of the main wing, as well as both tailplanes can be determined using the software. In Table 9.7, the lift slopes of all the aerodynamic surfaces as outputted by both the DATCOM-method and XFLR5 are visible, along with the difference. Moreover, the zero-lift angle

of attack for both methods is shown. In XFLR5, the ring vortex VLM (vortex lattice method) has been used, together with the aircraft's cruise speed, MTOW, altitude, and wing planform.

Table 9.7: Lift slopes, zero-lift angle of attack, and zero-lift drag coefficients for the aerodynamic surfaces as calculated with XFLR5 and the DATCOM-method or the Class II Drag Estimation.

Parameter	DATCOM or Class II Drag Estimation	XFLR5	Difference
C_{L_α} Main Wing [1/rad]	5.046	4.624	8.73%
α_0 Main Wing [deg]	1.987	1.548	24.8 %
C_{L_α} Horizontal Tail [1/rad]	3.404	3.421	0.498%
C_{L_α} Vertical Tail [1/rad]	2.526	2.429	3.92%
$C_{D,0}$ Main Wing [-]	0.00688	0.00615	11.2%
$C_{D,0}$ Horizontal Tail [-]	0.00111	0.00530	131%
$C_{D,0}$ Vertical Tail [-]	0.00205	0.00528	88.1%

It can be observed that all lift slopes can be considered validated, while the zero-lift angle of attack and the drag coefficients are not. The airfoil value for the zero-lift angle of attack was used, which may explain the difference with the result generated by XFLR5. It is recommended that a further look is taken at the estimation of the zero-lift drag coefficients of the aerodynamic surfaces.

9.6.2. XFOIL

With the help of XFOIL, the assumption that the aerodynamic center is at 25 per cent of the chord can be validated. The location around which the moment coefficient is calculated can be varied, and if the outputted moment coefficients do not change with angle of attack, the aerodynamic center is found. It is determined that at a location of 0.262c, the moment coefficient does not vary in the first three decimals. This location differs 4.69% from the initial assumed value, and is therefore considered validated.

9.6.3. Design Variable Step Sizes

A last verification test that can be performed is varying the step size of the design variables (A_h,A_v,$\Lambda_{c/4,h}$,$\Lambda_{c/4,v}$) over the iteration ranges, and investigating the convergence of the solution. The output for different step sizes is visible in Table 9.8. It can be observed that the solution converges.

Table 9.8: Output of the design variables for different step sizes of the iteration intervals.

Stepsize	0.5	0.1	0.01	0.001	0.0001
A_h	3.0	3.3	3.39	3.398	3.3999
A_v	1.8	1.9	1.93	1.932	1.9327
$\Lambda_{c/4,h}$	0.5	0.0	0.00	0.007	0.0007
$\Lambda_{c/4,v}$	0.0	0.0	0.91	0.800	0.7950

Note that the result for the smallest step size differs from that discussed in Table 9.5, it may even be a more optimised solution. However, as decreasing the step size becomes rather expensive rapidly, a smaller step size needed to be used in the total iteration, leading to slightly different results as those presented in Table 9.8.

Then, the iteration threshold can be varied. Again, setting a smaller tolerance should lead to convergence of the solution, something that can indeed be observed when looking at Table 9.9.

Table 9.9: Output of the design variables for different tolerances of iteration.

Tolerance	0.5	0.1	0.01	0.001	0.0001
A_h	3.4	3.3	3.3	3.3	3.3
A_v	1.9	1.9	1.9	1.9	1.9
$\Lambda_{c/4,h}$	0.0	0.0	0.0	0.0	0.0
$\Lambda_{c/4,v}$	0.0	0.0	2.0	2.0	2.0

Again, the computation becomes greatly more expensive with decreasing tolerance. A tolerance of 0.1 was deemed to give accurate results, while keeping computational time to a minimum.

10. Structural Analysis

An important part of the aircraft design is to make sure that all the structures inside the aircraft can carry the loads that they need to. In this chapter an elaborate analysis will be given on the different structural parts of the aircraft. In Section 10.1 the structural design of hydrogen tank will be done in order to store the cryogenic hydrogen in an efficient and safe way. This will be followed by a wing box analysis in Section 10.2. In Section 10.3 the fuselage design will presented so it can withstand all the loads that it is subjected to after which an aeroelastic analysis of the tilt rotor wing of the aircraft is done in Section 10.4. This chapter will be concluded with a section on the landing gear placement and design.

10.1. Hydrogen Tank Design

Storing liquid hydrogen at cryogenic temperatures onboard of an aircraft results in a challenging design both mechanically as thermally. The materials used for these applications should have sufficient mechanical properties at cryogenic temperatures where most materials become brittle. For the thermal design, the spontaneous heat transfer from the ambient environment to the cryogenic hydrogen should be as low as possible for long and safe storage. No active cooling system is used since this significantly adds up to the weight of aircraft. Therefore a passive insulation thermal design is required. The critical design temperature range is between the storage temperature of LH_2, $T_{min} = 20$ K and the maximum ambient temperature taken at $T_{max} = 323$ K. The midterm design of the H2-VTOO mission uses swappable tanks that reduce the refuelling time and complexity. However, detailed design of the mission increased the required hydrogen fuel mass at such extend that swappable tanks would result in a too large fuselage length for easy maneuverability on helipads. Therefore it was opted for a single tank design that allows for more compact storage of the hydrogen. A detailed discussion on this design change is provided in Section 10.1.7. The single tank requires an extra maximum 1 hour storage duration on top of the 4.5 hours range duration for ground time between refuelling and end of mission, as discussed in Chapter 6.

10.1.1. Aspects of liquid hydrogen

Molecular hydrogen occurs in two states; ortho-hydrogen and para-hydrogen [102]. Ortho hydrogen (with parallel nuclear spin) and para-hydrogen (with anti-parallel nuclear spin) have the same chemical properties but slightly different physical properties due to their different spin orientation. At room temperature, an equilibrium mixture of hydrogen consists of 75% ortho-hydrogen and 25% para-hydrogen. This mixture changes with temperature since para-hydrogen has higher stability at low temperatures. The reason being that the anti-parallel nuclear spin is the ground state and therefore at T = 0 K, 100% para-hydrogen will be present. The ortho-para conversion is an exothermic reaction and the released conversion heat will evaporate liquid hydrogen, which is called boil-off and is detrimental for the safe storage of liquid hydrogen. In order to minimise boil-off during storage, the amount of ortho-hydrogen should be minimised and the ortho-para conversion should be performed during liquefaction. At equilibrium at storage temperature 20 K, 99.8% para-hydrogen and 0.2% ortho-hydrogen are achieved after a lengthy natural conversion process. However the conversion is shortened with the use of suitable catalysts such as iron oxide (Fe2O3-2%H2O,IONEXs), and chromium(II) oxide doped silica catalyst (CrO-SiO2,OXISORBs) [61]. Since the hydrogen storage mixture consists of 99.8% para-hydrogen, the physical properties of para-hydrogen will be used during the design.

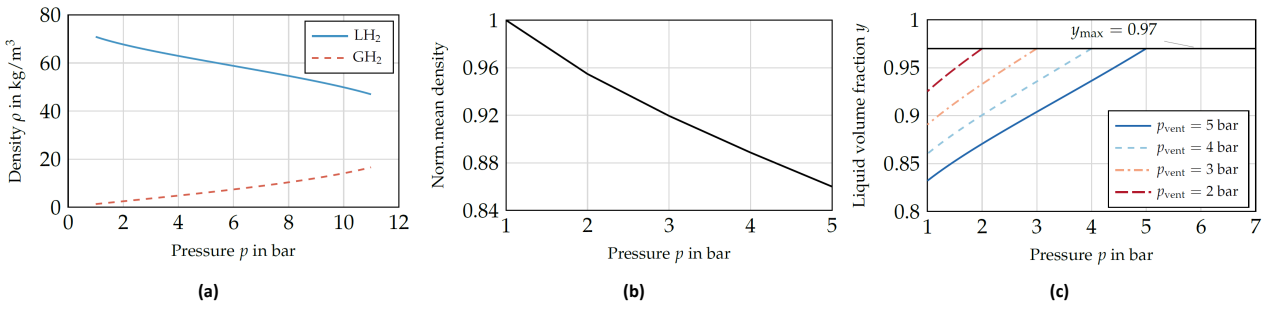

Figure 10.1: Density of both LH_2 and GH_2 as function of pressure (a), (b) density of LH_2 mixture normalized with respect to density at 1 bar and (c) the effect of filling pressure p_{fill} on the achieved volume fraction [154].

10.1.2. Tank sizing

Hydrogen is stored at its saturation condition to reduce the high volumetric energy density of gaseous hydrogen [151]. Therefore both liquid and gaseous phases of hydrogen are present in the storage tank. When the tank is stored in the aircraft, a non-zero heat input will exist that increase the pressure in the tank due to boil-off. Boil-off is the evaporation of liquid hydrogen LH_2 to gaseous hydrogen GH_2. When the pressure becomes too high, some gaseous hydrogen hydrogen should be vented to avoid structural damage. This prescribed pressure is the venting pressure p_{vent}. Figure 10.1a shows that the density of LH_2 decreases with increasing pressure while the density of $CH2$ increases but less steep. Overall, the density of the hydrogen mixture decreases with increasing pressure as shown in Figure 10.1b. Therefore the maximum storage pressure, i.e. venting pressure p_{vent}, should be minimised to have the highest density, hence lowest storage volume. However an important safety concern to be considered is that when p_{vent} is lower than the ambient pressure, air would penetrate the tank in case of leakage which creates an explosive mixture. Therefore, LH_2 should have a venting pressure higher than ambient pressure. However the venting pressure is set slightly higher than the required hydrogen feed pressure of the fuel cells in order to have a spontaneous feed flow to the fuel cells, i.e. $p_{vent} = 2.5$ bar. To allow for this venting of gaseous hydrogen, the tanks should be designed with a 3% volume for the gaseous hydrogen, resulting in a volume fraction of liquid hydrogen of $y = 97\%$. Another important aspect is the filling pressure p_{fill} at which the hydrogen is added to the tank. When p_{fill} is increased, the achievable LH_2 volume fraction is increased and more hydrogen can be stored. Therefore $p_{fill} > p_{vent}$ is used and a liquid volume fraction of $y = 97\%$ is reached.

For $p_{vent} = 2.5$ bar, the LH_2 density is obtained from Figure 10.1a and is 67.3 kg/m^3. The density of the gaseous hydrogen is 2.9 kg/m^3, obtained from the ideal gas law with p $= 2.5$ bar. The density of the saturated hydrogen mixture is now given by

$$\rho_{stored} = (1 - y) \cdot \rho_{cH_2} + y \cdot \rho_{LH_2} \tag{10.1}$$

and yields ρ_{stored}= 65.1 kg/m^3 for $y = 97\%$. To account for boil-off, c% of the required fuel volume m_{req} should be taken as reserve, resulting in a required fuel volume of

$$V_{req} = \frac{m_{req} \cdot (1 + c)}{\rho_{stored}}. \tag{10.2}$$

10.1.3. Tank geometry

The lowest heat losses are obtained by the lowest surface area to volume ratio (S/V). This ratio is the lowest for a spherical tank design and will therefore result in the lowest insulation mass. In addition, spherical tanks are excellent for the mechanical design since it has only circumferential stresses and has uniform thermal strains. However, due to diameter limitations on spherical tanks in the fuselage, cylindrical tanks with spherical end caps are required. The increase of (S/V) for cylindrical tanks is only 10% with respect to spherical tanks, hence no major influence on the heat losses is expected [102]. In addition, cylindrical tanks lead to less drag due to lower frontal surface area compared to spherical tanks with equal volume. The cylindrical tank geometry is shown in Figure 10.2. An optimal value of 1 for $\phi = \frac{a}{c}$ was opted for because it had a significant higher gravimetric efficiency than elliptical tanks, leading to higher tank masses as discussed in [154]. A value of 1 for ratio $\psi = \frac{b}{c}$ was opted for to have spherical end caps with optimal (S/V) ratio. The influence of the ratio λ on the gravimetric efficiency is not significant and therefore its value was set conveniently to accommodate the required hydrogen volume to be stored in the fuselage.

The S/V ratio decreases for increasing tank size, hence decreasing the heat losses and boil-off. Therefore, a single tank design yields a lower insulation mass than a combination of smaller swappable tanks.

10.1.4. Mechanical design

Tank material

Materials with high specific strength & stiffness, high fracture toughness and low hydrogen permeability are desired as tank wall material for cryogenic applications. The high fracture toughness is required for damage tolerance at cryogenic temperatures where most materials become brittle. Monolithic metals, polymer matrix composites reinforced with continuous fibres (PMCs) and discontinuous reinforced metallic composites (DRXs) are suggested by NASA [**noauthor_nasa_nodate**]. An overview of their advantages and disadvantages are provided in Table 10.2.

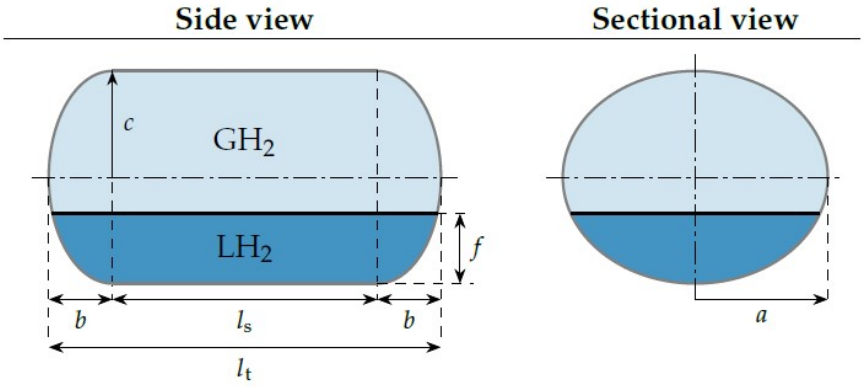

Figure 10.2: Cylindrical tank geometry. Ratios $\lambda = \frac{l_s}{l_t}$, $\phi = \frac{a}{c}$, $\psi = \frac{b}{c}$ [154].

Table 10.1: Tank wall material comparison obtained from [**noauthor_nasa_nodate**]. Monolithic metals, polymer matrix composites reinforced with continuous fibres (PMCs) and discontinuous reinforced metallic composites (DRXs) are considered.

Insulation material	Advantages	Disadvantages
Monolithic metals	High TRL, low cost, low manufacturing complexity, insignificant permeation	Higher mass
PMCs	High specific strength and stiffness	Highest cost, hydrogen permeation, microcracking due to CTE differences, manufacturing difficulties
DRXs	Lowest mass, lower cost than PMCs	CTE mismatches, manufacturing complexity, high cost

Main disadvantage of the composites PMCs and DRXs are the mismatches in CTEs between there constituents which result in microcracking during thermal cycling of the tanks. Therefore, despite their significant weight savings, it is opted for monolithic metals which also have great recycability characteristics compared to composites which are hard to recycle.

Within the monolithic metals class, hydrogen embrittlement at the cryogenic temperatures is an important trade-off criteria because the induced cracks result in material failure at stress levels significantly lower than their yield stress. High strength metals such as steel and titanium are very susceptible to this, while aluminium shows minimal effects to hydrogen embrittlement. The reason for this is aluminium's face-centered cubic structure that limits the solubility of hydrogen in its crystal structure [151]. It is opted for Alluminium alloy 2219 which is used in the LH_2 tanks of Ariane 4 and 5 [151]. Al-2219 has a density of 2825 kg/m^3 and limited stress K = 172.4 MPa [154].

Wall thickness

The tank consists of the cylindrical shell with two hemispherical end caps. The stresses in both sections are different which allows for a variable thickness. The wall thickness s_{wc} for the cylindrical shell is calculated with

$$s_{\mathrm{wc}} = \frac{p_{\mathrm{p}} \cdot d_{\mathrm{i}}}{v\left(2K/S - p_{\mathrm{p}}\right)} + c_1 + c_2 \tag{10.3}$$

where p_p is the design pressure, v the weld efficiency, S the safety factor, c_1 the allowance for permissible wall thickness shortfall, c_2 the allowance for corrosion and wear and K the material limited stress. The mandated safety factors for conservative materials are in the range 1.4-2.0 but a slightly higher safety factor of 2.25 is opted for. The reason for this is that behaviour of materials at cryogenic temperatures is not really well characterized [**noauthor_nasa_nodate**]. Since the tank wall material is surrounded and protected by insulation material, the allowances are both set to zero $c_1 = c_2 = 0$. The design pressure p_p includes venting pressure and dynamic loads. The dynamic loads are calculated with the ultimate load factor $n_{ult} = 4.9$ resulting in the induced stress σ_{dyn} of

$$\sigma_{dyn} = \frac{m_{req} n_{ult} g}{(2\pi r + 2l_{cyl}) s_{wc}} \tag{10.4}$$

where it is assumed that the acceleration causes a uniform stress along its circumference of the cylindrical tank. Stresses due to the venting pressure in the spherical end caps are halve as in the cylindrical part. However, to reduce manufacturing complexity and reduce induced stresses due to thermal expansion mismatches, s_{ws} is taken equal to s_{wc}.

10.1.5. Thermal design

A passive cooling system is preferred instead of an active cooling system that leads to large weight increases. Insulation material is placed at the outside of the tank wall rather than the inside because the latter case cripples the insulation material due to the cryogenic hydrogen temperature [154]. This is detrimental for its insulating performance.

Insulation material

The choice of insulation material is crucial in the LH_2 tank design to minimise LH_2 boil-off while minimising the tank mass. A good insulation material has a low thermal conductivity and diffusivity together with a low mass density preferred for aircraft applications. The thermal conductivity λ should be kept low to minimise thermal heat flux into the LH_2 tank. The thermal diffusivity a determines the time required to reach thermal equilibrium and should be minimised as well to allow for long storage.

Three material options were considered that are most promising for aviation applications; foams, aerogels and multi-layer insulation (MLI) [151]. A comparison of these three options is provided in Table 10.2. The materials are listed in order of increasing thermal performance, meaning that foam performs worst and MLI the best. Although MLI has a thermal conductivity of two orders of magnitude lower than foams, two thick tank walls are required for the vacuum. This increase in weight offsets the thicker insulation required for foams due to their higher thermal conductivity. In addition, the risk of mission failure when loss of vacuum is experienced, currently prevents their use in aviation. Aerogels have a slightly better performance than low-density foams. However their extremely low thermal conductivity ($40 \cdot 10^{-3}$ W/mK), caused by its low density and high porosity, also makes the material very brittle and fragile. Therefore their usage in load-bearing aircraft application are not yet ready. This makes foam the preferred insulation material for the H2-VTOO LH_2 tank. The usage of foam as tank insulation in aerospace applications has been demonstrated in among other the Ariane 5 [1].

Table 10.2: Insulation material comparison obtained from [**noauthor_nasa_nodate**]. Foams, aerogels and multi-layer insulation (MLI) are considered.

Insulation material	Advantages	Disadvantages
Foam	High TRL, light weight, low cost, safe & thermal performance characteristics	Relatively higher thermal conductivity
Aerogel	Extremely low thermal conductivity	New material (low TRL), limited mechanical properties
MLI	Very low density, high TRL, very low thermal conductivity and radiation heat transfer	Heavier tank wall mass required, safety risks when vacuum loss, high manufacturing & maintenance costs

Closed cell insulation foams are chosen instead of open cell foams insulation to avoid ”cryo-pumping” which is the condensation of atmospheric gases on the cold surface. The closed cell foams prevent penetration of the atmospheric gases through the insulation. Verstraete [151] recommended two closed foam cells materials; polyurethane foams (PU) and polymethacrylimide foam (PMI), also called the Rohacell. The properties of both materials are listed in Table 10.3.

Table 10.3: Properties of PMI and PU.

Insulation material	ρ (kg/m3)	σ_y (MPa)	λ (W/mK)	Thermal cycling (4000 cycl.)
PMI	51.1	3.3	0.022-0.035	Failed structurally but no thermal degradation
PU	32.0	1.0	0.005-0.035	No thermal & no mechanical degradation

Verstraete [151] modelled LH_2 tanks for a regional airliner with an endurance of 5 flight hours which is representative for the 4.5-hours design mission profile of the H2-VTOO mission. Tanks with polyurethance foam lead to an increase in gravimetric efficiency in the order of 1% to 3% when compared to tanks with polymethacrylimide foam. Due to this mass benefit and also the better thermal cycling performance after 4000 cycles (Table 10.3) makes the PU the preferred insulation material. The usage of polyurethane foams have been demonstrated as insulation material in the LH_2 tanks of the Saturn V, which stored 69, 000 kg of liquid hydrogen in cylindrical tank [74]. Currently PU-foam is being developed by ESA for usage as external thermal insulation on the Ariane 6 launch vehicle [1].

The thermal conductivity increases with increasing temperature for foams. Figure 10.3 shows this behaviour for PU and PMI foam. This variation is important to consider for the thermal since the temperature of the foam varies from approximately T = 323 K on the exterior to T = 20 K on the interior.

[1] https://www.esa.int/Enabling_Support/Space_Engineering_Technology/Greener_polyurethanes_for_space_and_beyond

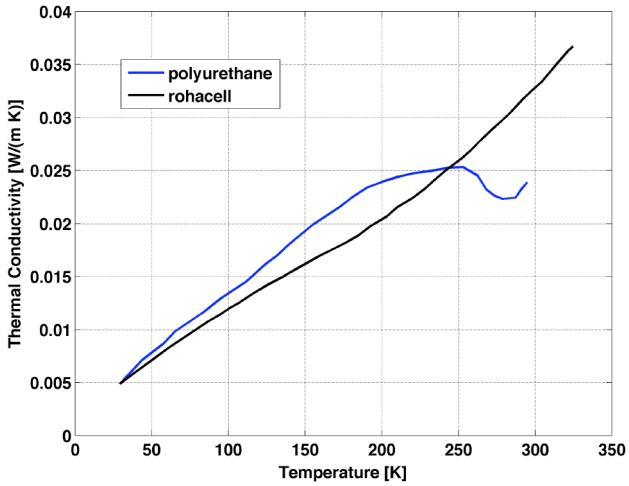

Figure 10.3: Variation of thermal conductivity PU and PMI foam [151].

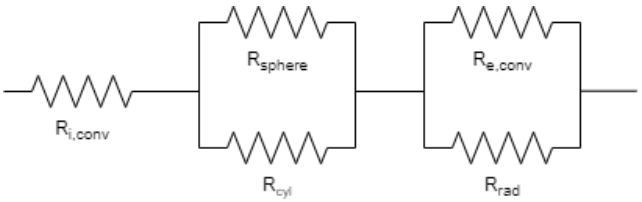

Figure 10.4: Thermal resistance model. R_{rad} the thermal resistance due to radiation, R_{sphere} the thermal resistance of the spherical end caps due to conduction, R_{cyl} the thermal resistance of the cylindrical shell, $R_{e,conv}$ the thermal resistance due to external convection and R_{rad} the thermal resistance due to radiation.

Thermal model

Thermal analysis of the closed PU-foam insulation is required to determine its thickness and the insulation mass. The thermal model developed for the tank is based on the electric circuit analogy [151]. The thermal resistance circuit is shown in Figure 10.4. The contribution of the internal and external convection $R_{i,conv}$ and $R_{e,conv}$ and radiation R_{rad} are not taken into account in this model. The reason is that their thermal resistance is small compared to R_{sphere} and R_{cyl} for low-conductive foams and are therefore omitted due to their calculation complexity. This approach is conservative since it lowers the thermal conductivity, hence thicker insulation required. The thermal resistance of the spherical end caps R_{sphere} and the thermal resistance of the cylindrical shell R_{cyl} are placed in parallel. These two components are the heat transfer due to thermal conduction through the insulation material. It is also assumed that solely the foam insulation contributes to the conduction and not the tank wall material with high λ. This is again a conservative approach since it results in a lower thermal resistance, hence thicker insulation required. The equations for R_{cyl} and R_{sphere} are provided in Equation 10.5 and Equation 10.6 respectively.

$$R_{cyl} = \frac{1}{2 \cdot \pi \cdot r_i \cdot l_{\text{tank}}} \cdot \frac{\ln\left(\frac{r_o}{r_i}\right)}{\lambda_{\text{foam}}} \tag{10.5}$$

$$R_{sphere} = \frac{r_o - r_i}{4\pi\lambda_{\text{foam}} r_i r_o} \tag{10.6}$$

The thermal conductivity of PU-foam changes with temperature as shown in Figure 10.3. Therefore the foam insulation layer was modelled in n-layers to account for these variations. To determine the temperature and conductivity in each layer, the principle of constant heat flux through each layer at steady state conditions was used.

$$R_{tot} = \left(\frac{1}{R_{sphere}} + \frac{1}{R_{cyl}}\right)^{-1} \tag{10.7}$$

$$Q = 1.3 \cdot \frac{T_{max} - T_{H_2}}{R_{tot}} \tag{10.8}$$

The total thermal resistance is given by the parallel resistor theorem in Equation 10.7. The heat flux though the material is now given by Equation 10.1.5 where the extra 30% is taken to account for the additional heat input through the supports [151]. The thermal resistance R_{tot} is iterated until it matches the maximum allowable heat input.

Two operational maximum heat fluxes should be considered. The heat flux through the tanks during storage is used to evaporate the boil-off concentration c and is given by Equation 10.9 where H_{evap} is the evaporation heat of liquid hydrogen (446 kJ/kg) and $t_{max} = 1$ hour, the maximum storage time between tank filling and loading in the aircraft, as

discussed in Chapter 6. The other operational heat flux is the heat flux through the tanks during flight which is used to evaporate the m_{req} to be used in gaseous phase in the fuel cells. This heat flux is given by Equation 10.10 with $t_{range} = 4.5$ hours the range duration. Since $Q_{max_1} < Q_{max_2}$, the insulation thickness was iterated for an allowable heat input of Q_{max_1}.

$$Q_{max_1} = \frac{c \cdot m_{req} \cdot H_{evap}}{t_{max}} \quad (10.9) \qquad Q_{max_2} = \frac{m_{req} \cdot H_{evap}}{t_{range}} \quad (10.10)$$

10.1.6. Integrated design

The tank consists of four layers; tank wall, thermal insulation layer, vapor barrier and fairing. An overview of this configuration is provided in Figure 10.5. The fairing protects the tank against foreign object damages. A kevlar epoxy composite is used with $t = 1.57$ cm and $\rho = 830.6$ kg/m^3. To prevent hydrogen permeation, a MAAMF vapor barrier with $\rho = 0.22$ kg/m^3 and t = 0.5 cm [154]. The foam insulation is applied externally to the tank wall that carries the mechanical loads. The open cell foam and purge channel filled with nitrogen allows for dimensional changes due to thermal cycling to reduce the induced stresses.

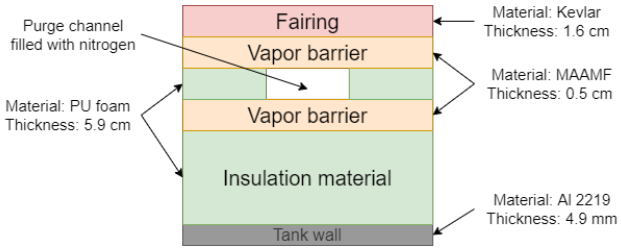

Figure 10.5: Overview of tank configuration.

From the thermal model, the required insulation thickness can be obtained. However the optimal boil-off concentration c should be determined based on the gravimetric and volumetric efficiency of the tank. The gravimetric and volumetric efficiency is given by respectively Equation 10.11 and Equation 10.12 with m_{req} and V_{req} the required hydrogen volume and mass and m_{tank} and V_{tank} the tank wall and tank insulation mass and volume.

$$\eta_{grav} = \frac{m_{req}}{(c+1) \cdot m_{req} + m_{tank}} \quad (10.11) \qquad \eta_{vol} = \frac{V_{req}}{(c+1) \cdot V_{req} + V_{tank}} \quad (10.12)$$

Both efficiencies are calculated in function of the boil-off concentration c for a tank that stores $m_{req} = 807$ kg with tank wall inner diameter d = 2.40 m. The results are shown in Figure 10.6 and $c = 3.5\%$ was chosen due to the high efficiencies η_{grav} and η_{vol}, while not having too much reserve fuel that increases the fuel costs. With this value of c, the insulation thickness s_i and wall thickness s_w were determined for a tank diameter d and cylindrical shell length l_{cyl} that fits the inner fuselage diameter of $d_{inner} = 2.6$ m with a clearance spacing of 5 cm. The results are listed in Table 10.4.

Table 10.4: Final design parameters for $m_{req} = 807$ kg for single tank design with boil-off reserve $c = 3.5\%$.

Parameter	Value	Unit
d	2.4	m
l_{cyl}	1.24	m
s_i	5.7	cm
s_w	4.9	mm
η_{grav}	63.4	%
η_{vol}	86.1	%

Table 10.5: Final design parameters for swappable tanks to store total of $m_{req} = 807$ kg with boil-off reserve $c = 3.5\%$.

Parameter	Value	Unit
d	0.95	m
l_{cyl}	0.68	m
s_i	16.9	cm
s_w	1.9	mm
n_{tanks}	16	-
η_{grav}	50.3	%
η_{vol}	51.2	%

The clearance spacing is used for the struts that are used to connect the hydrogen tank to the fuselage. Since the hydrogen should be replaceable after their lifetime, these connections should be removable. A detailed structural design is not covered in this design phase.

10.1.7. Comparison with single tank design

To justify the choice for single tank design instead of the initial swappable tank design, the final design parameters for swappable tanks placed laterally in the fuselage two by two are listed in Table 10.5 and compared with Table 10.4. A

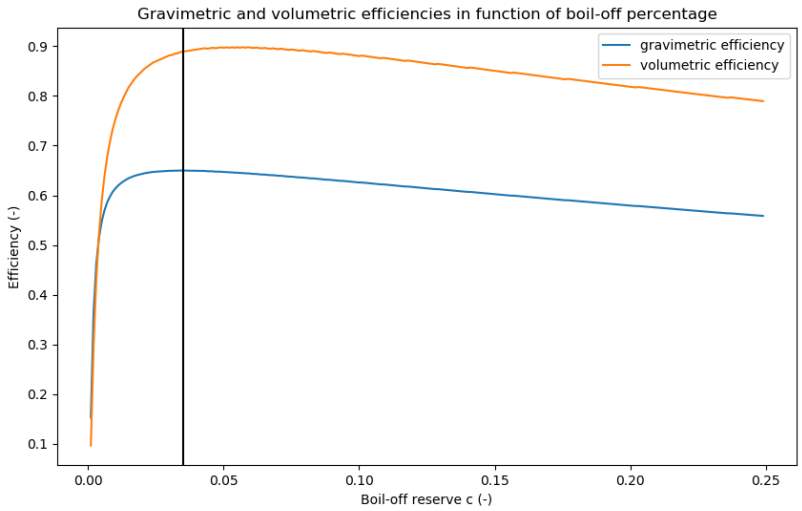

Figure 10.6: Gravimetric and volumetric efficiencies in function of boil-off concentration c for a tank with m_{req} = 807 kg and tank inner tank diameter d = 2.4 m.

total of 16 swappable tanks are required to store the 955 kg of hydrogen. This swappable tank configuration results in a storage length of 8.5 m, bringing the total fuselage length at a total of around 25 m. This large length is not desired for landing on helipads and decrease the aircraft's manoeuvrability. The single tank design only has a storage length of 3.2 m, making the fuselage shorter with 5.3 m and is therefore the preferred configuration.
An important advantage considered in the trade-off for swappable tanks is that for missions with ranges below the maximum range of 2500 km, a smaller number of tanks can be taken onboard of the aircraft, hence decreasing the structural mass. For a single tank design this is not possible and the whole tank should be carried during each mission. However, $\eta_{grav} = 50.6\%$ which is significantly lower than $\eta_{grav} = 64.4\%$ for single tank, might nullify this advantage and a detailed calculation was performed. An overview of the range distribution of flights within Europe was obtained from [109]. The number of tanks is scaled linearly with respect to the 16 tanks required for maximum 2500 km range, not taking into account the small snowball effect of the m_{req} due to lower structural mass. The average number of tanks is determined at 7.5 resulting in an average tank mass of 451 kg. This is indeed lower than the single tank mass of 550 kg. However the extra fuselage length of 5.3 m nullifies this mass benefit of 99 kg. From the class II weight estimation, the fuselage mass over length ratio equals 75.7 kg/m, yielding a mass of 401.1 kg for the additional 5.3 m. In addition, the total tank mass for the maximum of 16 tanks is 961 kg, meaning that the design aircraft mass will be around 812 kg higher than for single tank design which increases the mass of other subsystem due to the corresponding snowball effect. Therefore a single tank design is determined to the design option with the lowest mass.

10.1.8. Hydrogen Handling

The hydrogen should be transported to the rest of the aircraft safely and efficiently. An overview of the hydrogen handling system is depicted in Figure 10.7 and shows the venting, refuelling and fuel delivery system which will be explained in this subsection.

Venting system

As explained, the non-zero heat flux through the thermal insulation of the tank will generate GH_2. In order to avoid overpressurization, a venting valve is installed in the tank that self-activates itself when the prescribed p_{vent} is reached. Since malfunction of this pressure will result in catastrophic failure of the mission, a redundant safety valve is installed on a Y-junction. This safety valve has a slightly higher pressure threshold and self-activates in the event that the primary venting valve malfunctions and pressure is building up. A preliminary sizing of the venting valve system is derived from the Bernouilli equation for incompressible flow. The mass flow through the venting orifice is given by [71]

$$\dot{m}_{\text{vent}} = c_{\text{dis}} \cdot \pi \cdot \frac{d_{\text{valve}}^2}{4} \cdot \sqrt{2\rho_{GH_2}\left(p_{\text{vent}} - p_{\text{amb}}\right)} \tag{10.13}$$

with c_{dis} the discharge coefficient and d_{valve} the valve diameter taken equal to respectively, 0.09 and 7 mm from reference safety valves [156]. The ambient pressure is taken for the critical design case, i.e. p_{amb} = 1 bar. During flight

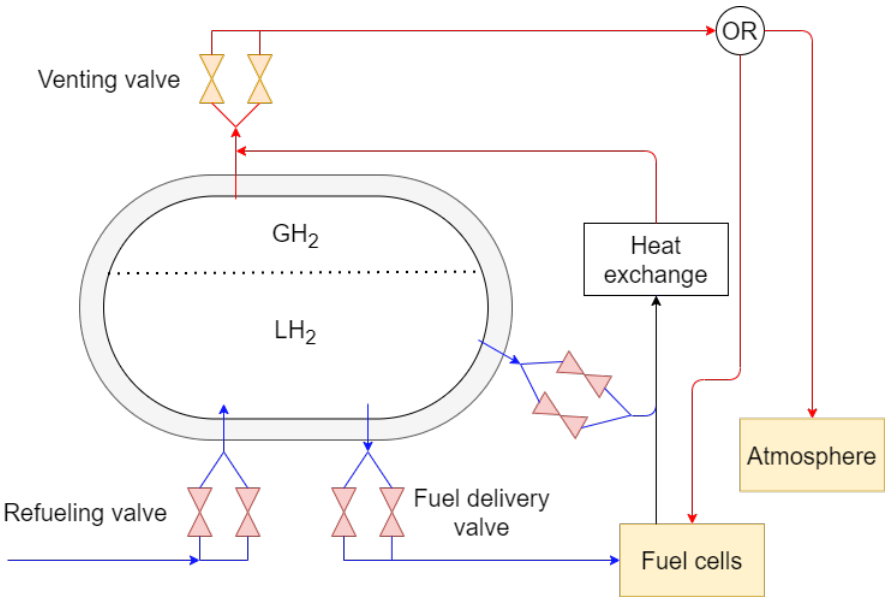

Figure 10.7: Overview of the hydrogen handling system in the propellant tank.

when the hydrogen compartment is not pressurized, the maximum mass flow will be higher due to the higher pressure difference. For the H2-VTOO tank this gives a maximum hydrogen mass flow of 149 kg/s which equals a maximum heat flux of $Q_{vent} = 6.66$ kW. This is higher than the maximum heat flux through the tank $Q_{max_1} = 3.32$ kW and therefore meets the requirements. When the extracted hydrogen flow rate to the fuel cells is too high for the low heat influx into the tank, some liquid hydrogen should be extracted and heated by the fuel cells in a heat exchanger to increase the pressure in the tank as shown in Figure 10.7. Otherwise, an underpressure could be generated that hinders the spontaneous hydrogen flow to the fuel cells.

The vented hydrogen will be processed in two possible ways as shown in Figure 10.7. When additional power is required for the aircraft, the vented hydrogen will be used in the fuel cells. The other scenario is that the hydrogen will be released in the atmosphere. Because hydrogen is non-toxic and disperses fast, this does not induce major safety problems.

Fuel delivery and refuelling

The single tank design is fixed in the aircraft and therefore requires a refuelling mechanism. The hydrogen should be transferred from the refuelling valve to the hydrogen tank and also from the LH_2 tank to the fuel cells. The sizing of these delivery pipelines is again based on Equation 10.13. A typical discharge coefficient $c_{dis} = 0.6$ for a pipeline is used while neglecting the small variations due to Reynold's number of the hydrogen flow [2]. For a tank pressure $p_{\text{tank}} = 2.5$ bar, maximum fuel cell pressure $p_{FC} = 2.0$ bar and a required LH_2 mass flow rate $\dot{m}_{LH_2} = 0.0436$ kg/s, a pipe diameter of $d = 1.9$ cm is required. The LH_2 flows spontaneously out of the hydrogen tanks due to the pressure difference. In order to control the flow through the pipelines, a solenoid valve is used that electro-mechanically opens the valve [3]. Again a Y-junction is used for redundancy. The liquid hydrogen will experience a heat flux when passing though the pipelines due to the extreme temperature difference. The same insulation material as for the hydrogen tanks, i.e. PU foam, is opted for making production less complex. The thermal model of the tank (discussed in Section 10.1.5) is reused to determine the required insulation thickness around the pipelines.

The pipelines for refueling are designed analogously to the fuel delivery pipelines. A refuelling time of 20 minutes was aimed for together with a filling pressure of 5 bar. Lower refuelling times are possible when higher filling pressure are used.

10.1.9. Verification tank design

Thermal model

The modelling of the insulation material in 40-layers is verified by plotting the temperature distribution within the insulation material in Figure 10.8. This shows the expected non-linear temperature behaviour due to the change of λ

[2] https://www.engineeringtoolbox.com/orifice-nozzle-venturi-d_590.html
[3] https://www.gemssensors.com

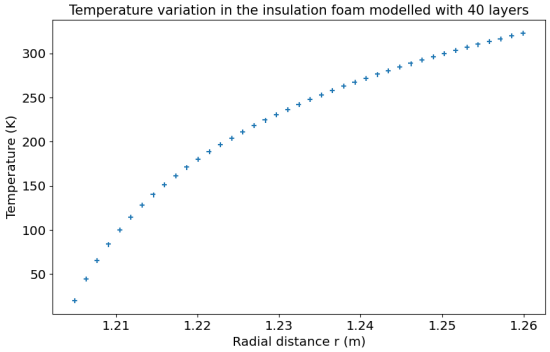

Figure 10.8: Foam modelled with 40 layers. Thermal conductivity varies within foam, but heat flux through each layer should be the same due to steady state principle.

with temperature. The low λ at low temperatures requires a higher slope to maintain constant heat flux at steady-state condition. This is verified in Figure 10.8.

Comparison single tank design with swappable tank design
The verification of the tank design model is combined with the comparison of the single tank design and the swappable tank design provided in Table 10.5 and Table 10.4. As discussed in Section 10.1.5, a hydrogen tank design with one single tank has a lower (S/V) ratio than multiple swappable tanks which results in lower heat transfer. This is verified by the total insulation mass $m_i = 480.8$ kg for swappable tanks, which is significantly higher than $m_i = 63.2$ kg for single tank.

The factor $\frac{m_{req}}{(2\pi r + 2l_{cyl})}$ in Equation 10.4 scales approximately with the square of the tank dimensions. Therefore a larger tank wall thickness is expected which is verified by the obtained $s_w = 4.9$ mm for single tank design and is significantly larger than the $s_w = 1.9$ mm for multiple tanks. However this larger thickness is counteract by the higher surface area of swappable tanks resulting in a total tank wall mass $m_{wall} = 451.4$ kg for single tank and $m_{wall} = 446.0$ kg for swappable tanks, leading to similar tank wall masses. Therefore, due to the significantly higher m_i, a single tank has $\eta_{grav} = 64.4\%$, much higher than $\eta_{grav} = 50.6\%$ for swappable tanks. Gravimetric efficiencies obtained from [154] which used identical tank material and similar insulation material ranges around the 60%. These higher efficiencies are similar and the small discrepancy is explained by the use of different tank dimensions.

10.1.10. Safety Assessment

An assessment of the failure scenarios of the hydrogen storage is crucial for hydrogen to be used in aviation as sustainable fuel . A common misconception is that hydrogen is inherently more dangerous than other fuels. The reason why this is incorrect is that although the explosive velocity/flammability of hydrogen is high, it has less explosive power than other fuel-air mixtures. However, usage of hydrogen can still lead to dangerous situations and therefore some precautions are taken in the design while assessing the failure scenarios.

Overpressurization of the tank, leading to structural failure is avoided by placing venting valves. Since this is a crucial system, a redundant safety valve is installed. The hydrogen flow is controlled by solenoid valves. In the case of a dangerous situation at the fuel cells or the refuelling station, these valves can be shut down, reducing the risk of an explosion. In addition passengers are loaded on board of the aircraft only when the hydrogen tank is fully filled to reduce the risk of damage. The electronics of the solenoid valves are protected to prevent sparks in the neighbourhood of the hydrogen. The hydrogen tank is stored after the pressurized cabin. Hence lower ambient pressure and higher dispersion rate. In addition the greater pressure difference makes it more difficult for oxygen to enter tank. The rear pressure bulkhead additionally provide an extra protection for the passengers in case of explosion. The LH_2 tanks are stored under low pressure, much lower than the burst pressure of metallic pressure vessels. In case tank rupture occurs, the LH_2 will escape from the tank and evaporate due to the temperature difference. The evaporation results in a fast volumetric expansion that can lead to an explosion. Therefore a safety venting system is installed in the fuselage compartment that expels the hydrogen into the atmosphere. In addition, the hydrogen tank compartment will also be insulated with PU-foam to limit the evaporation of escaped LH_2. When tank rupture has occurred, the H2-VTOO mission will be aborted with an emergency landing as soon as possible. The usage of foam is more safe compared to insulation with vacuum that leads to immediate mission failure when vacuum is lost. Furthermore, puncture of the tank due to the impact of objects, is mitigate by the Kevlar layer fairing around the tank. The detailed design of the external

refuelling system will be performed in the next design phase. However, it is crucial that the employees responsible for the refuelling, have an extensive training on the safety aspects of hydrogen handling and understand the procedures for handling hydrogen in a safe way. This is an essential step in enabling the usage of hydrogen in aviation.

10.1.11. Sustainability of hydrogen tanks

The usage of liquid hydrogen is far more sustainable than conventional aircraft fuel such as kerosene. The description of the liquid hydrogen production process is provided in Section 6.2. However this sustainable fuel comes at the expense of high production costs. Special effort was made in the choice for sustainable materials for the tank. The tank wall material Al 2024 is good recycable [60] and an environment friendly alternative for the insulation material was opted for. The insulation is made of polyurethane foam. This material is not inherently harmful but the current production of PU makes use of the toxic substances isocyanates and phosgene. Therefore, the H2-VTOO will strongly support and make use of alternative production processes to exploit the insulation strengths of this material in a sustainable manner without health or ecological risks. ESA has developed PU foams with 100% replacement of the isocyanates and usage of 50% of renewable resources such as vegetable oil [4]. The MAAMF vapor barrier consists of layers of Mylar, Aluminium foil and polyester fiber which are all recycable [151, 60].

10.2. Wing Box Design

The wing box design is of utmost importance in the design process. The wing will make sure that the aircraft can fly, store the batteries and it will carry the engines. In order to make all of this possible a strong structure in the wing should be made to carry all the loads that the wing will be subjected to without failing. For this, a wing box will be designed. A particular interest for this specific design is that the wing box should carry the loads during flight and during VTOL. The theory's and equations used in this section originate from the book *"Aircraft Structures for engineering students"* by T.H.G. Megson [94].

10.2.1. Assumptions and conventions

For the design of the wing box some assumptions will be made. These assumptions will simplify the design of the wing box since, due to time constraints, it is not possible to do a full detailed wing box analysis.

- The aerodynamic loads are assumed to be a constant distributed load over the span of the wing located at the quarter chord. The loads due to weight and thrust are assumed to be at 35% chord.
- For this analysis structural idealisation will be used. This structural idealisation will average out the shear flows for certain sections. For this reason the maximum stresses might not be as accurate. However, this is accounted for in a safety margin of 1.5 which is taken for the different stresses.
- The wing box is assumed to be symmetric over the x-axis which will make I_{xy} zero. This will simplify the calculations but might induce some discrepancies from the real values of the stresses. However, this is again accounted for in a safety factor of 1.5.

Furthermore, the conventions used for the wing box design can be seen in Figure 10.9.

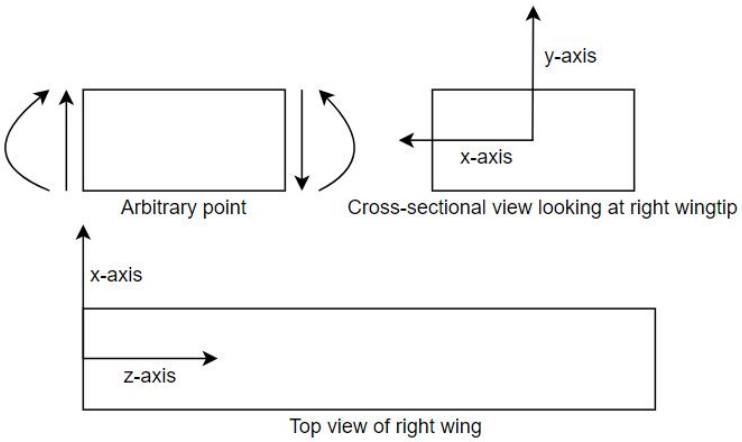

Figure 10.9: The conventions used for the wing box analysis

[4] https://www.esa.int/Enabling_Support/Space_Engineering_Technology/Greener_polyurethanes_for_space_and_beyond

10.2.2. Material and Stringer Selection

In order to determine the different dimensions of the wing box a material choice should be made. A selection will be done on two different kinds of materials namely metals and composites. From a literature study, several different kinds of metals and composites were taken into consideration. These materials are listed in Table 10.6 and a trade-off will be performed for these different materials Table 10.7.

Table 10.6: Materials selection [60] [135]

Material	Tensile strength [MPa]	Yield strength [MPa]	Density [g/cm^3]	Elastic modulus [GPa]	Shear modulus [GPa]	Corrosion resistance
Al-2024	482.6	344.7	2.78	73	27.6	Poor
Al-7075	572.3	503.3	2.81	72	26.9	Good
Al-7050	515	455	2.7	75	26.9	Good
Ti-6Al-6V-2Sn	1034	965	4.54	114	45	Good
Ti-3Al-2.5V	689	586	4.48	106.9	44	Good
CFRP	800	800	1.55	110	44	Good
GFRP	255.5	255.5	1.86	21.5	8.14	Good

Now that different considered materials are listed, a trade-off can be performed. From the trade-off criteria in Table 10.7 it becomes clear that CFRP is the best material structures-wise. However, because CFRP is hardly/not recyclable it still is not the optimal material sustainability-wise. For this reason the second best material, Al-7050, is determined to be the optimal material to construct the wing box since this material can also easily be recycled.

Table 10.7: Trade-off for selected materials

Material	Mass	Production cost	Strength	Stiffness	Torsional stiffness	Total
Al-2024	3	4	2	3	3	2.5
Al-7075	3	4	3	3	3	2.67
Al-7050	4	4	3	3	3	2.83
Ti-6Al-6V-2Sn	1	1	4	3	5	2.33
Ti-3Al-2.5V	1	1	1	3	5	1.83
CFRP	5	3	5	5	5	3.67
GFRP	5	3	1	2	1	1.83

Now that a suitable material is selected it is also important to select an optimal stringer type. From the various types of stringers it is determined that the Z-stringer is optimal for this design. The reason for this is that they have an efficient way of contributing to the moment of inertia. Furthermore, they are light, easy to inspect and just need to be riveted with on row of rivets what makes the Z-shaped stringer beneficial for manufacturing. Next to this, L-stringers are used in order to connect the spars to the skin of the wing box.

10.2.3. Loading

In order to construct the wing box it is of importance that the different kinds of loading on the wing are taken into account. In this particular case there are two loading cases. One where the aircraft is in cruise and one where the aircraft is in VTOL. An overview of the loading cases is given in Figure 10.10, Figure 10.102 and Figure 10.12.

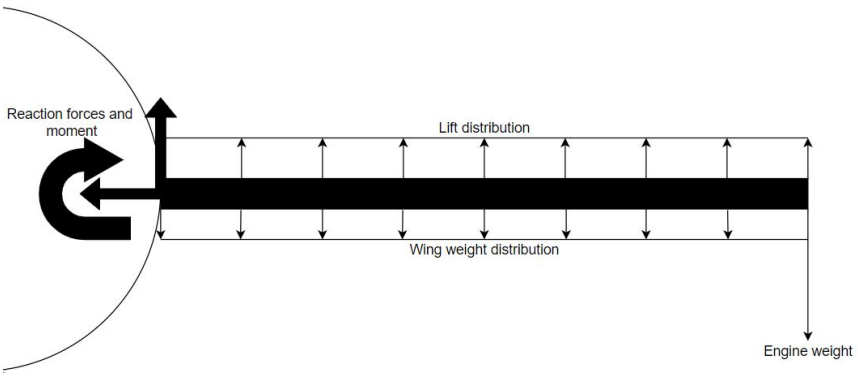

Figure 10.10: Free body diagram of the aircraft in cruise looking at the right wing from the end for the aircraft.

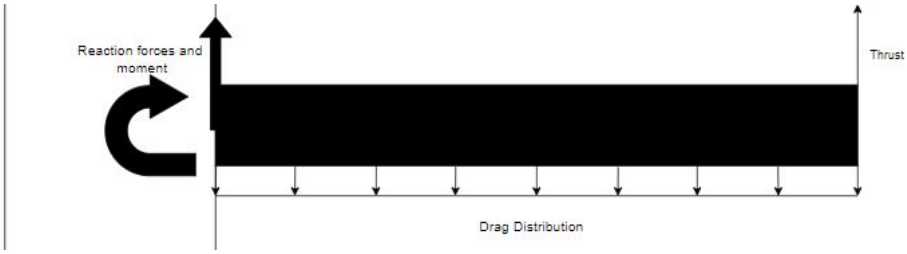

Figure 10.11: Free body diagram of the top view of the aircraft in cruise looking at the right wing.

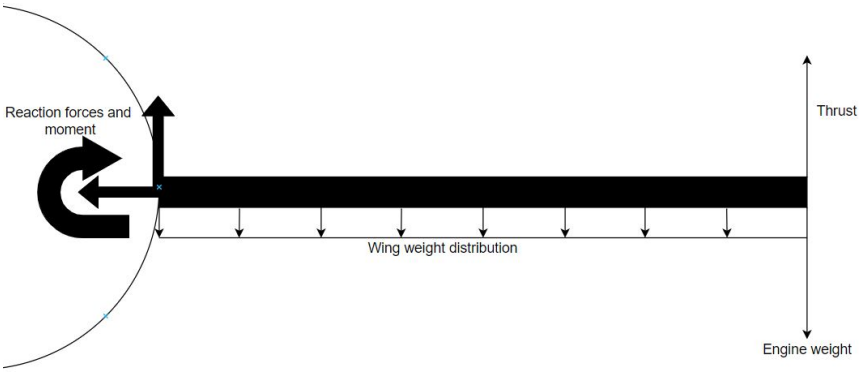

Figure 10.12: Free body diagram of the aircraft in VTOL looking at the right wing from the end for the aircraft.

From these loading cases the loading curves in Figure 16.1 could be constructed. In these curves there is a distinction between curves for cruise flight at sea altitude, since this is assumed to be the ultimate loading case, and VTOL. Furthermore, during cruise flight there can be made a sub-division in normal and transverse forces. These graphs show the distributions of forces, moments and torque on the wing under the ultimate load factor. It can be seen that the ultimate loading case is when the aircraft is in cruise since in this situation the shear force and the bending moment are the largest. For this reason the wing box will be designed for this loading case.

10.2.4. Wing box sizing

Now that it is clear what the different loads on the wing will be the wing box can be designed. For this design structural idealisation is used due to time constraints for this project. The wing box will run over the entire length of the wing. A front spar is located at 0.2 chord location, a middle spar at 0.4 chord location and a rear spar at 0.6 chord location. Furthermore, batteries are stored along the wingspan outside of the wing box so that regular inspection is possible.

Bending

Due to the bending moments in the wing, bending stresses will be induced. These bending stresses are in normal and transverse direction as can be deducted from the bending moment diagram in Figure 10.13b. The bending stress in different directions can be calculated by Equation 10.14.

In this equation σ is the bending stress, M is the bending moment, y is the distance from the respective axis and I is the MOI. The maximum bending stress is calculated by taking the maximum bending moment from Figure 10.13b and the maximum distance from the respective bending axis. The MOI for structural idealisation can be calculated the following way.

$$\sigma = \frac{My}{I} \tag{10.14}$$

$$I = \sum_{i=1}^{n} B_i y_i \tag{10.15}$$

.

Where y_i is again the distance of a boom to the respective aixs of interest and B_i is the boom area which can be determined by Equation 10.16 where $A_{stringer}$ is the stringer area, t_{di} is the plate thickness, b is the plate span and σ_i are the relative stresses between the two booms.

$$B_i = A_{stringer} + \frac{t_{di} b}{6}(2 + \frac{\sigma_{i+1}}{\sigma_i}) \tag{10.16}$$

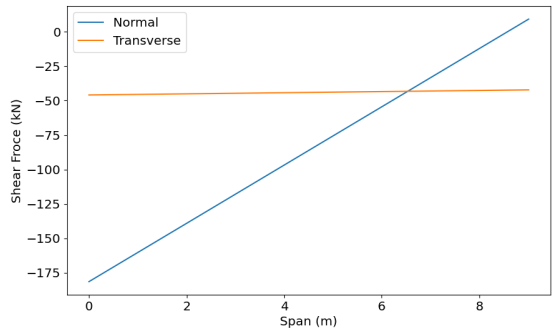

(a) Shear force distribution over the wing in normal and transverse direction for the ultimate load factor.

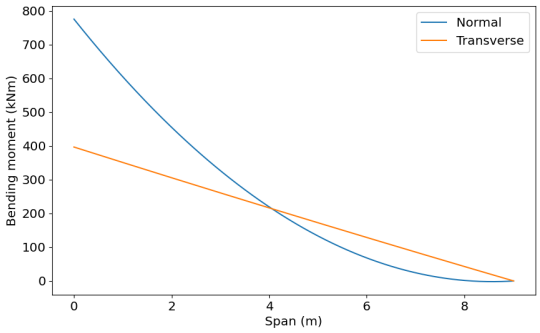

(b) Bending moment distribution over the wing in normal and transverse direction for the ultimate load factor.

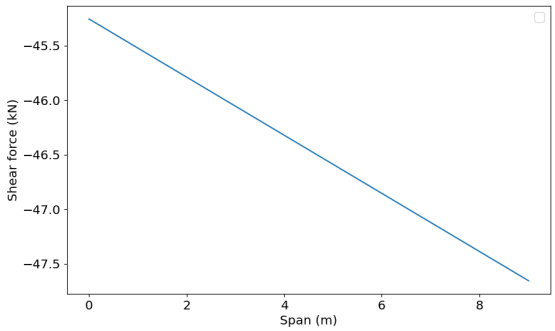

(c) Shear force distribution over the wing during VTOL.

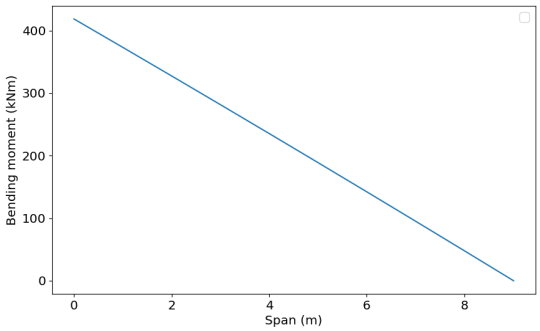

(d) Bending moment distribution over the wing during VTOL.

Figure 10.13: Internal loading diagrams for the different loading cases.

Eventualy the maximum bending stress should not exceed the material yield stress. In order to make sure that the yield stress is not exceeded, iteration is done on the calculation for the MMOI where the plate thickness, stringer number and stringer area can be varied.

Shear

During operation the aircraft should be able to withstand shear loads. These loads are induced by torque and shear forces. In order to design the wing box for shear stress due to shear forces, the following equation is used to calculate the shear flow in the different parts of the cross-section. For this analysis cuts are made in the horizontal parts of the wing box.

$$q_{ij} = -\frac{S_y}{I_{xx}} \sum_{r=1}^{n} B_r y_r - \frac{S_x}{I_{yy}} \sum_{r=1}^{n} B_r x_r + q_i \tag{10.17}$$

In this equation S_y/S_x are the shear forces in x and y direction respectively, I_{xx}/I_{yy} are the MOI around the x and y axis respectively and q_i is the redundant shear flow. By using Equation 10.18 the shear flows everywhere in the section could be calculated. The maximum shear stress can be determined by dividing the shear flow with the thickness of the respective part of the cross section.

In this equation A_R is the respective cell area, q the redundant shear flow, G the shear modulus, t the thickness per part of the cell and ds the length per part of the cell. Next to this, the torque induced on the wing box contributes to the shear flow. This torque is due to the forces that act on the wing box around the flexural axis. The shear flow due to the torque can be calculated using Equation 10.19 and again Equation 10.18.

$$\frac{d\theta}{dz} = \frac{1}{2A_R} \oint \frac{q ds}{Gt} \tag{10.18}$$

$$T = 2A_1 q_1 + 2A_2 q_2 \tag{10.19}$$

Design for buckling

The wing box should be designed for different kinds of buckling. In order to prevent column buckling inside the wing box it needs to be determined where the ribs are placed. The equation for column buckling is as follows.

$$\sigma_{cr} = \frac{K\pi^2 EI}{L^2} \tag{10.20}$$

σ_{cr} is the stress at a certain part of the wing box, K is a factor that depends on how the stringers are attached, E the Young's modulus, I the moment of inertia and L the length of the column. By rewriting this equation the maximum length of the column can be calculated. In order to optimise the wing box it is divided in three evenly large sections. For each of these sections the required rib pitch is calculated that is necessary to prevent column buckling.

Next to this, the wing box also needs to be designed for skin buckling. Skin buckling can be prevented by the placement of stringers and ribs. In order to determine the stringer pitch the following equation is used.

$$F_{cr} = \frac{\pi^2 k_c E}{12\,(1-v^2)}\left(\frac{t}{b}\right)^2 \tag{10.21}$$

In this equation k_c is a constant that depends on the way the skins are mounted, E is the Young's modulus of the material, v is the Poisson's ratio, t is the skin thickness, b is the short side of the respective plate and F_{cr} is the critical force. The critical force in this case is determined by the maximum stress per one of the three sections mentioned above. The stringer pitch can be found by rewriting Equation 10.21 in order to find the value of b.

Von Mises Stress

Now that all the different stresses can be determined, the Von Mises stress can be determined. This is a stress that takes into account all the different stresses in the different directions. The Von Mises stress can be determined by Equation 10.22.

$$\sigma_{VonMises} = \sqrt{\frac{\left(\sigma_{xx}-\sigma_{yy}\right)^2 + \left(\sigma_{yy}-\sigma_{zz}\right)^2 + \left(\sigma_{zz}-\sigma_{xx}\right)^2 + 6\left(\tau_{xz}^2 + \tau_{yz}^2 + \tau_{xy}^2\right)}{2}} \tag{10.22}$$

Final wing box design, dimensions and weight

Now that the methods are presented that are used to calculate the different loads and stresses, the wing box needs to be designed accordingly. The final design of the wing box can be seen in Figure 10.14. The upper and lower plate will be the same in order to also withstand the ultimate negative load factor and the wing box skin and spars will have constant thickness of 2.3 mm. However, the wing box layout can still be optimised due to further research on optimum stringer spacing. Next to the wing box layout, the stringer dimensions can be seen in Figure 10.15. The stringers are spaced evenly over the wing box where in the first section there are 26 stringers, the second section thirteen and in the third section eight. Furthermore, the wing box will be constructed with Al-7050 because of its beneficial characteristics. The wing box will be able to withstand the stresses presented in Table 10.8. The final weight of the wing will be approximately 700 kg also taking into account the ribs that will be spaced over the span of the wing box.

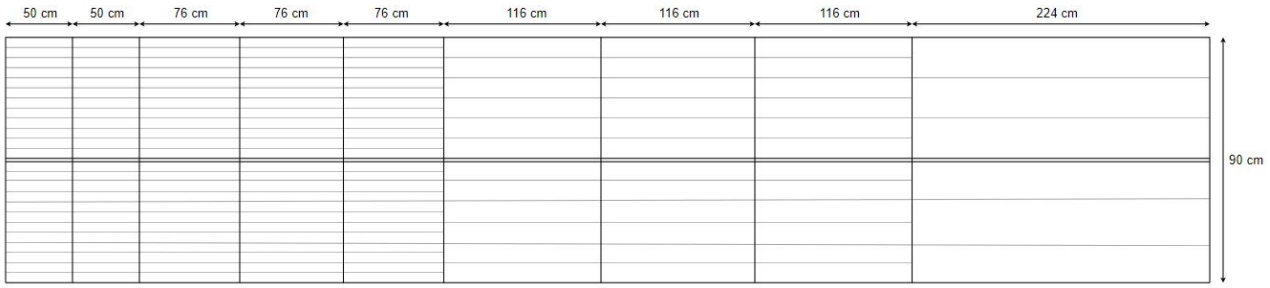

Figure 10.14: The final layout of the wing box

Figure 10.15: The final stringer layout.

Stress	Value
Maximum Bending stress [MPa]	445
Maximum Shear stress [MPa]	32.5
Maximum Von Mises stress[MPa]	451

Table 10.8: A table presenting different stresses that the wing box is designed for.

10.2.5. Verification and Validation

In order to verify the wing box calculations, code verification was performed by manipulating inputs and check whether and expected outcome occured. Furthermore, some hand calculations where performed on simplified loading cases to check whether they would yield approximately the same loading. This was followed by a validation procedure where the mass of the wing determined by the presented method compared to the wing mass determined by the class II weight estimation. The wing mass determined from the class II weight estimation estimation is 489 kg. As presented before the mass of the wing box is determined to be 700 kg after a structural analysis is performed. This is an increase of 43%, this might seem a lot. However, the class II weight estimation is a method for conventional aircraft where for example also the fuel, stored inside the wings, will cause some bending relief. For this reason the wing box structural analysis can be validated for now. However, a more thorough analysis can be performed where the wing box will be increasingly optimised.

10.3. Fuselage design

The fuselage offers protection to the payload and is a major load carrying structure. Detailed design of the fuselage structure is therefore important. The sizing of the fuselage is determined by the integration of the subsystems into the fuselage and is presented in Section 10.3.1. This sizing is followed by its structural design, discussed in Section 10.3.2.

10.3.1. Fuselage sizing

An exploded view of the H2-VTOO fuselage, showing the internal integration of the subsystems, is depicted in Figure 10.16. The fuselage should be sized to accommodate the 10 passengers, 2 crew members and cargo mass of 1000 kg. This high cargo weight is stored beneath the passengers and not after, in order to limit the fuselage length for manoeuvrability and landing on helipads. In addition, the large fuselage diameter increases the ground clearance for the tilt-rotor, hence enabling larger rotor tilt angles. It was opted for a two seats abreast configuration with a seat de Luxe classification to make H2-VTOO more competitive in the business jet market. This results in a seat pitch of 0.965 m, aisle width of 0.643 m and aisle height of 1.52 m [121]. A circular cross-section is used since this is the optimal geometry for pressurization of the fuselage, which is required to fly at the service ceiling of 7000 m (**REQ: HVA-AM-09** [7]).

In addition, the H2-VTOO mission will store the LH_2 tanks and the fuel cells as can be seen in Figure 10.16. The fuel cells are placed after the cargo in the cargo hold department, in front of the main landing gear. This allows for easy replaceability of the fuel cells which have a limited lifetime. The single hydrogen tank is at the back of the aircraft. Placement of the hydrogen tank podded to the wing was not desired due to the high drag penalty. In addition, placement in the front of the fuselage is not desired due to safety reason, despite the advantage of a more forward x_{cg}

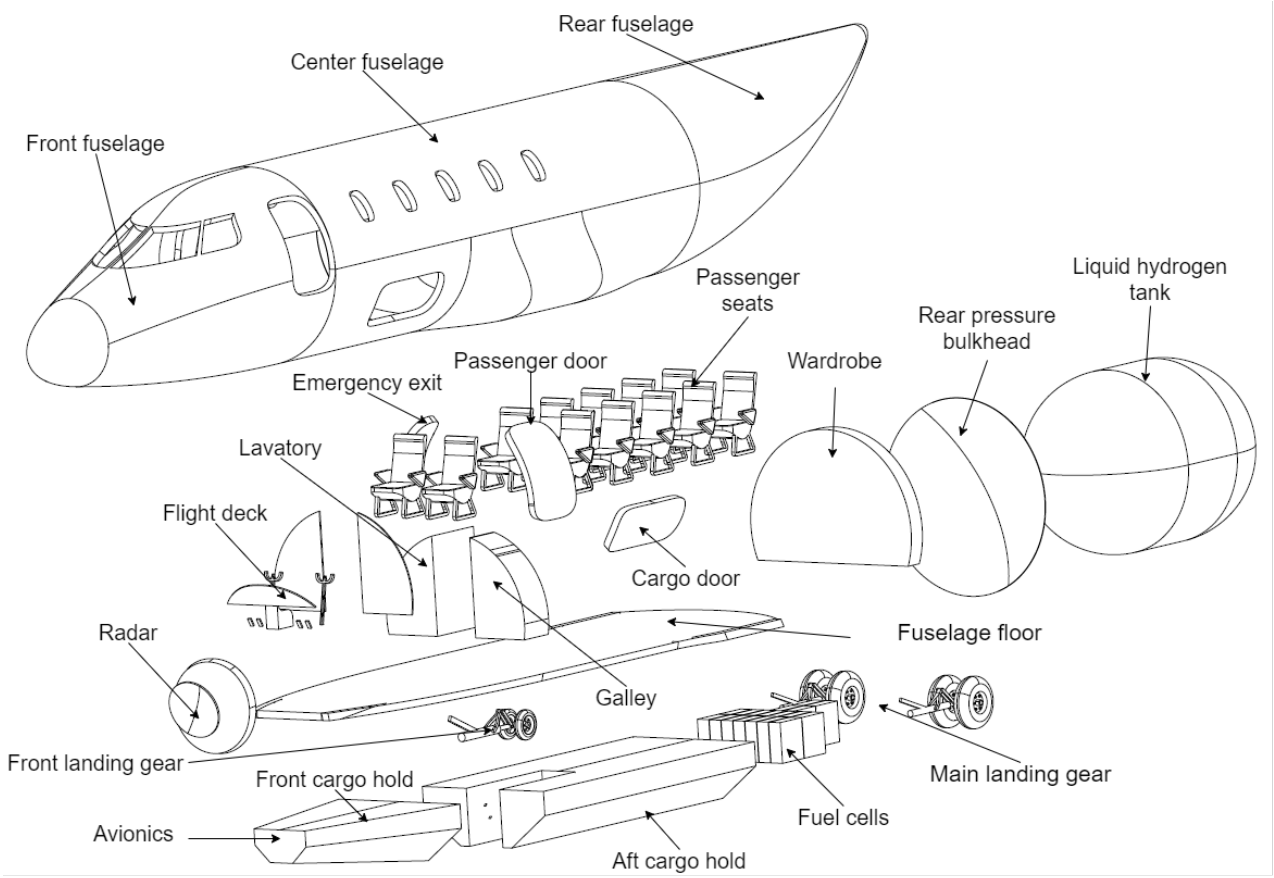

Figure 10.16: Exploded view of fuselage section.

position. The LH_2 tank is separated from the passenger compartment by the rear pressure bulkhead which ends the cabin pressurization.

The nosecone of the aircraft contains the flight deck with beneath storage for the avionics that are required to control the aircraft. The radar of the aircraft is protected by a radar dome. In front of the passengers and beginning of the nosecone, room is provided for 1 lavatory (0.61 m x 0.61 m), 1 galley (0.69 m x 0.46 m), 1 pax door (0.91 m x 1.30 m) and 1 type II emergency exit (0.51 m x 1.12 m) [121]. FAR 25 specifies a type IV emergency exist for a ten seater passenger aircraft [121], but since no above wing emergency exit is possible, it is opted for a type II emergency exit door.

The fuselage has a total length of $l_{fus} = 18.55$ m with nosecone length of $l_{nosecone} = 4.95$ m, cylindrical fuselage length of $l_{cyl} = 8.20$ m and tailcone length of $l_{tailcone} = 5.40$ m. The nosecone and tailcone lengths were optimised for lowest drag. This is determined by the fineness ratio l/d_f which results in lowest drag when in the range $1.5 - 2.0$ [121].

10.3.2. Fuselage structural design

For consistency, the method for designing the fuselage is taken from the same book as the wingbox design in Section 10.2, i.e. *"Aircraft Structures for engineering students"* by T.H.G. Megson [94].

The major loads carried by the fuselage and considered in its design are:

1. Loads in the cabin skin panels due to pressurization. This pressurization of the cylindrical fuselage structure results in circumferential stresses and axial stresses given by respectively, Equation 10.23 and Equation 1.

$$\sigma_{\text{circ}} = \frac{\Delta p R}{t} \quad (10.23) \qquad \sigma_{\text{axial}} = \frac{\Delta p R}{2t} \quad (10.24)$$

The fuselage is designed to sustain sea pressure in the cabin at the service ceiling height of 7000 m, resulting in a

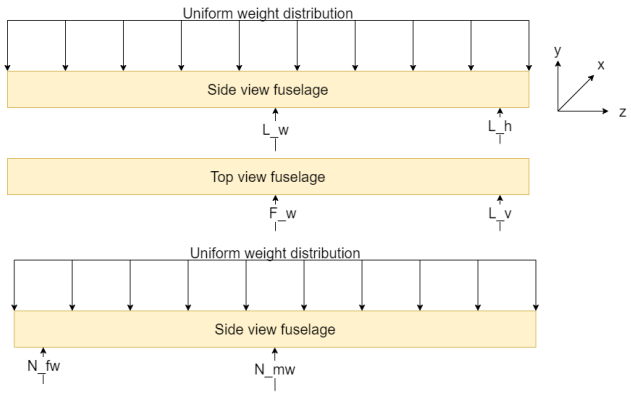

Figure 10.17: Free body diagram of fuselage for aerodynamic loading and landing gear loading.

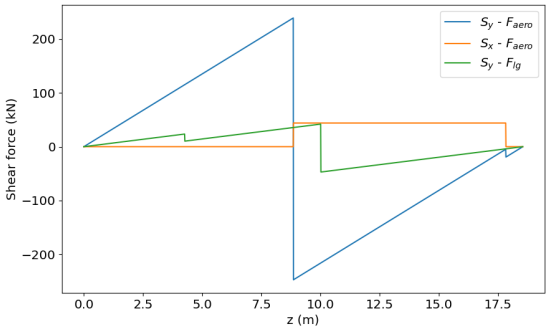

Figure 10.18: Shear loading S_y and S_x along the span of the fuselage.

pressure difference of 0.61 bar. This pressurization is slightly higher than for conventional aircraft which maintain a cabin pressure at typically 1800 m [5], but this results in more comfort of the passengers.

2. Aerodynamic forces from the main wing and empennage structure induced in the fuselage. It is assumed that the lift of the main wing is transferred as point load at the middle spar position of the center wing box. The total lift force includes the maximum load factor $n_{ult} = 4.9$ and consists of the lift provided by the main wing and the lift from the horizontal tailplane as shown in Equation 10.25. The lift L_h induces a moment that is counteracted by the center wingbox and is assumed to be applied at the middle spar location too.

$$L_{total} = L_w + L_h = n_{ult} \cdot MTOW \tag{10.25}$$

   In addition the forces induced by the vertical tailplane are considered. This creates a torsion in the fuselage. The vertical lift can act in two direction and therefore both load cases are considered. The drag of the aerodynamic surfaces is assumed negligible compared to lift forces.

3. Loads due to gravity. It is assumed that the MTOW is distributed uniformly along the fuselage length.
4. Ground reaction forces due to landing gear. This consists of the reaction force from the main landing gear and the nose landing gear given by

$$MTOW = N_{fw} + N_{mw}. \tag{10.26}$$

   The longitudinal position of the landing gear is discussed in Section 10.5.

A free body diagram of the fuselage for the described load cases is provided in Figure 10.17. Again, the vertical tail load is considered in both direction to determine the most critical load case. The fuselage is modelled as a beam in static equilibrium with skin thickness t and number of stringers n_{str}, evenly spaced along its cross-section. The coordinate system used consistently throughout this section is also shown in Figure 10.17. From the free body diagram the loading diagrams for the shear forces S_y and S_x, the bending moments M_x and M_y and the torsion T are determined. Their distribution along the span of the fuselage is shown in respectively, Figure 10.18, Figure 10.19a and Figure 10.19b. In each loading diagram, a distinction is made between aerodynamic loads F_{aero} and landing gear loads F_{lg}.

[5] https://abcnews.go.com/Health/Healthday/story?id=4507808&page=1

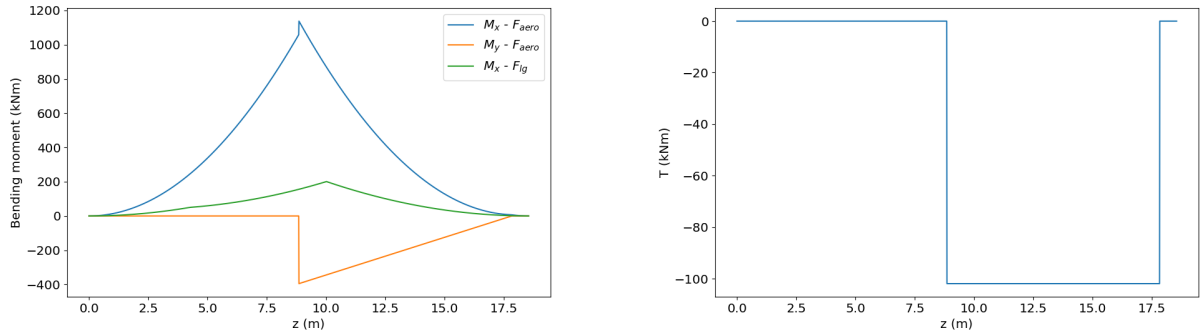

(a) (b)

Figure 10.19: Bending moment diagram M_x and M_y shown in (a) and (b) the Torsion T along the span of the fuselage.

The n_{str} stringers are idealised as point areas attached on the fuselage cross-section. Unlike the approach of the wing box, the skin thickness is not idealised for the fuselage and its effect is taken into account for the shear flow determined with Equation 10.27 and for the symmetric fuselage section ($I_{xy} = 0$ m^4, $x_{sc} = 0$ m and $y_{sc} = 0$ m). The reason for this is that with the constant thickness t the integral in Equation 10.27 can be solved analytically by expressing the skin in polar coordinates.

$$q_s = -\frac{S_x}{I_{yy}}\left(\int_0^s t_D x ds + \sum_{r=1}^{n} B_r x_r\right) - \frac{S_y}{I_{xx}}\left(\int_0^s t_D y ds + \sum_{r=1}^{n} B_r y_r\right) \tag{10.27}$$

The direct stresses σ_z, Von Mises stress σ_{vnm} and torsion T are determined with respectively Equation 10.14, Equation 10.22 and Equation 10.19 of the wing box design. In addition, the wingbox material Al-7050 is also opted as fuselage material. This allows for easier manufacturing and the same trade-off as in Section 10.2.2 is applicable. Stiffeners are necessary to prevent sheet buckling of the fuselage panels when loaded in compression. For the fuselage, it is opted for a hat-stringer with dimensions shown in Figure 10.21. The choice for hat-stringer allows for high moment of inertia, while all flanges are visible for inspection because only the flat centered section is attached to the wing. In addition, this requires only one rivet row which results in lower joining weight and less weaknesses in the fuselage structure. The fuselage is a curved surface unlike the flat sheet surface of the wing box. The same compressive buckling formula Equation 10.21 is used but now with k_c' which is obtained from [106] for curved surfaces. In addition, buckling of the cruved skin panels due to shear is determined similarly with constant k_s'.

The optimal n_{str} results in the design with the lowest fuselage mass. Therefore a tool was made that determines the required skin thickness for the critical loading case, for a given number of stringers. The distribution is plotted in Figure 10.21. The minimum fuselage mass of 1108.7 kg was obtained for $n_{str} = 30$ and $t = 1.25\ mm$. Sheet buckling was the limiting condition.

To prevent column buckling of the stringers, frames are uniformly spaced in the fuselage and the critical column buckling load was given by Equation 10.20 with $K = 1$ for the assumption that the stringers are simply supported by the frames. The stiffner's lowest moment of inertia is around its centroid of the x-axis and equals $I_{xx} = 6.272 \cdot 10^{-8}$ m^4 and with an area of $360 \cdot 10^{-6}$ m^2. With a maximum compressive strength of $\sigma_z = -53.9$ MPa this yields a maximum frame spacing of 1.54 m. Since the coefficients for column and sheet buckling depend on the stringer and frame pitch, the complete design process was iterative.

10.3.3. Verification & Validation of the fuselage

An important part is to verify and validate the correctness of the models used to design the fuselage. For this, the stress distributions σ_z, σ_{vnm} and τ are plotted along the fuselage length and shown in Figure 10.22. These distribution comply with the expected tendencies and act as verification. The stress distribution starts at non-zero σ_z and σ_{vnm} due to the pressurization loads. The stresses increase towards the center due to the fuselage. The spike at z = 8.85 m is due to the point load of L_w, resulting in a stress increase. The drop at z = 10.78 m on the other hand is due to the end of pressurization of the cabin, resulting in the expected decrease of stresses. This is not visible in the shear flow since pressurization only affects the direct stresses in the fuselage. The drop at z = 17.84 m is due to the horizontal and vertical tail load. As expected the stress go to zero at the end of the fuselage. A peculiar finding is the change in the slope at z = 4.10 m in the Von Mises stress and change in slope of z = 6.45 m for compressive direct stress σ_z. This is

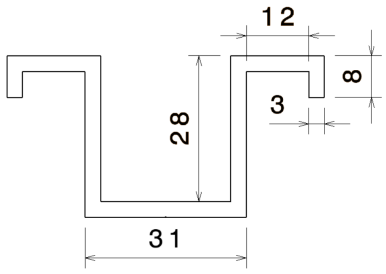

Figure 10.20: Hat stringer with corresponding dimensions listed in mm.

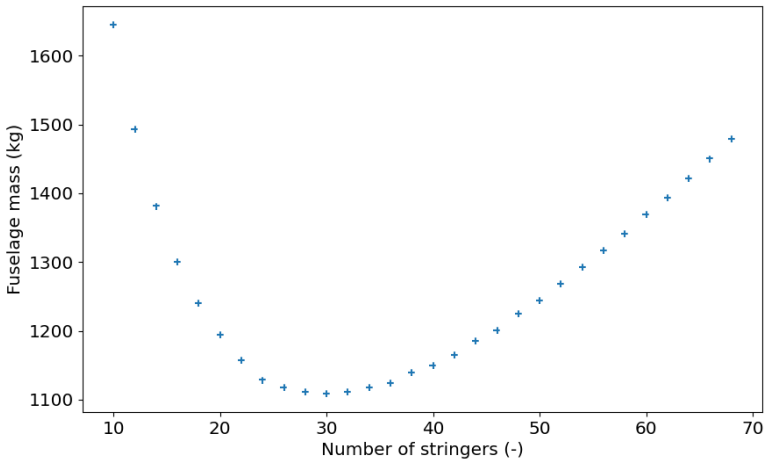

Figure 10.21: Fuselage mass in function of number of stringers. Optimal number of stringers is determined for lowest fuselage mass.

explained by the fact that Figure 10.22 shows the maximum for each stress and therefore the point at maximum Von Mises stress is not the same point as for maximum τ and maximum σ_{vnm}, hence explaining the change in slope.

After verification of the loading diagrams, the direct stress distribution calculation is verified by plotting its cross-sectional stress distribution in Figure 10.23, Figure 10.24a and Figure 10.24b. The distribution is plotted at longitudinal location z $=$ 8.86 m which is the point of highest Von Mises stress. In addition, the location of the stringers is plotted as visual verification. The maximum and minimum σ_z occur at respectively the top and bottom panel with a small offset due to the moment M_y induced by the tailplane. Therefore sheet buckling occurs at the bottom skin panel of the fuselage which is expected due to the weight of the fuselage. The maximum and minimum τ occur in the middle of the side panels which is expected due to the large negative S_y as was seen in Figure 10.18. The stress distribution is also verified by using unit stress loads and verify it complies with the expected tendencies.

For validation of the model, the stringer and frame pitch are compared with reference aircraft. The obtained frame-spacing of 1.55 m is higher than the prescribed frame spacing of 0.762 m specified by Roskam for small commercial aircraft [121]. A reason for this discrepancy is that the model of H2-VTOO did not take into account fuselage weaknesses such as windows, doors and rivets that result in stress concentrations, hence a lower frame-spacing. The stringer pitch is 0.28 m, obtained by spacing the 30 stringers evenly along the cross-sectional circumference. This stringer pitch falls in the range of 0.25 $-$ 0.38 m, specified by Roskam for small commercial aircraft [121]. The total fuselage mass determined by the class II weight estimation from Roskam [122] was estimated at 1407.1 kg. This value is higher than the H2-VTOO fuselage mass of 1108.7 kg obtained in Figure 10.21. This is expected since this value does not include the mass of the frames and the window and door reinforcements. Therefore the fuselage is in accordance with reference aircraft.

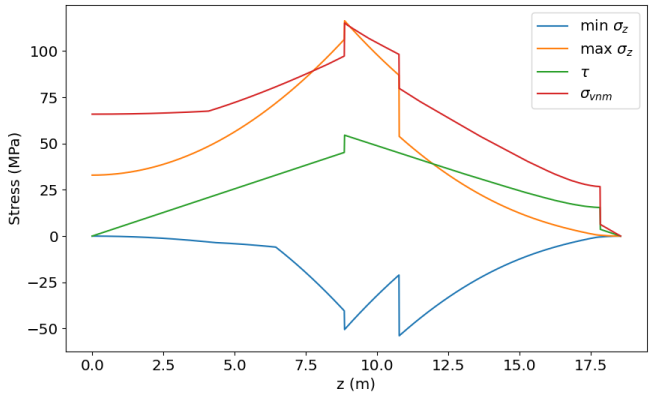

Figure 10.22: Longitudinal maximum stress distribution in the fuselage. Maximum τ, maximum σ_z, minimum σ_z and maximum σ_{vnm} along the cross-section are plotted for each longitudinal z position.

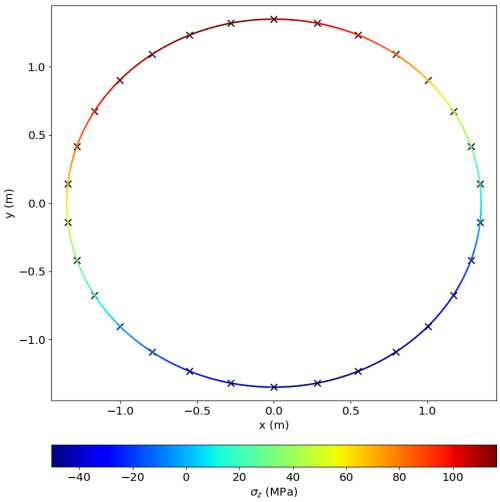

Figure 10.23: Direct stress σ_z distribution along the cross-section at maximum achieved σ_{vnm} = 115 MPa. The location of the stringers are visualized with crosses.

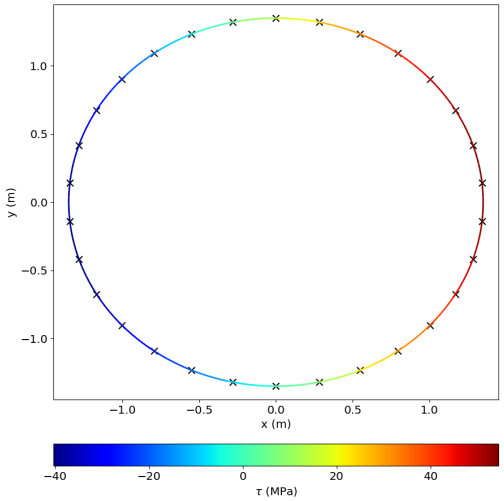

(a)

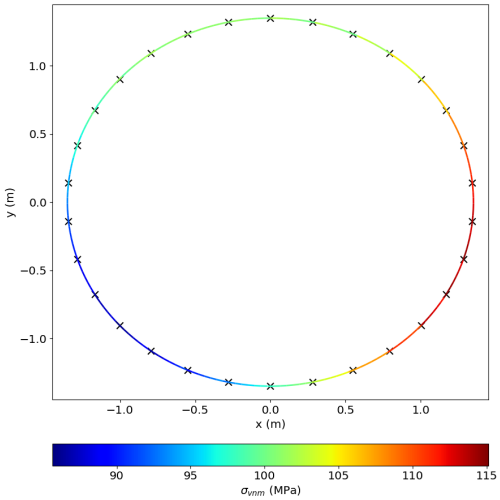

(b)

Figure 10.24: Shear stress τ shown in (a) and (b) the Von Mises stress σ_{vnm} along the cross-section at longitudinal location of maximum achieved σ_{vnm} = 115 MPa.

10.4. Aeroelastic stability of tilt rotor

The tilt rotor mechanism is beneficial for VTOL because it combines the advantages of VTOL as a helicopter and cruise flight in regular aircraft configuration. However, in the 1960's an instability called whirl flutter was discovered during wind tunnel tests of tilt-rotor aircraft [59]. Whirl flutter occurs during cruise configuration at high inflow speed due to the forces induced by the rotating propellers. The rotational motion of the propellers at high cruise speed results in aerodynamic interference that may induce unstable vibrations between the wing structure and the propeller. This instability is eventually the interaction between the aerodynamic forces experienced by the propeller and wing with the elastic and inertial forces of the wing [29]. The point at which this instability occurs, is the critical flutter point. Velocities above this speed lead to structural damage. Therefore an analysis has to be performed to verify that H2-VTOO will not encounter this flutter whirl instability in its flight envelope. However, this analysis is complex and a preliminary discussion on the problem is provided but definite conclusions on flutter stability of the H2-VTOO aircraft

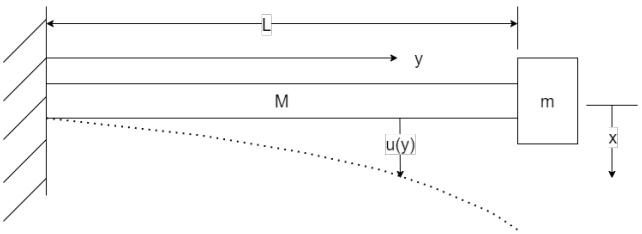

Figure 10.25: Static deflection for wingbox with mass M, moment of inertia Ixx, Young's modulus E and engine tip mass m.

require further investigation.

10.4.1. Natural frequency

The large engine mass at the end of the wing, raises the concern of low natural frequencies. Therefore the resonance frequencies of the vibrational modes of the wing are determined. The first vibrational mode considered is the vertical bending mode. The mass of the wing is significant compared to the engine tip mass and therefore the wing's inertia can not be neglected in the natural frequency determination. The wingbox is modeled with a clamped edge at its root to the fuselage and is shown in Figure 10.25. The used method supports on the conditions u(L) = x and $\frac{d}{dt}$u(L) = $\frac{d}{dt}$x in Figure 10.25. Considering these conditions a total kinetic energy of

$$T = T_{\mathrm{M}} + T_m = \frac{1}{2}\left(\frac{33}{140}M + m\right)\dot{x}^2(t) \tag{10.28}$$

is obtained which is equivalent to a simply vibrating point mass with $M_{eq} = \frac{33}{140}M + m$. The natural frequency f_{nat} for this vibrating point mass is given by Equation 10.29 [65] with stiffness K_x given by Equation 10.30.

$$f_{nat} = \frac{1}{2\pi}\sqrt{\frac{K_x}{M_{eq}}} \tag{10.29}$$

$$K_x = \frac{3EI_{xx}}{l^3} \tag{10.30}$$

The method to determine the natural frequency of lateral bending is identical to the vertical bending. The only difference is the moment inertia for which now I_{yy} is taken. The third vibrational mode is the torsional bending mode which has a natural frequency given by Equation 10.31 with J the polar moment of inertia of the engine and K_T the torsional stiffness of the wingbox. The torsional stiffness K_T is given by Equation 10.32 with J_p the polar moment of inertia of the engine and l the length of the wingbox. An overview of the natural frequencies of the aircraft wing is listed in Table 10.9 and shows that the vertical bending mode has the lowest natural frequency.

$$f_{nat} = \frac{1}{2\pi}\sqrt{\frac{K_T}{J}} \tag{10.31}$$

$$K_T = \frac{GJ_P}{l} \tag{10.32}$$

Table 10.9: Overview of the natural frequencies of the vibrational modes.

Vibrational mode	Natural frequency (Hz)
Vertical bending	2.14
Longitudinal bending	3.58
Torsional bending	14.30

10.4.2. Flutter

The aerodynamic forces that have an effect on the flutter phenomenon are the lift forces over the wing and the aerodynamic forces over the propeller that is rotating at a certain rpm. For the flutter analysis over the wing, a two-dimensional pitching-plunging model airfoil model is used and is shown in Figure 10.26.

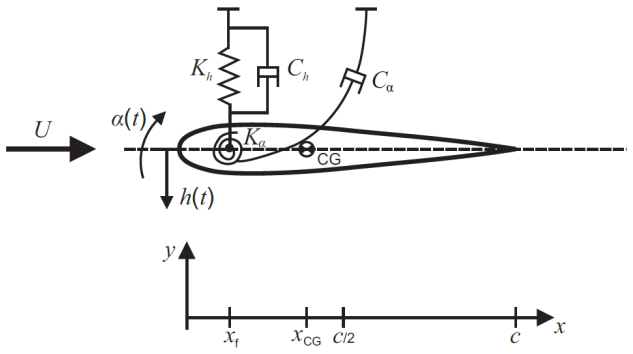

Figure 10.26: Two degrees of freedom aeroelastic model for flutter analysis [14].

The equations of motion corresponding to this two dimensional aero-elastic model are

$$\begin{bmatrix} m & S_\alpha \\ S_\alpha & I_\alpha \end{bmatrix} \begin{bmatrix} \ddot{h} \\ \ddot{\alpha} \end{bmatrix} + \begin{bmatrix} C_h & 0 \\ 0 & C_\alpha \end{bmatrix} \begin{bmatrix} \dot{h} \\ \dot{\alpha} \end{bmatrix} + \begin{bmatrix} K_h & 0 \\ 0 & K_T \end{bmatrix} \begin{bmatrix} h \\ \alpha \end{bmatrix} = \begin{bmatrix} -L \\ M_f \end{bmatrix}. \tag{10.33}$$

with α the torsional deflection (positive clockwise), h the vertical deflection (positive downward), $S_\alpha = m(x_{cg} - x_f)$ the product of the wing mass m and the distance $(x_{cg} - x_f)$ and x_f is the elastic axis of the wing, taken through the shear center of the wingbox. K_h and K_T the stiffness for the vertical bending and torsion as discussed in Section 10.4.1. L is the lift through the shear center. M_f is the aerodynamic moment through the elastic axis x_f, obtained from the moment around the aerodynamic center M_{ac} and the moment due to the lift. I_α is the mass moment of inertia of the wingbox though x_f. The center of gravity of the wing is taken as the centroid of the wingbox cross-section. The structural damping of the wing is given by the coefficients C_h and C_α. Equation 10.33 is a statically couple second order differential equation in two dimensions. In addition, the lift force L and moment M_f are not constant and depend on the degrees of freedom (h and α) and their derivatives (Dr. J. Sodja, personal communication, June 18, 2021). No exact solution exist for this equation and use must be made of partial differential solvers for an assessment of the flutter stability with the use of an eigenvalue analysis. It is required that the eigenvalues have negative real parts to have flutter stability. However, the aeroelastic model in Figure 10.26 is only for the wing. The model should be adapted to account for the aerodynamic interference of the rotating propeller at its rpm during cruise. This adapted model is complex and not considered in this report.

For the case whirl flutter instability is experienced, this could be solved by the use of an active control filter [59]. This uses a control loop with the wing deflection, velocity and acceleration as input to a feedback system consisting of the swashplate of the propeller. Another method to prevent flutter, is to redesign the wingbox such that the flexural axis (location of shear center) coincides with the center of gravity (refer to Figure 10.26). This eliminates the aerodynamic, elastic and inertial coupling. In addition, it is desired to have the center of gravity in front of the flexural axis. Therefore the heavy propeller blades are placed well in front of the wing [94]. However eliminating of the coupling is not always possible, and therefore increasing the stiffness of wing is advised when flutter instability is encountered. It is recommended to increase the (t/c)-ratio of the wing to increase stiffness of the wing, hence increasing flutter stability. However this comes with a drag penalty during cruise. The (t/c) ratio of the NACA 63(2)-215 used in the main aircraft wing has a (t/c) = 15% while the current tilt rotor aircraft have a (t/c) typically of 21% to 23% [59]. Therefore increasing (t/c) can be considered in the next design process when flutter instability might be discovered.

10.5. Landing Gear

The design of the landing is important as is has to support the aircraft. It must be strong enough to cope with the load and also well positioned, so that it does not influence the aircraft's configuration in a harmful way.

10.5.1. Landing Gear Configuration

Firstly, the possible configurations of the landing gear are investigated. These configurations differ in the positioning of the wheels but also in the way they can be stored. An overview is presented:

- **Fixed:** This is often used on lighter aircraft. It is a more simple design as no storage location and retracting mechanism has to be designed. However, the drag increases substantially with increasing speed.

- **Retractable:** The landing gear is often retractable to decrease the drag. However, it increases the weight and costs.

Next, the possible position configurations are presented:

- **Conventional/Taildragger:** This configuration has two wheels in front of the center of gravity and a small one behind. The biggest problem is that the center of gravity is located behind the main wheels and therefore ground loop may occur. Besides, it provides poor visibility for the pilot[131].
- **Tricycle:** Here the nose wheel is in front of the center gravity and the main wheels behind. This configuration can both be used for heavy as light aircraft and easier to land. Furthermore, the aircraft is at a low angle of attack. So the engine is more in line with the travelled direction and provides faster acceleration when taking-off [131]. The largest drawback is the weight it adds as they have to be retractable.
- **Tandem/Bycicle:** Here the (two) main wheels are on the center line of the aircraft. The nose wheel is on the same line in front of the center of gravity. It results in a lower weight but is hard to land. It is mainly reserved for high aspect ratio wing aircraft [131].
- **Quadricycle:** This configuration has four wheel that are positioned in a rectangular fashion. This configuration results in a higher weight and is sensitive to crosswinds. The main advantage is that the floor can be low to the ground which is beneficial for (un)loading cargo [131].
- **Multi-Bogey Gear:** Here multiple wheels are used for each landing gear strut. This can be done in combination with the tricycle configuration. However, this is only done for heavier aircraft, starting around 22680kg [131].

Now, a configuration has to be selected. First, convectional configuration may result in instability during landing and is this not desired. Secondly, the tricycle provides more stability and provides better acceleration during convectional take-off and VTOL. On the other hand, it is heavier as it has to be retractable. Thirdly, the bicycle is not optimal for the H2-VTOO as at has not a very big aspect ratio. Fourthly, the quadricycle provides good loading capabilities but also adds more weight. Now, the Multi-Bogey Gear is useful for heavier aircraft but adds weight to the H2-VTOO that is not necessary.
In conclusion, the tricycle is the landing gear configuration that is selected for the H2-VTOO.

10.5.2. Position of landing gear

When dealing with the positioning of the landing gear, the two most important parameters to consider are the scrape/ tip back angle(θ) associated with pitch, and the turnover angle(ψ) associated with roll. Firstly, it is important that the tip back angle is greater than 15deg to avoid the empennage from tipping backwards. The angle between the vertical of the aircraft c.g and the main landing gear must also be either 15deg or equal to the scrape angle if this angle is larger[117]. To prevent tip over, the main landing gear will be placed 10%-15% of MAC behind the most aft c.g.[115]. A value of 15% behind most aft c.g. will be used to avoid tip over. ψ must also be less than 55deg to ensure that the aircraft is within the landing gears such that the engines or wing tips do not touch the ground during steep turns. In addition to this, the loading on the nose landing gear must also be taken account for; typically, to avoid inefficient steering and braking of the aircraft, the load on the aircraft will be be 8% [115].

To estimate a position of the landing gear both longitudinally and laterally, the constraining values of 15deg and 55deg tip-over and turn-over angle were used along with a simple moment equilibrium.

The lateral distance of the main landing gear from the c.g. was computed using Equation 10.5.2

$$y_{\text{MLG}} > \frac{l_{\text{n}} + l_{\text{m}}}{\sqrt{\frac{l_{\text{n}}^2 \tan^2 \psi}{z^2} - 1}} \tag{10.34}$$

By performing all calculations, a longitudinal nose landing gear position of 4.27 m from the nose of the aircraft can be determined, the main landing gear will be 4.64 m behind the nose landing gear. The y_{MLG} will be a lateral distance of 1.08 m from the centre of the fuselage

10.5.3. Tire and wheel sizing

As mentioned previously majority of the weight will be supported by the main landing gear wheels. First, an LCN of 10 was used such that the tire pressure could be determined. An LCN of 10 was chosen as the aircraft will mainly operate on paved surfaces for CTOL and this would be the critical condition for the pressure of the tires [125]. The static loads on the nose and main wheels were determined based on the expected percentage of the MTOW they would support. The static loads and tire pressure could then be used to determine tire dimensions from statistical data presented by Torenbeek [145]. The chosen tire dimensions along with their respective tire pressures are presented in Table 10.10

Table 10.10: Dimensions of tires chosen for nose and main landing gear

Dimension	Nose	Main
Nominal tire diameter (m)	0.4064	0.711
Nominal tire width (m)	0.1118	0.2286
Rim diameter (m)	0.254	0.305

10.5.4. Shock Absorber

The landing gear must be able to absorb the shock the aircraft experiences while landing. That is why shock absorbers are used. The most commonly used sturt is the oleo strut. Which uses a hydraulic absorber that provides the required wheel deflection that depends on the vertical touch down speed. The speed assumed for STOL aircraft is 4.572m/s as this is the most critical landing mode of our aircraft. When a VTOL is performed a more steady landing operation can be conducted.
The shockabsorber stroke can be calculated with Equation 10.35. Where N_{gear} is the gear load factor and equals three, η is the shock absorbing efficiency of 0.75, η_T is the shock absorber efficiency of the tire and equals 0.47[117]. Finally, S_T is the stroke of the tire and is half of the tire radius minus the rolling radius.

$$S = \frac{V_{vertical}^2}{2g\eta N_{gear}} - \frac{\eta_T}{\eta} S_T \tag{10.35}$$

With a S_T of 0.1397m, a stroke of 0.3860m can be found. According to Raymer, one inch has to be added as a safety margin[117]. This results in a total of 0.3952m
Now, the dimension of the oleo shock absorber are determined. This is done with Equation 10.36. Where L_{oleo} and P are the load on the oleo in pounds and the internal pressure of 1800 psi. Furthermore, the total length of the shock absorber equals about two and a half times the stroke that was already calculated. [117]. This results in a diameter of the front and main shock absorber of 0.1199m and 0.090m.

$$D_{oleo} = 1.3\sqrt{\frac{4L_{oleo}}{P\pi}} \tag{10.36}$$

Finally, a material for the strut is chosen. The most commonly used materials for the landing gear are steel and titanium as they have high static strength, a sufficient fracture thoroughness and fatigue strength[83]. It is preferred to use steel for the H2-VTOO as it is much cheaper than titanium. The AISA 4340 alloy is used for the landing gear and undercarriage as it has a higher strength-to-weight ratio relative to other steels. [83]

10.5.5. Landing Gear Sustainability

After sizing the landing gear, its sustainability has to be assessed. The part consists primarily out of steel and rubber. A weight distribution of 75% steel and 25% rubber is assumed. Furthermore, this ratio is also assumed to be the recycling rate of the entire landing gear as steel has a very high recycling rate while rubber does not. Furthermore, since rubber is a plant based material, it can be very sustainable, under the right conditions. The problem with rubber however lies in not being biodegradable, which means that the huge quantities that are deposited in landfills stay there forever. During this project special focus will be put on ensuring both a sustainable production and a adequate end-of-life for the rubber, this however requires further investigation in the further stages of the project.

11. Stability and Control Analysis

For the design of an aircraft, the most important things arguably are the stability and control of the aircraft. Due to safety, design, and for future piloting of the aircraft, these topics are given a preliminary discussion and sizing in this chapter. Firstly, the static and dynamic stability will be discussed in Section 11.1. Secondly, this is followed by the design of the control surfaces in Section 11.2. These encompass the ailerons, rudder and elevators. This sizing is done on several criteria based on the regulations and critical conditions of each surface. Thirdly, an overview of the aircraft control is provided in Section 11.3. This section briefly gives an overview of what the automatic pilot and control diagrams of the aircraft look like, and how certain inputs correspond to the correct outputs. Fourthly, the longitudinal static stability and controllability are assessed in Section 11.4. This is done by means of a potato diagram to explore the outer c.g. ranges, and a scissor plot. Fifthly and lastly, the stability of the aircraft and control surfaces are verified and validated in Section 11.5.

11.1. Stability Analysis

In this section, the static and dynamic stability of the aircraft will be discussed. First, the regulatory requirements will be briefly touched upon, as they state which topics are of most importance at what scenarios. Than, the stability derivatives, vital for the stability calculations, will be calculated with the use of AVL. Finally, the static and dynamic ability of the aircraft will be assessed.

11.1.1. Stability Regulatory Requirements

When assessing the regulatory aircraft requirements, one has to look at the Part 25 Aircraft regulations, due to the MTOW being above 12500 lbs or ±5700 kg. The Federal Aviation Requirements (FAR) states in Sec. 25.173, 175, 177 and 181 that the aircraft must be provide static longitudinal and lateral-directional stability, and should provide dynamic short-period and Dutch Roll stability at a speed of $1.13 \cdot V_{SR}$. These conditions must be met at the MTOW, landing gear retracted and flaps retracted [47].

11.1.2. Calculation of Stability Derivatives

In order to assess the static and dynamic stability of the aircraft, the stability derivatives must be computed. Generally, they are defined as shown in Equation 11.1. Here, Y is the aerodynamic force and β the independent variable. This is then made dimensionless by using the corresponding surface area S and flight speed V.

$$C_{Y_\beta} = \frac{\partial C_Y}{\partial \beta} = \frac{\partial Y}{\partial \beta} \frac{1}{\frac{1}{2}\rho V^2 S} \tag{11.1}$$

When computing these derivatives, one compares the free stream V_∞ velocity to the perturbed velocity V' at a certain point on the surface with rotation vector $\Omega = [p, q, r]^T$. and position vector **r**, extended from the aircraft's c.g. This is shown in Equation 11.2.

$$\mathbf{V}' = \mathbf{V}_\infty + \Omega \times \mathbf{r} \tag{11.2}$$

In the case that a stability derivative is computed with a rotation between the body-fixed reference frame F_b and the aerodynamic reference frame F_a (also called the wind frame), the perturbed velocity V' has to be transformed from the body frame to the aerodynamic frame using Equation 11.3. The b- and a-frames are depicted in Figure 11.1, from which $\mathbb{T}_{ab}$ can be found.

$$\mathbf{x}^a = \mathbb{T}_{ab}\mathbf{x}^b \tag{11.3}$$

These stability derivatives have been calculated using the software Athena Vortice Lattice method (AVL) [30]. This program makes use of the same principles as mentioned above, combined with a central difference scheme to computationally model the aerodynamic effects [31]. This central difference scheme can be seen in Equation 11.4.

$$\frac{\partial Y}{\partial \beta} = \frac{Y(\beta + \Delta\beta) - Y(\beta - \Delta\beta)}{2\Delta\beta} + \mathcal{O}\left(\Delta\beta^2\right) \tag{11.4}$$

For AVL to know what it should model, a $.avl$ file describing the geometry of the aircraft, together with a $.run$ file describing the aircraft and flight properties must be set up. The $.run$ has been set up for the corresponding conditions

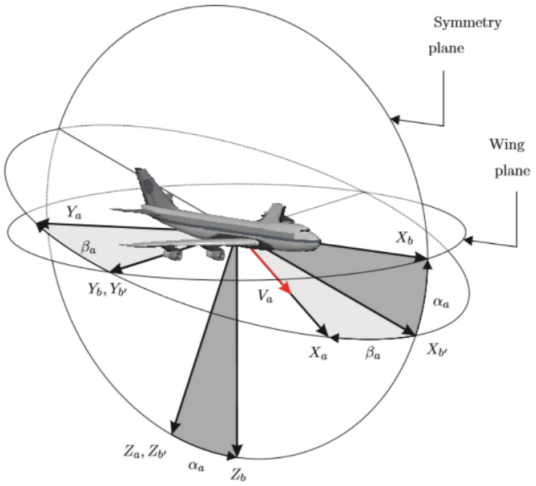

Figure 11.1: Transformation from body-fixed reference frame F_b to the aerodynamic reference frame F_a. [150]

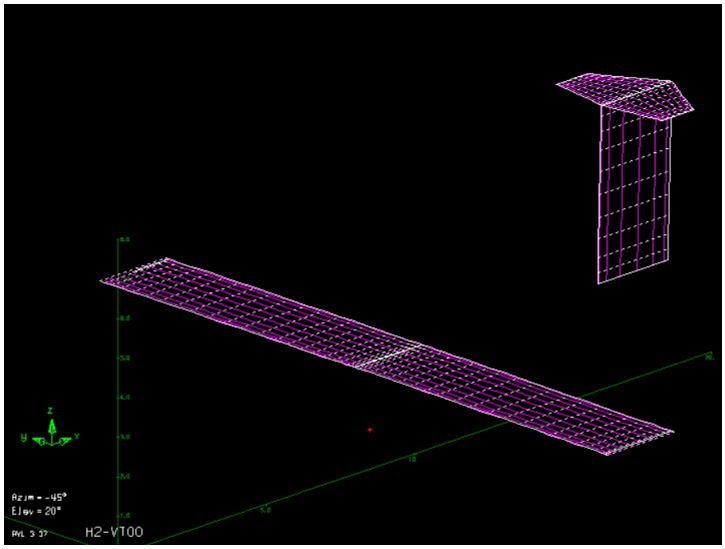

Figure 11.2: Simplified aerodynamic geometry of the aircraft in the AVL software package used to find the stability derivatives and eigenvalues.

to be analyzed. The $.avl$ file has been set up for the main wing and empennage only, neglecting the fuselage, as shown in Figure 11.2. This assumption is stated to be valid in the AVL documentation, and possibly improve results due to the fact that the slender-body theory being used has limited results. Therefore, if the fuselage does not have major influence on the aerodynamic loads, it is deemed more accurate to leave it out [31]. Note that C_{D_0} of the entire aircraft will not be used from AVL, but from the value calculated in Chapter 9.

11.1.3. Static Stability Analysis

To satisfy the condition of providing static stability as required by the FAR, the aircraft must provide an inversely proportional relationship between the pitching moment and the angle of attack. This is expressed mathematically in Equation 11.5.

$$\frac{dC_m}{d\alpha} < 0 \tag{11.5}$$

$$C_m = C_{m_0} + C_{L_h} + C_{L_{A-h}} \cdot (x_{cg} - x_{np}) \frac{S_h V_h}{SV} \tag{11.6}$$

When one combines Equation 11.5 and Equation 11.6, it can be found that the main stability requirement is that the C.G. is located in front of the neutral point, as shown in Equation 11.7. This requirement has to be assessed based on

the range of possible C.G.'s the aircraft can obtain, which is further explored in Section 11.4. Here, the stability and controllability of the aircraft are analysed based on the potato diagram and scissor plot methods.

$$(x_{cg} - x_{np}) < 0 \tag{11.7}$$

11.1.4. Dynamic Stability Analysis

Assessing dynamic stability can be performed by solving the approximated linearized symmetric and asymmetric equations of motion. Due to the equations of motion being linearized, some error is introduced, however, finding the exact solution would become to laborious for the time-scope of the project. These equations of motion have the general form as in Equation 11.8, where **x** is the state vector describing the states of the aircraft, and **u** the input vector, describing the control surface deflections. The worked out equations of motion for both symmetric and asymmetric flight can be seen in Equation 11.9 and Equation 11.10 respectively.

$$\frac{d\mathbf{x}}{dt} = A\mathbf{x} + B\mathbf{u} \tag{11.8}$$

$$\begin{bmatrix} C_{X_u} - 2\mu_c D_c & C_{X_\alpha} & C_{Z_0} & C_{X_q} \\ C_{Z_u} & C_{Z_\alpha} + \left(C_{Z_\alpha} - 2\mu_c\right) D_c & -C_{X_0} & C_{Z_q} + 2\mu_c \\ 0 & 0 & -D_c & 1 \\ C_{m_u} & C_{m_\alpha} + C_{m_\alpha} D_c & 0 & C_{m_q} - 2\mu_c K_Y^2 D_C \end{bmatrix} \begin{bmatrix} \hat{u} \\ \alpha \\ \theta \\ \frac{q\bar{c}}{V} \end{bmatrix} = \begin{bmatrix} -C_{X_{\delta_e}} & -C_{X_{\delta_t}} \\ -C_{Z_{\delta_e}} & -C_{Z_{\delta_t}} \\ 0 & \\ -C_{m_{\delta_e}} & -C_{m_{\delta_t}} \end{bmatrix} \begin{bmatrix} \delta_e \\ \delta_t \end{bmatrix} \tag{11.9}$$

$$\begin{bmatrix} C_{Y_\beta} + \left(C_{Y_\beta} - 2\mu_b\right) D_b & C_L & C_{Y_p} & C_{Y_r} - 4\mu_b \\ 0 & -\frac{1}{2} D_b & 1 & 0 \\ C_{l_\beta} & 0 & C_{l_p} - 4\mu_b K_X^2 D_b & C_{l_r} + 4\mu_b K_{XZ} D_b \\ C_{n_\beta} + C_{n_j} & 0 & C_{n_p} + 4\mu_b K_{XZ} D_b & C_{n_r} - 4\mu_b K_Z^2 D_b \end{bmatrix} \begin{bmatrix} \beta \\ \phi \\ \frac{pb}{2V} \\ \frac{rb}{2V} \end{bmatrix} = \begin{bmatrix} -C_{Y_{\delta_a}} & -C_{Y_{\delta_r}} \\ 0 & 0 \\ -C_{l_{\delta_a}} & -C_{l_{\delta_r}} \\ -C_{n_{\delta_a}} & -C_{n_{\delta_r}} \end{bmatrix} \begin{bmatrix} \delta_a \\ \delta_r \end{bmatrix} \tag{11.10}$$

Solving these equations is done by coupling the design parameters and stability derivatives obtained from AVL, and solving the systems for the eigenvalues, as shown in Equation 11.11. In particular, the eigenvalues come from the state matrix A. Note that these matrices are simplified based on the dynamic motion to be analyzed: short period, phugoid, aperiodic roll, dutch roll and spiral. Elaboration on the meaning of each control derivative is omitted for brevity, and assumes familiarity from the reader.

$$|A - \lambda I| = 0 \tag{11.11}$$

One requires the real part of the eigenvalue of a certain motion, Re(λ), to be negative for the motion to be stable. In Table 11.1 below, the results of the five discussed motions, are shown in the complex plane, which are also listed in Table 11.1. As can be seen, the aircraft is stable in all eigenmodes, except for the spiralling motion. This however, is a very small instability, which is typical behaviour for most aircraft, and can be reacted upon by the pilot and/or control system.

Table 11.1: Eigenvalues for the five discussed motions.

Eigenmode	Real Value	Imaginary Value
Short Period	-0.9795	±3.5592
Phugoid	-0.8591E-02	±0.1013
Aperiodic Roll	-4.1700	0
Dutch Roll	-0.7376	±3.5592
Spiral	0.4273E-02	0

11.2. Control Surface Design

In this section, the control surfaces of the aircraft are sized preliminary. These comprise of the ailerons, the rudder and the elevator. Providing controllability in the roll, yaw and pitch axes respectively.

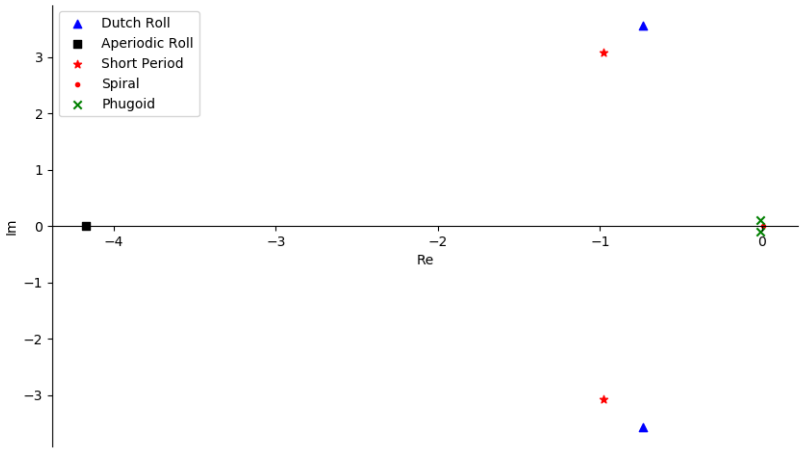

Figure 11.3: Eigenvalues of the analysed dynamic motions.

11.2.1. Ailerons

The ailerons of an aircraft provide the vital function of roll control. The main starting point when sizing ailerons comes from the roll rate requirement. It has been chosen that the aircraft shall be capable of rolling at 20 deg/s, based on typical business aircraft roll rates [103]. This is based on a minimum control speed based on 0.8 times the stall speed as a safety factor [126]. The first step is to calculate the roll damping coefficient C_{l_p}, based on the 2D aerodynamic characteristics of the main wing airfoil as shown in Equation 11.12.

$$C_{l_p} = -\frac{4\left(c_{l\alpha} + c_{d_0}\right)}{S_{ref} b^2} \int_0^{b/2} y^2 c(y) dy \tag{11.12}$$

Next, the aileron control derivative $C_{l_{\delta a}}$ is calculated in Equation 11.13. This is based on an aileron deflection angle δ_a of 15 degrees up and down on both sides, a commonly used value for aircraft in the business jet category [126]. The speed at which this is evaluated is the minimum control speed $V_m c$.

$$C_{l_{\delta a}} = -\frac{P C_{l_p} b}{\delta_a 2 V_{mc}} \tag{11.13}$$

Lastly, the aileron span can be determined using Equation 11.14 and a chord ratio τ of 0.2. This value has been chosen such that an adequate amount of space was left for the wingbox, and a reasonable aileron span was concluded.

$$C_{l_{\delta a}} = \frac{2 c_{l\alpha} \tau}{S_{ref} b} \int_{b1}^{b2} c(y) y dy \tag{11.14}$$

The specific design parameters used for the aileron sizing are listed again in Table 11.2 below, together with the final values describing the aileron dimensions. It is important to also discuss the event of having roll control during VTOL. Since the ailerons do not have any roll authority due to the low (or zero) airspeed, the engines will have to be used to provide roll control by using asymmetric vertical thrust.

Table 11.2: Specific parameter values used for the aileron sizing and final aileron dimensions.

Parameter	Symbol	Value	Unit
Roll rate	P	20	deg/s
Aileron deflection angle	δ_a	±15	deg
Aileron to mean aerodynamic chord ratio	τ	0.2	-
Aileron span	b_a	5.82	m
Aileron chord	c_a	0.45	m

To improve the lift performance during conventional take-off and landing, it is chosen to also let the ailerons work as flaps, so called 'flaperons'. These flaperons will have a maximum deflection angle equal to that of the ailerons, with an additional mechanic system allowing the flaperons to simultaneously move down or up together. This is the opposite from normal aileron configurations, in which the ailerons always move in opposite direction from each other. An estimate on the extra lift coefficient generated by the ailerons can be found using the linear relation as shown in Equation 11.15, where δ_a is the flaperon deflection. Note that it is assumed that the lift coefficient will remain in the linear part of the curve, and that the drag coefficient does not increase drastically. These assumptions can be deemed valid knowing that in conventional aircraft, a 10-20 degree flap setting is used during take-off, without any significant loss in performance. In these flap deflection ranges, the drag remains in the vertical part of the drag bucket, and the lift coefficient in the linear part.

$$C_l = C_{l_0} + C_{l_\alpha}\left(\alpha + \tau\delta_a \frac{b_a}{b/2}\right) \tag{11.15}$$

11.2.2. Rudder

To size the rudder, one has to comply with several flight criteria conditions and see which ones are most critical, and hence have to be designed for. For a double propeller transport aircraft, these will be asymmetric thrust and crosswind landings [128]. For an preliminary sizing, it has been assumed that the rudder will cover the entire vertical tail span. The maximum rudder deflection angle was chosen to be ±30 degrees, which is a common value for business aircraft [132], hence, the rudder chord (and thus the control derivative $C_{n_{\delta_r}}$) will be sized according to this requirement.

The first critical condition to be analyzed is the asymmetric thrust. This condition applies to when one of the engines fails and creates a yawing moment. Due to the long moment arm of the engines w.r.t. the fuselage, this is an important condition to consider. The required rudder deflection to compensate for this yawing moment can be calculated by Equation 11.16. This results in a required rudder deflection angle of 7.3 degrees.

$$\delta_R = \frac{T_L y_T}{-qSbC_{n_{\delta_r}}} \tag{11.16}$$

The second critical condition is that of the event of a 90 degree crosswind landing. With a crosswind speed based on the FAA requirement of it being 20% of the stall speed. Note that it does not mean that the aircraft cannot land when a larger speed crosswind is present. The pilot and/or control system will simply not be able to continue a straight flight path in that case, and will have to anticipate the landing by aiming to the right/left of the runway. The rudder deflection angle δ_r and crab angle σ can be found by solving the system of equations constructed by Equation 11.17 and Equation 11.18. These equations come from the force equilibrium that comes forth when looking at the lateral forces during a crosswind landing, as depicted in Figure 11.4. With a rudder deflection angle of 29 degrees at a crosswind of 13 knots the aircraft can keep flying straight and level. Therefore, the maximal rudder deflection angle is decided to be ±30 degrees.

$$\frac{1}{2}\rho V_T^2 Sb\left(C_{n_o} + C_{n_\beta}(\beta - \sigma) + C_{n_{\delta_R}}\delta_R\right) + F_w \cdot d_c \cos\sigma = 0 \tag{11.17}$$

$$\frac{1}{2}\rho V_W^2 S_S C_{D_y} - \frac{1}{2}\rho V_T^2 S\left(C_{y_o} + C_{y_\beta}(\beta - \sigma) + C_{y_{\delta_R}}\delta_R\right) = 0 \tag{11.18}$$

Note that for the H2-VTOO aircraft, if a crosswind is present during the VTOL, one does not have yaw authority by means of the rudder. Therefore, correct inputs by the control system and/or pilot must be given to control the yaw by means of (intentional) asymmetric thrust. The aircraft will rotate itself into the wind this way, and than provide sufficient forward thrust to not get blown backwards. This process is similar to that of a helicopter landing, and can be combined with the roll control during a VTOL landing. This maneuvre can also be used to stay in a straight flight when the crosswind speed is larger than that specified in Table 11.3.

From combining these two critical conditions, and evaluating which condition requires the largest rudder, the rudder can be sized. It has been found that the crosswind landing is the most critical condition, which is shown in Table 11.3 together with the required rudder dimensions.

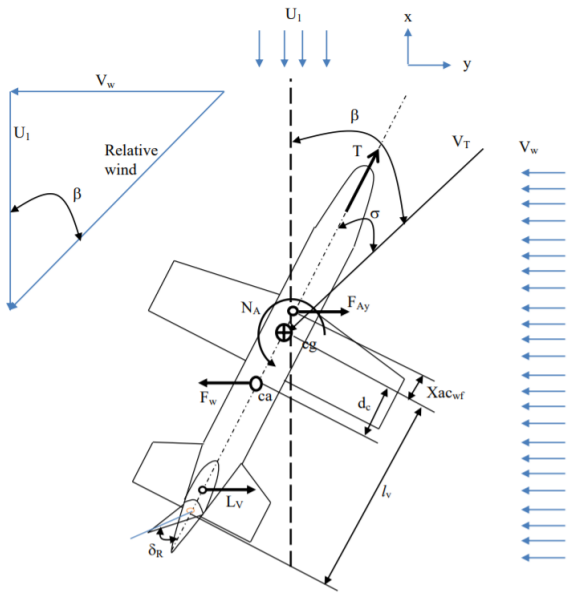

Figure 11.4: Forces and angles in crosswind crabbed landing. [128]

Table 11.3: Rudder dimensions, parameters and critical condition.

Parameter	Symbol	Value	Unit
Maximum rudder deflection angle	$\delta_{r_{max}}$	±30	deg
Rudder chord length	c_r	0.71	-
Rudder span	b_r	4.51	m
Critical condition	Crosswind landing at 13 kts		

11.2.3. Elevator

To size the elevator, one has to design for two main criteria: being able to rotate the aircraft at take-off conditions into the desired pitch, and providing longitudinal trim during cruise. To size the elevator properly, three design parameters must be chosen: the elevator span, chord length and maximum deflection angles up and down. The span is chosen to be the full span of the horizontal tail surface, this leaves the chord and maximum deflection angles free to be sized. It is assumed that the maximum upwards deflection angle is equal to the maximum downwards deflection angle.

Firstly, the take-off condition is analyzed. To start off with finding the required elevator deflection angle needed for take-off, with certain elevator dimensions, one has to analyze to FBD as shown in Figure 11.5. Note that, unlike this FBD, the thrust force is located on the top of the fuselage due to the high wing configuration, under a nacelle angle for take-off, needed for propeller clearance with the ground, as described in Section 8.4.

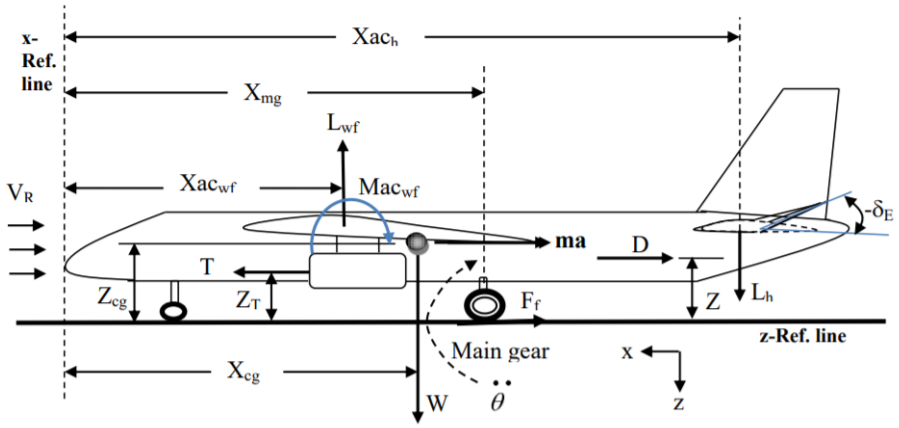

Figure 11.5: Free body diagram depicting the forces and moments used for elevator sizing during take-off. [127]

From this diagram, one can set up the moment equilibrium to find the required downforce needed at the tail section in order to rotate the aircraft. From this required force, the required elevator deflection angle for take-off $\delta_{e_{TO}}$ can be found using Equation 11.19. Typically, one inspects the rotation rate of the aircraft that is needed in order to ensure proper rotation. However, since H2-VTOO makes use of rotating engines, it is decided to not perform an intensive analysis on this matter. Therefore, the required elevator deflection angle is the calculated angle +5deg. The required elevator deflection angle for take-off is listed in Table 11.4. Note that the maximum elevator deflection angle will follow from this condition, and it is assumed that the elevator will have an equal amount of maximal upwards deflection as downwards deflection.

$$\frac{L_h}{0.5\rho V_R^2 S_h} = C_{L_{h_0}} + C_{L_{\alpha_h}} \left(\alpha_h + \tau_e \delta_{e_{TO}}\right) \tag{11.19}$$

Secondly, to find the required elevator trim angle during cruise, the free body diagram as depicted in Figure 11.6 can be used to derive the set of equations needed to analyze the required angle of attack α and elevator deflection angle δ_e. Note that this FBD is not corresponding to that of the H2-VTOO aircraft, but can be used nonetheless. The set of equations result in Equation 11.20 and Equation 11.21, which can be solved as a system of two equations with two unknowns. The required δ_e for this condition is listed in Table 11.4.

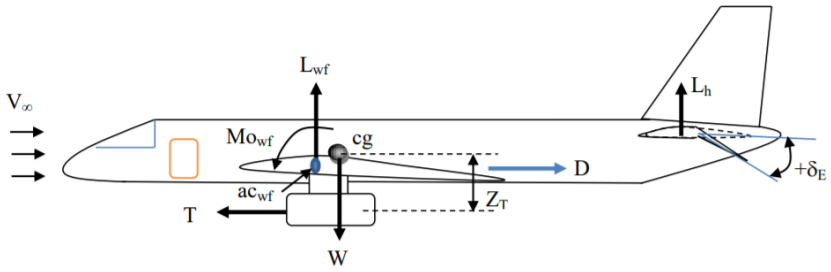

Figure 11.6: Free body diagram of the aircraft configuration during cruise conditions. [127]

$$C_{L_0} + C_{L_\alpha}\alpha + C_{L_{\delta_e}}\delta_e = \frac{W}{q \cdot S} \tag{11.20}$$

$$C_{m_0} + C_{m_\alpha}\alpha + C_{m_{\delta_e}}\delta_e = -\frac{T \cdot z_T}{q \cdot S \cdot c_{MAC}} \tag{11.21}$$

Table 11.4: Elevator dimensions, parameters with required trim and take-off deflection angles.

Parameter	Symbol	Value	Unit
Elevator deflection for cruise trim	$\delta_{e_{trim}}$	4.6	deg
Elevator deflection for take-off	$\delta_{e_{TO}}$	-12.9	deg
Maximum deflection angle	$\delta_{e_{max}}$	±15	deg
Elevator span	b_e	5.67	m
Elevator chord length	c_e	0.71	m

11.3. Aircraft control overview

The H2-VTOO aircraft has functions similar to a helicopter and an aircraft. In principle the control diagrams of both a helicopter and an aircraft can be simplified as seen in Figure 11.7.

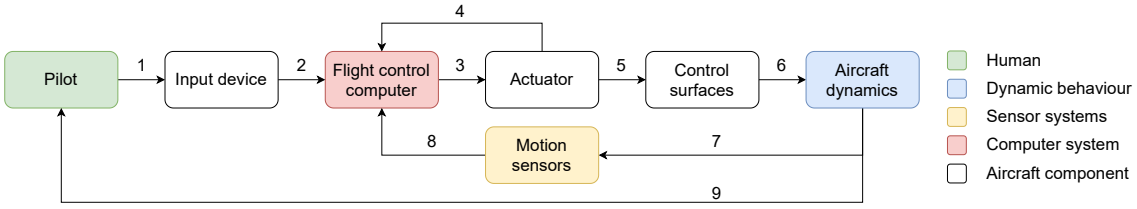

Figure 11.7: Simplified overview of the control of an aircraft.

Table 11.5: Explanation of numbers of Figure 11.7

Number	Explanation
1	Movement as per required input
2	Electrical signal
3	Electrical signal
4	Electrical feedback signal
5	Movement of actuator
6	Movement of control surfaces
7	Motion
8	Electrical feedback signal
9	Visual feedback

The H2-VTOO aircraft uses an all-electric configuration. Next to a fly-by-wire system, the actuator is controlled electrically as well. The main difference between the H2-VTOO and a conventional aircraft is how the flight control computers reacts on the inputs of the pilot. The computer has to predict which flight mode the aircraft is in and change the control response accordingly. This system cannot fail, that's why the H2-VTOO has all sensors redundant and a redundant flight computer.

The computer changes its response based on the angle the motor nacelles makes with the body axis and the airspeed. In Section 8.4 the combination of producing lift with the wing and the turned nacelle is discussed. During a transition phase, either from the turned rotors during conventional take-off, or a full transition from helicopter mode, the aircraft has to constantly balance the lift generated by the rotor and by the wing to keep level. In the mean time the flight computer needs to give a proper response to the input of a pilot. Generally the computer has three different modes:

Firstly, *Aircraft mode*: The Thrust Control Lever (TCL) acts as a normal thrust controller and controls the electrical power delivered to the propellers. The control stick should control the ailerons and elevators.

Secondly *Helicopter mode*: The TCL acts similarly to the collective of a helicopter. Moving the TCL forward and backwards changes the pitch angle of the rotor blades, hence increasing or decreasing thrust. The control stick influences the orientation of the lifting surface and allows for flight control in helicopter mode.

Lastly, *Hybrid mode*: The aircraft flies with its propellers partly tilted upwards. The wing cannot yet deliver the necessary lift for stable flight. After an input from the pilot, the flight computer is programmed to send a signal to the appropriate actuators. This will be a combination of the control actuators used during aircraft mode and helicopter mode.

An example control loop for transitioning is displayed in Figure 11.8. To transition from helicopter mode into aircraft mode the pilot needs to gradually pitch up and reduce the motor nacelle angle. During this manoeuvre horizontal speed is increased, and the wing begins to generate lift. The flight control computer senses the airspeed and calculates the lift produced by the wing. Based on that data the rotors can gradually be placed in parallel with the aircraft body. In order to transition, the H2-VTOO in helicopter mode needs to be able to provide the necessary thrust to stay level at a rotor nacelle angle of around 75° to provide forward velocity as well. This is only necessary for the short time the aircraft's wing is not yet generating any lift. The mechanism to turn the engines is relatively straightforward. The entire rotorblock is attached to a beam, supported by bearings. A double redundant electric motor is connected to the beam via a gear to rotate the system.

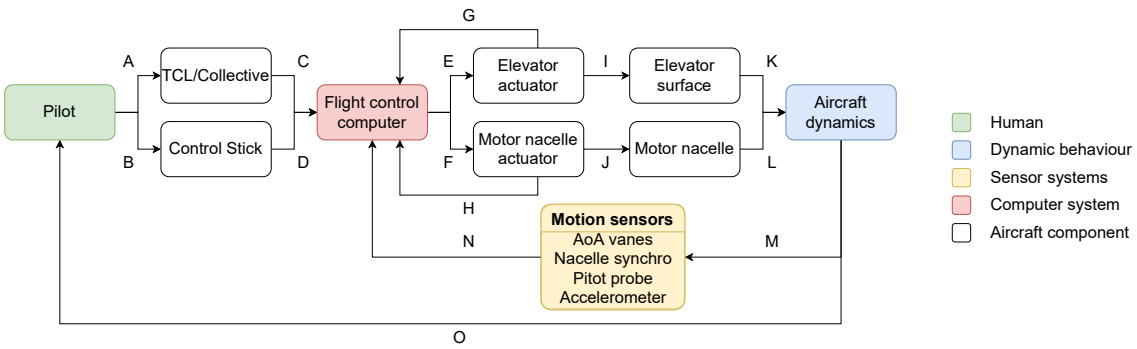

Figure 11.8: Overview of control of the transition phase.

Table 11.6: Explanation of letters in Figure 11.8.

Indicator	Explanation
A	The pilot pushes the nacelle control nob located on the TCL forward
B	The pilot pulls slightly on the Control stick to raise the attitude
C	The analogue input of the TCL is transformed to an electrical signal
D	The analogue input of the control stick is transformed to an electrical signal
E	The flight computer looks at the current flight phase and sends a signal to the elevator actuator
F	The flight computer looks at the current flight phase and sends a signal to the motor nacelle angle actuator and the propeller pitch angle actuator
G	The elevator actuator sends a feedback response back to the flight computer
H	The motor actuator sends a feedback response back to the flight computer
I	The elevator surface is moved based on the actuator input
J	The motor nacelle angle and the rotor pitch is moved based on the actuator input
K	The elevator changes the aircraft dynamics
L	The propeller pitch and angle change the aircraft dynamics
M	Motion sensors receive information on the pitch, nacelle position and velocity
N	An electrical signal on the motion is sent to the flight computer
O	The motion of the aircraft is seen and felt by the pilot

11.4. Assessing Longitudinal Static Stability and Controllability

In this section, the longitudinal static stability and controllability will be assessed. This will be done by first choosing the optimal longitudinal wing position in terms of CG location. Than, the extreme CG locations will be found by means of a potato diagram. Finally, a scissor plot will be constructed which will show whether or not the extreme CG cases lie within the limits of the stability and controllability of the aircraft.

11.4.1. Longitudinal wing position determination

To find the optimal location of the wing, one can construct the change in forward and aft CG with respect to the wing position (noted by X_{LEMAC}) as shown in Figure 11.9. From this diagram, one can find the minimum distance between the most aft and most forward CG, the corresponding wing position is the most optimal. This is due to the fact that the CG range will then lay more easily within the stability and controllability limits as described in Section 11.4.3.

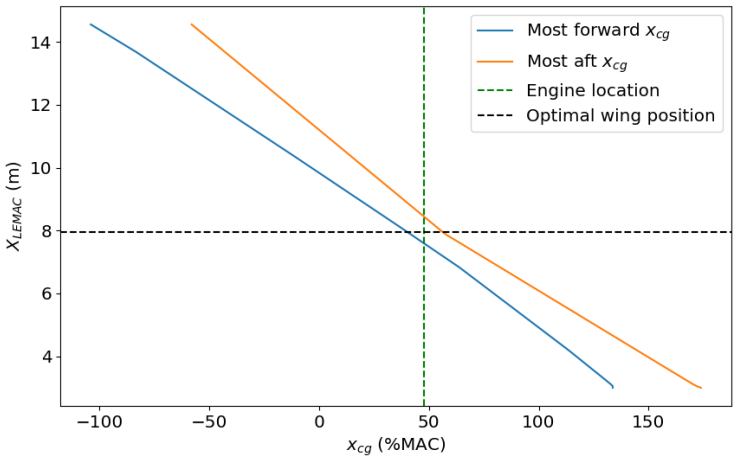

Figure 11.9: Engine placement: x_{cg} = 47.8% and $X_{LEMAC} = 7.95\ m$.

11.4.2. Potato Diagram

To find the proper range of CG's that the aircraft will be subjected to, one can construct a potato diagram, as shown in Figure 11.10. In this diagram, all possible load conditions are explored, together with their influence of the CG position. From this, one can extract the most aft and most forward CG values, while using a safety margin of 2%, which is based on experience. The different loads which the aircraft is subjected to are shown in the legend of Figure 11.10. It can be concluded that the most aft CG is located at 44.27% of the MAC, and the most forward at 22.63% of the MAC.

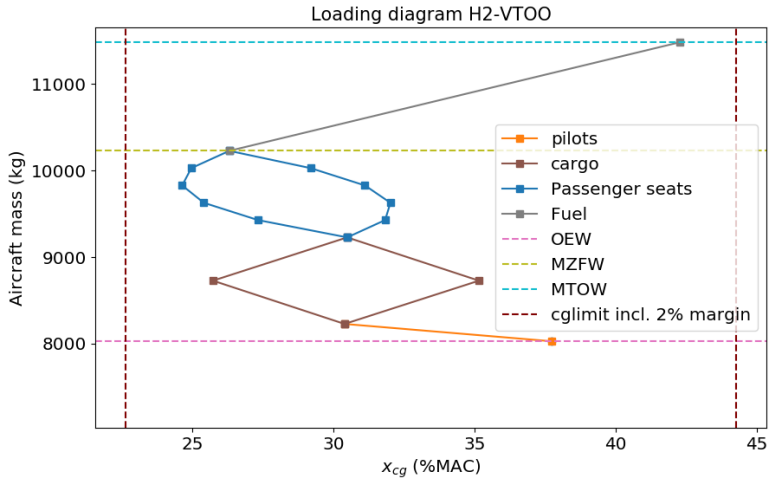

Figure 11.10: Loading diagram, Most aft xcg = 44.27% and most forward xcg = 22.63%.

11.4.3. Scissor Plot

To assess whether or not the aircraft is statically stable and controllable, a scissor plot, shown in Figure 11.11, can be constructed. The stability line is plotted using Equation 11.22, where S.M. is the stability margin, which equals 0.10 in this case and has been chosen rather high for a more redundant design in terms of c.g. fluctuations. The controllability line is plotted using Equation 11.23. Then, the most forward and most aft cg locations are plotted and checked if they lie between the two curves. From this plot, one can alter the stability and controllability by either changing the wing location or horizontal tail surface area. This is incorporated in the iteration program described in Section 7.1. As can be seen, the aircraft is just statically stable and controllable, but also with a slightly overdesigned horizontal tail. This is done on purpose, since the vertical tail will take up some of the surface area of the horizontal tail surface, therefore the extra surface will guarantee that the tail can generate the required lift. However, it should be noted that the tail surface can be further optimised.

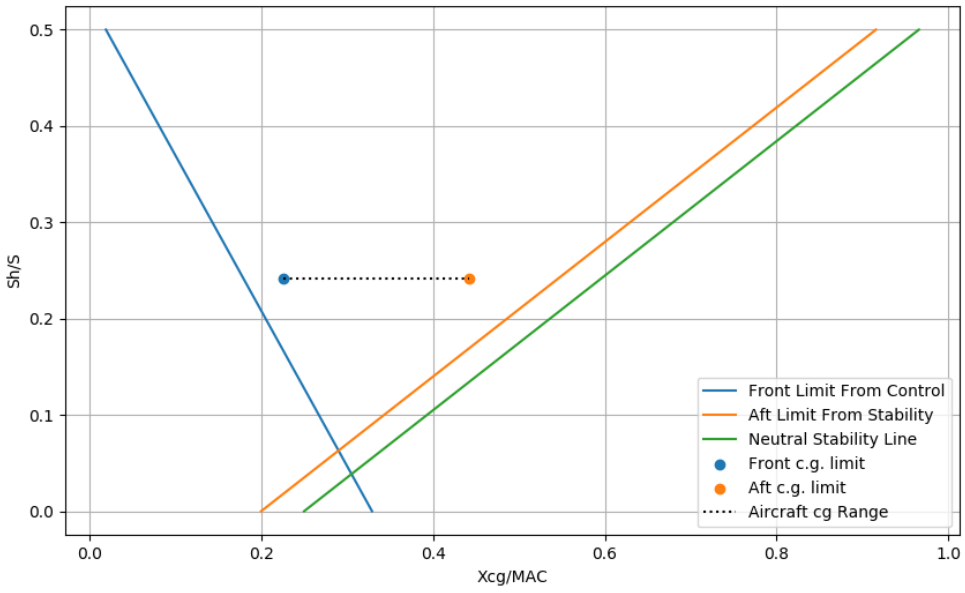

Figure 11.11: Scissor plot describing the stability and controllability lines and c.g. range of the aircraft.

$$\bar{x}_{cg} = \bar{x}_{ac} + \frac{C_{L\alpha h}}{C_{L\alpha A-h}}\left(1 - \frac{d\epsilon}{d\alpha}\right)\frac{S_h l_h}{S\bar{c}}\left(\frac{V_h}{V}\right)^2 - S.M \tag{11.22}$$

$$\bar{x}_{cg} = \bar{x}_{ac} - \frac{C_{mac}}{C_{L\alpha A-h}} + \frac{C_{Lh}}{C_{L\alpha A-h}}\frac{S_h l_h}{S\bar{c}}\left(\frac{V_h}{V}\right)^2 \tag{11.23}$$

11.5. Verification and Validation

11.5.1. Stability Analysis

Verification of the stability analysis can be performed by determining how accurate the model is. The system that is used to analyse dynamic stability was linearised. This introduces some error due to neglecting the higher order terms. However, in academia this is an error that is often deemed so small that it is a perfectly valid assumption. Apart from this, the assumption is made that the stability derivatives are independent of surface area. This assumption is proved to be valid due to the fact that in AVL, the same stability derivatives could be obtained when using scaled wings.

To validate the stability model, one can use the geometry from the Cessna Citation aircraft, used in the SVV course. For this aircraft, the stability derivatives are known and dynamic stability has been analyzed before. Therefore, the output of AVL can be compared to that of the course's output, and found to be equal.

11.5.2. Control Surfaces

The calculation of the control surfaces can be validated by comparing them with similar aircraft in their category, namely business aircraft. This category is chosen due to the weight, and typical control-surface requirements.

The aircraft chosen for this is again the Cessna Citation III, with an MTOM of 9979 kg. For this aircraft, three tables are made comparing several factors for each control surface to that calculated for H2-VTOO. It is then validated if the results are realistic and do not deviate too drastically from the Cessna Citation III. In Table 11.7, b is the wing span, C_a/C the aileron chord ratio, also referred to as τ in the formulas. The span ratio is split into two parts, the inboard ratio and the outboard ratio respectively. These indicate where on the half-wing span the aileron starts and ends. For Table 11.8 and Table 11.9, the surface area ratios with respect to the vertical and horizontal tail, and the chord ratios are listed as well.

Table 11.7: Validation of aileron dimensions.

Aircraft	b [m]	C_a/C	Span ratio	$\delta_{a_{max}}$ [deg]
Cessna Citation III [126]	11	0.2	0.46/0.95	+20, -14
H2-VTOO	5.82	0.2	0.07/0.90	±15

Table 11.8: Validation of rudder dimensions.

Aircraft	S_r/S_v	C_r/C_v	$\delta_{r_{max}}$ [deg]
Cessna Citation III [128]	0.26	0.26	±25
H2-VTOO	0.3	0.3	±30

Table 11.9: Validation of elevator dimensions.

Aircraft	S_e/S_h	C_e/C_h	$\delta_{r_{max}}$ [deg]
Cessna Citation III [127]	0.37	0.37	+15, -15.5
H2-VTOO	0.41	0.3	±15

As can be seen, the values for the rudder and elevator are very comparable to that of the cessna citation. However, two things can be noted. The first being the difference in surface area ratio and chord ratio for the elevator. This is due to the assumption that the chord of the elevator has constant length throughout the span, with the chord length being equal to that 0.3 times the chord of the root of the horizontal tail. Secondly, it can be seen that the aileron takes up 83% of the span, compared to 49% for the cessna. This is rather high and requires further investigation. The effects however are minimal, due to the unused space behind the wingbox before the aileron. Therefore, this is simply an overdesign of the ailerons, which can be further optimized.

12. Power Analysis

One of the main design challenges is the generation and delivery of the necessary power for propulsion and electric systems in all mission phases. This chapter details the design of the two primary sources of power in operations: the batteries and the fuel cells. A thermal analysis for the fuel cells is also completed and a system to accommodate the heat generated by them is determined and sized for. Along with this, the engine selection and sizing is also conducted in Section 12.4. Lastly, Section 12.6.1 and Section 12.6.2 present the verification and validation procedures performed and analyse the outcomes of each test.

12.1. Power Budget

To design and size the power and propulsion system, a power budget has to be made. This power budget exists out of the required shaft power needed for every flight phase to which efficiencies must be added, power to recharge the batteries during cruise and all remaining electrical subsystems.
The required power for each phase of flight has already been determined in Section 7.5, where the design choice was made to let all conventional flight phases be fully powered by fuel cells , whereas batteries will provide the additional power required during VTOL operations. In Section 7.5, it was found that the most demanding conventional flight phase is the cruise phase where 2239 kW is required. The most demanding VTOL operation is hovering at the hover ceiling where 3452 kW is required. These values already take into account the propeller efficiency, however two additional efficiencies must still be added, the engine efficiency and the efficiency of the DC/DC converter that will be discussed later on. Multiplying the engine efficiency of 96% and the DC/DC converter efficiency of 95% results in a total efficiency of 91.2%. Note that the reasoning behind these efficiencies will be explained later on. Dividing the power required for cruise and hovering at the hover ceiling by the total efficiency gives a required power during cruise of 2455 kW and 3785 kW for hovering at the hover ceiling.

As already mentioned, the fuel cells must provide enough power to fully recharge the batteries during cruise flight within a reasonable time. Therefore, the power required to recharge the batteries within one hour is added, which after multiple iterations turned out to be 156 kW as will be explained further on in this chapter.
Finally, the power required for the remaining electrical subsystems has to be determined and added. For most of the subsystems, a statistical estimation can be made based on other aircraft data, where the Boeing 787 [18] was the main example, since this aircraft is also fully electric. The estimation then can be done by using the number of passengers and maximum takeoff mass as a ratio of power required. For some subsystems, such as the actuators, the power can be estimated in a more theoretical way.

To determine the power required for the actuators, an estimation can be made based on some small calculations. The hydraulics will power the actuators for which five different groups can be distinguished: the ailerons, the elevator, the landing gear, the rotation mechanism and the rudder. For each different group, the mass moment of inertia is calculated. Together with this, the required torque to achieve a certain acceleration is calculated by using Equation 12.1, for which the sum of the torque induced by drag and gravity are taken into account. With this torque, the minimum power required can be calculated by my multiplying this torque with the maximum angular velocity as can be seen in Equation 12.1. By doing this same calculation for each single group, a power estimate can be found for the actuators, which can be seen in Table 19.3.

$$\sum torque = I \cdot a \tag{12.1}$$

$$P = \tau \cdot \omega \tag{12.2}$$

Adding the power required to charge the batteries during cruise flight, and the power required for each of the mentioned subsystems to the cruise power, gives the total power to be generated by the fuel cells which equals 2669 kW.

12.2. Fuel Cell Design

This section generates a fuel cells stack system design. First, available fuel cells on the market are evaluated with the best performing being chosen. The fuel cell stacks are then sized according to the power required. After this, a thermal analysis is conducted such that a cooling system can be sized for. To conclude this section, the resulting fuel cell stack system per power unit can be presented in Section 12.2.6

Table 12.1: Electrical power required for subsystems.

Subsystem	Power required (kW)
Conventional aircraft loads	17.96
Lighting	1.172
Fuel	1.562
Water/waste	2.343
Ice/rain protection	0.185
FCS	0.195
Consumer loads	11.33
Navigation	0.391
IPS	0.585
Communication	0.195
Electric actuators	9.374
Electric ECS	28.32

12.2.1. Fuel Cell Selection

This subsection determines a fuel cell for which to base the fuel cell stack design and configuration. There exists multiple types of fuel cells to choose from, first, each type of fuel cell must be assessed for their performance and how relevant they are for the project itself. The types of hydrogen fuel cells to be evaluated are: polymer electrolyte membrane (PEM), alkaline fuel cell (AFC), phosphoric acid fuel cell (PAFC), molten carbonate fuel cell (MCFC) and solid oxide fuel cell (SOFC).

Both SOFC's and MCFC's have the highest power output per stack, however they operate at temperatures over 500˚C, this is way too high a temperature and would not be feasible, both for the safety of the passengers as well as the performance of the aircraft itself. In addition to this, they are also heavier as they are generally used as stationary power sources and are not meant for mobility. PAFC's, will not be considered due to the higher start up time, which is not desirable for the project when one of the main requirements is to reduce door-to-door travel time [7] [39].

PEM fuel cells are chosen as they use pure hydrogen as a fuel, making them more sustainable than the other fuel cells. They also operate at lower temperatures. After this decision was made, fuel cell stacks offered by different manufacturers were assessed. The fuel cell efficiency (E_{FC}) was broken into three corresponding efficiencies: voltage efficiency (E_v), fuel utilisation efficiency (E_f) and thermodynamic efficiency (E_t)[48].

E_v was calculated by simply dividing the output voltage of the chosen fuel stack per cell by the theoretical electric potential for the liquid hydrogen fuel cell reaction of 1.23 V. E_t which accounts for the fact that not all energy from the reaction can be converted to electrical energy, was calculated by dividing the Gibbs free energy by the change in enthalpy of the reaction; this gave a value of 0.83. Finally, E_f was assumed to be 100% such that the fuel is consumed immediately as it is delivered [53]. Solving for the product of these three efficiencies gives the total fuel cell efficiency from hydrogen fuel to DC power for the fuel cell selection in Table 12.2.

Table 12.2: Selection of Fuel cells [144].

Manufacturer/Model	Power [kW]	Mass [kg]	l x w x h [m x m x m]	Efficiency [%]
Toshiba/ H2Rex [146]	100	-	2.900x2.000x2.350	45.54
Ballard/ FCGen-HPS [139]	up to 140	55	0.484x0.555x0.195	44.13
Hydrogenics/HyPM HD 180 [63]	198	654	0.955x1.525x0.690	41.46
PowerCell/ S3-455C [36]	100	98	0.75x0.750x0.520	62.02

From Table 12.2, it can be seen that the clear all-round chosen winner is the FCGen-HPS from Ballard. The hydrogenics model while providing the most power, loses out on both its larger size and mass. The other two fuel cell stack models lack in the power they can deliver along with mass and size. The powercell fuel stacks have the highest efficiency but are still nearly double the mass of the Ballard fuel cell stacks. Fuel cells stacks are chosen for convenience in sizing the new stacks. This is because the stack mass and specific performance will also account for the housing around the fuel cells and therefore, the resulting values from the sizing will be more realistic. Designing fuel cells and then the housing along with them would be too tedious a task for this stage of the conceptual design.

12.2.2. Fuel Cell and Stack Sizing

As discussed before, the PEM fuel cell chosen to model the fuel cell stack to be used is the Ballard FCGen-HPS due to its superior energy density and specific energy. An estimation for the properties of a single cell within the chosen stack could then be computed. In fuel cell stacks, the fuel cells are stacked in series, this means that the current of the stack and the current of a single fuel cell are equal. Therefore, the area of the fuel cells themselves dictate the current of the

stack.

The voltage of each fuel cell is determined by simply dividing the voltage of the stack by the number of fuel cells, this was found to be 0.654 V. The current density of a cell was then determined by dividing the current of each cell by its area-yielding a value of 0.683 A/cm^2. The mass of each cell was also calculated by dividing the total mass of the fuel stack by the number of cells. With the required properties of a single fuel cell now derived, the fuel stacks to be used by H2V-TOO can now be sized.

While keeping the area the same and therefore obtaining the same current, the power output of a stack is only increased by adding more fuel cells thereby increasing the voltage. The stacks in each power unit were chosen to be in series, this is because having even one line of stacks in parallel would result in too high a mass for the fuel cells as the stacks must provide a high enough power. While one might argue that the current could be increased to accommodate a lower voltage for a parallel configuration, this would not be feasible as a fuel cell with a larger area would have significant temperature differences from end to end and would therefore interfere with the performance of the fuel cells themselves [136].

Following these decisions, the number of fuel cells and fuel stacks were varied to determine an optimum configuration for each power unit. For this, close attention was payed regarding the number of fuel cells per stack; while having a few stacks with large cells may be compact, this would result in a severely high voltage per stack which would be hazardous to the operation of the aircraft. Additionally, a large number of cells per stack would also result in a more complex and therefore more failure prone [108] thermal system because all cells along the entire stack would have to be maintained at the same temperature for optimum efficiency. 6 fuel cell stacks of 339 fuel cells each per power unit was then determined to be the optimum configuration for both weight and volume. The stacks would be placed in series along the length of the fuselage in the relevant compartment assigned to them as it would not be possible to place them along the cross section of the fuselage as both the spacing between fuel cells and the size of the fuel cells themselves would not be contained. Furthermore, the temperature range of the fuel cell stacks is between -40 to 95 degrees Celsius. This is important for the performance of the fuel cells during operation and will therefore be analysed in Section 12.2.3. Lastly, the pressure and humidity at which the fuel cells are maintained and fuel delivered to them must be maintained. These systems are discussed in Section 12.2.6 and must be designed later in the design phase.

The final sizing parameters for the fuel cell stacks can be found in Table 12.3

Table 12.3: Parameters of fuel cells and fuel cell stacks.

Number of cells in a stack	Power of a stack[kW]	Mass of a stack[kg]	Total number of stacks	Total mass of stacks[kg]	Total volume of stacks[m^3]
339	142.94	60.34	18	1086.12	1.03

12.2.3. Thermodynamic Analysis

With the sizing of the fuel cells complete, a thermodynamic analysis will now be conducted in this subsection. Firstly, it is important to elaborate more on the efficiencies mentioned in Section 12.2.1. In this section, a total efficiency of 44.1% was determined for the fuel cells, this was the product of three sub-efficiencies. One would think that the heat lost from the fuel cells could be calculated using this efficiency, however, the thermal efficiency relates the theoretical maximum amount of thermal energy from the reaction in the fuel cells that can be converted to electrical energy-the Gibbs free energy. This means that the fuel cell can have a maximum efficiency equal to the thermal efficiency component. However, in reality, this is not the case and other factors further lower the efficiency of the fuel cell; this is due to the resistance of the materials used to make the fuel cell and voltage drops that may occur [136]. Therefore, the energy the fuel stacks lose as heat must be evaluated with a different method. This is done by setting up an energy balance using Equation 12.3[136]:

$$\sum Q_{in} - \sum Q_{out} = W_{el} + Q_{dis} + Q_c \tag{12.3}$$

Q_{in} represents the energy produced from the reactants, in this case hydrogen and oxygen. Similarly, Q_{out} represents the energy produced from the products, in this case the water. W_{el} is the electricity generated by the fuel cells. Q_{dis} and Q_c represent the energy dissipated and the energy needed for cooling respectively, for the energy balance, these aforementioned parameters are set equal to each other. Additionally, Equation 12.3 can be simplified to chemical form resulting in Equation 12.4:

$$H_2(g) + {}^1/2O_2(g) \rightarrow H_2O(l) + \text{electric energy} + \text{waste heat} \tag{12.4}$$

The energy produced per second from the products and reactants was calculated by first determining their mass flow $\dot{m}$ to meet the power requirement, and then multiplying it with the relevant molecule's specific internal energy at the

operating temperatures of the fuel cells [139]. By doing this, a maximum value for the heat generated from them can be analysed and a cooling system can be sized for this worst-case scenario.

By applying Equation 12.3, the total heat dissipated is computed as 1988 kW. When dividing this by the total energy generated and subtracting it by one, leads to 32.9% of the energy produced being lost as heat from the fuel cells. The results of the energy balance and thermal analysis will be later analysed in Section 12.6.

12.2.4. Cooling System

Taking away the dissipated heat of the fuel cells will be done by a cooling system which consists of two subsystems. The first subsystem is using cold hydrogen leaving the fuel tank to cool down the fuel cells before entering the fuel cell for power generation. Secondly, a radiator based cooling system will be deployed to take away the remainder of the heat. The sizing and preliminary design of these two subsystems will be further discussed below, however it must be noted that further research and analysis is required to arrive at a functional final cooling system design. Also, an air based cooling system was considered as an alternative cooling method but was deemed unfeasible as the required contact area on the fuel cells would be too large.

Fuel cell cooling by hydrogen

The hydrogen leaves the fuel tank in a gaseous state with an extremely low temperature of 20 K. Heating the hydrogen to 273.15 K by letting it flow past the fuel cells before using as fuel, will withdraw a considerable amount of heat from the fuel cells. In addition, it will be beneficial for operation of the fuel cell itself as the operating temperature lies between 245.15 K and 368.15 K. To calculate how much heat the cold hydrogen can absorb, Equation 12.5 is used [10]. $\dot{Q}$ represents the joules per second which that can be absorbed by the cold hydrogen, $\dot{m}$ is the hydrogen mass flow, $C_{p_{H_2}}$ the specific heat of hydrogen and ΔT the temperature difference. The specific heat of hydrogen at different temperatures is found in literature, from these values, an average of 12620 J/(kg K) is used [42][1]. The total temperature difference which the hydrogen will experience is 253.15 K. Finally, the hydrogen mass flow can be calculated by using Equation 12.6 with the previously computed fuel cell efficiency η_{fc} of 44.13%, the required fuel cell power to be generated and the gravimetric energy density of hydrogen $E_{gravimetric}$ which is $120 * 10^6$ J/kg[64][2]. From this, a mass flow of 0.05 kg/s of hydrogen is found which can be put in Equation 12.5. A thermal power of 161 kW can be absorbed by the cold hydrogen by redirecting it along the fuel cells to cool them down.

$$\dot{Q} = \dot{m} C_p \Delta T \tag{12.5}$$

$$\dot{m} = \frac{P_{fc}}{\eta_{fc} E_{gravimetric}} \tag{12.6}$$

Radiator cooling

The radiator based cooling system will have to transport the remaining dissipated heat of 1827 kW to the outside of the aircraft. It will do this by first absorbing the heat of the fuel cells via tubes running along the surface of a fuel cell stack, using thermal conduction. This heat will heat up the cooling liquid inside the tubes, after which the cooling fluid will flow to the actual radiators outside the aircraft. Here, the cooling fluid will lose its heat by conducting it to the radiator fins where finally the heat will be transferred to the air, by forced convection. Hereafter the cooled cooling liquid will return to the fuel cells were this entire cycle will recommence. To sustain the cooling cycle, a pump is used which ensures a constant flow velocity and mass flow of the cooling liquid. This entire process is visualised in Figure 12.1.

The first step in sizing the cooling system is to determine which cooling liquid will be used. Water has excellent cooling capabilities due its high specific heat coefficient. However, when flying at the service ceiling of 7000 m, the outside temperature drops to -31˚C for standard ISA conditions. When pure water would flow through the radiator outside aircraft, it could freeze and cause sever problems for the cooling of the fuel cells. Therefore a water-glycol mixture will be used with a 50% glycol concentration, which lowers the freezing temperature to -36.8°C. In addition, the use of a water-glycol mixture is beneficial in terms of corrosion of the tubes [41][3]. Secondly, it must be decided out of which material the tubing and radiator will be made. For this, two main materials were considered: aluminium and copper. Copper has a thermal conductivity of 401 W/(m K), whereas aluminum has a thermal conductivity of 236 W/(m K), from this point of view, copper is significantly better [143][4]. However, copper costs 4.2 times as much as aluminium at the time of writing, and weighs 3.3 times as much [100][91][5][6]. Therefore, the decision is made to have a radiator fully made from aluminium which is in line with the current trend in radiator technology.

[1] https://www.engineeringtoolbox.com/hydrogen-d_976.html
[2] https://hypertextbook.com/facts/2005/MichelleFung.shtml
[3] https://www.engineeringtoolbox.com/ethylene-glycol-d_146.html
[4] https://www.engineeringtoolbox.com/thermal-conductivity-metals-d_858.html
[5] https://www.indexmundi.com/commodities/?commodity=copper&months=60&currency=eur&commodity=aluminum
[6] https://www.engineeringtoolbox.com/metal-alloys-densities-d_50.html

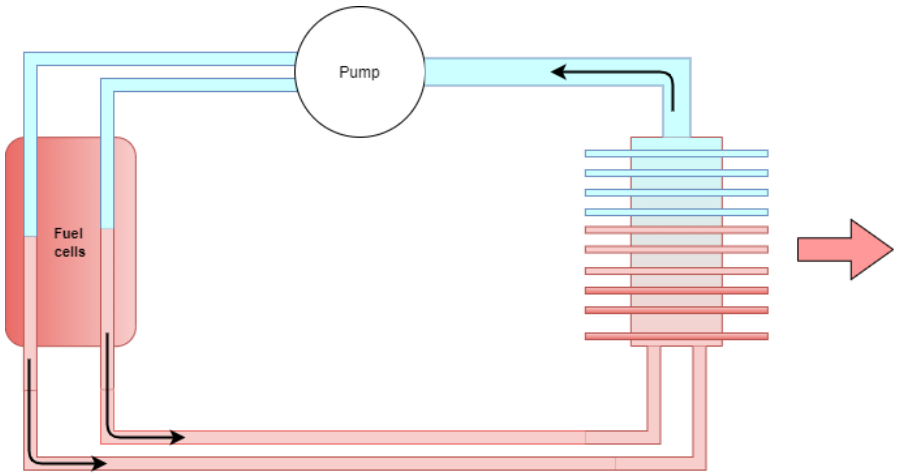

Figure 12.1: Radiator based cooling of a fuel cell stack.

With the cooling liquid and radiator material chosen, the sizing of the radiator system can done. For this, multiple simplifying assumptions are made.

- The maximum temperature of the fuel cells during operations is decided to be 358.15 K.
- In the most critical case, the cooling liquid is heated up from an ambient air temperature of 298.15 K to 358.15 K whilst absorbing all heat being dissipated by the fuel cell.
- The conductive surface area between the fuel cells and the tubes is assumed to be equal to the surface area of the bottom half of the tubes.
- The conductive surface is assumed to be a flat plate.
- All the heat dissipated by the fuel cells is assumed to be conducted through the tubes.
- At the end of a cooling cycle, the cooling fluid is fully cooled such that its temperature is equal to that of the ambient air.
- The heat transfer rate between the fuel cells and the cooling fluid is assumed to be a fully conductive process where the tubes act as medium through which the heat must conduct.
- The cooling fluid is able to transfer all its heat to the radiator fins without any energy losses.
- The heat transfer rate between the radiator fins and the outside air is a pure convective process.

First, a required coolant mass flow is computed such that enough coolant flows by the fuel cells to absorb the remaining dissipated heat. Equation 12.5 is used again, but now it must be solved for $\dot{m}$. $\dot{Q}$ is equal to the remaining dissipated heat of 1759.7 kW, ΔT is 60 K in the most critical case considered and C_p is the specific heat coefficient of the water-glycol cooling fluid, equal to 3488.3 (J/kg K) [41]. Solving for the mass flow, leads to a total required coolant mass flow of 8.7 kg/s.
The tubes in contact with the fuel cells should be sized such that they offer enough contact area to conduct all dissipated heat. For this Equation 12.7 is used where again $\dot{Q}$ is the dissipated heat to be conducted as mentioned before, k is equal to the thermal conductivity of aluminium mentioned before, T_2 is the temperature of the cooling fluid and assumed to be 298.15 K and T_1 is the temperature of the fuel cells which is assumed to be 358.15 K [10]. The unknown variables are the contact surface area A and the tube thickness d, the ratio of these two can be computed which results in a contact surface over tube wall thickness ratio of 129 m, this ratio can be considered as a design variable used for further, more detailed design of the cooling system.

$$\dot{Q} = k\frac{A}{d}(T_1 - T_2) \tag{12.7}$$

$$\dot{m} = \rho V A_{tube} \tag{12.8}$$

Sizing of the tubes must be done such that they can accommodate the required coolant mass flow of 8.4 kg/s, by using Equation 12.8 a cross-sectional area of the tube can be calculated. The density of the cooling fluid is equal to 1079 kg/m^3 and a flow velocity of 1.5 m/s is chosen as initial estimate as it is a common flow velocity for cooling water in tubes[41][142][7]. Solving for A_{tube} results in a total required cross-sectional tube area of 54 cm^2.
Finally, the total radiator fin area has to be determined such that all of the heat can be dissipated to the air stream and consequently cool down the cooling fluid. Solving Equation 12.9 for A where $\dot{Q}$ is again 1760 kW and h is the forced

[7] https://www.engineeringtoolbox.com/flow-velocity-water-pipes-d_385.html

convective heat transfer coefficient of air for which an average value of 255 W/m^{2}K was taken[111]. Finally T_2 is the temperature of the radiator fins equal to 358.15 K and T_1 is the ambient air temperature assumed to be 298.15 K. This assumption is deemed accurate enough as the aircraft is often flying at higher altitudes and thus lower temperatures. In addition, a redundancy of ten degrees is present such that the temperature of the fuel cells is allowed to increase further on a hot day. Solving for A leads to a total required fin surface area of 119 m^2. The radiators are to be located underneath the wing at the root as illustrated in Figure 12.2 where the location of the radiator is marked in red. Here they are exposed to the incoming airflow during regular flight phases which will enhance the convection of heat to the air. During VTOL however, the radiators are not directly exposed to an airflow. To solve this problem, a flap will be placed in front of the radiators to redirect the vertical airflow onto the radiators. This will not be sufficient to fully cool down the radiators and the cooling liquid, however the VTOL phases at which the fuel cells deliver maximum power, lasts only 90 seconds at maximum. A time period in which the fuel cells will not heat up beyond the maximum allowable temperature of 368.15 K.

$$\dot{Q} = hA(T_2 - T_1) \tag{12.9}$$

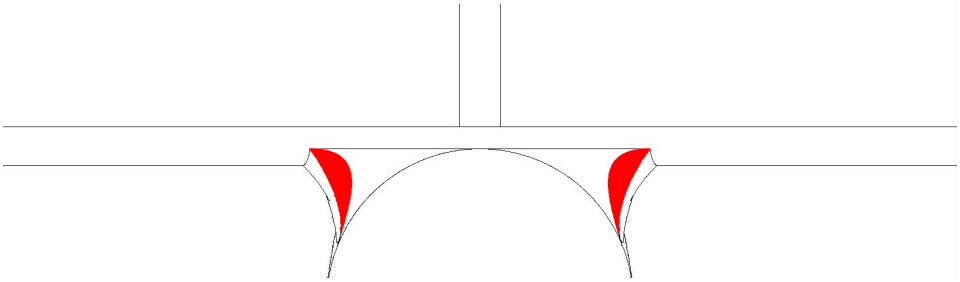

Figure 12.2: Radiator location between the wing and the fuselage.

The resulting conceptual design of the cooling system is summarised in Table 12.4. However, due to the time constraint and the scope of the conceptual design, an abundance of simplifying assumptions was used, therefore a more detailed and accurate thermodynamic analysis is required for the next design phase. In addition, the detailed sizing and configuration of the cooling system, such as tube location and tube thickness are subject to further research and analysis. One last note to be made on the design of the cooling system is that as mentioned in Section 10.1 if there is insufficient boil-off due to excess LH2 being extracted, the heat generated by the fuel cells is used to counter this effect. While this may not significantly alter the design of the cooling system, it makes the design slightly conservative.

Table 12.4: Fuel cell cooling system properties and dimensions.

$\dot{Q}_{total}$ [kW]	$\dot{Q}_{H2}$ [kW]	$\dot{Q}_{coolant}$[kW]	$\dot{m}_{coolant}$[kg/s]	$\frac{A}{d}$ [m]	A_{tubes}[m^2]	A_{fins}[m^2]
1987.7	161.0	1826.6	8.7	129.0	53.9	119.4

Fuel cell cooling by water emissions

A factor not considered in the radiator cooling system sizing, is the heat absorbed by the water emissions. These absorb a portion of the fuel cells' dissipated heat, by increasing in temperature. However, due to the conceptual level of this design phase and the time constraint, no analysis was done on this. What can be concluded is that the radiator cooling system has to absorb less heat and thus has been sized more conservatively than initially expected.

12.2.5. Air Inlet Sizing

Power production by the fuel cells does not only depend on the hydrogen carried on-board, but also on the amount of oxygen available. The inlet should be sized such that the incoming mass flow of air, contains enough oxygen to sustain the chemical reaction as shown in Equation 12.4. From this formula it can be calculated what the minimum required oxygen mass flow should be, if the hydrogen mass flow is known. In Section 12.2.4 the hydrogen mass flow at maximum fuel cell power was computed to be 0.05 kg/s, converting this to moles per seconds by using the molar mass of hydrogen of 0.002 kg/mole results in a molar mass flow of 25.2 mole/s. Following from Equation 12.4, the oxygen molar mass flow should be 12.6 mole/s, multiplying this by the molar mass of oxygen of 0.032 kg/mole gives a required oxygen mass flow of 0.4 kg/s.

The most critical condition for which the inlet needs to be sized occurs at the lowest airflow velocity. The design choice

is made to have an inlet big enough to accommodate a sufficiently large mass flow at service ceiling conditions at the take off speed of 56.4 m/s. At lower velocities, an internal fan or compressor will be used to obtain the required mass flow.
The required mass flow of air can be computed by dividing the required oxygen mass flow by the oxygen concentration at the service ceiling which is equal to 8.7% [8]. Resulting from this is a required air mass flow of 4.63 kg/s. Using Equation 12.10 where ρ is the service ceiling density of 0.59 kg/m^3 and V is the take-off velocity of 56.4 m/s. Solving for A gives a required inlet area of 0.14 m^2.

$$\dot{m} = \rho A_{inlet} V \tag{12.10}$$

12.2.6. Fuel Cell System Layout

With the stacks and main cooling system design, a diagram depicting how the fuel cell power system works can be generated, this is presented in Figure 12.3

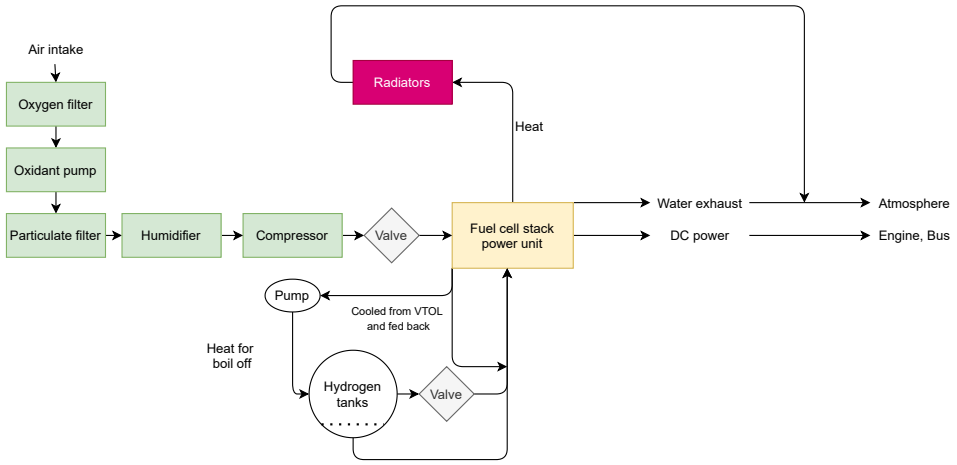

Figure 12.3: Fuel cell stack system diagram.

As PEM fuel cells are used, only oxygen and hydrogen are needed as reactants. The oxygen is obtained from the air intake of the aircraft, this is then filtered to remove nitrogen and other molecules present in air. The oxidant is then pumped through a particulate filter to remove any impurities in the oxygen to avoid interference with the fuel cell electrodes[136]. A humidifier is then used to ensure the fuel cells operate at optimum humidity conditions, and lastly the compressor is used to increase the pressure that the oxygen is delivered to the fuel cells a the desired value[139].

A loop is present to visualise the cooling of the fuel cells during VTOL by using the stored hydrogen and then feeding it back into the fuel cell power unit when needed. The majority of the heat produced from the fuel cells is then transferred to the radiators using tubing as described in Section 12.2.4. The radiators, placed near the wings of the aircraft, then emit the heat into the environment.

The water tank and heat vent both are used to absorb heat generated by the fuel cells and then expel these into the atmosphere. The water vapour produced from the fuel cells is also passed through the water tank to condense and be used for cooling before the excess vapour is dumped harmlessly into the atmosphere. The valves are used for both hydrogen and oxygen to monitor their mass flow into the fuel cells to ensure optimum fuel usage efficiency. Lastly, the power produced by the fuel cell stack power units is then distributed as DC power to the engines and bus of the aircraft.

12.2.7. Fuel Cell Sustainability

The positive effect of the fuel cell on the sustainability is clear: no combustion means no greenhouse gasses (apart from potential contrails, which has already been discussed as not relevant for our considered altitudes), on top of the already

[8] https://hypoxico.com/altitude-to-oxygen-chart/

extensively discussed benefit of using hydrogen. However, it has to be investigated whether there are negative sides to fuel cells.

PEM fuel cells, which will be used in the H2-VTOO design, consist primarily out of two electrodes, anode and cathode, usually made out of platinum, and a electrolyte, which is a polymeric membrane. These three together make up the Membrane Electrode Assembly (MEA) [17], which is the primary focus of the fuel cell recyclability. The rest of the fuel cell consists out of plates and hardware made of trivial metals and materials which are easier to recycle. The MEA can be recycled by specialised companies, who claim to be able to recycle 95% of all precious metals in the MEA [17]. Furthermore, at end-of-life of the fuel cell, which is significantly shorter than that of the rest of the aircraft, it is possible to merely replace the MEA, instead of the entire fuel cell. As a conservative approach, a 95% recyclability is taken for the entire fuel cell, even though it is guaranteed to lay higher in practice. Even though the fuel cells perform well in terms of recyclability, it still requires quite some precious metals to be produced, meaning it does have an impact on the planet.

An additional sustainability benefit is that there are no toxic or dangerous materials involved in the production, which means that there will be no possible adverse effect at end-of-life disposal of the parts that can not be recycled [17]. Finally, all packaging used for transport or storage will be fully recyclable.

One important aspect of sustainability to consider for the fuel cells are the emissions it produces. In this case, only water is produced as a product of the reaction within the fuel cells. The rate of water produced from the fuel cells is derived from the power requirement of the fuel cells by first computing the rate of hydrogen required to meet this. The mass flow of water is then determined using the ratio from Equation 12.4. It is found that the rate of water emitted is 0.4371 kg/s. For the 4.5 hour duration of the flight, this results in 7081.02 kg of water vapour emitted into the atmosphere. The vapour is emitted into the atmosphere as it was determined that the aircraft flies at a low enough altitude such that the water vapour does not form contrails which are harmful to the environment as they contribute to global warming[110].

12.3. Battery Design

This section encompasses the design of the batteries on-board the aircraft. These will primarily be used to provide the extra power required by the aircraft for VTOL operation. A selection of the type of batteries to be used is first made after which the sizing of the batteries can be computed using various electrical and dimensional properties.

12.3.1. Battery Selection

In order to perform VTOL operations, additional batteries are needed to obtain the high amount of power required. To obtain this high amount, it is required to select a battery with high power specifications. This mainly results in a high C-rate, the rate at which the battery can discharge all its energy. A battery can have a high energy density, but can have a low c-rate making the battery even heavier to achieve a high power. Therefore it is of high importance that the right battery will be chosen.

A selection of possible candidates for the battery has been made. These batteries and their specifications can be seen in Table 12.5. The aim here is that the battery should be able to deliver a high power, but still be lightweight. This can either be achieved by a very high specific energy, or a very high discharge rate. As can be seen in the table, the Lithium Iron Phosphate battery has the highest discharge rate, however the Lithium Nickel Cobalt Aluminum Oxide has the highest specific energy. The main drawback of the latter, is that its discharge rate is significantly lower than the former. The best option for the H2-VTOO is to use Lithium Iron Phosphate batteries, since they can achieve high powers at a relatively low weight. Also, they have a relatively high life cycle and also are not that expensive. Therefore this battery is the best option.

Table 12.5: Selection of Battery [148].

Type	Voltage [V]	Specific energy [Wh/kg]	Discharge rate	Life cycle	price [$/kWg]
Lithium Manganese Oxide	3.8	100-150	1-10	300-700	420
Lithium Iron Phosphate	3.3	90-190	1-25	2000<	580
Lithium Nickel Cobalt Aluminum Oxide	3.6	200-300	1	500	
Lithium Titanate	2.4	50-80	10	3000-7000	1005

12.3.2. Battery Sizing

Now that the battery type has been chosen, the battery can be sized. This will be done in two different ways, one based on the maximum power, and one based on the total energy required for VTOL. First, the maximum power required for

the batteries needs to be determined. With this maximum power and the discharge rate, the required energy can be calculated using Equation 12.11, where C is the discharge rate.

$$E_{battery} = \frac{(P_{hover} - P_{horizontal} - P_{charge})}{C} \tag{12.11}$$

Another way to determine the amount of energy is the amount of energy needed for the whole VTOL operation. This can be done using Equation 12.12. From both these equations, the maximum was taken and it was found that required energy should be 156.1 kWh.

$$E_{battery} = 2(t_{hover} \cdot P_{hover} + t_{ceiling} \cdot P_{ceiling} + t_{vclimb} \cdot P_{vclimb} + t_{trans} \cdot P_{trans} - E_{cell}) \tag{12.12}$$

Now with the calculated energy; the mass, volume and price of the battery can be estimated. This can be done using the values from the table. The mass is estimated to be 821.6 kg. The price is estimated to be $90544 and the volume is estimated to be 480.34 l. Also, these values can be seen in Table 12.6.

Table 12.6: Total engine configuration characteristics

Battery type	Capacity [kWh]	Discharge/Charge rate	mass [kg]	Volume [l]	Price [$]
Lithium Iron Phosphate	156.1	25/1	821.6	480.34	90544

12.3.3. Battery Sustainability

Much like the fuel cells, the sustainability of the batteries can be broken down as well. Batteries have a reputation of not performing well in terms of sustainability. The batteries used by the project at hand are Lithium Iron Phosphate batteries. First of all, these batteries are not toxic and are chemically stable. Furthermore, this type of battery uses commonly available metals, rather than for example nickel and cobalt, which take significantly more energy to mine. Contrary to the historically used lead-acid battery (which are also quite toxic), lithium iron phosphate batteries do reasonably well in terms of recyclability. In recent years the recycling of these batteries has been under heavy investigation. In laboratory environments, recyclabilities of around 90 wt% have been achieved, where mostly the recovery of the cathodic material seems troublesome, with recovery rates of about 50 wt% [51]. However, batteries made with the recycled materials have shown to have at least 99% of the capacity of the original battery [51]. Even though these results are currently just for laboratory environments, due to the increasing number of lithium and more specifically lithium iron phosphate batteries that will retire in the coming 20 years, a comparable commercial recycling rate is expected by 2040. However, as a contingency, a battery recycling rate of 85% is assumed.

12.4. Engines

This section design the final main component of the power system, the engines. Similar to previous sections, a selection process is first conducted. Following this the sizing of the engines and their configuration can be determined.

12.4.1. Engine Selection

All power sources on-board the aircraft are required to provide electric power, therefore, only electric motors are considered for the engine. The selected engine or engines should be able to deliver the maximum required power to the propellers whilst minimising the engine mass, in other words: a high engine power density is desired. In the last couple of years, a new type of electric motor is being developed which uses an axial flux without a stator yoke. The companies behind this development are MAGNAX and YASA, both claiming that these engines provide a power density, 3 to 5 times higher than traditional electric motors. On top of that, these engines use less materials and have efficiencies higher than 96 % [155]. These high efficiencies are due to the patented built-in oil cooling system which both engines have. An additional benefit is that these engines can be put onto one shaft to provide more power and a higher torque. This allows to use multiple smaller standardised engines, instead of a larger custom made engine, which decreases the overall engine costs.

To determine which engine fits H2-VTOO's needs the best, the most power dense engine of both of the mentioned companies was analysed and their properties listed to compare both engines as can be seen in Table 12.7. For the MAGNAX AXF290 engine, both the expected final product and the measurements on the prototype were analysed as the engine is still under development, however it is expected that by 2040 the final product will have been in production for years.

From Table 12.7 it becomes clear that the YASA-750R has only two properties which are better than those of the AXF290, being the maximum torque and the axial length. Both are seen as less important than the peak power and the power density which happen to be the areas in which the AXF290 performs extremely well. An engine configuration using the AXF290 prototype will be 2.4 times lighter compared to a configuration using the YASA-750R engine whilst delivering the same amount of power. This in combination with the even better properties of the expected final product led to the design choice of using the MAGNAX AXF290 engine.

Table 12.7: Engine selection [99] [155].

	YASA-750R	MAGNAX AXF290 prototype	MAGNAX AXF290 expected final product
Peak power [kW]	200	325	420
Peak power duration [sec]	-	15	-
Mass [kg]	37	25	< 25
peak power density [kW/kg]	5.41	13	16.8
Diameter [mm]	368	290	290
Axial length [mm]	98	138	124
Maximum RPM	3250	10000	> 12000
Maximum torque [Nm]	790	510	> 520

12.4.2. Sizing

Sizing the engine configuration is based on the required maximum shaft power to be delivered to the propellers. As previously discussed in Section 7.5, this maximum power occurs when hovering at the hover ceiling, where a total shaft power of 3462 kW is required. Dividing this power over the two propellers, a shaft power of 1731 kW is required on each side. The final version of the MAGNAX AXF290 is expected to deliver a peak power of 420 kW, dividing the maximum required shaft power on each side by the engine's available peak power, results in 4.41 engines required on each side. Rounding this number up gives that five MAGNAX AXF290 engines are required to drive the shaft on each side of the aircraft. It must be noted that the engines are not able to continuously provide this peak power of 420 kW, however in the mission profile it was determined that the maximum hover time at the hover ceiling before transitioning is ten seconds, a duration of peak power which can be easily achieved by the engines. Finally a summary of the engine configuration can be seen in Table 12.8.

Table 12.8: Total engine configuration characteristics.

Engine type	MAGNAX AXF290
Total Number of engines on each side	5
Total peak power [kW]	4200
Total mass [kg]	250
Total torque [Nm]	5200
Total axial length on each side [mm]	620
Diameter [mm]	290

An important factor to consider is the power level at which the engines must operate as electric motors are designed to operate at 50% to 100% of their rated power. In addition, the maximum engine efficiency is achieved when operating 60% to 80% of the maximum rated power, therefore it is desirable that the engines operate within this range throughout the entire mission[28]. When comparing the maximum power output of a ten engine configuration which delivers a maximum of 4200 kW with the required power during each phase of flight as illustrated in Figure 7.8, it becomes evident that only for both hovering phases and for vertical climb, the 10 engines operate within the 60% to 80% range. To ensure all engines are operating at their maximum efficiency, some engines are turned off during specific flight phases depending on the required power. The amount of operative engines per flight phase percentage of the maximum rated power are given in Table 12.9.

Table 12.9: Optimal amount of operative engines for each phase of flight.

	Hover at sea level	Vertical climb	Hover at hover ceiling	Transitioning	Cruise	Conventional take-off	Climbing flight
Amount of engines	10	10	10	6	8	6	6
Percentage of maximum rated power	70.25 %	77.5 %	82.4 %	70.7 %	66.66 %	59.8 %	76.1 %

12.4.3. Engine Sustainability

The engines that are used in the concept, namely the MAGNAX AXF290, are made out of a wide range of metals. Some of these are simple alloys, like steel alloys, on the other hand there are some more rarer materials incorporated, for

example magnetic metals. These magnetic metals are very hard to recycle. In theory it is possible, but many companies do not believe it to be worth the energy and money investment for the limited return. Therefore, the percentage of these rare materials within the engine it also takes as the assumed recycling rate of the engines. Since the engine can provide 16 kWp per kg, and has a magnetic material content of 7.1 g per kWp, a magnet mass of 113.6 g/kg is found, which is equal to 11.4 wt% [99]. Due to some uncertainty in these numbers, a safety factor of almost two is taken, leading to a recycling rate of 80 wt%.

12.5. Gearbox

The chosen engine has a relatively low torque and a relatively high rpm. A reduction gearbox needs to be designed in order to let the propeller spin at the necessary rpm. In Section 8.6 it was found that the rpm for cruise was around 450 rpm and for VTOL around 597 rpm. for the gearbox design, to limit complexity of the system, a maximum amount of gear wheels was chosen as the main constraint. This maximum was set to 3 wheels per gear shift, not counting the gear wheels on the propeller shaft and the motor shaft. The power required for cruise and hovering at the hover ceiling were taken as the power requirements for the engines. The engines are in both cases consistently run at maximum torque, only the rpm varies.

Before the gearbox could be sized, the maximum tip speed of the propeller blades V_{tip} was determined, to check whether the flow at the tip does not become trans-sonic. The maximum tip speed was chosen to be mach 0.8 to keep away from the drag divergence mach number M_{dd}, at which a spike in drag occurs. Since the hover ceiling and cruise altitude are in the same region, the maximum tip velocities are similar, at 267.1 m/s and 267.6 m/s for cruise and VTOL respectively. The tip speed can be estimated as a function of the circular velocity of the propeller ω_{prop}, the rotor radius and the velocity at which the aircraft flies, as seen in Equation 12.13.

$$V_{tip} = \sqrt{(\omega_{prop} r_{prop})^2 + V_{flight}^2} \tag{12.13}$$

Table 12.10: Gear ratio's for the gearbox.

Phases					Total
Cruise gear ratio's	1.81	1.81	1.81	1.54	9.14
VTOL gear ratio's	1.81	1.81	1.81	1.80	10.65

It can be seen that the tip speed constraint is met, as the tips speeds are 229.4 m/s (mach 0.69) and 249.6 m/s (mach 0.75) for cruise and VTOL respectively for the rpm's stated above. Knowing that the tip speed does not enter the trans-sonic region, the gearbox can be designed to meet the rpm's. The torque could be calculated using the power required for the two stages, and the respective angular velocity of the propeller. The total gear ratio could then be calculated for both stages. Using the constraints stated above the individual gear ratio's between all gear wheels for the 2 flight stages could be calculated, as seen in Table 12.10.
It can be sen that the first few gear ratio's are identical, hence the gear-shifter only needs to switch out one gear wheel to change from VTOL to cruise mode. In order to do this properly, during transition the engines need to gradually lower their rpm until they match the rpm for the cruise phase, then you switch gear. The rpm from the engines are 4112 and 6357 during cruise and VTOL respectively. The maximum rpm of the engines is around 7713.

12.6. Verification and Validation of Power Systems

The sizing and power parameters obtained from the computations performed in this chapter are preliminary. Nevertheless, these values still need to be assessed for their feasibility and confirmed that they meet the power requirements. Along with this, it also needs to be confirmed that the sizes determined will be feasible and function as required in reality. This section will accomplish this by verifying and validating the power systems.

12.6.1. Verification of Power Systems

This subsection will verify the various calculations used to perform the sizing of the power system. The methods used will be tested to confirm whether they perform as required and retrieve expected values. The fuel cells, followed by the batteries and engines, and lastly the thermal system design will be verified.

Fuel cells
As multiple parameters such as fuel stack dimensions, power generated and number of stacks in each power unit were calculated during the fuel cell stack sizing, these values can be varied and their outputs can be analysed to confirm whether they are as expected and hence, verified. The values did indeed change as expected, for instance the number of cells per stack to accommodate an increase in power. Along with this, the length of the stacks increased but the area of the fuel cells stayed the same as expected. Additionally, the sizing calculations carried on into the thermal analysis

calculations and the heat generated also varied as expected. The results of this test show that all relations between power required, fuel cell sizing and thermal output show the correct correlations. This verification testing is crucial to verify the program used.

The mass of the fuel cells can also be verified by comparing it to the value estimated for the class 2 weight estimation (571.2 kg). The percentage error between both outputs of the methods is rather large-65.92%. However, the class 2 weight estimation used a much more efficient power densities that are predicted for the future while the relatively more detailed design of the fuel cells used current high end fuel cell stacks such that numeric values could be obtained for all sizing parameters.

Batteries and engines

The design of the batteries and engines were mainly done by the use of a python program. As already explained, this was done by comparing two methods and selecting the best one. The python program has been verified by using hand calculations in order to find the power required for the batteries. The formulas are checked for consistency of the units and then the values are calculated and compared to the program. In addition, different inputs have been used and their outputs are calculated and compared to the programs output in order to know how sensitive the program is.

Thermal system

The method used to calculate the heat generated from the fuel cells can also be verified. This is done by comparing the resultant value to that generated from a different method used to approximate the heat generated for fuel cells[136]: (Equation 12.14):

$$Q_{gen} = (1.254 - V_{\text{cell}})\,\text{In}_{\text{cell}} \tag{12.14}$$

Using Equation 12.14, the total power generated by the fuel cell stacks is 2362569.397 W which is only a percentage error difference of 23.4%. This difference may seem quite significant, however the magnitude of the power values are similar. This difference is expected as both estimates are very preliminary and therefore their comparison should function more as a sanity check. For future verification a more detailed thermal analysis should be conducted and compared to the values produced by the energy balance method.

12.6.2. Validation of Power Systems

After verification and confirming that the designed systems and methods used to design them perform as required, the validation can be conducted. This testing will ensure that the designed components fulfill their functions and therefore validate them to be used for the design.

12.6.3. Fuel Cell Validation

The sizing of the fuel cells can be validated by using the method for sizing the fuel cells and applying it to other fuel cells in general. Since the sizing of the fuel cells are based on the electrical properties of the fuel cells, these properties are validated by comparing them to the standard fuel cell current density in Figure 12.4[107] The current density obtained from the fuel cells by dividing the current output by the area of a fuel cell was calculated to be 0.6834 A/cm^2.This was verified by calculating the voltage per cell (0.6537 V) and checking the corresponding current density from Figure 12.4. The graph gives a value of close to 0.7A/cm^2 which lies very close to the previously calculated value, therefore validating the calculations for the electrical properties of the fuel cells. Sizing the fuel cells using the values from Figure 12.4 also results in minimum changes.

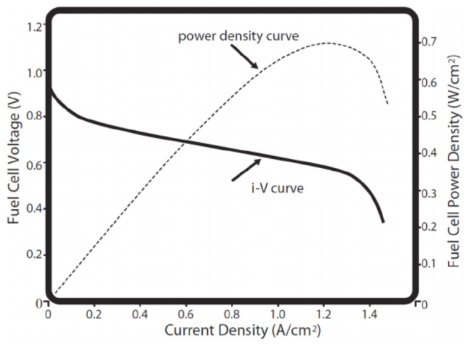

Figure 12.4: Standard fuel cell current density and power density curve.

13. Electrical Analysis

In the electrical analysis, the system interface as well as the electrical layout will be discussed. It will give an overview on how the subsystems interact with each other. First, the hardware of the aircraft will be elaborated. Thereafter the software will be shown. Next the electrical block diagram will be explained after which the data handling diagram will be elaborated. Lastly, the communication diagram will be explained.

13.1. Hardware diagram

A hardware diagram shows all the hardware on the aircraft. It is a way to show the relations between different hardware systems. The hardware diagram can be seen in Figure 13.1. Note that it does not include every single subsystem of the aircraft, only the ones that are of importance in the electrical diagram. As can be seen, the pilot and the CPU are in the middle of each subsystem. This is rather logical, as they both have to operate the aircraft. Around these, seven subsystems can be defined. These subsystems contain the components which are the most important of their subsystem. The communication system does not have the components shown, as these will be explained further in Section 13.5.

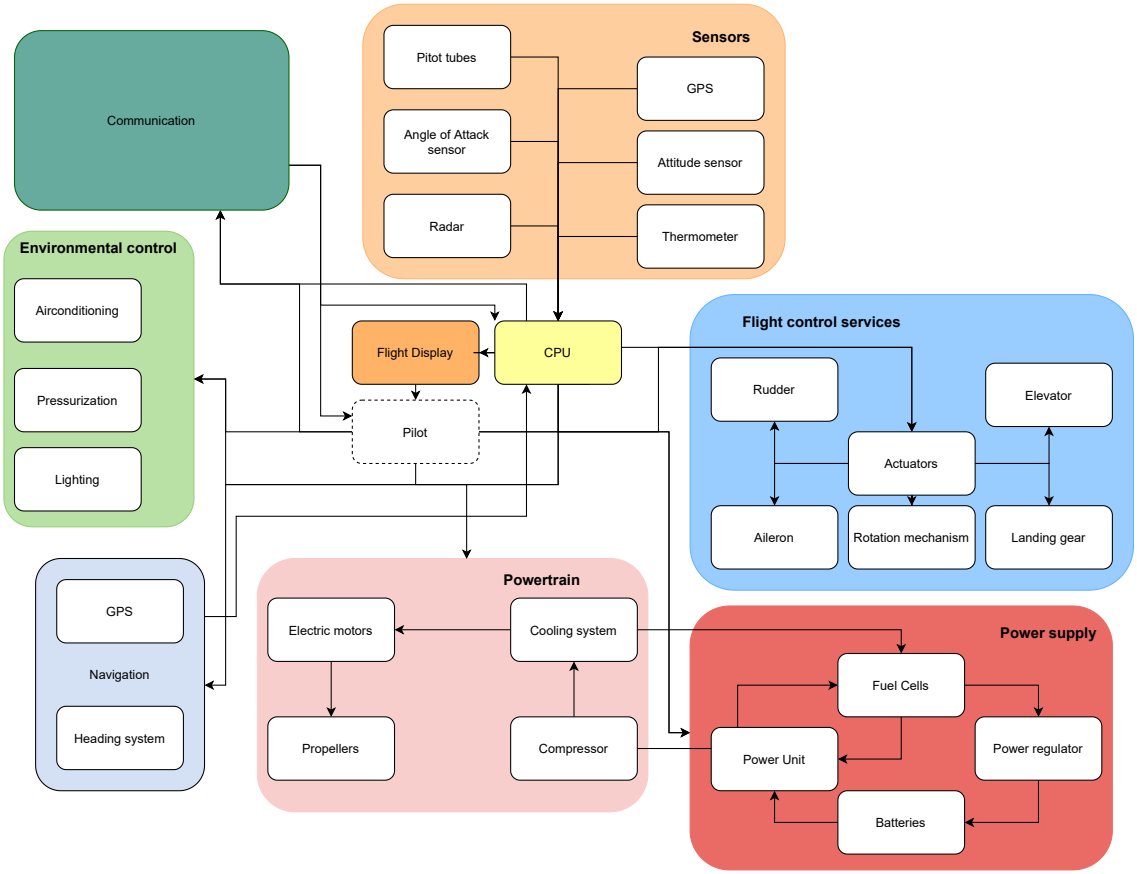

Figure 13.1: Hardware diagram of the H2-VTOO aircraft.

13.2. Software Diagram

The software diagram shows all the software the aircraft uses and how they relate to each other. The H2-VTOO is a manned aircraft, however it has an autopilot and a CPU that need software. The software diagram of this aircraft can be seen in Figure 13.3. As can be seen, the pilot and the CPU can control all the software. This is similar as indicated in the hardware diagram. As can be seen, the software is a small feedback loop that ends with the VTOL transition software. How the data is processed of these loops will be explained in Section 13.4.

13.3. Electrical Block Diagram

The power from the fuel cells has to go to the electric motors in some way. Therefore an electrical block diagram has to be made, in order to get a better understanding of the electrical layout. The electrical block diagram of the H2-VTOO can be seen in Figure 13.2. The red lines indicate a voltage of 1323 V, the orange lines 682V, the green lines 28 V and the yellow lines 3.6V.

The red box indicates one power unit, for which there are three in total. As has been explained in Section 12.2, the voltage that the fuel cells in one power unit are able to generate is equal to 1323 V and the power equals 857 kW . This then goes to the input power regulator. This power regulator is needed, since the fuel cells are not able to generate constant power and are relatively slow in changing power levels. It makes sure that the power unit receives a constant power and voltage; and that, if needed, the power required from the fuel cells can change relatively quickly. Apart from the fuel cells, the power unit also contains a battery. The battery is connected to a switching system, which makes it possible to recharge the batteries during cruise, but also use the batteries during VTOL. As has been explained in Section 12.3, the batteries are able to deliver a voltage of 3.6 V. The voltage required to charge the batteries equals 3.6V as well. From the power regulator and the batteries, the voltage goes to the power unit. The power unit (PU) makes sure that the voltage output is kept constant and works as the main regulator of the total power output. All of this combined makes one PU.

The three PU's are independent from each other. They come together at a certain point in the block diagram, which makes them in parallel. If one PU would completely fail, then there are still two more that can provide enough power to make a safe landing. Also, there is a switch at the end of the power unit, so that if one unit may fail, it will not drain voltage from the other two, since voltage is the same in parallel.

From the power units to the subsystems, there are two different circuits: The powertrain bus and the main bus. For each circuit, two DC/DC converter are used, which are connected in parallel, so that if one fails, it is not detremental to the system. The powertrain runs on 682 V while the main bus runs on 28 V. Each bus has its own circuit breaker, so that if it gets overloaded, it will automatically break the circuit so that other busses do not get overloaded as well. If this happens, the pilot can manually switch these circuit breakers if he wants to.

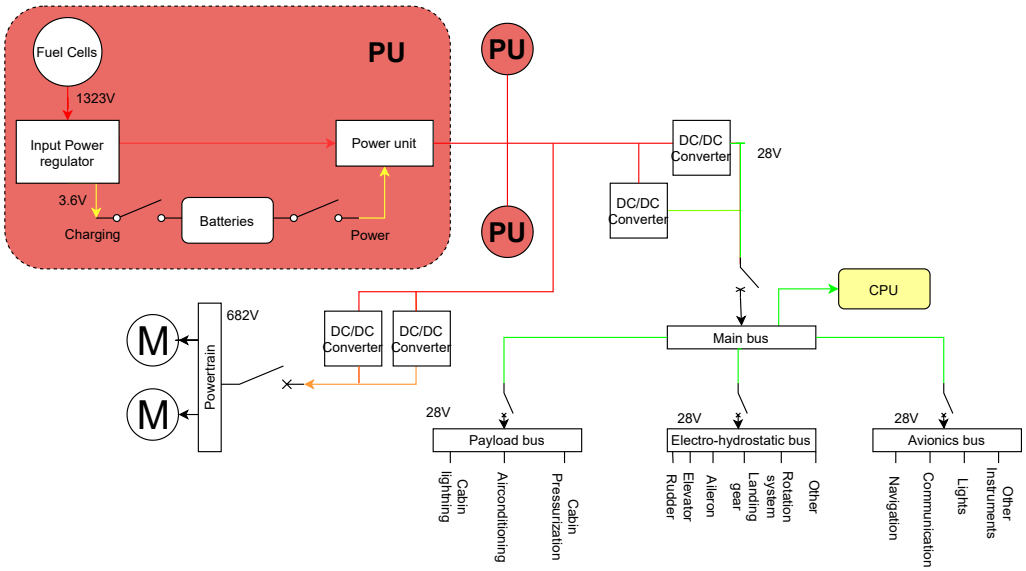

Figure 13.2: Electrical block diagram of the H2-VTOO aircraft.

13.4. Data Handling Diagram

In the data handling diagram one can see how the data is processed between the subsystems. The data handling diagram for the H2-VTOO aircraft can be seen in Figure 13.3. As can be seen in this diagram the CPU[67] processes all the data from each subsystem, and has a 1.7 GHz 8 core processor. The incoming data is transferred to the black box of the aircraft where the positional data, communication data and subsystem data is stored. As also can be seen, the CPU sends data to other systems, such as the communication subsystem, which will be further elaborated on in Section 13.5. In addition, the CPU transfers data to the actuators and VTOL sensors, since they both need operational input in order to move. Subsequently, the power regulator, as has been explained in Section 13.3, needs data input on how much power is needed, but also gives data output on how much power is available. The power unit needs data input as well, since the electrical switches need to be turned on or off in order to charge the battery. This all makes the data handling diagram.

13.5. Communication System

An important part of any aircraft is the communication system. This system provides the communication between the pilots, the passengers, air traffic control and air traffic management. This system is shown in Figure 13.4. In this diagram, five main parts can be distinguished: the cockpit segment, audio control unit (ACU), mainframe, antennas and external communication links. The round shaped boxes depict the components of the system that cannot be controlled by the design of the aircraft. As can be seen, some links have an accompanying number, this number is listed in Table 13.1 together with the explanation of the particular link. The most important parts of this diagram are the operating crew, audio control panel, central computer and ATC. As explained in Section 13.2 and Section 13.4, the central computer takes care of all of the data transmission in the aircraft, hence also the communication.

Table 13.1: Legend for enumeration of flows from the communication system diagram.

Number	Description	Number	Description
1	Customer provides destination and time slots	10	Access and transmit information
2	Pilot receives mission data	11	Data transfer
3	Direct contact between customer and pilot	12	Data transmission for ACARS
4	Access and transmit info, send messages	13	Data transfer ATC
5	Usage of avionics by pilot to operate aircraft	14	GPS satellite communication
6	Central computer processes data to and from ACP	15	Weather, gusts, birds, terrain, ...
7	PA system provides communication between pilot and passengers during flight	16	System state
8	Voice recordings	17	System response
9	Aircraft position, system status, diversion, weather		

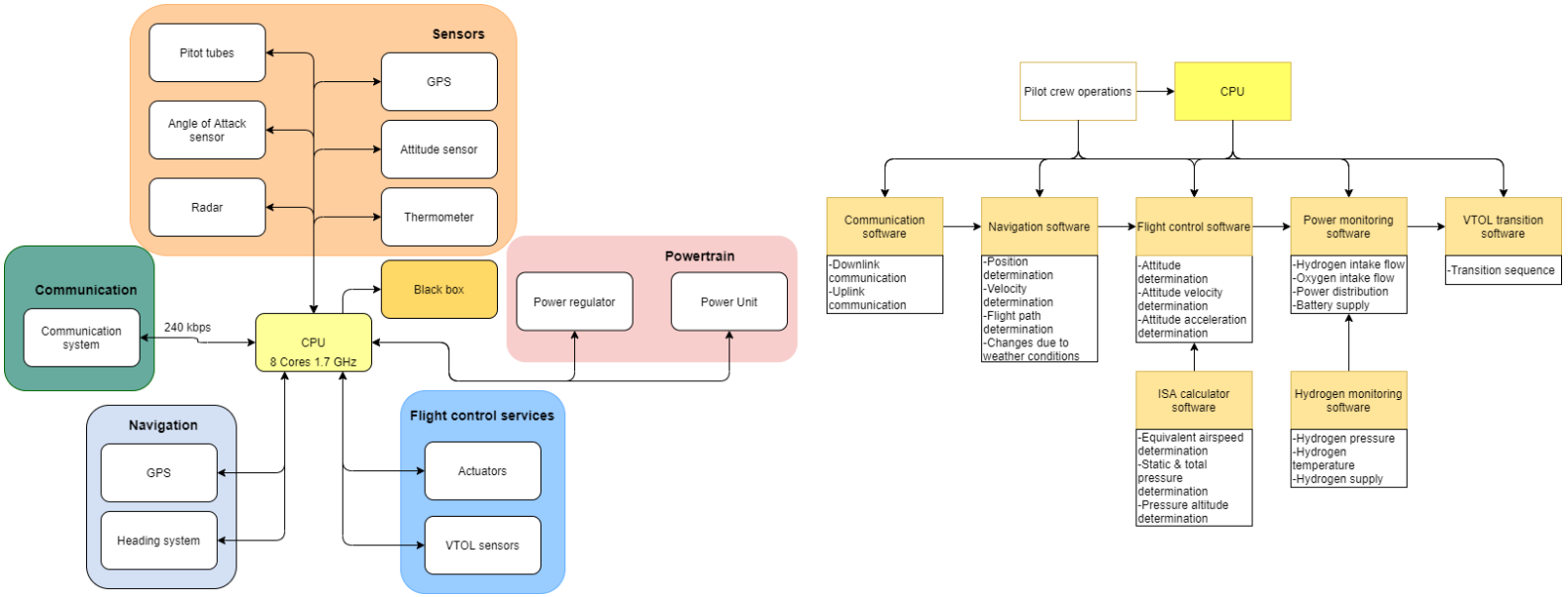

Figure 13.3: Software and Data handling diagram of the H2-VTOO aircraft.

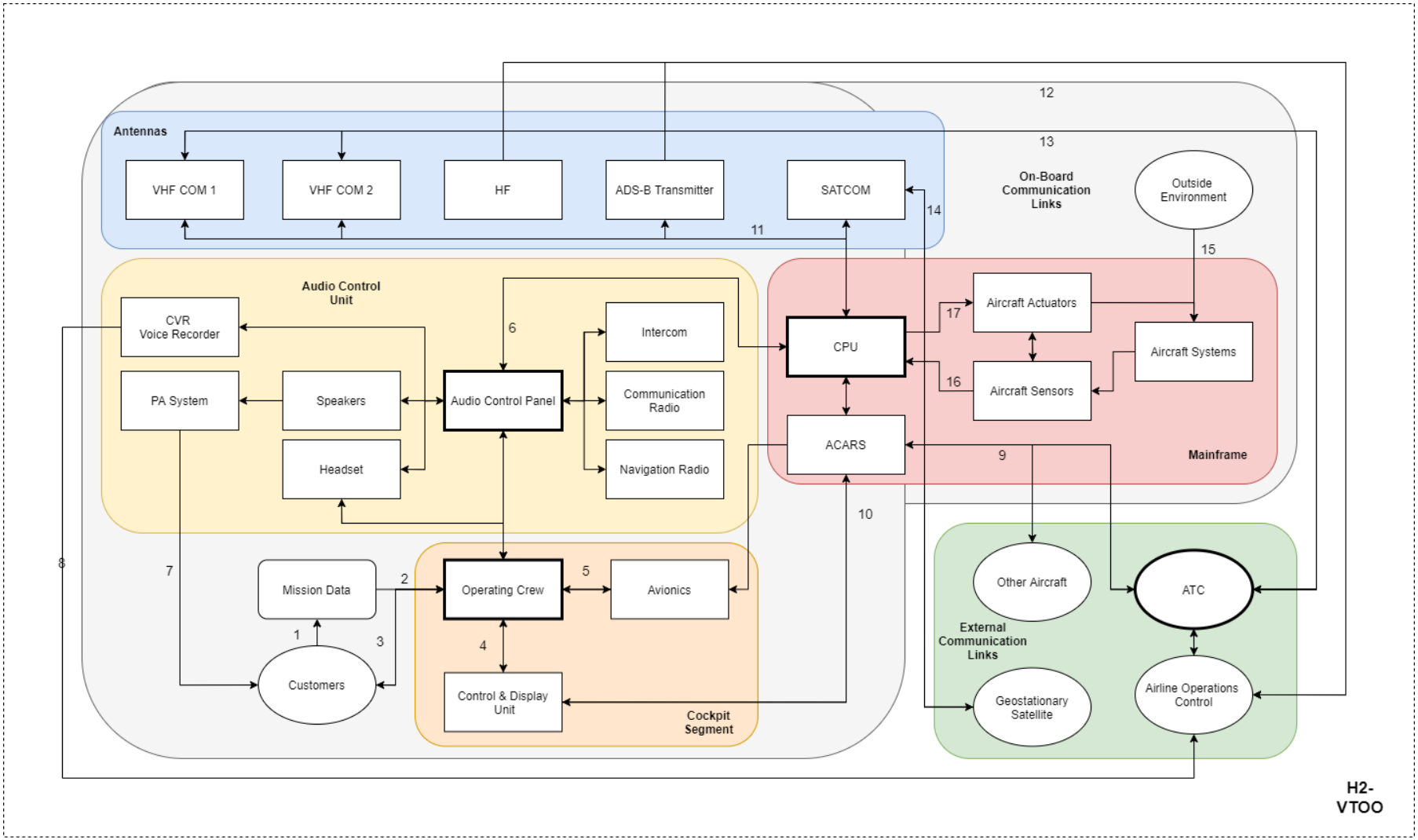

Figure 13.4: Communication system diagram of the H2-VTOO aircraft.

14. Technical Risk Assessment

In this chapter, the technical risk assessment and contingency management is presented. This is done according to the following structure. Firstly, the SWOT analysis is shown and discussed. It provides an overview of the technical strengths, weaknesses, opportunities and threats of the project. Next, the risks are identified and assessed and the top risks are indicated. Thirdly, a risk map is presented which is a tool to visualise the severity of specific risks. Finally, the mitigating and contingency actions of the risk events are discussed.

14.1. SWOT analysis

In order to get a better understanding of the strengths and weaknesses of the product, a SWOT analysis is performed. It gives an overview of the technical **S**trengths, **W**eaknesses, **O**pportunities and **T**hreats for the internal and external factors of the product. The SWOT analysis is necessary, since it provides help deducting risks and mitigating actions based on the properties and characteristics of the product. The results of this SWOT analysis can be seen in Figure 14.1.

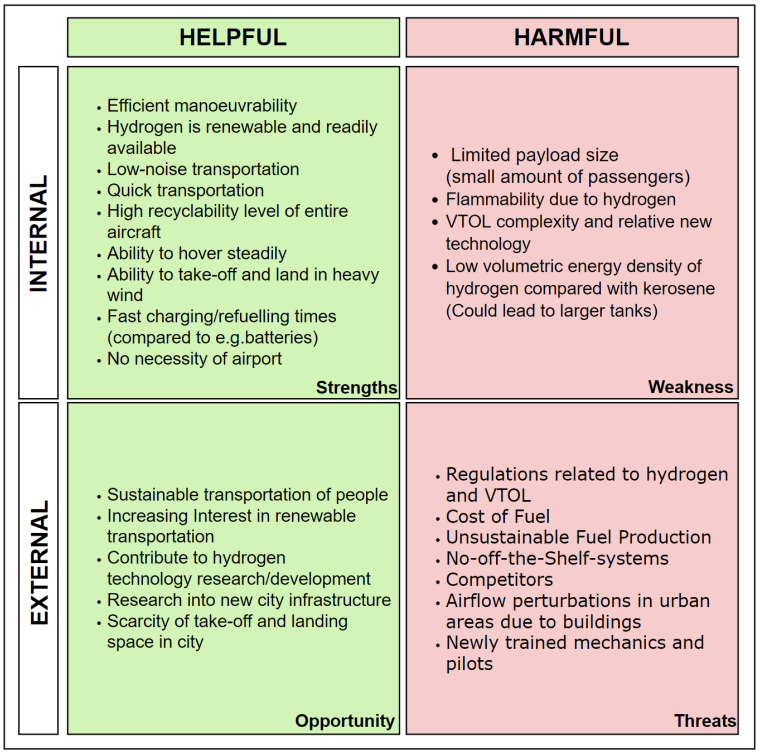

Figure 14.1: Technical SWOT Diagram.

14.2. Risk Identification and Assessment

In the following section, the technical risks are identified by an ID, described and assessed in function of their likelihood of occurrence, impact and their risk score. Important to note is that risks come from the uncertainty of accomplishing a target, aim or requirement due to technical performance, cost or scheduling. Some risk in this analysis refer to a failing design process that can cause the failure of meeting a design requirement. These are included as they can have an impact on the schedule and the cost of the project and can influence other objectives.

Next, the risk are assessed in the following way: both the likelihood and impact are scaled from one to five. A likelihood of one indicates that a risk event is (very) improbable to happen. While a five indicates that an event is almost inevitable. For the impact, a score of one means that the effect is negligible. A five indicates that the event is catastrophic. These scores were given on the basis of the experience of the team. The risk (score) is determined by multiplying the likelihood and the impact of an event. This shown in Table 14.1.

Next, the events, their likelihood and impact are visualised in the risk map that is shown in Figure 14.2. The events that are located to the right of the diagonal running from the top left to the bottom right are high risk events as their

risk scores are higher than or equal to ten. These can also be identified by a red box in Table 14.1.

The identifiers[1] consist out of three parts. Firstly, the TRM is the abbreviation of Technical Risk Management. Secondly, the risk category is shown. These are: Materials (MAT), Performance (PER), Reliability (REL), Market (MKT), Safety (SAF), Sustainability (SUS) and Organisational (ORG). The category is followed by the number of the event.

Table 14.1: Technical Risks with their respective likelihood, impact and risk score.

ID	Risk Description	Likeli-hood	Impact of the risk	Risk Score
TRM-MAT-02	The materials provided by the suppliers do not meet the expectations. **Reasoning:** The likelihood is small that a manufacturer has pour quality assurance. The impact is catastrophic as it could result in an under performing structure and even failure.	2	5	10
TRM-MAT-03	The provider cannot deliver materials in a timely fashion. **Reasoning:** It is moderately likely that a supplier fails to deliver in time, the impact would mean a delay of a batch of aircraft, which is not deal breaking.	3	2	6
TRM-MAT-04	Fuel tank material failure. **Reasoning:** If the fuel tank cracks, the aircraft won't be able to fly, and toxic gas will be released. As cryogenic tanks are not used often yet in mobile application, for contingency the likelihood is set to 2.	2	5	10
TRM-MKT-01	Green hydrogen production is too expensive. **Reasoning:** Green hydrogen is relatively rare and this influences the price. In 2040 however, green hydrogen might be the least expensive form of hydrogen [55].	3	3	9
TRM-MKT-02	Production of new systems ask too much resources. **Reasoning:** The likelihood is moderate as a hydrogen VTOL aircraft is more complex than a conventional aircraft. The impact is moderate as it impacts the schedule.	3	3	9
TRM-MKT-03	Hydrogen infrastructure is inadequate. **Reasoning:** The likelihood is relatively low by 2040 as hydrogen aircraft are on the rise. The impact is high as the aircraft will not be able to fly to many locations.	2	4	8
TRM-MKT-04	Design process goes overtime and cannot enter by 2040. **Reasoning:** The likelihood is moderate due to the hydrogen propulsion and VTOL mechanism. The impact is moderate as most likely it does not threaten the potential market share in a radical way.	3	2	6
TRM-MKT-05	The cost price of one unit is higher than 12 000 000 euros. **Reasoning:** The likelihood of going over-budget is moderate due to the hydrogen propulsion and VTOL mechanism. The impact is small due to its unique position in the market without much competition.	3	2	6
TRM-MKT-06	Competitors make a better performing sustainable aircraft **Reasoning:** The impact is large as it results in being out competed. The likelihood is moderate as there is not much direct competition.	3	4	12
TRM-MKT-07	Global economic crisis **Reasoning:** The likelihood is high due to the corona crisis. The risk can be mitigated over a long period so this tempers the impact.	4	3	12
TRM-MKT-08	New more efficient transportation methods are developed **Reasoning:** The impact is large as it can result in being out competed. The likelihood is small as the H2-VTOO will be efficient itself.	2	4	8
TRM-MKT-09	Business organisations are not interested in sustainability for their business jets. **Reasoning:** The impact is large as this results in the evaporation of the aimed market segment. The likelihood is small due to a general large interest in sustainability.	2	4	8
TRM-ORG-01	The design time of the aircraft exceeds 10 weeks. **Reasoning:** The likelihood is small due to a thorough planning. The impact is catastrophic as it would result in the failure of the project.	2	5	10
TRM-PER-11	The aircraft cannot land on a rooftop **Reasoning:** The likelihood is small due to the VTOL capability. The impact is moderate as it influences the flexibility of the aircraft.	2	3	6
TRM-PER-15	A bird strike limits the air intake of the fuel cells **Reasoning:** Bird strikes do happen, but not often. The air intake will probably not be completely blocked, hence the impact is moderate. The aircraft will need to return for checks.	2	3	6
TRM-PER-16	The most aft cg is farther aft than anticipated. **Reasoning:** The aircraft can become statically unstable when too many people stand too far aft. This would fail the aircraft. However during the design multiple stability margins are taken into account to mitigate this.	1	5	5
TRM-POW-01	The batteries provided by the supplier do not meet the expectations. **Reasoning:** The likelihood is small as suppliers have quality controls. The impact is large as it implies not enough power is available for the VTOL.	2	4	8
TRM-POW-02	The fuel cells do not meet the expectations. **Reasoning:** The likelihood is small as suppliers have quality controls. The impact is large as it implies not enough power is available.	2	5	10
TRM-REL-01	The reliability of the VTOL mechanism is insufficient. **Reasoning:** The likelihood is moderate as a VTOL mechanism is complex. The impact is moderate as it implies maintenance.	3	3	9
TRM-REL-02	The Reliability of the hydrogen propulsion system is insufficient. **Reasoning:** The likelihood is small due to big developments and testing of hydrogen propulsion. The impact is moderate as it results in more maintenance.	2	3	6
TRM-REL-04	Leak in the fuel cell cooling system. **Reasoning:** A leak in the cooling system is possible, however fuel cells need to be maintained regularly, hence small fractures should be found in time. A leak is also not dramatic, as the system can still operate long enough to land.	2	3	6
TRM-REL-05	Power decrease due to electrical cable failure. **Reasoning:** The H2-VTOO requires an extensive amount of cabling, hence failure is moderately likely. The effects are mitigated by the fact that the power supply is split in multiple engines per rotor.	3	2	6
TRM-REL-06	Fuel cell stack failure.	2	4	8

[1] Identifiers are not reused. Some risks are removed, which explains the perceived numbering inconsistency.

	Reasoning: The aircraft has multiple power units with a stack of fuel cells, losing one power unit will force the aircraft to land, landing however is still easily possible with the remaining fuel cell stacks.			
TRM-REL-07	Flight control sensor failure. **Reasoning:** The H2-VTOO is very sensitive for sensor failure, especially during the transition phase. The flight computer then determines either to let the aircraft react like a helicopter, or like a plane. Failures are moderately likely and the impact is high.	3	4	12
TRM-REL-08	Flight computer error. **Reasoning:** Same reasoning as for the flight control sensor failure, TRM-REL-07.	3	4	12
TRM-REL-09	Electric motor failure. **Reasoning:** Electric motors have become quite reliable, failure is not likely. The impact is large if every rotor is driven by a single engine.	2	5	10
TRM-REL-10	Rotor nacelle turning failure. **Reasoning:** If either the actuator or the motor needed for turning the rotor fails, the rotor is stuck in its current position, depending on the flight mode, this can be catastrophic.	2	5	10
TRM-REL-11	Refueling system failure. **Reasoning:** If refueling fails, the aircraft cannot take flight. The likelihood is low and the effects are lost profit and angry customers, hence moderate.	2	3	6
TRM-REL-12	Battery charging failure. **Reasoning:** The changes of the battery not charging is low. If the battery does not charge, vertical take-off and landing is impossible, taking off and landing conventionally would still be possible.	2	2	4
TRM-SAF-01	Risk of explosion/fire **Reasoning:** The likelihood is moderate due the precaution taken in storing and transporting the hydrogen. However, hydrogen is a highly flammable substance. The impact is severe as it implies life-threatening events .	3	5	15
TRM-SAF-03	The safety venting in the cabin cannot control the boil-off of the hydrogen **Reasoning:** The likelihood is small as venting systems are reliable. The impact is severe as it harms the safety of the passengers.	2	5	10
TRM-SAF-04	Built up of debris/material in the engines. **Reasoning:** The likelihood is moderate as engines are not airtight. The impact would be moderate as it implies more maintenance and checking.	3	3	9
TRM-SAF-05	Control surfaces get stuck or break. **Reasoning:** The likelihood is low as the system are often used without failure. The impact is severe, as certain angles would require an emergency hard landing.	2	4	8
TRM-SAF-06	Control surface actuators become stuck. **Reasoning:** Same reasoning as for TRM-SAF-05.	2	4	8
TRM-SAF-07	Gearbox failure. **Reasoning:** If the gearbox fails one of the rotors will become inoperative, this will force a landing procedure. Due to the large rotorarm, if the vertical tail is improperly designed, the other engine needs to shut off as well, leaving only gliding as a possibility.	2	5	10
TRM-SAF-08	Complete propeller failure. **Reasoning:** If the propeller fails, by literally falling off, the same severe impact holds as with the gearbox, TRM-SAF-07. The likelihood, however, is deemed very low.	1	5	5
TRM-SAF-09	Brakeshaft failure. **Reasoning:** The likelihood of the shaft completely breaking is low. If it does happen, the impact is similar to that of the gearbox, TRM-SAF-07.	1	5	5
TRM-SAF-10	Fuel tank venting system failure. **Reasoning:** The likelihood of improper venting is low, as the venting system is passive and will vent automatically after a certain pressure. The impact is severe, because if the venting is done wrong, the fuel tank might fail explosively.	1	5	5
TRM-SAF-11	Complete failure of the fuel cell cooling system. **Reasoning:** If the fuel cells fail completely, both rotors won't be able to operate, meaning that a crash landing after glide is inevitable.	2	5	10
TRM-SUS-02	The life cycle of hydrogen is not climate neutral. **Reasoning:** The likelihood is moderate as due to the hydrogen production. Besides, hydrogen is also an indirect greenhouse gas. The impact is small due to it still being eco-friendly.	3	2	6
TRM-SUS-03	The aircraft is not recyclable for 80 %. (Where recyclable indicates the reusability of material post-processing.) **Reasoning:** The impact is high as sustainability is an important aspect of the project. The likelihood is low as aircraft are often made out of metals, which are recyclable.	2	4	8
TRM-SUS-04	The company tasked with compensating the CO_2 that cannot be removed in the manufacturing process gives improper oversight on how it is compensated. **Reasoning:** Due to H2-VTOO's strict requirement on sustainability, the impact is high. The likelihood is low, since it will damaga a companies reputation.	2	4	8
TRM-SUS-05	Extreme weather causes contrails (water vapour as clouds) to form at low altitudes. **Reasoning:** H2-VTOO's cruise altitude as fairly low, hence the weather has to be quite extreme for it to happen. The impact is moderate as contrails dissipate quickly at lower altitudes, hence the longer term environmental impact is reduced .	1	3	3

14.3. Risk Mitigation and Contingencies

In this section, the risk mitigating and contingencies actions are examined. Risk mitigation tries to reduce the likelihood of occurrence. On the other hand, one should provide contingency actions for when the event does actually happen. Especially, high risk events should be provided with contingency actions. The mitigation and contingency actions are shown in Table 14.2 and Table 14.3.

Important to note is that the risks and actions can change over time and be updated throughout the project. The risk manager is responsible for following up these changes and updating both the risk map and actions. On the other hand, it is the responsibility of all team members to help with reducing the likelihood of risks.

Finally, a new risk map is presented that includes the effect of the mitigating actions in Figure 14.3. It is clear that there

are no unaccepted high risk anymore.

Table 14.2: Top risks with their corresponding mitigating actions.

ID	Mitigating Action: Action to mitigate the risk
TRM-MAT-02	Test samples of the material.
TRM-MAT-03	Contact multiple suppliers for the same item.
TRM-MAT-04	Regularly inspect the tank structure and the integration in the fuselage.
TRM-MTK-01	Maximise the engine efficiency.
TRM-MKT-02	Use off-the-shelf-systems.
TRM-MKT-03	Study the production methods of hydrogen and seek out reliable sources.
TRM-MKT-04	To reduce the unforeseen delay, apply lean manufacturing.
TRM-MKT-05	Minimise waste in the manufacturing process which reduces the cost.
TRM-MKT-06	Perform a thorough study of the competition and their alternatives.
TRM-MKT-07	Perform a study of the contemporary economic environment and future predictions.
TRM-MKT-08	Perform a thorough market analysis and investigate other potential concepts of other projects.
TRM-MKT-09	Perform a thorough market analysis.
TRM-ORG-01	Provide overall management to the group and all members have to be transparent over the work they are performing.
TRM-PER-11	Study the strength of rooftops that can be used to VTOL.
TRM-PER-15	Design inlet to minimise debris accumulation.
TRM-PER-16	Ensure people don't gather at the most aft point of the cabin.
TRM-POW-01	Verify if the battery meets the expectations by checking the customer satisfaction data.
TRM-POW-02	Verify if the fuel cell meets the expectations by checking the customer satisfaction data.
TRM-REL-01	Perform an operational readiness test.
TRM-REL-02	Perform an operational readiness test.
TRM-REL-04	Perform an operational readiness test.
TRM-REL-05	Ensure proper inspection intervals.
TRM-REL-06	Properly manage the cabling layout to reduce friction and interference.
TRM-REL-07	Properly heat manage all systems and install sensors to turn off a stack when close to failure.
TRM-REL-08	Install multiple redundant systems to reduce the likelihood.
TRM-REL-09	Frequently maintenance the software to reduce the error rate.
TRM-REL-10	Use multiple engines per rotor to reduce the effect of a single engine failure.
TRM-REL-11	Install redundant system to reduce the likelihood of complete failure.
TRM-REL-12	Write up a protocol for proper cryogenic hydrogen refueling to minimise the likelihood of failure.
TRM-REL-13	Structure the battery in multiple cells, such that failure does not mean total system failure.
TRM-SAF-01	Research the use of a firewall.
TRM-SAF-03	Research the quality provided by the suppliers of ventilation systems.
TRM-SAF-04	Isolation Material can be used to prevent from debris entering the engines.
TRM-SAF-05	Most control surfaces come in pairs, the likelihood of rudder-lock can be reduced by the introduction of a dorsal fin.
TRM-SAF-06	Regularly inspect the actuators for wear and tear.
TRM-SAF-07	Regularly replace the gears. Inspect the shaft for wear.
TRM-SAF-08	Inspect shaft and bolt for torsional wear regularly.
TRM-SAF-09	Inspect shaft for small fracture regularly.
TRM-SAF-10	Install a redundant pressure regulator.
TRM-SAF-11	Install a redundant coolant pump.
TRM-SUS-02	Minimise transport of hydrogen on the ground.
TRM-SUS-03	Perform a literature study over (the forming of) recyclable materials.
TRM-SUS-04	Request for monthly reports on the compensated carbon, and the methods.
TRM-SUS-05	Unfortunately no one can control the weather.

Table 14.3: Top risks with their corresponding contingent actions.

ID	Contingent Action: Action for when the risk does happen
TRM-MAT-02	Consider another supplier.
TRM-MAT-03	Contact all suppliers to find out whether one can deliver sooner.
TRM-MAT-04	Emergency landing procedure should be started to let everyone disembark.
TRM-MKT-01	Increase the price of a flight per person.
TRM-MKT-02	Reallocate resources to limit delay on other aspects of the project.
TRM-MKT-03	Consider providing/developing own infrastructure.
TRM-MKT-04	Consider contacting the customer to negotiate the delivery time.
TRM-MKT-05	Consider contacting the customer to negotiate the price.
TRM-MKT-06	Consider a new market for the aircraft or make the aircraft more economic competitive than the competition.
TRM-MKT-07	Consider cutting back on the budget of the project.
TRM-MKT-08	Search a new function or niche for the aircraft.
TRM-MKT-09	Consider branding the aircraft for a different target audience.
TRM-ORG-01	Consider the distribution of the group's resources.
TRM-PER-11	Consider other locations landing in urban environments.

TRM-PER-15	Fly to closest airport and check for damage to the fuel cells.
TRM-PER-16	Deflect elevator, command passengers to take their proper seating.
TRM-POW-01	Consider another supplier of batteries.
TRM-POW-02	Consider another supplier of fuel cells.
TRM-REL-01	Reduce the time between inspection rounds and maintenance.
TRM-REL-02	Reduce the time between inspection rounds and maintenance of the propulsion system.
TRM-REL-04	Land immediately and reduce time between inspection.
TRM-REL-05	Replace cabling, increase inspection rate.
TRM-REL-06	Replace stack, improve layout to decrease impact of a single stack failure.
TRM-REL-07	Increase inspection rate.
TRM-REL-08	Consider adding a redundant flight computer.
TRM-REL-09	Turn off an engine on the other side of the fuselage to ensure parallel thrust.
TRM-REL-10	Increase inspection rate.
TRM-REL-11	Introduce an emergency cut-off system to pump away hydrogen if the system fails.
TRM-REL-12	Analyse battery data to find out what triggered the failure. Improve batteries if necessary.
TRM-SAF-01	Keep the fire controllable and try to safely land the aircraft as soon as possible.
TRM-SAF-03	Consider isolating the propulsion system more and consider another supplier.
TRM-SAF-04	More maintenance can fix the problem. Adding a layer of protection can prevent the debris from entering.
TRM-SAF-05	If the rudder locks, introduce differential thrust with the propellers and start landing procedure.
TRM-SAF-06	Use other control surfaces to land, increase inspection rate.
TRM-SAF-07	Increase gear tear inspection rate.
TRM-SAF-08	Land with single rotor at nearest airport.
TRM-SAF-09	Land with single rotor at nearest airport.
TRM-SAF-10	Land and research failure of passive pressure regulator.
TRM-SAF-11	Land, increase inspection rate.
TRM-SUS-02	Consider a new supplier.
TRM-SUS-03	Consider the use of other materials.
TRM-SUS-04	Switch supplier if it does not improve.
TRM-SUS-05	Nothing, the contrails dissipate quickly at lower altitudes.

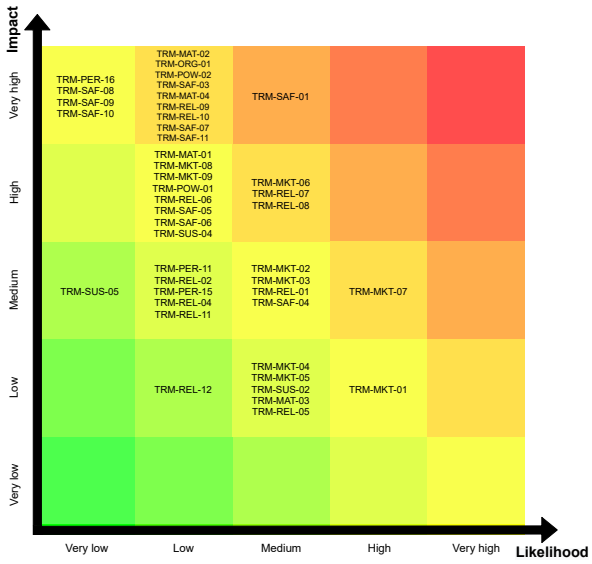

Figure 14.2: Technical Risk Map.

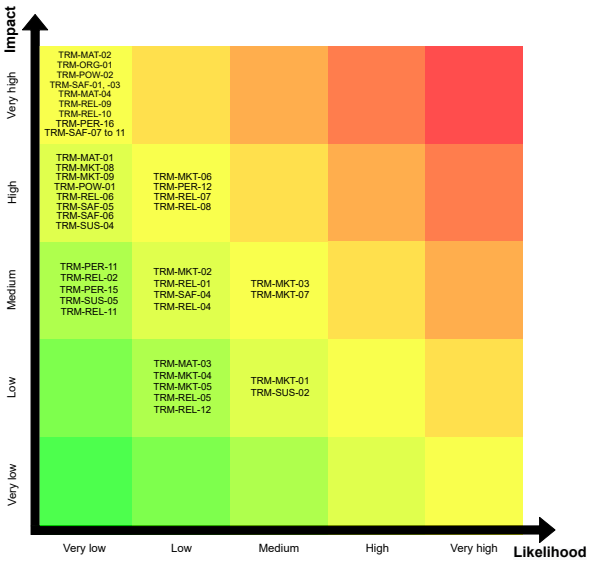

Figure 14.3: Post-Mitigation Technical Risk Map.

15. RAMS Analysis

RAMS is the abbreviation of reliability, availability, maintainability and safety. All of these are essential for a successful operation of the aircraft as they influence the functionality of the aircraft. That is why a thorough analysis is performed. Each subsection contains the definition of one the four concepts. A more elaborate explanation is given in the following sections.

15.1. Reliability

Reliability can be defined as the probability that a system or product performs its intended function in an adequate fashion for a given period of time under certain operating conditions[13].
The aircraft's reliability stems from the reliability of the individual systems. That is why an overview of certain subsystems is presented.

The reliability assessment strategy is presented. Firstly, it is important to choose a reliability distribution. Due to its simplicity, an exponential distribution is chosen. This is a special case of the Weibull distribution where the failure is assumed to be random. Moreover, it is assumed that all components/systems have a constant failure rate over time. This is a simplification of reality. The exponential distribution can be seen in Equation 15.1. Where, the λ represents the failure rate of a component/system and t is a period of time for which the reliability is analysed. An aircraft is generally checked around every 400-600 flight hours or about 200-300 flights [76]. As our aircraft is quite complex and innovative, an interval is taken of 400 hours to analyse its reliability.

$$R = e^{-\lambda * t} \tag{15.1}$$

Secondly, one has to grasp that there are two main categories of how systems are structured in terms of reliability. There is the series-configuration, wherein the functionality of one component/system is dependent on the reliability of another. Hence, if one component/system fails, the entire system fails. This configuration is visualised in Figure 15.1a. A parallel configuration is one that fails only when all components systems fail. This is visualised in Figure 15.1b

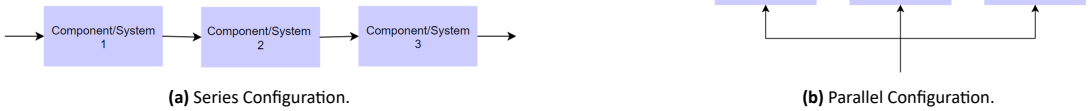

(a) Series Configuration. **(b)** Parallel Configuration.

Figure 15.1

The reliability of a series configuration can be computed by Equation 15.2[96]. Where, R_x is the reliability of a component or subsystem.

$$R = R_1 \cdot R_2 \cdot \ldots \cdot R_{n-1} \cdot R_n \tag{15.2}$$

The reliability of a parallel configuration can be modeled by Equation 15.3 and Equation 15.4[96]. In Equation 15.3, F is the probability of the failure of the totality of components/systems and can be computed with Equation 15.4 [96]. Where F_x is the probability of the failure of a component or system.

$$R = 1 - F \tag{15.3}$$

$$F = F_1 \cdot F_2 \cdot \ldots \cdot F_{n-1} \cdot F_n \tag{15.4}$$

Next, the reliability of individual subsystems are examined.

15.1.1. Electric Motors

Electric motors have been around since the nineteenth century and are a proven technology. H2-VTOO uses five electric motors per propeller. These are configured in parallel from a reliability standpoint and are connected to the shaft that drives the propeller. This means that a failure of one engine is less severe in comparison with an aircraft that has less motors. The failure rate of one electric engine can be assumed to be 3.33 $*10^{-5}$ $\frac{failures}{hours}$ as manufactures estimate their engines to last 30000-40000 hours [38]. One can estimate the reliability of a single electric motor to be 0.9867. This results in a total reliability of 0.9999 of the subsystem for a period of 400 hours.

15.1.2. Fuel Cell

Fuel cells are already used in the automotive industry and are being tested in the aerospace industry [6]. H2-VTOO has 18 fuel cell stacks. These stacks are grouped in parallel in three groups. Internally, these groups consists out of six fuel cells that are linked in series. Fuel cells for transportation applications are designed to last around 5000h [40]. This leads to a failure rate of $2*10^{-4}\ \frac{failures}{hours}$, and a reliability of one fuel stack of 0.9231 while the fuel cell system has a reliability of 0.9446 for a period of 400 hours.
It is clear with a reliability of 0.9446, that the fuel cells are a vulnerable part of the aircraft. The main causes of this are the membrane and catalyst[77]. To prevent membrane failure, one has to counteract the dehydration of it. This can be done by counteracting the electro-osmotic drag[77]. This happens when the hydrogen protons take water molecules with them through the membrane. This can be mitigated by humidifying the fuel cells with a humidifier[77]. In terms of the catalysts, the usage of high pulses from time to time can mitigate the oxide coverage[77].

15.1.3. Battery

The battery pack is essential in the operation of the aircraft as it is mainly used for the take-off and landing. Batteries are constantly evolving and are expected to have been drastically improved by 2040. The H2-VTOO uses three main battery packs that can be considered to be linked in parallel with respect to failure modes. If one fails the other should still be able to continue to work. It is estimated that a Lithium Iron Phosphate battery are able to support at least about 2000-2500 cycles[69]. Each flight means one cycle if one assumes that all flights use the VTOL capability for take-off and landing. No information was found about the average trip within Europe. If one assumes an average flight time of 1.5 hours, than a failure rate of $2.67*10^{-4}\ \frac{failures}{hour}$ is found. More information will be given in Section 15.2 why an average flight time of 1.5h was chosen. However, this leads to a reliability for one battery of 0.8988. Consequently, this results in a total reliability of 0.9989 for a period of 400 hour.

15.1.4. Hydrogen Tank

The liquid hydrogen tank is one of the most important components of the H2-VTOO as it carries the energy carrier. Hence, it is essential that the hydrogen tank is reliable. However, a tank can fail in multiple ways like a rupture, fracture, temperature variations, buckling and plastic deformation. The tank can be seen as a single component where the reliability can be estimated using the failure rate. One can assumes the failure rate to be $1.11*10^{-5}$ as the lifetime for a liquid hydrogen tank is about 20000 cycles [113]. One cycle can provide a flight up to four and a half hours. This results in a reliability of 0.9956 for a duration of 400h.

15.1.5. Tilt mechanism

When investigating the reliability of the H2-VTOO's tiltrotors, the reliability the electro-hydrostactic actuator was analysed. In each nacelle, there are two of these devices that help to rotate the engine. There was not a lot of information to be found concerning the lifetime of an EHA. However, the ones in a F-18 aircraft can last to 5000000 cycles[101]. Hence, this value was used to determine the failure rate. Recognising that there are at least two cycles per flight, a failure rate of $2.67*10^{-7}$ is retrieved. As there are two EHA in parallel a reliability of 0.9897 is retrieved for one engine. For both engines this leads to a outcome of 0.9998.
It is important to realise that this is an exaggeration of the reliability as only the EHA are examined. The motor can also get stuck due to debris or corrosion and so on. However, proper maintenance should help to reduce these issues.

15.1.6. Summary of the Reliability

The reliability of all the subsystem can now be combined in estimate of the total reliability of the aircraft. This is done by multiplying the values in Table 15.1. A combined reliability score of these subsystems of 0.9391 is found.

Table 15.1: Reliability scores of the subsystems.

Subsytem	Reliability
Electric Motors	0.9999
Fuel Cells	0.9446
Battery Pack	0.9989
Hydrogen Tank	0.9956
Tilt Mechanism	0.9998

15.2. Availability

Availability can be defined as the probability that a system or product is going to be ready to perform its function [52]. To be profitable, the aircraft has to be available as much as possible. This means that the downtime has to be minimised. It is clear that availability is closely related to reliability and maintainability.
Now, there are multiple types of availability. Firstly, there is the inherent availability which is the availability only in terms of operating time and corrective maintenance and can be calculated by Equation 15.5 [27]. Where MTBF is the mean time between failures and MTTR is the mean time to repair. This does not include preventive maintenance, logistical and administrative delay. It indicates the efficiency of the maintenance personnel.[119]

$$A_i = \frac{MTBF}{MTBF + MTTR} \tag{15.5}$$

Secondly, one has the achieved availability. This is the same as the inherent availability but takes the preventive downtime also into consideration. However, it does not include logistical, administrative nor supply delays into consideration [119]. It can be seen as the availability seen from the perspective of the maintenance team. The achieved availability can be computed with use of Equation 15.6[119]. Where MTBM is the mean time between maintenance and MMT is the mean maintenance time.

$$A_a = \frac{MTBM}{MTBM + MMT} \tag{15.6}$$

Thirdly, the operational availability is presented. This could be seen as the real availability as it includes all sources of delay or downtime and can be defined as Equation 15.7[119].

$$A_o = \frac{Uptime}{OperatingCycle} \tag{15.7}$$

However, as the H2-VTOO has not been fully developed, it is hard to estimate the reliability of the aircraft with use of the previous equations. That is why a different strategy is used by estimating how much the aircraft is required to be maintained and so determining the availability of the aircraft on a yearly basis. Firstly, the H2-VTOO has to undergo an A-check every 400 flight hours and this takes about 10 working hours[2]. Secondly, a B-check is performed every six months and last about 3 days [2]. Next, a more thorough investigation is performed on the aircraft by the C-check. This has to be done every 2 years and takes around two weeks[2]. Fourthly, a D-check is done every six to twelve years. An aircraft gets dismantled and this last around four to six weeks [2]. Furthermore, line maintenance is also performed. These are the most basic routine checks and are normally performed before and/or after the flights. These checks happen every 24 to 60 hours of flight time [2]. These last around 45 minutes [129].

The average yearly maintenance time is estimated. If we look at the competition one can see that the average business jet has around 448 flight hours a year[58]. Keeping in mind downtime, this can be rounded of to an average flight time of 1.5 hours a day. This accounts to a exaggerated downtime of 60 days of an aircraft per year. When keeping this in mind for the H2-VTOO, one retrieves a total time spend on A-checks of 10 hours a year. This leads to a total days spent on maintenance of 21 days a year for all checks. Besides, one has to remember that on each up day a total 45 minutes has to be subtracted. This accounts to a total line maintenance time of 273.75 hours or an equivalent of 10.757 days per year. However, these can be split over the days on which the aircraft is operational and have therefor little effect on the amount of days the H2-VTOO is operational and available. Next, the aircraft also has to be refueled, passengers have to board and disembark. Besides, the battery needs to be charged. It was chosen to refuel without any passenger on board for safety reasons. However, the passengers can board while recharging the battery. It is assumed that boarding the aircraft last 15 minutes and recharging the battery for 50% takes about 30 minutes as the battery can charge the other half while flying. The aircraft can perform one VTOL manoeuvre with half a charge.

This leads to a total availability due to the maintenance, boarding and refueling of the aircraft of 344 days per year. However, it should be clear that this is an overestimate of the total availability. As not all logistical nor any administrative delays are considered. Besides, the effect of random failures of components are not factored in.

15.3. Maintainability

Maintainability can be defined as the measure of ease and speediness by which a system or components can be restored to an operational status[98]. It is thus essential that maintenance is performed to prevent and fix failures. As the H2-VTOO has an unconventional and complex configuration, more maintenance will be needed. Especially, the fuel cell, electric motors, battery and tilt rotor will have to be extra carefully checked.

Generally, there are multiple types of maintenance for an aircraft. These presented in the first section and are followed by some critical subsystems.

15.3.1. Types of Maintenance

Line Maintenance
Line maintenance is the maintenance that can be done in the open, outside of the hangar. Line maintenance is needed every 24-60 hours and takes around 45 minutes [129]. It covers basic inspection of things such as fluid levels, landing gear, brakes, etc.

A-check
As already mention in Section 15.2, an A-check is performed every 400-600 flight hours and takes around 10 hours that can be performed in the hanger. During this check, the interior and the fuselage are checked for damage or other types of deterioration [2]. Furthermore, the engine is also investigated, as are the emergency lights, the retract system of the noise gear and the parking brake [2].
As the reliability of the components in Section 15.1 were calculated on a time frame of 400 hours, all these subsystems also need to be checked in some form during every A-check.

B-check
Some airliners have absorbed the B-check in the A-check due to efficiency reasons. However, when it is performed separately, it takes about 3 days and has to be performed every six to eight months [2]. This is a more thorough inspection of the aircraft. As an example, the calibration and torquing of the noise landing gear spotlight are executed and the hydraulics of the wheel well are examined [2].

C-check
C-checks are considered to be heavy maintenance. They often require the aircraft to be out of service for 1-2 weeks. Typically, C-checks are about 6000 man hours [2]. During C-checks, technicians perform tasks such as the examination of structures for corrosion and damage, checking the electrical subsystems and fuel cells and an lubrication of the cables and fittings. For the C-check, there are different levels depending on the aircraft. One might perform the C1 check tasks on one day, the C2 on the next and so on.

D-check
Lastly, the D-check is discussed. This is also called the heavy maintenance visit [2]. It is performed every six to ten years and lasts from four to six weeks. The aircraft gets completely stripped and components are checked. Interiors can also be updated [2]. An aircraft usually undergoes two to three D-checks before being disposed [2].
However, the H2-VTOO has a complex and unconventional design. This may result in the fact that more maintenance may be required. This is especially the case for some of components that will be analysed in the next section.

15.3.2. Analysis of Critical subsystems

Some of the critical subsystems are analysed in terms of maintainability. These are critical as they are not often used in the construction of the aircraft, and should therefore be examined with extra caution.

Electric Motors
The electric motors are a vital part of the aircraft and therefore it has to be guaranteed that they work perfect. That is why regular visual inspections are needed especially when it operates in a though environment [112]. This is to prevent dirt and corrosion from interfering with the motor. Furthermore, the winding can be checked for burning marks by means of smell. This could be due to overheating. Next, a brush and communicator inspection can be performed [112]. Deterioration of this could lead to communication problems of the engine. The communicator also has to be checked for grooves, inconsistencies, corrosion and so on. These can cause sparks. Besides, the stator, rotor and belts need to be checked[112]. Next, a winding test can be executed. Here, irregularities in and burn marks in the winding are sought [112]. For this, the engine needs to be dismantled. In case of (serious) damage, the motor must be rewound [112]. Fourthly, the bearings need to be checked for noise, vibrations, pour lubrication and overheating [112]. Next, a vibration test is carried out as vibration can reduce the life time of a motor [112]. Finally, infrared thermography can used for making thermal images of the motor and help by mapping the heat patterns of the engine [112]. This can detect insufficient cooling, insulation failures or deterioration of the stator.

Power Unit
The power unit encompasses both the battery and the fuel cell. They both have no moving parts and is therefore potentially more reliable than a combustion engine. However, the H2-VTOO is fully electric and therefore the power unit becomes of higher importance. Due the the high temperatures within the fuel cells and their intensive use, the chance of failure increases significantly. Therefore maintenance is of high importance. The fuel cells and batteries have to be checked regularly. This can be done by inspecting them for possible cracks or loose fittings. In addition, leak tests should be performed in order to find possible leaks within the fuel cell. This can be done by using hydrogen leak sensors and doing a small engine start. The indicators would show if hydrogen is detected outside of the fuel cell, which therefore means a leak in the fuel cell[80]. Furthermore, action to counteract the failure of the membrane or catalyst were already mentioned in Section 15.1.

Fuel tank
During its lifetime, a liquid hydrogen tank is loaded in a diverse set of ways. However, the main concerns are failures due to the thermal cycles and fatigue due to the pressure of 2.5 bar. Hence, the tank has to be checked on a regular basis to prevent a (catastrophic) failure. This can be done by a visual inspection in case of crack formation. However, a proper fatigue test may be periodically needed where the tank is tested for leakage to ensure safe operations. This could be done using a noise analysis to detect a rattling sound [97]. Ultrasonic and X-ray inspection may also be useful. Fluorescent dyes are also an option to make cracks visible [97].

Tilt Rotor
When performing the maintenance, it is important to check the electro-hydro-static actuators. This can be checked by rotating the engines at least once before a flight. More thorough tests can be performed by analysing the the electronic and hydraulic system in the hangar. Furthermore, the tilt mechanism has to be checked for the buildup of dirt and corrosion. These could counteract the tilt mechanism and therefore hurt the reliability. Finally, the bearings need to be checked and lubricated.

15.4. Safety
Safety is of huge importance in aviation. Therefore, right countermeasures should be taken in order to guarantee the safety of not only the passengers, but also for the environment. This section will contain certain countermeasures in different scenarios.

Lightning
Lightning always has been something people are scared for when flying through a storm. It mostly impacts the aircraft around the wing, tips, rudders and nose[104]. However, when lightning strikes an aircraft, the passengers rarely notice it as measurements are taken. A first measure is to make the external parts out of metal from a sufficient thickness to be used as basic protection and controlling electromagnetic energy form interfering with the electrical wires and systems. Secondly, the cabin and interior are layered by a metal mesh that functions as a Faraday cage that blocks the electromagnetic fields. Thirdly, ground straps, composites and bundle straps can be used for lightning prone/sensitive areas of the aircraft[86].
Next, the H2-VTOO has a hydrogen tank on board, which is highly flammable. That is why the tank and fuel lines have to be fully enclosed by protective material to make an explosion impossible. Most dangerous are the ground operations, especially during refueling. So, a good lightning detecting systems is required[104]. Besides, a proper Airport lightning protocol has to be created for the operations of the H2-VTOO.

VTOL
The VTOL capabilities of the aircraft is has great potential for making the H2-VTOO a flexible vehicle. However, it also brings great dangers mainly during the transitioning of the tiltable rotor. Firstly, there is the possibility that an actuator gets stuck. Than, the electric motors can still provide sufficient thrust to bring the aircraft safely to the ground, both for the VTOL and conventional configuration. Besides, each rotor has two actuators. This implies that the redundant one can take over the control and thus, increasing the reliability of the aircraft.
Secondly, there is the possibility that an actuator uncontrollably starts to change the pitch of the propeller. Here, the second actuator can counteract the first to limit the movement of the rotor. The other nacelle can then move to the same pitch to guarantee the aircraft's stability and be followed by a safe landing.

Power unit failure
A power unit failure is something that can happen due to a battery failure, power regulator failure or fuel cell failure or perhaps the cabling in between those. If the power unit of an aircraft fails, this could cause catastrophic effects. For example, if the internal combustion engine of a regular turboprop aircraft fails, than the whole engine fails as well, and therefore causes unwanted effects. For the H2-VTOO, it was decided to have three power units which are all independent of each other. This way, if one power unit fails, the aircraft still has 2/3 of the maximum power available which is sufficient enough to get the aircraft on the ground safely for maintenance.

Electric Engines
It is possible that an engine fails while in flight. This can happen during a VTOL or a conventional manoeuvre. For the latter, only six engines are needed to take-off and land. So, four engines can fail while the aircraft still can safely take-off or land. Next, if an engine fails during the VTOL, the other ones can spin up to compensate the thrust loss. The spin up of eight is enough to safely land the aircraft. This results in the conclusion that an engine failure is not a catastrophic event as it can be compensated by the other engines.

Propeller blade breakage
Due to the load on the propellers, it is possible that one of the blades of the propeller breaks. The loads are the largest during VTOL and therefore it is most likely that a failure happens during such a manoeuvre. If a failure happens, the engine on the side of the break can spin up and the ones on the other side can adapt to an appropriate RPM to counter the moment of the aircraft. Furthermore, if the aircraft hits the ground, the landing gear has to absorb absorb the impact. Secondly, if a break happens during conventional flight, the rudder and aileron can be applied to keep the aircraft going in the right direction and stable. Lastly, when a failure happens during transition, the engines on the side of the broken propeller needs to spin up and the actuators have to rotate the aircraft as fast as possible. The rudders and ailerons can once again be used to keep the aircraft stable and going in the right direction. Then, a emergency landing can performed.

Hydrogen fuelling
When on the ground, the most dangerous part of the ground operations is the refuelling of the H2-VTOO aircraft. This has to be done with a lot of care. Therefore, it is essential that the refueling crew receives specialized training to be able to safely fuel the aircraft. This comes with a special protocol that indicates very clearly and unambiguously what, when and how all the crew members have to do. Besides, the H2-VTOO cannot be refueled with passenger on board for fire and explosive safety measures.
Furthermore, special zones can be considered near the fire brigade for refueling. This could allow a shorter reaction time and reduce the harm produced of an accident.
Lastly, it was mentioned in Section 15.4 what measures should be taken for a potential lightning strike during refueling.

16. Manufacturing Plan

In order to make the post-DSE manufacturing as smooth as possible, a preliminary manufacturing plan will be presented. The manufacturing plan will present the different manufacturing processes, materials, production of several subsystems and the working environment.

16.1. Material breakdown

The major material groups that will be used for the manufacturing of the aircraft are presented in Table 16.1. The material breakdown contains the materials that will be used in the work stations during the manufacturing of the aircraft. It does not include the materials used in products procured from other companies.

Table 16.1: Material breakdown showing the weight percentage of the materials processed in the production of the aircraft. Materials in components purchased by H2-VTOO are not included in the material breakdown.

Material	Components	Mass (%)
Al-7050	Wing, fuselage, empennage, nacelles and propellor blade	46.5
Al-2219	Tank wall	5.6
Polyurethane foam	Tank and pipeline insulation	0.8

Aluminium 7050 is the major material used in the aircraft and is mainly used in the aerodynamic surfaces, fuselage and propulsion unit structure. Aluminium 2219 is used as tank wall material due to their excellent resistance against cryogenic temperature. Due to the excellent recyclability of both Aluminium 7050 and 2219, the usage of these materials contribute strongly to the sustainability of the aircraft. The polyurethane insulation material is used in the hydrogen tanks and is produced with an environmental production process, as discussed in Section 10.1.11. Table 16.1 only contains the major material components decided at this point of the design phase. Other materials will be needed in for example joining methods that contribute slightly to the total aircraft mass. For joints loaded in only shear, rivets will be used. Rivets are easy to apply both for double-sided assembly where solid rivets are preferred and for single-sided assembly where hollow rivets are preferred. They are preferred because of their easy applicability and fatigue-sensitivity. However, special attention should be taken for their corrosion-sensitivity due to for example, galvanic corrosion due to the difference in material between the structure and the rivets. Rivets can be made from Aluminium alloys such as the Al 7050 used in the other parts of the fuselage. For axial loads, rivets can not be used and bolts are used instead. These bolts are also made from Aluminium alloys or from Titanium when higher strengths are required.

16.2. Manufacturing processes

During the manufacturing of the aircraft, different forming processes will be used to produce different parts of the aircraft. These different processes will be elaborated upon in the following sections.

16.2.1. Metals

In the H2-VTOO aircraft, use will be made of different metals. In order to form these metals in their desired shape, several different forming processes can be used [133]. These processes will be elaborated upon in the following sections.

Extrusion

In this process, which is suitable for aluminium alloys, a heated metal is forced through a die having a constant cross sectional shape. This process is good at making longs bars of constant cross sectional shape. Furthermore, the process is beneficial for large product series. An example of extrusion can be seen in Figure 16.1a.

Roll bending

This is a process where sheets of metal pass through three rolls. This is done so that every part inside the sheet's cross section has the same bending moment applied. Furthermore, roll bending is a universal process which can be applied for many different parts of the aircraft. Roll bending is mainly used for single curved sheets. An example can be seen in Figure 16.1b

Rubber forming
Rubber forming is a cheap universal process where metal sheets can be bent by a rubber press. However, since the rubber forming process takes quite long and the rubber press will deteriorate over time it is only beneficial for a small production series. An example of rubber forming can be seen in Figure 16.1c

Stretching
Another process that is used in the manufacture of an aircraft is stretching. This process is mainly used for double curved parts such as the cockpit and tail cone. During stretching a metal sheet is stretched over a die. This will induce plastic deformation which will form a sheet in a desired shape. An example of stretching can be seen in Figure 16.1d.

Casting
Casting is a forming technique where liquid metal is poured inside a cats where it will solidify. This solidified liquid can be of any desired shape. For this process in particular gravity based, reusable mould casting is selected. This might be expensive at first, however for production series larger than 1000 it becomes a feasible option.

Machining
This forming process entails a lot of different principals. However, it comes down to the point that machining is mechanically removing material form a part in order to get a desired shape.

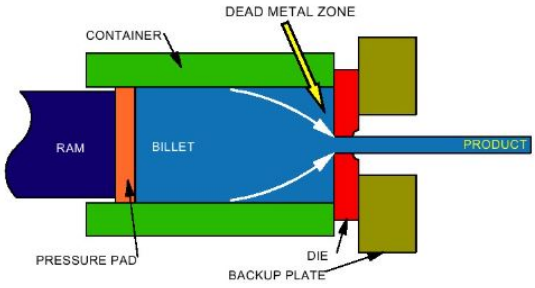

(a) The extrusion forming process.

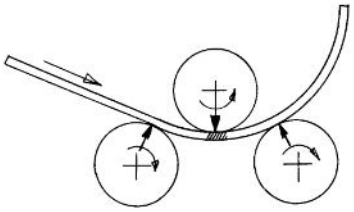

(b) The roll bending process.

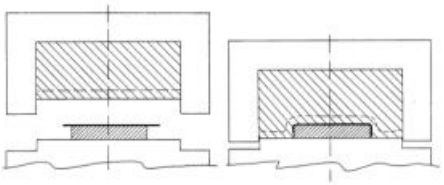

(c) The rubber forming process.

(d) The stretch forming process.

Figure 16.1: Different mtal forming processes [133].

16.2.2. Foams

In order to produce the required poly urethane foam several different steps have to be taken [1]. The first step is to identify the different raw materials needed for this production process which are Isocyanates, Polyols and some additives. Isocyanates are crucial for the production of poly urethane and are produced by adding nitrogen with toluene. Polyols are the chemicals that the isocyanates will react with and have a characteristic alcohol (OH) group in their molecule. Last of all, additives are added in order to increase the performance of the foam. Now that the different materials that are necessary to produce the foam are identified, the following steps indicate the actual production processes:

1. The raw materials presented above are stored in big tanks where they are kept liquid.
2. After this, the materials pass through a heat exchanger where the actual polymerization happens that forms the foam.
3. This is followed by a process were the reacted polymer is dispensed on a sheet of paper on the production line where it reacts with carbon dioxide which makes it expand.

[1] http://www.madehow.com/Volume-6/Polyurethane.html [120]

4. Now that the expansions reaction has started the remainder of the foam is covered by paper. This is done so that the foam can be shaped in a desired form due to the forces exerted by a series of panels.

An example of this production process can be seen in Figure 16.2.

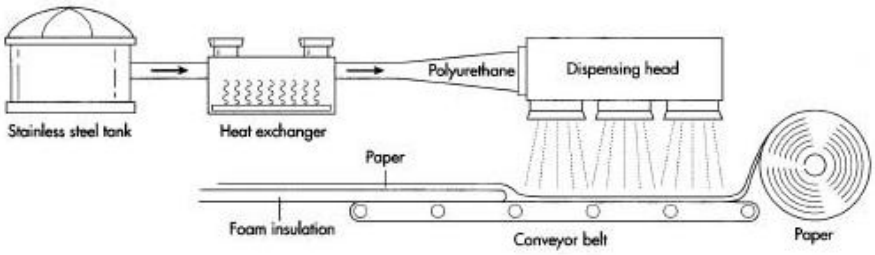

Figure 16.2: The production process of poly urethane foam [120].

16.2.3. Production Process Overview

In this subsection a table is presented where the different production processes for the different parts are presented.

Table 16.2: Different parts in the assembly procedure and their respective production process.

Part	Production process
Front fuselage skins	Stretching
Center fuselage skins	Roll bending
Rear fuselage skins	Stretching
Gears	Casting
Stringers	Extrusion
Ribs	Rubber forming
Wing box skins	Machining
Empennage sheets	Roll bending, stretching
Radiator piping	Extrusion
Hydrogen piping	Extrusion
Propeller	Casting, machining
Tank skin sheets	Stretching
Hydrogen tank insulation	Foam production process

16.3. Assembly

The assembly line of H2-VTOO is shown in Figure 16.3. First, most of the subsystems are produced separately after which they will be assembled into the final product. The process of assembly is executed in series; sub-assemblies are joined into larger sub-assembly until the final product is finished. The choice for an assembly line is based on the following reasons:

- Efficiency: Because several subsystems can be produced concurrently, the manufacturing process will become increasingly efficient as no time is wasted on waiting for other subsystems to be finished. This will also have a positive economic effect on the project.
- Accessibility: Since most of the subsystems are produced separately and then assembled, it will also be easier to produce the systems since they are more accessible. If the aircraft was to be one big part, it would be hard to access certain parts of the aircraft.
- Size: In order to transport and move systems in an easy way it is of importance that they are not too big. the principle of assembly is important for this point since due to assembly there are multiple smaller parts that can be easily transported if necessary.
- Operation and maintenance: Because the final system is constructed by assembling several subsystems it will also be easier to remove certain subsystems for maintenance or replacement. Complex tasks can be performed in smaller sub-assemblies, separate from the main assembly line. Because operation and maintenance are easier the cost can be reduced since less advanced equipment and crew is needed to perform certain operational and maintenance tasks.

In order to break down the aircraft into different assemblies, divisions are made between various sub-assemblies. These divisions consist of mounting divisions and manufacturing divisions. Mounting divisions should be detachable and exchangeable. These divisions are used for movable components or components that should be replaced or inspected regularly. For the H2-VTOO mission these include the electrical motors, fuel cells, batteries, hydrogen tank, control surfaces and landing gear. Manufacturing divisions on the other hand, are fixed connections. These include the fuselage divisions, fuselage-wing integration and wing divisions. An overview of the assembly sequence for joining all these divisions of the H2-VTOO is provided in Figure 16.3. Besides the assembly process, the time required per work station is estimated for an experienced crew, taking into account the learning curve. The times are based on a total assembly time of 45 working days, since the typical assembly time of an aircraft was in the range of 1-2 months[2].

In the H2-VTOO manufacturing plan, most of the subsystems will be produced in parallel. For example, the wing, fuselage and empennage will be constructed separately to be assembled together later on in the process, hence making optimal use of the assembly advantages described in this section. However, some processes should be performed in series and cannot be performed in parallel. For example, integration of the rear and center fuselage can only be done when the hydrogen tank is integrated in the center fuselage due to the large dimensions of the hydrogen tank. This division should also be a mounting division to exchange the hydrogen tanks after their end of life. It should be noted that the wing should be produced twice per aircraft in Figure 16.3. As indicated, a quality check is performed after each sub-assembly/assembly is completed.

H2-VTOO makes use of several principles that increase the efficiency and quality of its assembly. The rigid-flexible principle dictates that a rigid assembly is always connected to a flexible assembly and vice versa. Connecting two rigid or two flexible assemblies result in induced stresses. For example, the flexible fuselage skin panels are attached to a rigid fuselage keel of stringers and frames. The second principle is hole-to-hole assembly. All holes are made before entering the main assembly line. In the main assembly, the holes only need to be joined by fasteners. This leads to higher accuracy and a more efficient assembly process. The last principle is the lean manufacturing. A constant effort is made to investigate different kinds of waste and eliminate them accordingly. This is a continuous process in order to increasingly optimise the manufacturing process and contribute to a sustainable manufacturing process.

[2] https://travelupdate.com/how-long-does-it-take-to-build-a-commercial-aircraft

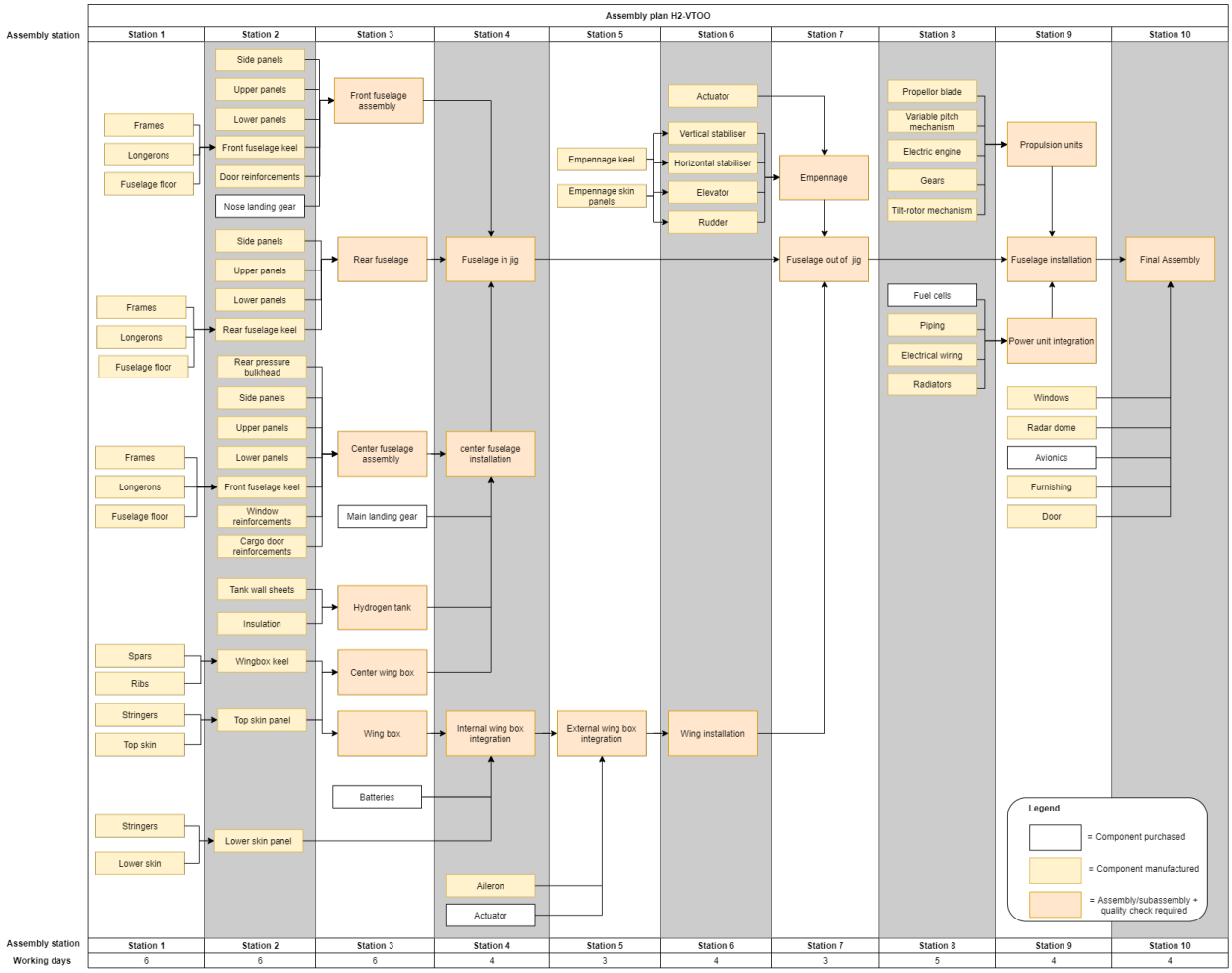

Figure 16.3: Assembly plan of H2-VTOO aircraft.

17. Sustainability Analysis

In this section the sustainability of the H2-VTOO is discussed. This is done in the following way. Firstly, the life cycle assessment is made of the aircraft. Secondly, the noise estimation strategy is discussed for the propeller, rotor, engine, gearbox and airframe. Finally, the recyclability of the aircraft is presented.

17.1. Life Cycle Assessment

In this section the total amount of CO2 emissions throughout the product life will be determined through use of a life cycle assessment (LCA), also referred to as Cradle-to-Grave analysis. Determining this amount is required for both comparing the environmental effect of this aircraft to similar ones in terms of range and passengers and for seeing what order of magnitude compensation should be made.

At this point in the design, a preliminary version of the LCA analysis is performed. This method uses mass fractions of the operational empty weight of H2-VTOO versus that of similar design concepts. The design concept that was used to compare the H2-VTOO aircraft with is the Futura project [54], which is a smaller hydrogen VTOL aircraft. These values are than compared to the H2-VTOO design and changed accordingly if necessary, as can be seen in Table 17.1. For example, one can already decide that the combustion part of the LCA will equal 0 tons of C02 and 0 MJ of energy consumption in of itself, due to the nature of the hydrogen. This assessment is than compared to the Airbus H145 [5] helicopter using a mass fractions. Values such as those used in manufacturing, end-of-life and process have been extracted from the CES LCA software [11] and from the Futura project [54].

Table 17.1: Preliminary LCA estimate for the H2-VTOO aircraft compared to the Airbus H145 10-seater helicopter.

		Process CO2 Emissions [ton]		**Process Energy Consumption [MJ]**	
Stage	**Substage**	**H2-VTOO**	**H145**	**H2-VTOO**	**H145**
Production	Material extraction	105	21	1.6E06	3E05
	Manufacturing processes	11	2	1.5E04	2.5E04
Operational Life	Fuel production & Transportation	4.4E04	5000	5.6E08	5.2E07
	Combustion	0	1.22E05	0	1.3E09
EOL	Recycling process	2.6	8.96E-02	1.8E02	1.3E03
	Recyclability potential	-329	-10	-1.9E04	-1.5E05
Total		2.18E04	1.32E05	5.61E08	1.35E09
Normalized total		1.95	34.74	5.00E04	3.55E05
Difference		-94.4%		-85.9%	

When comparing the values of the LCA analysis, it has to be kept in mind that the MTOW of the H145 is 3800kg, while that of H2-VTOO is 11200kg. Also, it is more important to assess the relations between each emission, rather than the numbers themselves. When comparing the values, one should normalize the emissions and energy consumption by their mass. Firstly, as can be seen from Table 17.1, the H2-VTOO aircraft emits almost 89% less C02 during its lifetime. This is a logical consequence from the fact that it uses hydrogen as its main fuel. Secondly, one can see the large difference between the fuel production and transporation. These emissions are kept very low due to the hydrogen being assumed to be produced in a 'green hydrogen' style, from which the energy needed to produce to hydrogen comes directly from renewables. The transportation on the other hand, largely come from pipeline systems. However, there will always be some kind of involvement of trucks and cars transporting the hydrogen to the customer buildings, as described in Section 6.4. Therefore, until all transportation is fully renewable, there will be a certain amount of CO2 emitted during transport.

One can also note that it uses a large amount of materials and uses quite some energy and produces emissions. This is due to the subsystems required to fly on hydrogen, that are not needed in normal flight. Think of the fuel cells and cooling systems. Generally, it can be concluded that the H2-VTOO by far outperforms the H145 helicopter, and all conventional aircraft, in terms of emissions produced. The largest challenges in terms of emissions are that of material extractions, and emissions of hydrogen production.

For future analysis, the substages can be assessed in more detail. This can be done by further analyzing the

material distribution of the aircraft, and finding corresponding substage values using the LCA software. This can than be combined with the manufacturing processes that are used in each part, which can also be implemented in the software.

17.2. Noise Analysis

In this section, the noise that will be produced by the aircraft is estimated. The noise that is produced by this particular aircraft is divided in five different kinds: rotor, propeller, engine, gearbox and airframe noise. These different sources of noise will be evaluated separately after which they will be added to determine the final noise that the aircraft will produce.

17.2.1. Propeller Noise

In order to determine the propeller noise, an estimation method of the NASA is used. More specifically, this subsection is entirely based upon the noise estimation method provided by Jack E. Marte and Donald W. Kurtz[72]. For this specific application, the far-field noise is analysed. This models the noise at locations that are further from the propeller tip than one propeller diameter.

The first step is to retrieve a reference noise level L_1. this is done with Figure 17.1a. Secondly, a correction factor is added that is in function of the number of blades B and the diameter of the propeller D. Their contribution can be determined by Equation 17.1 and Equation 17.2 .

$$C_1 = 20log\left(\frac{4}{B}\right) \tag{17.1}$$

$$C_2 = 40log\left(\frac{15.5}{D}\right) \tag{17.2}$$

Thirdly, the tip speed of the propeller has to be computed. This is done by multiplying the propeller rotational speed by the radius of the propeller. On the basis of this, a third correction factor C_3 can be determined with use of Figure 17.1b where Z equals 1ft.

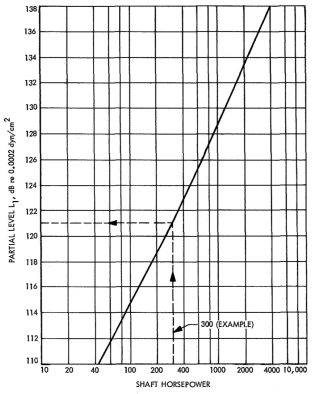

(a) Shaft power vs noise diagram.

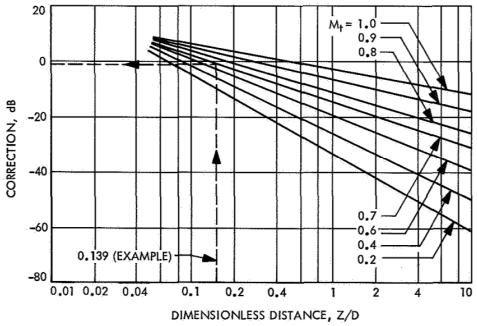

(b) Correction factor due to the propeller radius and tip speed.

Figure 17.1: Correction Factor due to Tip-Mach Number and Diameter [72].

Next, a new correction factor C_4 is determined on the basis of the heading angle of the propeller. This factor can be determined by Figure 17.2a. Furthermore, another correction factor has to be subtracted due to the distance to the point of interest from the propeller r in feet. This contribution be calculated with Equation 17.3.

$$C_5 = 20log(r - 1) \tag{17.3}$$

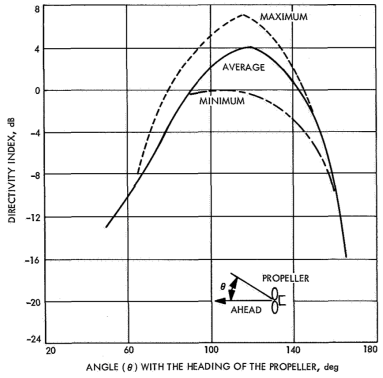

(a) Correction Factor due heading of the propeller.

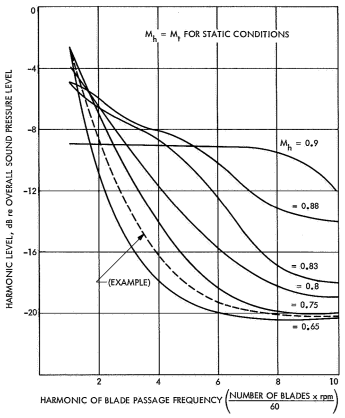

(b) Harmonic of Blade Passage Frequency and Harmonic Level Overall Sound Pressure Level.

Figure 17.2: Correction factor due to azimuth and effect of incidence and effective mach number diagrams [72].

Now, the reference sound pressure level L_1 and all the correction factors have to be combined. Next, the blade passage frequency is calculated by $\frac{Bn}{60}$ where B is the number of blades and n the propeller angular speed. With the use of Figure 17.2b a correction factor for each harmonic is found and these harmonics can be divided over octave band levels.

Next, one has to correct for the molecular absorption of sound in the air. These have to be subtracted from the sound pressure levels of the octave band levels.

Finally, the unweighted sound pressure levels will now be transformed to the A-weighted scale. This is a scale in which the sound pressure levels at the frequencies that cannot be heard by the human ear are reduced in importance and thus in dB. This is done by adding the result of Equation 17.5 [137].

$$R_A = \frac{12194^2 f^4}{(f^2 + 20.6^2)\sqrt{(f^2 + 107.7^2)(f^2 + 737.9^2)}(f^2 + 12194^2)} \tag{17.4}$$

$$A = 20 \log R_A + 0.17 \tag{17.5}$$

17.2.2. Rotor Noise

Rotor noise is the noise that is generated by the propellers when the aircraft is in VTOL configuration. In order to predict the noise generated by the propellers in this configuration, a noise estimating method constructed by NASA is used [72].

Rotor Rotational Noise

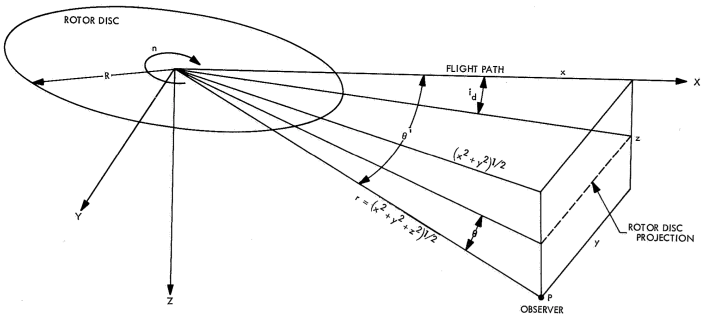

Figure 17.3: Overview of rotor-observer configuration [72].

Firstly, the distance to the observer is calculated by Equation 17.6 and the rotational Mach number by Equation 17.7. Where R is rotor radius, n the rotor angular velocity and c the speed of sound. Thirdly, the flight mach number is determined by Equation 17.8 and the angle between the flight direction and the line that connects the rotor with the observer is determined by Equation 17.9.

$$r = \sqrt{x^2 + y^2 + z^2} \tag{17.6}$$

$$M = 0.8n\frac{R}{c} \tag{17.7}$$

$$M_F = \frac{V}{c} \tag{17.8}$$

$$\theta' = \arccos\frac{x}{r} \tag{17.9}$$

These equations are combined to attain the effective rotational mach number which is determined by Equation 17.10. Then, the angle between the rotor plane and the line connecting the rotor and observer by formula Equation 17.11. Here, i_d is the disc incidence, as visualized in Figure 17.3.

$$M_E = \frac{M}{(1 - M_F \cos\theta')} \quad (17.10) \qquad \theta = \arctan\left(\frac{z}{\sqrt{x^2+y^2}}\right) - i_d\left(\frac{x}{\sqrt{x^2+y^2}}\right) \quad (17.11)$$

Next, the harmonic sound pressure levels I_N has to be estimated based upon M_E and θ. This is done by the graph that can be found in [72]. Then, these harmonic sound pressure levels are corrected by formula Equation 17.12. Here, the T is the thrust in lb and A the disc area in ft^2. The final step of the rotor rotational noise is calculating the fundamental frequency that can be found by Equation 17.13.

$$SPL_N = \left[I_N + 11 + 10\log\frac{T}{r^2}\left(\frac{T}{A}\right)\right] \quad (17.12) \qquad f_{fund} = \frac{nB}{2\pi(1 - M_F\cos\theta)} \quad (17.13)$$

Rotor Vortex Noise

In this part, the rotor vortex noise is estimated. Firstly, the linear speed of the rotor is calculated at 0.7 of the radius. This results in Equation 17.14 [72]:

$$V_{0.7} = 0.7\frac{n\pi D}{60} \quad (17.14)$$

Next, the thrust in hovering condition has to be determined by setting it equal to the weight of the H2-VTOO aircraft. Then, the total blade A_b are is retrieved by multiplying the number of blades and blade plan form [72].

The following step is the determination of the sound pressure level at a distance of x ft by Equation 17.15 which holds for sea level conditions at 21°C [72].

$$SPL_x = 10(2\log V_{0.7} + 2\log T - \log A_b - 3.57) - 20\log\frac{x}{300} \quad (17.15)$$

Now, the sound pressure level is ordered by octave bands. This is done calculating the peak frequency with the use of Equation 17.16. Here, the h is the projected blade thickness and can be computed by use of Equation 17.17. In this equation b is the blade thickness, a is the chord length and α is the angle of attack.

$$f = \frac{0.28V_{0.7}}{h} \quad (17.16) \qquad h = b\cos\alpha + a\sin\alpha \quad (17.17)$$

Next, a correction factor is subtracted from the the rotor vortex noise that is in function of the measured frequency. This is clear when one looks at Figure 17.4.

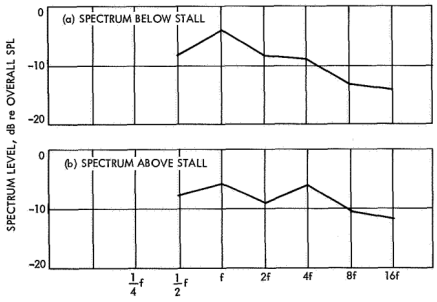

Figure 17.4: Correction of the Rotor Vortex Noise[72]

Finally, the sound pressure levels can be ordered according to a certain frequency range and the sound pressure levels have to be converted to an A-weighted system as explained in Section 17.2.1

17.2.3. Engine Noise

In this subsection, the noise generated by the engine will be calculated. As this aircraft uses fuel cells, almost no noise is emitted by this part of the engine. However, the noise generated by the electric motors can be determined with the help of Equation 17.18 [25], at 1 m distance from the motor. Here, P_{shaft} is the shaft power, S is the conformal surface area and ω is the angular velocity of the engine in rpm. The latter can be calculated by Equation 17.19[25]. Where L, W and H are the length, width and height of the reference box and d is the distance form the reference box which is chosen to be one. The final sound pressure level will be scaled to the correct distance.

$$L_W = 27 + 10\log P_{shaft} + 15\log\omega + 10\log S \quad (17.18)$$

$$S = LW + 2H(L + W) + \pi d(L + W + 2(H + d)) \tag{17.19}$$

17.2.4. Gear Box Noise

In this subsection, the noise generated by the gear box is analysed. This is done on the basis of Equation 17.20 [25] that predicts the sound power levels of gear boxes that cope with a power ranging for 200kW to 17500kW [25]. Here, Ω is the rpm of the slower gear shaft, $P_{gearbox}$ is the power the gearbox transfers. Finally, S is the conformal area discussed in Equation 17.19[25].

$$L_W = 86 + 3\log\Omega + 4\log P_{gearbox} + 10\log S \tag{17.20}$$

17.2.5. Airframe Noise

The airframe noise that this aircraft will make is estimated by another technique from NASA [50]. In this estimation, the airframe noise is mainly dependant on the the weight of the aircraft. The equation for the aircraft noise estimation can be seen in Equation 17.21[50]. U is the airspeed and W is the weight of the aircraft.

$$\text{OASPL [dB]} = 10\log U^5 + 10\log W - 74.0 \tag{17.21}$$

17.3. Noise Mitigation Strategy

Isolation materials are often used to reduce noise for multiple applications. Here, the material is considered for the electric motors and the gearbox as it can be easily applied in contrary to the propeller, rotor and airframe.
It is important to select the right material. The focus is on the weight, flammability (safety) and sustainability. That is why polyester was chosen as the material. It has a density of 50 kg/m^3, it is about 3cm thick and is recycled for 80% out of PET[12]. Besides, polyester is considered a non-flammable insulation material[43]. However, attention should be payed as it can melt at high temperatures. This could be emitted by placing an extra layer of a reflective material on the material. Furthermore, water can pass through the material without deteriorating its quality. Most importantly is its sound reduction index ΔL of 48 dB [12].

17.4. Results

An overview is given of the noise that is generated for the cruise and VTOL phase. Furthermore, the summation of the different kinds of noise is shown as well. Important to mention is the fact that it is assumed that all the noise originates from the same point source. However, this overestimate of the total sound level of the aircraft as the sound waves of the suggest that all subsystems are located in the place and will amplify each other noise in all positions around the aircraft. However, this is not the case in reality.
Now, the noise levels are shown for two situations. The first is shown in Table 17.2 and is for the VTOL phase. The second one can be seen in Table 17.3 and shows it for the cruise phase.

Table 17.2: Results for VTOL at 100m.

Subsystem	SPL [dBA]
Rotors	81.63
Engines	37.66
Gear Box	32.31
Airframe	27.53
Total	81.63

Table 17.3: Results for cruise flight at a distance of 1650m.

Subsystem	SPL [dBA]
Propellers	23.99
Engines	9.51
Gear Box	6.78
Airframe	57.93
Total	57.93

It is clear from Table 17.2 that the aircraft does not meet the constraint for the VTOL phase according to the calculations. The main source of the noise is the rotor system. This consists out of two rotors. This is followed by the engines. The engines themselves were quite loud without the sound isolation material as they produced around 90.6 dBA. However, the polyester counteracted this. The same holds for the gear boxes. Without the polyester, it produced 81.94 dBA at a distance of 100m. Lastly, The airframe noise is negligible due to the low speed.
The main problem is that the rotors have to spin too fast. This mainly has an effect in the rotor vortex noise that increases drastically with rotation speed. A reduction in rpm would have a beneficial effect on the noise. This could be done by increasing the radius. As the thrust produces by the rotor is related to the radius in a parabolic fashion while the tip speed is only linearly related to the rpm.

However, there is not a problem in terms of noise for the cruise phase as can be seen in Table 17.3. The propellers seem to produce a limited sound pressure level. This is due to the a moderately low rpm of 450, five blades per propeller

and large distance of the observer. The engines produce less noise than for the VTOL configuration as only 8 engines and less power are needed. In combination with the noise reduction factor of the polyester and large distance, this leads to a sound of 6.78 dBA. Next, one can see that the gearbox's contribution is negligible. Now, the airframe noise is higher than for the VTOL as the speed of the aircraft is higher than for the conventional take-off and is the main source of noise for the VTOL phase.
Finally, no estimation is given for the conventional take-off or landing. This is because no reliable rpm could be provided for the propeller in this situation. However, as the aircraft already exceeds 70 dB for VTOL, it is clear that the requirement is not met.

17.5. Verification

The noise estimation was performed with the use of python program. Now, that program will be subject to a verification. This is done in the following way: the used source for the estimation method included sample solutions/calculations in the appendices for both the propeller and rotor configuration to estimate the sound pressure levels. Consequently, the inputs of the python program were changed to equal the ones in the appendices. Next, unit tests were performed for each step of the method, so that all steps could be checked and therefor no errors could compensate each other to result in the correct final solution. It is an important fact that the verification does not cover all the steps that one encounters in this method. This is as the method also exist out of a couple of manual steps. For the rotor and propellers, the outcomes of the comparison can be found in Table 17.4 and Table 17.5 for both the analytical solution retrieved from the source and the solution that was retrieved from the program.

When comparing the results of the python file with the analytical solution of the rotor, it is clear that for all parameters but one, the deviation is smaller or equal to 1%. This an acceptable deviation that does not influence the result in a drastic way. However, the Correction$_1$ factor deviates 5.58%. This is due to the fact that the analytical solution assumes a disc loading of 7 $\frac{lb}{ft^2}$ while the program calculates it based upon the other values that are given. Hence, the five percent is also due to the difference of the disc loading. This leads to the conclusion that the rotor program is verified and supplies the correct values that the model intends to produce. It is important to note that a sign error was detected in the analytical model for the value of SPL_N. Consequently, this was fixed in the python file.

Table 17.4: Verification of the Rotor.

Parameter	Analytical Solution	Python Solution	Deviation [%]
M [-]	0.4290	0.4333	1.00
M_F [-]	0.179	0.1790	0
θ' [°]	20	20	0
M_E [-]	0.516	0.5210	0.96
SPL_N [dB]	-0.5490	-0.5797	5.58
$V_{0.7}$ $[ft/s]$	421	423.5	0.59
A_B $[ft^2]$	64	64.20	0.31
SPL_{300} [dB]	78.7	78.76	0.08
SPL_{1000} [dB]	68.2	68.3	0.15
h [ft]	0.212	0.2121	0.05

Now it is time to take a look at Table 17.5 to perform the verification of the propeller noise estimation. Here, the results are even better. There are no parameters that deviates more than 1.18%. This leads the the conclusion that the program works in the right fashion.

Table 17.5: Verification of the Propeller.

Parameter	Analytical Solution	Python Solution	Deviation [%]
C_1 [dB]	2.5	2.4987	0.05
C_2 [dB]	9.5	9.5635	0.66
d_{ref} [-]	0.1110	0.1118	0.72
V_{tip} $[ft/s]$	746	741.3	0.63
C_3 [dB]	-59.2	-59.9	1.18
SPL_1 [dB]	72.8	72.1	0.96
f_{bp} [Hz]	79	79.2	0.25

17.6. Validation

Due to the fact that there is no sufficient data available of a hydrogen powered VTOL aircraft it is not possible to validate the noise that is generated by the H2-VTOO by comparing it to reference data. In order to validate the noise, physical tests should be conducted. The proposed test to validate the rotor, propeller and airframe noise is to make a scale model of H2-VTOO and analyse this inside a wind tunnel for its dimensions. In this experiment acoustic measurement equipment will be attached to the aircraft as well as to the surrounding of the aircraft in order to measure the noise. In order to validate the engine and gearbox noise a proposed experiment is to operate these systems in a representative environment where again acoustic measurement equipment will be used to measure the produced noise.

17.7. Recyclability of the Aircraft

One of the main sustainability goals and requirements was to achieve a recycling rate of at least 80 %, as was discussed in Chapter 2. Throughout the report, including in the production plan, this recyclability has been discussed for all considered subsystems. By, multiplying the weights of these subsystem by their assumed recycle rate and dividing this by the total system weight, a total recycling rate can be found. This will be done in Table 17.6. Note that only certain parts of the aircraft have been designed in detail, including what material is used. For the rest of the aircraft, statistical values in terms of material used are assumed, together with their recycling rate. Modern aircraft currently have a recycling rate of 92% [37]. For subsystems made entirely out of aluminium (fuselage, propellers, etc), a recycling rate of 1 is assumed. Note that in the previous chapters, these parts have not received a seperate sustainability section for this exact reason.

Part	Weight [N]	Recyclability [-]
Battery	8060	0.85
Engines	2453	0.8
Propeller	7336	1
Fuel cell	5603	0.95
Fuselage	13803	1
Empennage	2704	1
Landing gear	4120	0.75
Wings	4797	1
Tanks	4455	0.5
Nacelles	6602	1
Rest	21982	0.92
Total	79462	0.943

Table 17.6: The different parts of the aircraft, along with their weights and recycling rate

Taking the weighted averages of the recycling rate of the many parts within the design, a total recycling rate of 94.3% has been found. This means requirement HVA-GP-03 can be considered to be met. One could note that this requirement is met by quite a margin, meaning it could be considered to be overdesigned. However, due to the design approach and view of the team, an overdesign in terms of sustainability is not deemed as a negative aspect. Furthermore having a higher recycling rate means the design will be relevant longer, even when authorities introduce tighter laws and regulations.

18. Cost Analysis

It is stated by the requirements that the total cost of the aircraft should be below 12 million euros. In order to achieve this goal, a thorough cost analysis needs to be conducted on several different aspects of the aircraft. In total, 500 aircraft are predicted to be sold from the year 2040 till the year 2060. It should be noted that this is a preliminary cost analysis and further investigation is necessary.

18.1. Cost Breakdown Structure

For a cost analysis it is important to identify all the different aspects of cost. This is done by making a cost breakdown structure where costs for different phases of the project are estimated. This cost breakdown structure can be seen in Figure 18.1. All the different parts of the aircraft are developed and manufactured specifically for the H2-VTOO where exceptions are made for the avionics which are purchased according to prices of Roskam [123] and for some other systems such as the fuel cells, electric motors and batteries, the landing gear and for the interiors of the aircraft. All these costs of different purchases are included in the cost analysis presented below.

18.2. Research, Development, Test and Evaluation (RDTE) Cost

The first step in the cost analysis is to estimate the the RDTE cost. This cost encompasses all the activities that are conducted during the DSE as well as a much more elaborate research after the DSE. In order to estimate the cost for this phase, an estimating method of Roskam [123] is used. In this method the RDTE cost is divided in seven different categories:

- C_{aed_r}**:** The airframe engineering and design cost which encompasses the planning, conceptual design and cost analysis. Furthermore, this cost will cover system integration studies and the design and construction of test facilities.
- C_{dst_r}**:** The development support and testing cost which mainly covers the actual testing of for example the propulsion and the structure.
- C_{fta_r}**:** The cost of flight test aircraft which will take into account the cost for manufacturing a test aircraft.
- C_{fto_r}**:** This is the flight test operational cost which covers all the operations and hours necessary for test operations.
- C_{tsf_r}**:** The test and simulation facility cost which takes into account the cost of operating the test facilities. From Roskam it was determined that this cost is 0.2 of the final RDTE cost.
- C_{pro_r}**:** This cost takes into account the profit that should be made during this phase. From Roskam it was determined that this cost is 0.1 of the final RDTE cost.
- C_{fin_r}**:** This cost will take into account the cost to finance the RDTE phase including the interest from the required loanes. From Roskam it was determined that this cost is 0.1 of the final RDTE cost.

With help of Roskam these different cost could be determined for this particular aircraft. The last three mentioned types of cost are a percentage of the final cost. Therefore, the sum of the first four types of cost should be divided by 0.6. The different cost values are presented in Table 18.1. The total cost of this phase can be determined by adding these numbers and dividing it by the aforementioned 0.6. However, this would result in a cost estimate for the year 1989. By assuming an average inflation of two percent per year the total necessary cost for this phase is determined to be 619.7 million euros.

Table 18.1: The total cost values for the first four types of cost excluding inflation.

Type of cost	Cost [€Million]
C_{aed_r}	22.1
C_{dst_r}	6.7
C_{fta_r}	123.2
C_{fto_r}	0.5

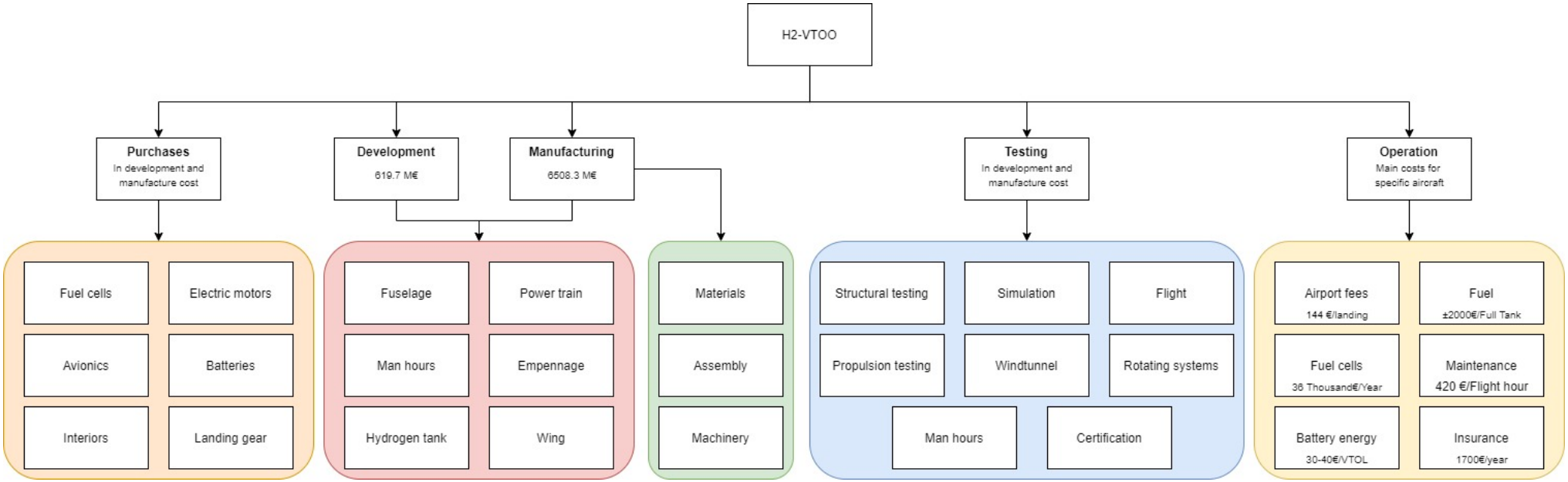

Figure 18.1: Cost Breakdown Structure for the different phases.

18.3. Manufacturing and Acquisition Cost

After the RDTE phase cost is determined, the manufacturing phase cost can be estimated. This is again done with help of a method determined by Roskam [123]. The manufacturing and acquisition cost is divided in four separate parts:

- C_{aed_m}: This is again the airframe engineering and design cost. However, this is mainly the cost to resolve problems and errors that were encountered in the RDTE phase. Furthermore, the cost of a RAMS analysis is incorporated in this cost.
- C_{apc_m}: Aircraft program production cost is the cost which covers material, interior, labour, tooling and quality control cost.
- C_{fto_m}: The flight test operations cost is again considered in this phase. It is mainly based on the aircraft operating cost per hour and the number of flight hours.
- C_{fin_m}: This is the cost to finance the manufacturing phase including the interest rates of loans. From Roskam it was determined that this cost is 0.1 of the final manufacturing cost.
- C_{pro_m}: This cost takes into account the profit that should be made during this phase. From Roskam it was determined that this cost is 0.1 of the final manufacturing cost.

These different costs are separately calculated with help of Roskam [123]. The final values for these calculations can be seen in Table 18.2. In this case again, the total manufacturing cost is determined by dividing the sum of the values listed in the table by 0.8. Assuming that this phase will be started in the year 2038 the total cost for this phase, with inflation taken into account, is 6508.3 million euros.
By adding the cost for developing, manufacturing and testing the aircraft and estimating the percentage every part will be of the total aircraft, the eventual cost per part of the aircraft could be made. These values are presented in Table 18.3. These costs per part are based on percentages given by [90]. Note that the values are for conventional aircraft, further investigation is necessary to determine whether they also comply for this particular aircraft. Furthermore, these are cost values for developing, manufacturing and testing of the aircraft that will be sold in the first twenty years.

Table 18.2: The total cost values for three types of cost excluding inflation.

Type of cost	Cost [€Million]
C_{aed_m}	34.4
C_{apc_m}	2017.2
C_{fto_m}	6.7

Table 18.3: Cost for different aspects of the aircraft testing and manufacturing taking inflation into account.

Type of cost	Cost [€Million]
Fuselage	2128.4
Wing	1150.5
Engines	460.2
Landing gear	57.5
Empennage	517.7
Systems (avionics etc.)	977.9
Manhour Cost	1375.6

18.4. Final Cost Summary

Now that the cost for these phases is determined it can be determined what the total cost of the project will be. This will be 7128.0 million euros in this value safety factors are incorporated for uncertainties. With the total cost to develop and manufacture this aircraft known the return of investment (ROI), break even point and total profit can be determined. In order to determine these parameters it first needs to be stated what the cost of one aircraft will be and for what price an aircraft will be sold. It is assumed that 500 aircraft will be sold over 20 years time, which would result in a cost price of 14.2 million euros per aircraft. The maximum aircraft price as determined by the requirements is 12 million euros for today's worth. However when taking into account inflation, the maximum allowable selling price will be 17.8 million euros by 2040. It is assumed that in the first three years, five, ten and 20 aircraft are sold in each of these three consecutive years. Hereafter it is assumed that every year a constant amount of aircraft will be sold until the total of 500 sold aircraft has been reached by the year 2060. It should be noted that this cost estimation based on empirical relations is for conventional aircraft and do not accurately takes into account the cost of a hydrogen tank for example. This will induce some error in the estimation which might result in a higher cost.

18.4.1. ROI

The return of investment can be determined by the following equation where the total profit can be determined by Equation 18.2.

$$ROI = \frac{\text{Total Profit}}{\text{Total Cost}} \cdot 100\% \tag{18.1}$$

$$\text{Total Profit} = (\text{Selling Price per Unit} - \text{Cost Price per unit}) \cdot \text{Amount of Units} \tag{18.2}$$

All the values in Equation 18.1 and Equation 18.2 are known hence the ROI could be determined and is equal to 25.1 %. Next to this, the total profit of this aircraft will be approximately 1.8 billion euros. This project therefore looks like a worthwhile investment. Since the H2-VTOO is one of the first hydrogen powered aircraft on the market it will also most probably take quite a part of the market. However, it should be noted that this will be an investment with quite some risk since hydrogen technology in aviation is still in early development stages. In order to actually get enough investors to finance the project, proper marketing needs to be conducted where as much investors as possible need to be attracted.

18.4.2. Break even point

The break even point is the point where all of the accumulated costs equals the amount of revenue. In Figure 18.2 a line can be seen which represents the total investment and a blue line can be seen which represents the revenues. The break even point is where these lines intersect and this is determined to be after approximately 16.5 years after which every sold aircraft contributes to the profit.

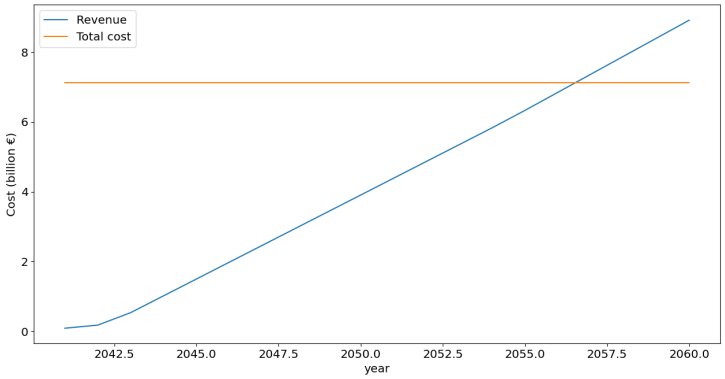

Figure 18.2: A plot showing the total cost vs the amount of revenues where the intersection of the two lines is the break even point.

18.5. Operational Cost

Now that it is determined what the cost will be to develop, manufacture and test the aircraft it is also of importance to approximate the cost of operation. The reason for this is that if it will be too expensive to operate, the aircraft will not be appealing to customers which will most likely reduce the amount of aircraft sold. The main cost factors of the operation of this aircraft, next to the standard cost factors of airport fees and such, are the price of fuel and the price of the fuel cells that need to be replaced every 5000 flight hours [40]. The standard cost of this aircraft are identified to be 202 euros for the landing fee [1], 420 euros per flight hour [2] for maintenance and approximately 1700 euros per year for insurance [3].

18.5.1. Fuel price

This aircraft will make use of cryogenic *green* hydrogen. The cost of green hydrogen by 2040 is approximately 2.10 €/kg [55] and the cost to liquefy hydrogen is approximately 0.52 €/kg [138]. This would result in a total cost of 2.6 €/kg of hydrogen. If the hydrogen tank is completely filled, it would result in a cost of approximately 2098 €per full tank. This is actually quite comparable to other business jets like the learjet 75 where a full tank approximately costs 2016 €per full tank [57] [35]. Moreover, it is expected that in the future a subsidy will be given on sustainable aircraft and that kerosene will be increasingly taxed which will make the refuelling price of the H2-VTOO more appealing [62].
Next to this, the H2-VTOO uses batteries for take-off and landing which need to store 156 kWh. For take-off this amount of energy needs to be charged to the batteries. This will approximately cost 33 euros [84].

18.5.2. Fuel cell price

Because fuel cells deteriorate quite quickly over time they need to be replaced frequently. The cost of a of fuel cells that is used for this aircraft is 200 €/kW [92]. Knowing the maximum power which the fuel cells need to be able to deliver, it is determined that the cost for the entirety of the fuel cells is approximately 512 thousand euros. These fuel cells will need to be replaced every 5000 flight hours [40]. This would mean, by knowing the availability of the aircraft, that the fuel cells need to be replaced every 10 years. This will result in a cost of 51 thousand euros per year for the fuel cell replacement. However, certain processes exist where parts of the old fuel cells are recovered and sold again [17]. This will save approximately 30% of the total fuel cell cost and would mean that the price of replacing the fuel cells will be approximately 358 thousand euros or 36 thousand euros per year. Although this sounds expensive, it is expected that the price of fuel cells will drop over the coming twenty years due to further developments and subsidy's [92].

[1] https://simpleflying.com/the-cost-of-flying/
[2] https://www.opshots.net/2015/04/aircraft-operating-series-aircraft-operating-expenses/
[3] https://www.investopedia.com/articles/wealth-management/121415/economics-owning-small-plane.asp

19. Compliance Matrix and Feasibility Analysis

As one of the final steps of the conceptual design phase, it has to be checked whether the user requirements are met. Throughout this entire report, these requirements and how they were achieved was discussed. An overview of these requirements is shown in Table 19.1. In this table the requirements are iterated, along with their identifier. In the third column it is shown whether the requirement is met, by using a ✓ when it is achieved, and a ✗ when it is not. In the final column the relevant section, where the requirement is discussed, is shown. Requirements that are not met will be elaborated upon, explaining why they have not been met. Furthermore, there are certain requirements that have not been discussed yet. Due to the nature of these requirements, they should be investigated and implemented later on in the design process.

Table 19.1: Compliance matrix indicating what requirements are achieved and where they are discussed.

Identifier	Requirement	Achieved	Section
HVA-US-01	The system shall have a door-to-door travel time of less than 4.5 hours within Europe for 90% of the business jet market, for a maximum range of 2500 km.	✓	8.1, 8.2
HVA-US-02	The user shall be able to choose their own preferred lay out, including seating and desk arrangement.		Not discussed
HVA-US-03	The aircraft shall be able to take off and land from corporate office rooftops.	✓	8.3
HVA-US-09	The aircraft shall be able to land on corporate office rooftops.	✓	8.3
HVA-US-04	The aircraft shall allow for advertisements on the exterior.		Not discussed
HVA-US-05	The aircraft shall be available whenever it is required.	✓	6.3
HVA-US-06	The aircraft shall have a positive influence on the public image of the user.		Not discussed
HVA-US-07	The final product shall have a cargo payload of 1000 kg.	✓	8.2, 10.3
HVA-US-08	The aircraft shall endure a payload of 10 passengers (100 kg + 15 kg per passenger).	✓	8.2, 10.3
HVA-GP-01	The final product shall be climate neutral.	✓	2.2, 2.3, 2.4, 2.5
HVA-GP-02	The final product shall use hydrogen as energy carrier.	✓	2.2, 2.4, 12.2
HVA-GP-03	The final product shall be able to repurpose 80% of its materials as spare parts or scrap.	✓	17.7
HVA-GP-04	The final product shall have Aviation Induced Cloudiness (AIC) levels not higher than conventional aircraft.	✓	2.2, 2.5
HVA-GP-05	The final product shall have a noise level of 70 dB within a 100 m distance during VTOL.	✗	17.2
HVA-AL-01	The final product shall have an operational infrastructure for refuelling with hydrogen.	✓	10.1
HVA-AL-02	The final product shall enter service in 2040.	✓	20
HVA-AL-03	The final product shall have a unit cost below 12 000 000 EUR.	✓	18.4
HVA-AL-04	The final product shall have an average unit cost according to the expected production of 500 units over 20 years.	✓	18.4
HVA-AL-05	The final product shall be designed for 30000 flight hours.	✓	18.4
HVA-AM-01	The final product shall have a range of 2500 km.	✓	8.2
HVA-AM-03	The final product shall be able to take off from sea level and ISA+15 ambient conditions.	✓	8.3
HVA-AM-04	The final product shall be able to land from sea level and ISA+15 ambient conditions.	✓	8.3
HVA-AM-05	The final product shall be able to perform landing and take off halfway.	✓	8.1
HVA-AM-07	The final product shall accommodate 2 crew members (100 kg + 15 kg per crew member) in the cockpit.	✓	8.2, 10.3
HVA-AM-08	The final product shall have a design cruise speed of 650 km/h.	✗	4.2, 8.1
HVA-AM-09	The final product shall have a service ceiling of 7000 m.	✓	8.1, 8.5
HVA-AM-10	The final product shall have a maximum climb rate of 9 m/s.	✓	8.5
HVA-AM-11	The final product shall have an assessment of failure scenarios of the hydrogen storage system.	✓	15.4
HVA-AM-12	The final product shall have an assessment of failure scenarios of the VTOL system.	✓	11.3, 15.4
HVA-AM-13	The final product shall have VTOL capability.	✓	8.3
HVA-AM-14-n	The conceptual design time of the aircraft shall be 11 weeks.	✓	20
HVA-AM-15	The components supplied by subcontracters shall account for CO2 emissions of no more than 125 kg.	✓	17.1
HVA-AM-16	The subcontracters shall be located within the European Union.	✓	2.4
HVA-ES-01	The final product shall have a level of safety equivalent to CS23 or CS29 regulations.	✓	15.4
HVA-GVNM-01	The hydrogen generation shall comply with regulations.		Not discussed
HVA-GVNM-02	The aircraft project shall create extra jobs in the hydrogen supply path.	✓	2.4
HVA-GVNM-03	The aircraft project shall create extra jobs in the aerospace engineering sector.	✓	2.4
HVA-AP-01	The final product shall have capability to take off as a regular fixed wing aircraft.	✓	8.4
HVA-AP-02	The final product shall have capability to land as a regular fixed wing aircraft.	✓	8.4

Requirement HVA-AM-08 is, as indicated in the table, not met. This is due to the change in the door-to-door travel time requirement. By raising the time by half an hour, a lower cruise speed is allowed. By lowering this speed, a significantly lower drag and thus power required is found. This in turn results in a lower fuel and powerplant weight, which is ofcourse beneficial. Because of the looser door-to-door time requirement, requirement HVA-AM-08 is not considered relevant anymore. Instead, a cruise speed of 131 m/s is designed for.

Another requirement that is not met is requirement HVA-GP-05. As was discussed in Chapter 17, the aircraft noise exceeds the allowed 70 dB at a distance of 100 m. During vertical take off, the aircraft, in its current design, shall produce a noise of 82 dB. However, due to the limited depth of this design phase, a slight decrease in this noise is expected when the rotors will be discussed further, as a smart design, like shaping the blade edges, decreases the noise. This will however most likely not amount to a decrease of 12 dB. Therefore, a looser requirement will be discussed with the client before starting the next design phase.

To conclude this chapter, the final operational empty mass and power budgets are assessed in Table 19.2 and Table 19.3, based on several discussions throughout the report. In the mass breakdown, a category is added for remaining systems, who do not weigh enough to put in the list or that are not designed in depth enough yet. Examples of systems included in this are the gearbox and the cooling system. On the other hand the power budget is kept to the primary systems. A further breakdown of these can be found in Chapter 12.

Table 19.2: OEM budget breakdown.

System	Mass (kg)
Engines	250
Propeller	748
Fuel cell	571
Battery	822
Nacelles	673
Fuselage	1407
Wing	489
Empennage	276
Landing gear	420
Tank	454
Rest	2164
Total	8024

Table 19.3: Power budged breakdown.

System	Power required (kW)
Propulsion	3462
Conventional aircraft loads	19.5
Electric actuators	9.4
Electric ECS	28.3
Total	3519.2

The OEM mass and power budget are likely to be subjected to unexpected changes and therefore a contingency factor should be included in the design process. The same applies to other parameters such as the MTOM, thrust and range. These contingency factors decrease during the design process. An overview of the contingency factors applied in the various phases of the design process are shown in Table 19.4. The team is currently in the conceptual design phase for which a contingency factor of 30% was taken for both OEM and MTOM and a contingency factor of 20% for both power, thrust and range. These large contingencies are commonly used for this conceptual design phase due to the large uncertainties [82]. For the preliminary design phase the contingency factors are halved and when the flight testing is reached, no contingencies are allowed anymore. Important to note is the reason why a contingency of 30 % was chosen for the OEM and MTOM instead of 20% for the other parameters. This is because the fuel used is hydrogen. This is a relative new trend in the aircraft business and data for these kind of aircraft is not easily available. This introduces extra risk and to deal with this, a higher contingency factor was introduced.

Table 19.4: Contingency factors used in different design phases.

Design phase	OEM [%]	MTOM [%]	Power [%]	Thrust [%]	Range [%]
Conceptual design	30	30	20	20	20
Preliminary design	15	15	10	10	10
Detail design	2	2	2	2	2
Flight testing	0	0	0	0	0

20. Future Development

Now that a conceptual design of the aircraft has been performed, several different steps need to be taken in order to get the aircraft fully operational by 2040. These steps can be broadly divided into preliminary design and development, detailed design and development, testing, production, certification and finally operation.

During the preliminary design, the conceptual design is improved and done in more detail. By obtaining a more elaborate design, a proper analysis can be conducted on, for example, the market, cost and sustainability. This will all direct to the point where a go/no-go sign will be assigned to proceed forward with the development of the project which will start with a detailed design.

During a more detailed design and development phase every aspect of the aircraft will be designed into full detail. This means that all the different locations of every part are known and that the integration of the different subsystems is optimised to get an optimised aircraft that complies with the requirements and safety regulations. During this phase FEM and CFD simulations will also be done in order to already confirm whether the system will perform as desired. Next to this, these simulations can be used to further optimise the different systems.

After the detailed design is performed the testing phase can begin. In this testing phase all the different subsystems will be fully tested in order to check whether they work as required. Next to this, the different materials that will be used will be tested for their respective characteristics. For example, the insulating foams will be tested for their insulation capabilities and the metals will be tested for their strength and stiffness and such. After all the separate tests have been performed a prototype can be built. With this prototype a lot of tests will be performed to determine the physical performance and safety of the aircraft.

After the first testing phase is done it is necessary to produce a full scale aircraft that will also go through all the testing procedures. If this full scale aircraft will pass these tests it will be subjected to certification. The aircraft will pass through the entire certification procedure in order to make sure that it will operate safely according to all the set regulations.

If the aircraft is certified, the aircraft will be mass produced according to the production plan after which it will go into operation. After the aircraft is in operation, analyses will still be conducted on the environmental performance and impact of the aircraft. The aircraft will be improved where necessary. An overview of the different post-dse actions and their timing can be seen in the project design and development logic in Figure 20.1 and the post-dse gantt-chart in Figure 20.2. Some tasks in the gantt-chart are shown collapsed, hence the connection arrows do not always show. The full timeline is available upon request.

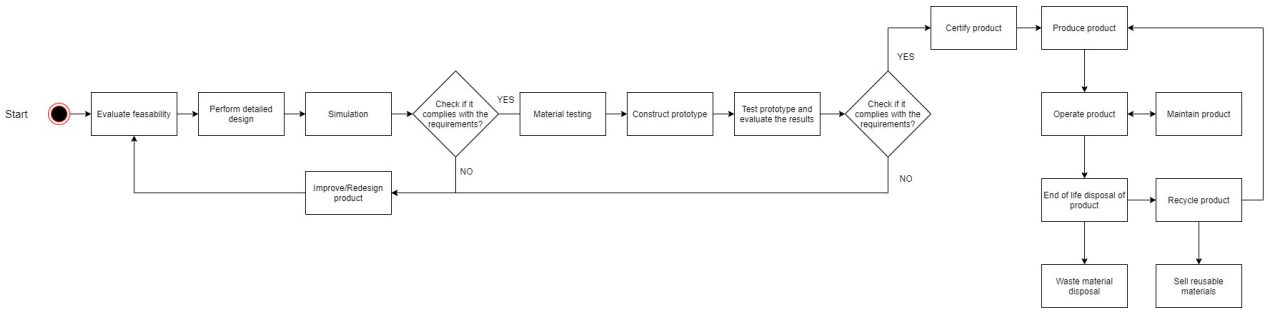

Figure 20.1: Project design and development logic.

ID	WBS	Task Name	Start	Finish
1	**1**	**Evaluate feasibility**	**Mon 2-8-21**	**Fri 14-7-28**
2	**1.1**	**Evaluate budget**	**Mon 2-8-21**	**Fri 14-7-28**
3	1.1.1	Evaluate ROI	Mon 2-8-21	Fri 20-8-21
4	1.1.2	Raise Funds	Mon 23-8-21	Fri 14-7-28
5	1.2	Evaluate conceptual design	Mon 2-8-21	Fri 27-8-21
6	1.3	Update market strategy	Mon 23-8-21	Fri 1-10-21
7	1.4	Receive go-ahead to continue project	Mon 4-10-21	Mon 4-10-21
8	**2**	**Perform detailed design**	**Mon 4-10-21**	**Wed 2-4-31**
9	2.1	Start detailed design	Mon 4-10-21	Mon 4-10-21
10	**2.2**	**Aerodynamic design**	**Mon 4-10-21**	**Wed 17-6-26**
11	**2.2.1**	**Design wing integration**	**Mon 4-10-21**	**Fri 1-8-25**
15	**2.2.2**	**Size the propellers**	**Tue 8-4-25**	**Thu 12-2-26**
18	2.2.3	Design final empennage	Mon 16-9-24	Fri 20-6-25
19	**2.2.4**	**Design landing gear**	**Wed 4-6-25**	**Tue 10-2-26**
22	2.2.5	Design rotor nacelle	Fri 29-11-24	Thu 4-9-25
23	2.2.6	Verify and validate the aerodynamic design	Thu 12-10-23	Wed 17-6-26
24	**2.3**	**Power and propulsion design**	**Thu 18-6-26**	**Wed 17-5-28**
25	**2.3.1**	**Design powertrain**	**Thu 18-6-26**	**Wed 8-3-28**
29	**2.3.2**	**Integrate engine**	**Thu 18-6-26**	**Wed 4-11-26**
32	2.3.3	Verify and validate power and propulsion design	Thu 18-6-26	Wed 17-5-28
33	**2.4**	**Design flight control system**	**Thu 18-6-26**	**Mon 30-4-29**
38	**2.5**	**Design structure**	**Thu 18-6-26**	**Wed 17-4-30**
45	**2.6**	**Design for function**	**Thu 18-4-30**	**Wed 2-4-31**
54	**3**	**Simulate system**	**Thu 3-4-31**	**Wed 17-3-32**
55	3.1	Build FEM model	Thu 3-4-31	Wed 29-10-31
56	3.2	Perform FEM analysis	Thu 30-10-31	Wed 17-3-32
57	3.3	Build CFD model	Thu 3-4-31	Wed 29-10-31
58	3.4	Perform CFD analysis	Thu 30-10-31	Wed 17-3-32
59	**4**	**Material testing**	**Thu 18-3-32**	**Wed 13-10-32**
60	4.1	Test for tensile stress	Thu 18-3-32	Wed 26-5-32
61	4.2	Test yield strength	Thu 18-3-32	Wed 26-5-32
62	4.3	test deformation	Thu 18-3-32	Wed 26-5-32
63	4.4	Investigate recyclability	Thu 27-5-32	Wed 13-10-32
64	**5**	**Design small-scale prototype**	**Thu 14-10-32**	**Wed 27-6-35**
65	5.1	Start prototype manufacturing	Thu 14-10-32	Thu 14-10-32
66	5.2	Manufacture the prototype	Thu 14-10-32	Wed 20-7-33
67	**5.3**	**Perform wind tunnel test**	**Thu 21-7-33**	**Mon 1-5-34**
72	**5.4**	**Stress test the system**	**Tue 2-5-34**	**Mon 10-7-34**
75	**5.5**	**Test propulsion system**	**Tue 11-7-34**	**Mon 25-6-35**
81	5.6	Evaluate green hydrogen availability	Tue 11-7-34	Mon 25-6-35
82	5.7	Contract parts and material suppliers	Thu 21-9-34	Wed 27-6-35
83	5.8	Establish production line	Thu 21-9-34	Wed 18-4-35
84	5.9	Establish contractor delivery system	Thu 21-9-34	Wed 27-6-35
85	**6**	**Produce first full scale aircraft**	**Tue 26-6-35**	**Tue 17-3-37**
86	**6.1**	**Manufacture the aircraft (by others or in-house)**	**Tue 26-6-35**	**Mon 9-6-36**
97	**6.2**	**Assemble the aircraft**	**Tue 10-6-36**	**Mon 5-1-37**
100	**6.3**	**Check readiness aircraft**	**Tue 6-1-37**	**Tue 17-3-37**
103	**7**	**Test full scale aircraft**	**Tue 17-3-37**	**Mon 1-3-38**
104	7.1	Test wing loading	Tue 17-3-37	Mon 25-5-37
105	7.2	Test pressurisation	Tue 26-5-37	Mon 3-8-37
106	7.3	Test control systems	Tue 4-8-37	Mon 12-10-37
107	7.4	Perform flight test	Tue 13-10-37	Mon 21-12-37
108	7.5	Evaluate testing	Tue 22-12-37	Mon 1-3-38
109	8	Go through certification procedure	Tue 2-3-38	Mon 30-1-40
110	**9**	**Deploy aircraft**	**Tue 31-1-40**	**Mon 2-9-41**
111	9.1	Start aircraft production	Tue 31-1-40	Tue 31-1-40
112	**9.2**	**Operate aircraft**	**Tue 31-1-40**	**Fri 24-5-41**
113	9.2.1	Fly aircraft	Tue 31-1-40	Fri 24-5-41
114	9.2.2	Maintain aircraft	Tue 31-1-40	Fri 24-5-41
115	9.2.3	Perform A checks	Tue 31-1-40	Fri 24-5-41
116	9.2.4	Perform B checks	Tue 31-1-40	Fri 24-5-41
117	9.2.5	Perform C checks	Tue 31-1-40	Fri 24-5-41
118	9.2.6	Perform D checks	Tue 31-1-40	Fri 24-5-41
119	9.3	Perform yearly environmental impact analysis	Tue 31-1-40	Mon 24-6-41
120	9.4	Improve environmental impact where necessary	Tue 25-6-41	Mon 2-9-41
121	**10**	**Retire aircraft**	**Tue 3-9-41**	**Mon 31-3-42**
122	10.1	Disassemble aircraft	Tue 3-9-41	Mon 11-11-41
123	10.2	Assess total recyclabilty	Tue 12-11-41	Mon 9-12-41
124	10.3	Recycle parts	Tue 12-11-41	Mon 31-3-42
125	10.4	Sustainably handle non-recyclable parts	Tue 12-11-41	Mon 20-1-42

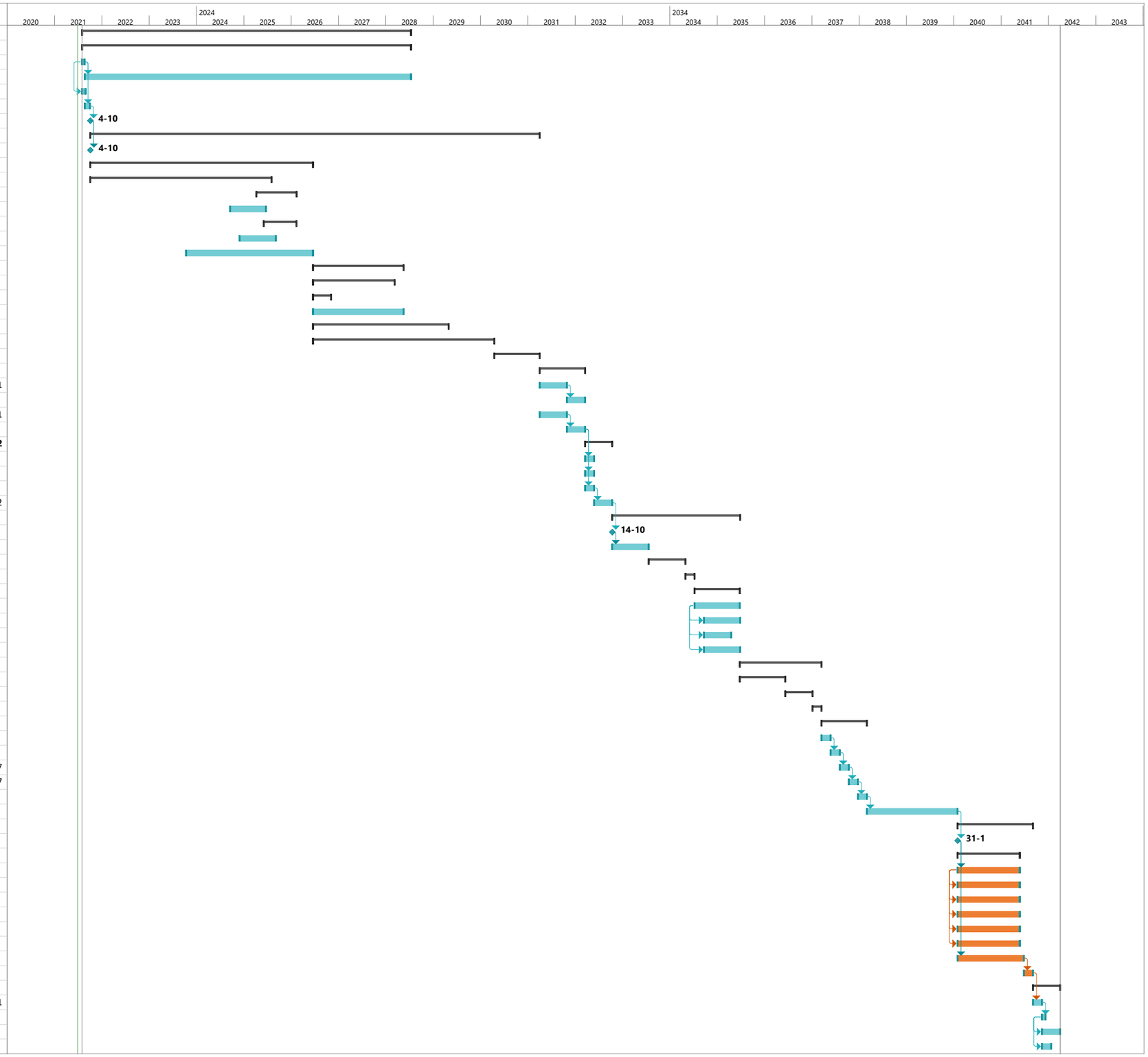

Project: Project Timeline
Date: Mon 28-6-21

Yearly Task | Summary | Task | Milestone

Figure 20.2: Post-DSE timeline

21. Conclusion and Recommendations

This final chapter provides the reader with a conclusion and future recommendations of the project. These recommendations are based on further work that is necessary such that the work the group has delivered can be improved upon.

21.1. Conclusion

Global warming plays an unequivocal role in our daily lives as it has the potential to threaten our way of living. Aviation is often seen as one of the most polluting industries. That is why the mission of this DSE project was to: *"Conceptually design a low capacity, 2500 km range, VTOL capable aircraft using H2 as energy carrier that reduces the door-to-door travel time in and between urban environments by 2040."* Achieving this will help contribute to a more sustainable future of aviation and strengthen inter-European travel. To do so, an elaborate conceptual design process was conducted. Firstly, the entire project was planned by dividing the main tasks and deciding upon the general strategy. The design process then became increasingly detailed and several straw-man concepts were developed. Next, a trade-off was performed to select the final concept. In the final phase of the project the scope was broadened again and several iterations were performed to see where the final design would fit on economical, social, environmental and technical aspects. Moreover, the subsystems were designed more elaborately.

The conceptual design process resulted in a hydrogen powered aircraft, called 'H2-VTOO'. This is an aircraft propelled by two tilt-rotors that also function as propellers for cruise or conventional take-off and landing. Each propeller is driven by five electric engines that are connected via a gear box to the crankshaft. The aim of the VTOL capability was to allow the aircraft to operate in an urban environment and for example land on a rooftop. To make this possible, fuel cells, a hydrogen tank and batteries were integrated to provide the required power to do so.

However, some concessions had to be made as the H2-VTOO produces 82dBA during VTOL at a 100m distance- this is louder than the 70dBA target. 80dBA Is about the same as the intensity of a door bell and therefore can be identified as annoying but does not make the aircraft unusable in urban environments. Besides this, the aircraft does not cruise at a speed of 650 km/h but at 475km/h. This was chosen because the speed would still allow for a travel time of 4.5 hours for 90% of the destinations in Europe for a better efficiency. Nonetheless, more research should be performed on these fronts to improve the H2-VTOO's performance.

Next, the contribution of aircraft to sustainability is discussed. The aircraft strives to improve on sustainability on several fronts. Green hydrogen is used as this does not emit any CO_2. As hydrogen can be very harmful for the environment, it was decided that the aircraft only flies at a certain range of altitudes to prevent the formation of contrails as these can be harmful to the climate and ozone layer. Furthermore, the H2-VTOO can be reused for at least 80% and some recycled materials are planned to be used in its construction. This should help counteract the draining of the earths natural resources.
Furthermore, this project can be identified as an effort to push the boundaries of hydrogen powered flight as they are known today. Hydrogen flight is a promising concept that has been subject to little research. Therefore, lots of new research is necessary to develop current technologies to such an extent to make hydrogen in aviation increasingly realistic and economic. The main problems at this point in time are efficiently storing and refuelling the hydrogen. Hence, further research should be performed. Some of the topics that require extra attention are elaborated upon in the recommendations.

21.2. Recommendations

In order to improve the future design, several steps can be taken on the following subjects to improve the validity and completeness of the design:

1. **Perform more iterations:** If an increasing amount of iterations can be performed on all the parts of the aircraft, this will lead to more reliable data for the design process. This will result in a better optimized aircraft that comes closer to reality.
2. **Detailed design of the propeller:** If the propeller can be designed in more detail in terms of dimensions, material and shape of the blade, the lift generated per rotation and per propeller blade can be determined. This would

allow to estimate the exact rpm at which the propeller is turning. If this data would have been acquired, a more detailed and exact estimation or design could have been made of the generated noise, the gearbox, the lift generation and the thrust generation. Furthermore, the propeller's dimensions could have been altered to change the tip speed. This could result in meeting the noise constraint of 70dB. Besides this, the effect of the shape could have been examined and its effect on the sound pressure level.

3. **Noise estimation:** As mentioned earlier, the noise requirement of 70dB is not met. Further research should be performed to reduce the noise. The focus should be on the propeller and rotor. As mentioned in item 2, the dimensions and shape of the blades could be changed. Furthermore, a 3D analysis could be made. On the basis of this a more realistic estimation could be given as the noise would no longer be modelled as coming from a single source. Additionally, had a more detailed analysis of the propeller been made, a noise estimation of the propeller could have been provided for the conventional take-off and landing configuration.
4. **LCA improvement:** If due to further research more detail is determined on which and what amount of materials are used, the LCA can be improved. Furthermore, by using a LCA software the assessment can be even more improved since the existing software tools have more detail incorporated for the different aspects of an LCA.
5. **Control derivative accuracy:** The simplified model used to determine the control derivatives ignored the effect of the fuselage and propellers on the flight performance. Therefore, a new model can be created that integrates these components. This would lead to a more accurate estimation of the eigenvalues and eigenmotions of the aircraft. This in turn helps with the development of an autopilot software at later stages of the design, as these systems have to be able to accurately determine at what magnitude they have to operate.
6. **Cost:** For this design, electric motors were selected which are still in the prototyping phase. For this reason, the cost of the motor at this stage is based on the cost of comparable electric motors. In order to improve the cost analysis a more thorough research can be performed on this specific engine to determine its cost. Furthermore, the cost analysis is based on a method of Roskam for conventional aircraft. For this reason there is quite some margin in the cost analysis at this moment in time. A more thorough research on the cost of hydrogen VTOL aircraft should be performed in order to come up with a more accurate cost analysis.
7. **Whirl flutter:** A further detailed examination should be performed on the topic of whirl flutter as it can lead to the failure of the engines and wing. Therefore, it is an important aspect of the design as it can cause catastrophic events. This might lead to wing box redesign to make sure it can cope with the vibrations created by this effect, especially as the eigenfrequency is lower than the vibration that the wing experiences under cruise conditions.
8. **External fueling system:** The working of the possible external fueling systems should be further examined. At the time of writing this, there is no real plan on how the fuel system will operate and look on the rooftops of buildings. This is an important aspect for the functionality and economics of the H2-VTOO.
9. **Wing download:** During VTOL, the rotors are placed above the wing. As they create lift, some download on the wing is created. This is due to the air that is pushed down by the propeller and creates a down force on the wing. This force was not considered during the design of the wing. So, research should be performed on this topic. A flap along the wingspan, like on the V-22 Osprey, could be considered to reduce the download.
10. **Detailed thermodynamic analysis of the fuel cell cooling:** During the thermodynamic analysis multiple assumptions were made. A more detailed analysis could reduce the amount of assumptions. This could lead to a better understanding of the cooling system of the fuel cell and more accurate results in terms of contact area needed with the fuel cell and contact area of the radiators that are cooled by the airflow.

Finally, one can argue that this concept should focus on the hydrogen technologies and adapt to a more conventional aircraft for take-off and landing. The challenges that come with hydrogen in aviation are not to be taken lightly, and requires a lot of innovation in both energy supply chains, infrastructure and aeronautical engineering. Therefore, it is deemed that for future development of the project, the extra VTOL capability of the aircraft will be sacrificed for a more complete study on the viability of hydrogen propelled aircraft. This allows for a more streamlined development of hydrogen powered aircraft, without taking steps that are too large to be realistically accomplished, like combining exotic technologies such as VTOL together with new technologies such as hydrogen powered aircraft.

Bibliography

[1] *'Flight-shaming' could slow growth of airline industry, says Iata*. the Guardian. Section: Business. Oct. 17, 2019.

[2] National Avioation Academy. *The Different Types of Aviation Maintenance Checks*. en-US. July 2020.

[3] Central Intelligence Agency. *The World Factbook*. 2021.

[4] European Union Aviation Safety Agency. *Easy Access Rules for Standardised European Rules of the Air (SERA)*. 2020.

[5] Airbus. *H145 Specifications*. 2021.

[6] Airbus. *Hydrogen fuel cells, explained - Innovation - Airbus*. 2021.

[7] Group 05:H2-VTOO; M. Boersma et al. *Hydrogen Powered VTOL Aircraft Baseline Report*. May 4, 2021.

[8] Group 05:H2-VTOO; M. Boersma et al. *Hydrogen Powered VTOL Aircraft Midterm Report*. May 19, 2021.

[9] Vik Krishnan Andrew Curley Rachel Garber and Jillian Tellez. *For corporate travel, a long recovery ahead - McKinsey*. 2021.

[10] Donatello Annaratone. *Engineering Heat Transfer*. Berlin, Heidelberg: Springer Berlin Heidelberg, 2010. ISBN: 978-3-642-03931-7 978-3-642-03932-4. DOI: 10.1007/978-3-642-03932-4.

[11] Ansys. *Ansys (CES) Granta EduPack | Software for Materials Education*. 2021.

[12] Jorge Arenas and Francesco Asdrubali. "Eco-Materials with Noise Reduction Properties". In: Nov. 2017. DOI: 10.1007/978-3-319-48281-1_137-1.

[13] ASQ. *What is Reliability? Quality & Reliability Defined - ASQ*.

[14] *ASSESSMENT OF THE FLUID-STRUCTURE INTERACTION CAPABILITIES FOR AERONAUTICAL APPLICATIONS OF THE OPEN-SOURCE SOLVER SU2. - ECCOMAS Congress 2016 - EASD Procedia*. Eccomas Proceedia.

[15] *Aviation Fuel Market Size, Share Statistics | Forecast - 2026*. Allied Market Research.

[16] Alejandro Nunez Baladron, Frederik Hedegaard Larsen, and Iliana Bers. "A Study on the Ideologies Surrounding the Debate on Flight-shaming". In: ().

[17] Ballard. *FUEL CELL RECYCLING & PLATINUM RECOVERY*. 2017.

[18] Boeing. *Boeing: 787 Dreamliner Specifications*. 2021.

[19] Christopher Bolkcom. "V-22 osprey tilt-rotor aircraft". In: LIBRARY OF CONGRESS WASHINGTON DC CONGRESSIONAL RESEARCH SERVICE. 2004.

[20] Sheila Bonini and Steven Swartz. "How organizing for sustainability can benefit the bottom line". In: (2014), p. 11.

[21] *Business Model Canvas | Marketingbright*. Marketingbright NL.

[22] Brian Cantwell. *The NACA airfoil series*. 2015.

[23] Sean Goulding Carroll. *EU planning staggered increase in use of green jet fuel*. www.euractiv.com. Section: Alternative & renewable fuels. Mar. 16, 2021.

[24] McKinsey Company. *Hydrogen-powered aviation A fact-based study of hydrogen technology and economics and climate impact by 2050*. Tech. rep. 2020, p. 96.

[25] Malcolm J. Crocker. *HAND BOOK OF NOISE AND VIBRATION CONTROL*. New Jersey: John Wiley & Sons, 2007.

[26] Donovan C Curry. "Estimation of Real-Time Runway Surface Contamination Using Flight Data Recorder Parameters". In: (), p. 158.

[27] DAU. *Inherent Availability (AI)-Defense Acquisition Glossary[DAP]*. Apr. 2014.

[28] "Determining Electric Motor Load and Efficiency". In: (), p. 16.

[29] G. Alvin Pierce Dewey H. Hodges. *Introduction to Structural Dynamics and Aeroelasticity*. 1st edition. Cambridge Aerospace Series. Cambridge University Press, 2002. ISBN: 9780521806985,0521806984.

[30] Mark Drela. *AVL Main Website*. 2021.

[31] Mark Drela. *AVL User Manual*. 2021.

[32] Mark Drela. *XFOIL*. Version 6.99. 2013.

[33] Giovanni Droandi, Giuseppe Gibertini, and M Biava. "Wing-rotor aerodynamic interaction in tiltrotor aircraft". In: (2012).

[34] United Nations Department of Economic and Social Affairs. *THE 17 GOALS*. 2015.

[35] eia. *US kerosene wholesale/resale price by refiners*. Section: News Release. Aug. 25, 2020.

[36] Dr. Per Ekdunge. *PowerCell Sweden AB*. 2017.

[37] Abdelghafar Elsayed. *Towards a Circular Economy, chapter 8: Best Practices and Standards in Aircraft End-of-Life and Recycling*. 2019.

[38] U.S. Department of Energy. "Extend the Operating Life of Your Motor". en. In: (), p. 2.

[39] U.S. Department of Energy. *Fuel cells fact sheet*. Nov. 2015.

[40] Office of ENERGY EFFICIENCY & RENEWABLE ENERGY. *Fuel Cells*. en.

[41] EngineeringToolbox. *Ethylene Glycol Heat-Transfer Fluid*. 2021.

[42] EngineeringToolbox. *Hydrogen - Specific Heat*. 2021.

[43] Insulation essentials. *What Is Polyester Insulation?* en-US. May 2019.

[44] Eurocontrol. *A Common European Transition Altitude, An ATC Perspective*. 2013.

[45] *Europe leads world aviation towards net zero carbon emissions | CAPA*.

[46] European Commission. *The European Green Deal*. 2019.

[47] *Federal Aviation Regulations - Index of Part 25: AIRWORTHINESS STANDARDS: TRANSPORT CATEGORY AIRPLANES*.

[48] Arnold P Fickett. "Fuel cells for electric utility power generation". In: *Advances in energy systems and technology*. Elsevier, 1986, pp. 1–73.

[49] *Figure 23: Distance distribution of European flights (weighted by...* ResearchGate.

[50] Martin R Fink. "AIRFRAME NOISE PREDICTION METHOD". en. In: (), p. 141.

[51] Federica Forte et al. "Lithium iron phosphate batteries recycling: An assessment of current status". In: *Critical Reviews in Environmental Science and Technology* (June 2020). DOI: 10.1080/10643389.2020.1776053.

[52] FSES. *Reliability, Availability and Maintainability Study (RAMS)*. en-GB. Apr. 2017.

[53] *Fuel Cell Efficiency - an overview | ScienceDirect Topics*.

[54] *Futura Final Report*. Google Docs.

[55] Ben Gallagher. *Green hydrogen costs to fall by up to 64% by 2040*. Section: News Release. Aug. 25, 2020.

[56] Ginger Gardinier. *Carbon fiber in pressure vessels for hydrogen*. 2020.

[57] GlobalAir.com. *Learjet 75*. Section: News Release. Aug. 25, 2020.

[58] Doug Gollan. *How Many Hours A Year Do Private Jets Fly?* en-US. July 2017.

[59] Yves Gourinat et al. "A numerical study on active control for tiltrotor whirl flutter stability augmentation". In: *American Helicopter Society Journal* (2004). Publisher: American Helicopter Society, pp. 244–254. ISSN: 0002-8711.

[60] Granta, Cambridge. *Granta Edupack 2020*. June 15, 2021.

[61] Monika Hartl et al. "Hydrogen adsorption on two catalysts for the ortho- to parahydrogen conversion: Cr-doped silica and ferric oxide gel". In: *Physical Chemistry Chemical Physics* 18.26 (June 29, 2016). Publisher: The Royal Society of Chemistry, pp. 17281–17293. ISSN: 1463-9084. DOI: 10.1039/C6CP01154C.

[62] Bill Hemmings et al. *Taxing Aviation Fuel in Europe. Back to the Future?* 2020.

[63] Martin Tröger Hydrogenics GmbH. *Hydrogenics Fuel Cell Systems for mobile Heavy Duty applications*. 2021.

[64] Hypertextbook. *Energy Density of Hydrogen - The Physics Factbook*. 2021.

[65] Daniel J. Inman. *Engineering-Vibrations-2nd-Edition*. 2001.

[66] Fortune Business Insights. *Business Jet Market Size, Share & COVID-19 Impact Analysis, By Business Jet Type (Very Light Jet, Light, Super-Light, Mid-size, Super-Mid-Size, Large, Super Large, Ultra Long Range), By Platform (On-Demand Service, Aircraft Management Services), By System (Propulsion System, Aerostructures, Avionics), By End Use (Private and Operators), By Point of Sale (OEM and Aftermarket), and Regional Forecast, 2020-2027*. 2020.

[67] Intel. *Airworthiness Enablement of Systems Using Intel Multi-Core Processors*. 2019.

[68] Mordor Intelligence. *Business Jet Market - Growth, Trends, COVID-19 Impact, and Forecasts (2021 - 2026)*. 2020.

[69] Christos S Ioakimidis et al. *Life Cycle Assessment of a Lithium Iron Phosphate (LFP) Electric Vehicle Battery in Second Life Application Scenarios*. Tech. rep. 2019, p. 14.

[70] IRIS. *5 Reasons Why Leasing is Better than Buying*. 2021.

[71] ISO. *Measurement of fluid flow by means of pressure differential devices inserted in circular cross-section conduits running full — Part 1: General principles and requirements*. 2014.

[72] Jack Marte and Donald Kurtz. *A Review of Aerodynamic Noise From Propellers, Rofors, and Liff Fans*. English. Tech. rep. Technical Report 32-1462. PASADENA, CALIFORNIA: CALIFORNIA INSTITUTE OF TECHNOLOGY, Jan. 1970, p. 58.

[73] "Japan bets on hydrogen to lift its ambitious carbon-neutral plans". In: *Washington Post* (). ISSN: 0190-8286.

[74] Mike Jetzer. *Apollo Flight Journal - S-II Insulation*. 2010.

[75] Hakan Karaosman, Gustavo Morales, and Mercedes Grijalvo. "How Can Local Manufacturing Improve Economic Sustainability? Saint Brissant: a case study of local manufactur- ing in Spain". In: July 2014.

[76] Harry A. Kinnison. *Aviation Maintenance Management, Second Edition*. Second Edition. 2004. ISBN: 978-0-07-180502-5.

[77] Michael Knowles et al. *The State of the Art in Fuel Cell Condition Monitoring and Maintenance*. English. 2010.

[78] Axel Krein and Gareth Williams. "Flightpath 2050: Europe's vision for aeronautics". In: *Innovation for Sustainable Aviation in a Global Environment: Proceedings of the Sixth European Aeronautics Days, Madrid* 30 (2012).

[79] Gijs van Kuik. *The fluid dynamic basis for actuator disc and rotor theories*. Amsterdam, The Netherlands: IOS Press, 2018. 132 pp. ISBN: 978-1-61499-865-5.

[80] Andre Lanz, James Hessel, and Colin Messer. *Hydrogen Fuel Cell Engines and Related Technologies*. 1st ed. Palm Desert: College of the Desert, Dec. 2001.

[81] Karen Law et al. *Air passenger transport in the EU Record number of air passengers carried at more than 1 billion in 2017 Around 71 million more than in 2016*. Dec. 6, 2018.

[82] *Lecture 5: The Design of the Fuselage - AE1222-II Aerospace Design & Systems Engineering Elements (2018/19 Q3)*.

[83] D Scott MacKenzie. "The heat treatment of landing gear is a complex operation requiring precise control of time, temperature, and carbon control. Understanding the interaction of quenching, racking, and distortion contributes to reduced distortion and residual stress." en. In: (2008), p. 4.

[84] Wood Mackenzie. *Green hydrogen costs to fall by up to 64% by 2040*. 2020.

[85] Faisal Mahmuddin. "Rotor blade performance analysis with blade element momentum theory". In: *Energy Procedia* 105 (2017), pp. 1123–1129.

[86] Mainblades. *How does aircraft lightning protection work? | Mainblades*. 2020. URL: https://mainblades.com/article/how-does-aircraft-lightning-protection-work/ (visited on 06/28/2021).

[87] *Making Rotterdam Europe's hydrogen hub*. Port of Rotterdam. Mar. 8, 2021.

[88] Research and Markets. *Global $29.75 Bn Sustainable Aviation Fuel (Biofuel, Hydrogen Fuel, Power to Liquid Fuel) Market to 2026: Analysis by Fuel Type, Manufacturing Technology, Biofuel Blending Capacity, Platform*. GlobeNewswire News Room. Apr. 21, 2021.

[89] MarketsandMarkets. *Hydrogen Aircraft Market worth $7,427 million by 2030*. 2021.

[90] Jacob Markish. *Valuation Techniques for Commercial Aircraft Program Design*. Tech. rep. 2002.

[91] The World Material. *Density of Metals, All Common Metal Density Chart & Table PDF*. 2021.

[92] Ahmad Mayyas et al. *Manufacturing Cost Analysis for Proton Exchange Membrane Water Electrolyzers*. Tech. rep. 2019.

[93] Barnes W. McCormick. *Aerodynamics, Aeronautics, and Flight Mechanics*. Sept. 1994. ISBN: 9780471575061.

[94] T. H. G. Megson. *Aircraft Structures for engineering students Sixth Edition*. Elsevier, 2017. ISBN: 978-0-08-100914-7.

[95] Joris Melkert. *Lecture_3_Flight_Mechanics - AE1110-I Introduction to Aerospace Engineering I (2018/19 Q1)*. https://brightspace.tudelft.nl/.

[96] Jaroslav Menčík. *Reliability of Systems*. en. Publication Title: Concise Reliability for Engineers. IntechOpen, Apr. 2016. ISBN: 978-953-51-2278-4. DOI: 10.5772/62358.

[97] METINVEST. *Fatigue of metal: how to detect, fight, and prevent*.

[98] MITRE. "Reliability, Availability, and Maintainability". en. In: (Aug. 2013).

[99] Daan Moreels. *Axial flux motor topology: will it dominate the future?* 2020.

[100] index Mundi. *Copper, grade A cathode vs Aluminum - Price Rate of Change Comparison - IndexMundi*.

[101] Robert Navarro. "Performance of an Electro-Hydrostatic Actuator on the F-18 Systems Research Aircraft". en. In: *Systems Research* (1997), p. 37.

[102] T. Nejat Veziroglu, S. A. Sherif, and Frano Barbir. "CHAPTER 7 - Hydrogen Energy Solutions". In: *Environmental Solutions*. Ed. by Franklin J. Agardy and Nelson Leonard Nemerow. Burlington: Academic Press, Jan. 1, 2005, pp. 143–180. ISBN: 978-0-12-088441-4. DOI: 10.1016/B978-012088441-4/50008-3.

[103] Laura Newton. *Armstrong Flight Research Center*. NASA. Feb. 22, 2021.

[104] Earth Newtworks. *How Does Aircraft Lightning Protection Work?* en-US. Dec. 2019. URL: https://www.earthnetworks.com/blog/aircraft-lightning-protection/ (visited on 06/28/2021).

[105] M. Nita and D. Scholz. "Estimating the Oswald Factor from Basic Aircraft Geometrical Parameters". In: *Deutscher Luft- und Raumfahrtkongress* (2012).

[106] Michael C. Y. Niu. *Airframe Stress Analysis and Sizing*. 2nd ed. Technical Book Company, 2005.

[107] Ryan P O'Hayre. "Fuel cells for electrochemical energy conversion". In: *EPJ Web of Conferences*. Vol. 148. EDP Sciences. 2017, p. 00013.

[108] Fabrizio Oliviero. *AE2111-II Systems Design (Aircraft Part)*. 2021.

[109] Annika Paul and Ulrike Schmalz. *DATASET 2050 Deliverable 3.1 Current Passenger Demand Profile*. Mar. 6, 2017.

[110] Fred Pearce. "How Airplane Contrails Are Helping Make the Planet Warmer". In: *Yale Environment 360* (2019).

[111] George Wise Philip Kosky. *Convection Heat Transfer Coefficient - an overview | ScienceDirect Topics*. 2013.

[112] Jason Pitt. *7 Ways to Ensure Better Maintenance of Electric Motors - Reliabilityweb*. en-us.

[113] Hans Pohl and Bengt Ridell. "HYDROGEN STORAGE IN VEHICLES". en. In: (), p. 19.

[114] ITM Power. *Shell Hydrogen Refuelling Stations Update*. ITM Power. 2021-05-21.

[115] J.A.Melkert R. Vos. *AE1222-II Aerospace design and systems engineering*. 2019.

[116] C. K. Prahalad Ram Nidumolu. "Why Sustainability Is Now the Key Driver of Innovation". In: *Harvard Business Review* (Sept. 1, 2009). Section: Disruptive innovation. ISSN: 0017-8012.

[117] Daniel P. Raymer. *Aircraft design: a conceptual approach*. In collab. with American Institute of Aeronautics {and} Astronautics. AIAA education series. Washington, D.C: American Institute of Aeronautics and Astronautics, 1989. 729 pp. ISBN: 978-0-930403-51-5.

[118] *Report suggests up to $14.7 billion in eVTOL market growth by 2041*.

[119] Reliability Engeneering Resources. *Reliability Basics: Availability and the Different Ways to Calculate It*.

[120] Perry Romanowski. *How products are made, Polyurethane*. 2021-06-20.

[121] Jan Roskam. *Airplane Design Part III: Layout design of cockpit, fuselage, wing and empennage: cutaways and inboard profiles*. Vol. 3. Airplane Design. DARCorporation, 2002. ISBN: 9781884885563,188488556X.

[122] Jan Roskam. *Airplane Design Part V: Component Weight Estimation*. Vol. 5. Airplane Design. DARcorporation, 1985. ISBN: 1884885500,9781884885501.

[123] Jan Roskam. *Part VII: Airplane Cost Estimation: Design, Development, Manufacturing and Operating*. Vol. 3. Airplane Design. DARCorporation, 1889.

[124] Ger J.J. Ruijgrok. *Effect of altitude*. English. Vol. Chapter 10. Delft: Delft Academic Press. ISBN: 978-90-6562-232-7.

[125] *Runway Pavement Loading*. en-US. Aug. 2006.

[126] Mohammad Sadraey. "Chapter 12 Design of Control Surfaces: Ailerons". In: (), p. 25.

[127] Mohammad Sadraey. "Chapter 12 Design of Control Surfaces: Elevators". In: (), p. 28.

[128] Mohammad Sadraey. "Chapter 12 Design of Control Surfaces: Rudder". In: (), p. 40.

[129] Sanfoudry. *Routine Aircraft Maintenance Questions and Answers*. en-US. Section: Aircraft Maintenance MCQs. Dec. 2019.

[130] Dieter Scholz. *Aircraft Design 11 Empennage Design*. 2021.

[131] Jeff Scott. *Aerospaceweb.org | Ask Us - Aircraft Landing Gear Layouts*. Oct. 2004.

[132] Omran Al-Shamma, Rashid Ali, and Haitham S Hasan. "An Educational Rudder Sizing Algorithm for Utilization in Aircraft Design Software". In: 13.10 (2018), p. 6.

[133] Ir. J. Sinke. *Reader production of aerospace systems (AE3211-II)*. 2021.

[134] Tomas Sinnige. Personal Communication.

[135] Smiths Metal Centers. *Datasheets*. 2018.

[136] Colleen Spiegel. *Designing and building fuel cells*. OCLC: ocm85162236. New York: McGraw-Hill, 2007. 434 pp. ISBN: 978-0-07-148977-5.

[137] International Standard, ed. *Electroacoustics - Sound level meters*. 2nd ed. Vol. Part 1: Specifications. 2013.

[138] M.T. Syed et al. "An economic analysis of three hydrogen liquefaction systems". In: *International Journal of Hydrogen Energy* 23.7 (1998), pp. 565–576. ISSN: 0360-3199. DOI: https://doi.org/10.1016/S0360-3199(97)00101-8.

[139] Ballard Power Systems. *Ballard product data sheet*. 2021.

[140] David Szondy. *World's largest hydrogen-powered plane makes maiden flight*. 2020.

[141] Hemant Taneja and Ken Chenault. "Building a Startup That Will Last". In: *Harvard Business Review* (July 8, 2019). Section: Entrepreneurship. ISSN: 0017-8012.

[142] Engineering Toolbox. *Maximum Flow Velocity in Water Systems*.

[143] The engineering toolbox. *Thermal Conductivity of Metals, Metallic Elements and Alloys*. 2021-06-18.

[144] Airfoil Tools. *Airfoil database (NACA 6 series)*. 2021.

[145] Egbert Torenbeek. *Synthesis of Subsonic Airplane Design*. Sept. 1982. ISBN: 9789024727247.

[146] Toshiba. *Toshiba H2Rex leaflet*. 2021.

[147] UNESCO. *Sustainable Development*. 2015.

[148] Battery University. *BU-205: Types of Lithium-ion*. 2010.

[149] Christophe Van den Bulte and Stefan Stremersch. "Social contagion and income heterogeneity in new product diffusion: A meta-analytic test". In: *Marketing Science* 23.4 (2004), pp. 530–544.

[150] Alexander op het Veld. *AE3212-I Aerospace Flight Dynamics and Simulation*. 2021.

[151] Dries Verstraete. "The Potential of Liquid Hydrogen for long range aircraft propulsion". In: (Apr. 2009).

[152] R. Vos, Joris Melkert, and B.T.C. Zandbergen. *2 - Class I weight estimation + payload-range diagrams version 21-Feb-17 - AE1222-II Aerospace Design & Systems Engineering Elements (2018/19 Q3)*. Feb. 2017.

[153] William Wentz, Roy Myose, and Ahmed Mohamed. "Hydrogen-Fueled General Aviation Airplanes". In: *AIAA 5th ATIO and16th Lighter-Than-Air Sys Tech. and Balloon Systems Conferences*. AIAA 5th ATIO and16th Lighter-Than-Air Sys Tech. and Balloon Systems Conferences. Arlington, Virginia: American Institute of Aeronautics and Astronautics, Sept. 26, 2005. ISBN: 978-1-62410-067-3. DOI: 10.2514/6.2005-7324.

[154] Christopher Winnefeld et al. "Modelling and Designing Cryogenic Hydrogen Tanks for Future Aircraft Applications". In: *Energies* 11 (Jan. 2018), p. 105. DOI: 10.3390/en11010105.

[155] *YASA Advanced Manufacturing of Electric Axial Flux Motors*. YASA Limited.

[156] Yumpu.com. *ASME Relief Valves for Gas & Cryogenic Systems*. yumpu.com. 2021.

[157] Dan Zhao et al. "Chapter 1 - General introduction to wind turbines". In: *Wind Turbines and Aerodynamics Energy Harvesters*. Ed. by Dan Zhao et al. Academic Press, Jan. 1, 2019, pp. 1–20. ISBN: 978-0-12-817135-6. DOI: 10.1016/B978-0-12-817135-6.00001-6.